INNOVATIVE JOINTS | FOR GRIDSHELLS
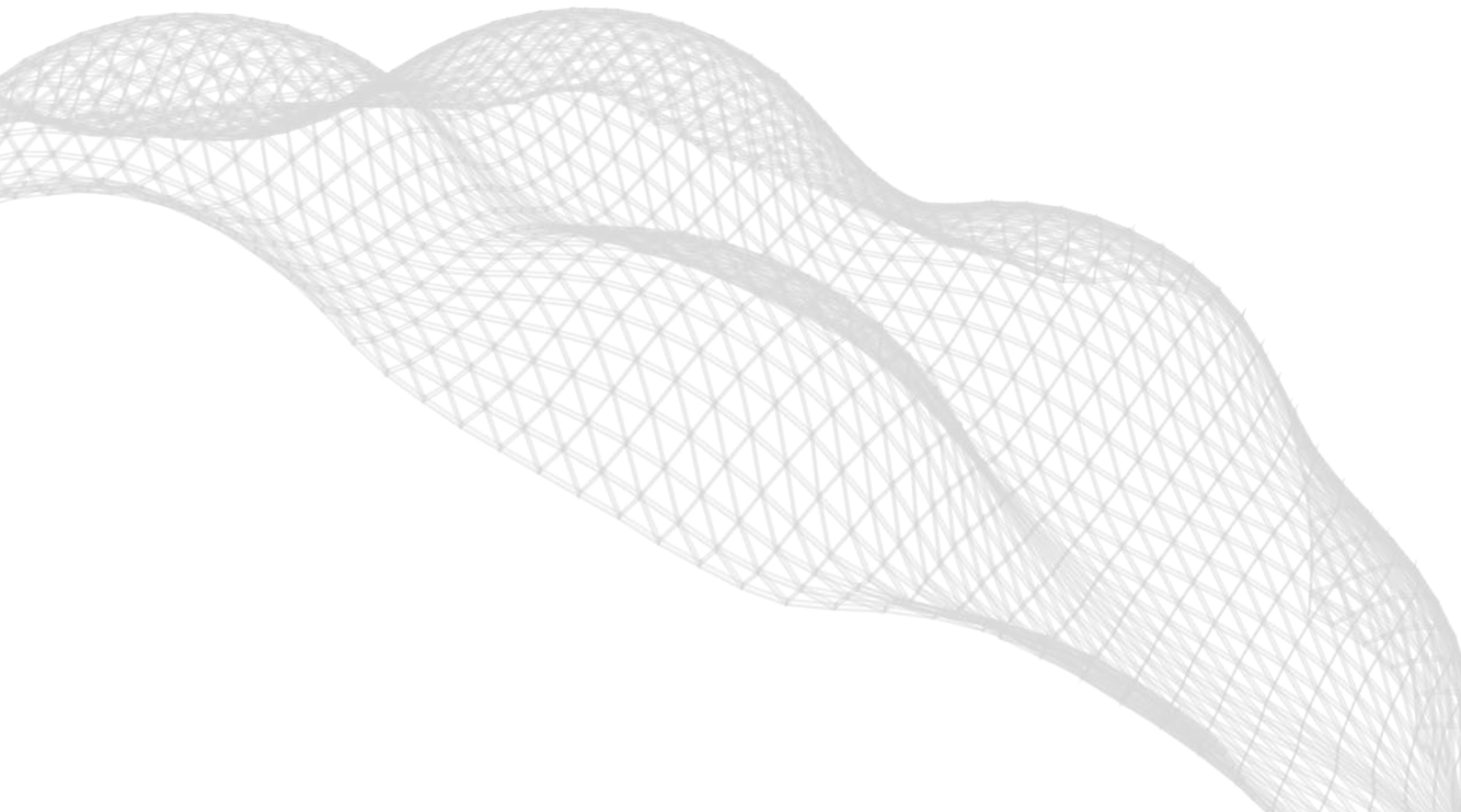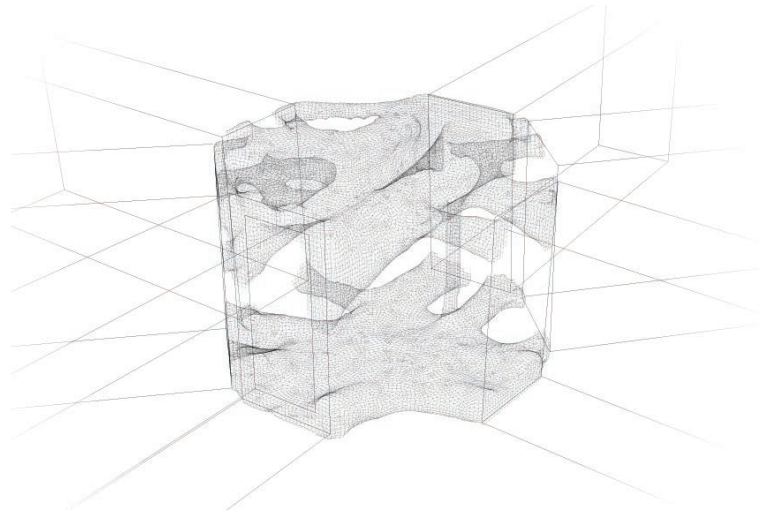
joints designed by topology optimisation and to be produced by additive manufacturing

TUDelft   ARUP

L.P.L. VAN DER LINDEN
MSc. THESIS, APRIL 2015

MASTER THESIS BUILDING ENGINEERING

FACULTY OF CIVIL ENGINEERING IN COOPERATION WITH ARUP

AUTHOR
Lennert van der Linden, BSc
lennertvanderlinden@gmail.com

APRIL 2, 2015

GRADUATION COMMITTEE
Delft university of technology:

prof. dr. ir. J.G. Rots	Faculty CiTG, Structural Mechanics
dr. ir. M.A.N. Hendriks	Faculty CiTG, Structural Mechanics
dr. ir. K.C. Terwel	Faculty CiTG, Building Engineering

Arup:

ir. S. Hofman	Amsterdam office

FINAL PROJECT GRADE: 8.5/10

PREFACE

"In November 2013 I only knew Additive Manufacturing (AM) by the well-known term of 3D printing. I associated AM with printing of plastic scale models, which would have little opportunity for structural purposes in building projects. I was sceptic and had not heard of the possibility to print with metals, concrete or human tissue yet. However, during my internship at Arup Amsterdam (November 2013 – January 2014) I became familiar with the advantages associated with AM. While researching different structural types that could benefit from the advantages of AM, I concluded that producing metal parts by AM could potentially be interesting for structures today.

In the same period during my internship I started questioning myself why AM produced metal elements have not yet been applied in building structures. Other industries such as aviation, automotive and aerospace already used structural AM produced elements for critical parts. I discovered that one of the reasons was the caution regarding the structural performance, the same as I had earlier on, amongst many structural engineers with respect to AM produced parts. This motivated me to try to open eyes in the building industry by showcasing an example of an improved structural element to be produced by AM.

Intrigued during my internship by the advantages that AM offers and helped by the knowledge gained in this period, I was ready to start my Master's thesis research on a topic involving AM in the building industry. I had the ambition to do research on a typical building element that had the potential to be produced by AM. Such building elements were preferably unique complex middle-sized elements like joints in freeform gridshells. This has led me to my research subject: Innovative joints for gridshells.

Looking into the future, 10 years from writing this thesis report, I hope to see structures in the built environment that consist of AM produced structural elements. I am aware of the fact it is still a big step to apply structural elements that has been produced by a production technique that has not been applied in the building industry yet. Therefore I hope that a visionary client has the courage to apply AM produced elements in his building, and competent engineers and designers can address the remaining challenges associated with this technique.

In order to make this come true, I hope that my research was a small link in the process to the first application of AM produced structural building elements. Moreover, I hope that from now on interest in the building industry will grow and further research will take place on this topic. However, it seems promising and, considering the fact other industries already apply AM structural components, I think it will certainly make impact in the near future."

<div align="right">Lennert van der Linden</div>

ACKNOWLEDGEMENT

SUMMARY

Additive manufacturing (AM) is a production technique that builds up successive layers of material to create a 3D object from a digital model. With this production technique, also known as 3D-printing, there are few restrictions to the shape of printed parts. Industries such as automotive and aviation have already implemented this technique, in order to build complex shapes and to reduce weight and material.

Additive manufacturing provides new opportunities for architects and structural engineers. New and better design solutions can be created with shapes that could not be produced before. However, AM has not yet been applied to realize structural elements of buildings. Freeform gridshells are typically lightweight structures built from slender members connected by structural joints. This type of structures can potentially benefit from AM. First, it is important in the design of gridshells to minimize the self-weight. Second, every individual joint in a gridshell has a complex and unique shape, which is difficult and costly to produce by conventional production methods.

Additive manufacturing could provide an economical alternative to produce these labour intensive, costly, and unique joints. Currently, this new production process is rather slow and associated with high production costs. However, AM can produce complex shapes that outperform existing production techniques and it can be used to minimize use of material and labour. Considering these points, a further investigation of the application of AM for structural joints in gridshells seems warranted. The following research question arises:

What opportunities are created by additive manufacturing in the design and production process of structural joints in gridshells?

To explore these opportunities, joints are designed for an existing gridshell. First, a literature study provides clear understanding of gridshells and their joints, the process of additive manufacturing, and topology optimization (TO). TO is a method to minimize the material of an object. The method finds an optimal distribution of material within a given domain in order to meet predefined boundary and loading conditions.

The structural behaviour of gridshells strongly depends on the behaviour of the joints. The behaviour can be identified by means of a classification system that classifies the joints as pinned, semi-rigid or rigid, based on the out-of-plane stiffness plastic moment capacity of the joint.

Three joints have been designed for the gridshell of the Złoty Tarasy roof in Warsaw, Poland, by taking different loading conditions into account. The shape of the joints are developed by using software that applies the Bi-directional Evolutionary Structural Optimization method. The software is a plug-in to the finite element analysis package of Abaqus. Detailing of the joints involved the integration of functional features, such as weld preparations and gusset plates. In this way, labour intensive on-site work will be reduced. This process fully utilized the design freedom offered by AM.

Subsequently, the joints were analysed and approved by design criteria. Two design criteria were based on the classification method for joints in gridshells: (i) the joints should have sufficient out-of-plane stiffness and (ii) sufficient plastic moment capacity. Moreover, the Von Mises stresses in the joint and in the adjacent steel members had to satisfy stated requirements.

Finally, the design and production process of the developed joints were compared with the traditional design and production method for the Złoty Tarasy gridshell. This comparison included a quantitative comparison on weight, costs, and production of the joints. A qualitative comparison was performed on various aspects to identify opportunities in the design and production. Based on this comparisons it can be concluded:

The opportunity of additive manufacturing is that lighter joints for gridshells can be developed and improved solutions for detailing can be found. This reduces the weight of the structure, labour intensity and, it speeds up the erection process. Although the use of additive manufacturing of structural joints for gridshells is not cost efficient yet, it can be in the near future when printing speed goes up and material costs go down.

AM enables designers and engineers to develop innovative solutions for design problems. Moreover, detailing of the joints can easily be adjusted to specific requirements. The design of the joints by topology optimization for the Złoty Tarasy gridshell, resulted in a weight reduction of almost 70%. In case of large joint-to-roof weight ratios, it seems feasible that the wall thickness of the applied members of gridshells can be reduced.

The high costs associated with printing of the joints are not yet compensated by the reduction of labour costs. It is expected that new generation AM devices will have higher printing speeds, which will reduce costs for printing. With increased knowledge of the applied design and production method, it might become economically and technically feasible to produce structural joints in gridshells by AM.

TABLE OF CONTENTS

1

INTRODUCTION

1.1 RELEVANCE OF RESEARCH

Additive manufacturing (AM) is a production technique that lays down successive layers of material to build a 3D object from a digital modal. This production technique, also known as 3D-printing, is already used in several industries such as aerospace, automotive and aviation. In aviation for example, various components are redesigned to minimize the self-weight, contributing to fuel cost savings for every flight [1]. Figure 1 shows an example of a light-weight door hinge that is produced by AM.

With additive manufacturing there are hardly any restrictions to the shape of the developed parts. Due to this advantage, parts can be designed from the design perspective, rather than from the manufacturing perspective. Despite of the fact that it has not yet been applied in structures for buildings, AM enables new opportunities for architects and engineers. They will be less restricted to manufacturing limitations and will be able to create innovative or improved structures and building elements. One could think of the application of more complex forms, the integration of other building disciplines in the structure and the design of parts with improved performance.

At this moment, although the price per AM produced unit is decreasing, it is still high due to the printing time and the material costs. On the other hand, traditional manufacturing processes include high tooling costs. Large numbers of produced parts are necessary to reduce unit costs. In contrast, costs per AM produced unit are constant leading to the possibility of mass customization.

Figure 1: Door hinges in airplanes are redesigned to save on fuel costs [2].

1

Typical buildings that can potentially benefit from the possibilities offered by AM are freeform gridshells. Gridshells are light-weight structures built from slender members connected by joints and containing an outer skin of translucent (glass) panels. They are able to provide stunning architectural experience for new buildings and renovation projects (Figure 2 and Figure 3).

The advantages of AM respond to the difficulties faced in the production of the joints today. Each joint in a freeform gridshell is required to connect the members under unique angles. Therefore all joints are unique which makes production of these joints highly complex and costly. In some cases, joints are assembled from 20 parts yielding in a highly labour-intensive process requiring thorough inspection [3].

Furthermore, during the design of a gridshell, engineers are trying to minimize the self-weight of the structure since this is a large part of the total load. Reducing the weight of the joints would therefore be beneficial to the forces in the structure. Also, this would have a positive effect for the loads on the foundation or on existing structures. The weight reduction of the joints could be achieved by using topology optimization (TO) as a design tool for the joints. TO is used to find the best possible material lay-out in a given design space. Similar to the redesigned door hinge in Figure 1, TO can be used to reduce the weight of the joints. These optimization processes are capable to develop very complex geometries, which outperform traditional manufacturing techniques.

Concluding, AM seems to be an interesting alternative for the current production techniques for the manufacturing of joints for gridshells. Reducing the weight by TO would be beneficial for the forces in the structure, but considering the opportunity for mass customization, AM might also be economical as well. However, until today there are only few examples that study these potential benefits. Researching this topic will create understanding of involved factors, help to find limitations, but most importantly explore the potential benefits of this production method.

1.2   RESEARCH QUESTION

What opportunities are created by additive manufacturing in the design and production process of structural joints in gridshells?

1.3   OBJECTIVE

The objective of this research is to design joints produced by additive manufacturing, for an existing steel gridshell by topology optimization, and to compare the design and production processes of the new developed joints.
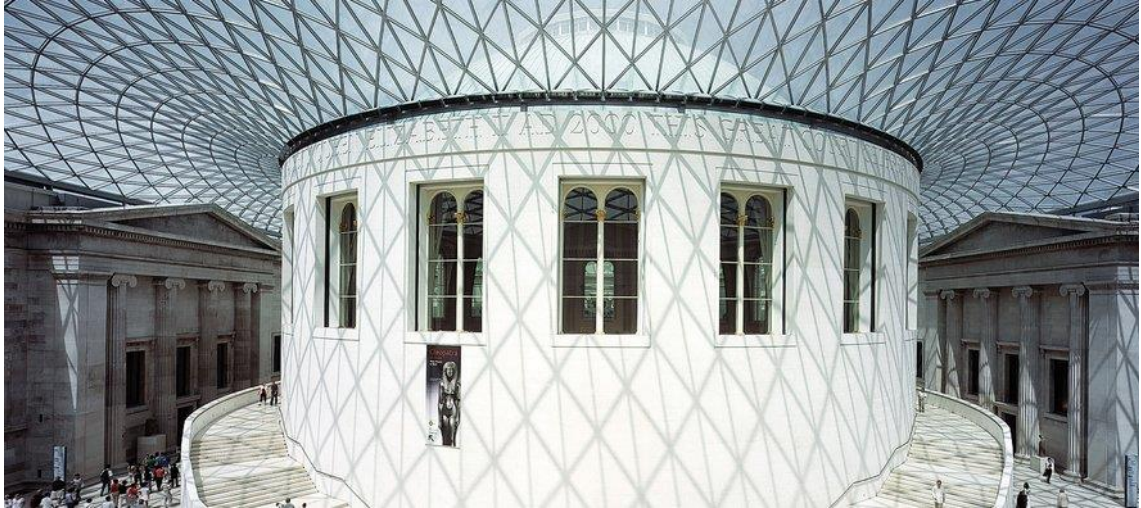
Figure 2: Example of a renovation project: The Queen Elizabeth II Great Court, British Museum (London, UK) © 2012 Waagner-Biro AG.

Figure 3: Example of a new building project: Yas Hotel (Abu Dhabi, UAE) © 2012 Waagner-Biro AG.

1.4 RESEARCH METHODOLOGY

Figure 4 shows the research methodology and the report structure with corresponding chapter numbers. The following sections explain the content by presenting the research questions of every chapter.

Chapter 2 – Background of research

The purpose of this chapter is to create a clear understanding of gridshells, joints, topology optimizations (TO) and additive manufacturing (AM), by means of a literature study. The case study that will be used for designing and comparing the joints in chapter 3 and 4 will be elaborated in this chapter as well. The following subquestions will be answered:

   2.1   What is a gridshell structure and what are its structural principles?
   2.2   What are the design requirements for joints in gridshell structures?
   2.3   What is topology optimization and how can it be applied to design lightweight metal joints of a gridshell structure?
   2.4   What is additive manufacturing and what are the advantages compared to traditional design and production techniques?

Chapter 3 – Joint design

This chapter explains how the shape of the joints are optimized and detailed, and how these joints can be produced by additive manufacturing. The following subquestions will be answered:

   3.1   What are the topology optimized shapes of representative structural joints?
   3.2   What is the best option to connect the joints to the beams?
   3.3   Which steps need to be taken to prepare the joint for AM production?

Chapter 4 – Comparison

Chapter 4 compares the developed joints, and its design and production process, with a traditional joint design. The following subquestions will be answered:

   4.1   What are the quantitative results by the applied design method compared with a traditional design approach?
   4.2   What qualitative opportunities and pitfalls exist for the application of additive manufacturing in order to produce joints for gridshells?

Chapter 5 – Conclusions and recommendations

In the final chapter, the results obtained in the different parts of the research will contribute to the answer of the research question. Moreover, conclusions and recommendations with respect to future consequences will be given.
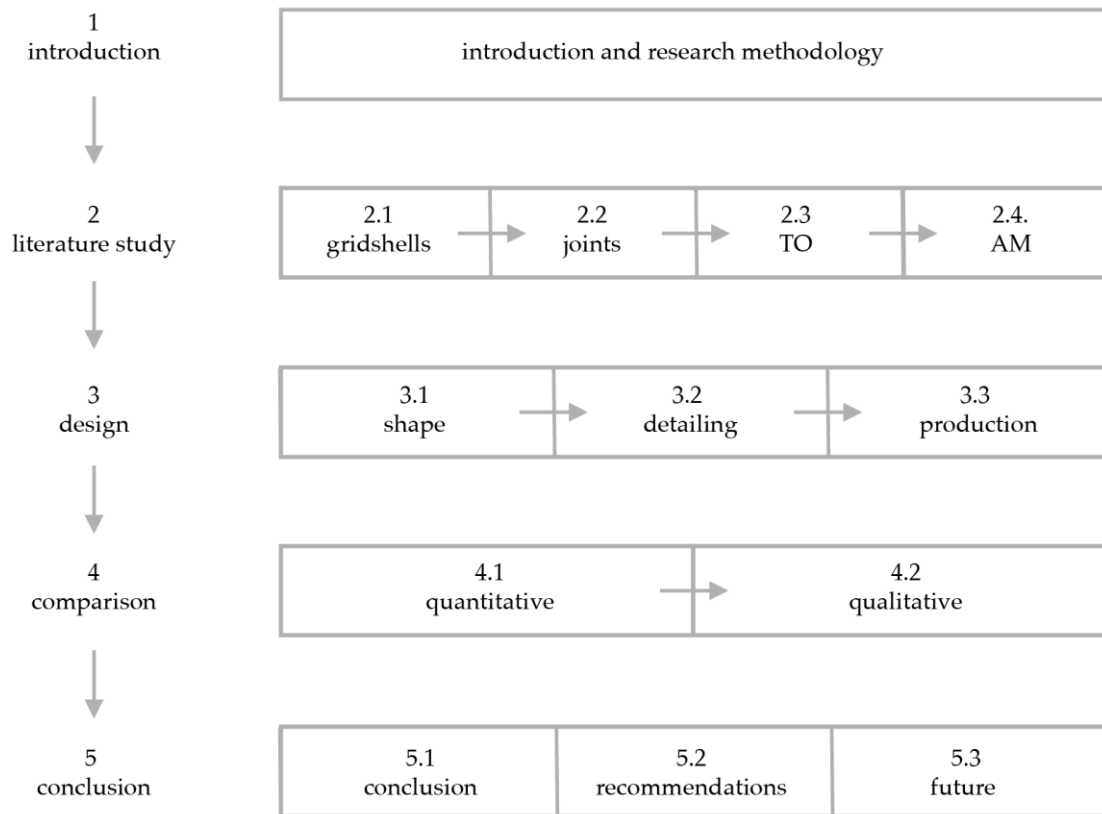
Figure 4: Schematic view of the research methodology and the report structure.

1.5   SCOPE AND LIMITATIONS

This study will mainly focus on the design process of structural joints in gridshells and the future consequences it might have when topology optimization and additive manufacturing are used for the design and production of the joints.

Different AM techniques will be explained, but not compared. Whereas Direct Metal Laser Sintering (DMLS) is used for the production of the joints, other AM techniques might result in similar or even better outcomes. The same holds for the applied material.

For the design of the joints by topology optimization, an existing optimization tool will be used instead of developing a custom made tool for this typical design purpose. To create a workable scope for this thesis, three joints are topology optimized. A larger set of optimized joints could demonstrate whether the found weight reductions are valid.

The study uses computer models for the design of the joint. Physical tests are beyond the scope of this research. The computer models are verified with simplified examples.

This study will focus on AM techniques that produce metals. Other techniques that produce plastics, concrete or any other material are not considered. The material applied for the joints is selected from existing data of manufacturers rather than studying the best suitable material for the design purpose.

2

BACKGROUND OF THE RESEARCH

"If we knew what it was we were doing, it would not be called research, would it...?"

Albert Einstein

Designing joints of a gridshell structure by making use of topology optimization and the possibility of additive manufacturing requires knowledge of diverse subjects. First of all it is necessary to understand the structural principles of gridshells and the function of the joints in these type of structures. Secondly, topology optimization will be applied as a design tool and therefore it is very important to understand this operation. Especially to prevent the optimization tool to work as a black box. Thirdly, the application of additive manufacturing plays a big role in the proposed joint design method. Finally, a case will be used in order to compare results of the proposed method to traditional design methods. Information about this case cannot be lacking.

This chapter includes all relevant information about the above mentioned topics. The information is gathered prior to the start of the design of the joints. The knowledge is united in this chapter and forms the *background of the thesis*. This chapter presents the results and provides the reader of the most relevant information. The conclusion to this chapter will focus on the answer to the sub-questions:

    2.1   What is a gridshell structure and what are its structural principles?

    2.2   What are the design requirements for joints in gridshell structures?

    2.3   What is topology optimization and how can it be applied to design lightweight metal joints of a gridshell structure?

    2.4   What is additive manufacturing and what are the advantages compared to traditional design and production techniques?

2.1 GRIDSHELLS

Gridshell structures are closely related to shell structures, but do have one main difference. The difference is that shell structures consist of a continuous surface while gridshells consist of discrete members connected in nodal points which lie on the surface of an imaginary shell. Therefore their shapes function almost identically.

This paragraph will provide general information about gridshells regarding the history and the design method of gridshells. More important, the structural principles of gridshells will be discussed. Additional information such as the analytic relation of the structural principles and the failure of gridshells can be found in appendix A.3. This paragraph will provide insight and understanding of the flow of forces in shell structures. Subsequently, the relation between shells and gridshells will be discussed.

As gridshells are not common building structures, a clear definition of what is exactly meant by a *gridshell* reads as:

> *A gridshell is a form- and cross-section-active, lightweight structure, composed of discrete members connecting nodal points following a curved shape* [4].

2.1.1 HISTORY

In the second half of the 19th century the first gridshell structures appeared. The advantage of such light-weight steel structures is that the lightness of the structure is fully visible and daylight can enter. In 1890, Vladimir Shukhov constructed two steel single curved gridshells with a span of approximately 9 m to cover two pump stations in Grozny. In 1897, Shukhov was able to build the first steel doubly curved gridshell in the world. [5].

Today, freeform gridshells are very popular, and without a doubt, a way to create attractive (public) spaces. Examples are the well-known Queen Elizabeth II Great Court (Figure 2), covering the court of the British Museum in London and the Joe and Rika Mansueto Library in Chicago (Figure 5). For more information on the history of gridshells see appendix A.1.

Figure 5: Example of a gridshell, Joe and Rika Mansueto Library, Chicago (2011) [6].

2.1.2 DESIGN OF GRIDSHELLS

Double curved gridshells are light-weight structures and designers try to reduce the weight of the structure as the dead load is a large ratio of the entire load on the structure. As gridshells are non-standard structures with complex geometries, the way of designing is different in contrast to straightforward structures. Over the years the design approach has changed.

Classical way: Form finding by physical models

Hanging chain (Figure 6) or hanging fabric models are a very simple way to find an optimal form for a shell surface. As a chain cannot resist bending moments as well as compression and shear forces, it will take the *funicular shape* in which only tension forces are present. Given this characteristic of a chain it is possible to create a net which can be seen as a three-dimensional supporting element. Loaded by its dead weight, the net will deform in a spatially curved surface. The inverted form can be found when it is flipped over a horizontal axis. Only axial compression will be present in the shell structure loaded by its dead weight.

It should be noted that the found form belongs to a particular load case. As there are many load cases to consider, the task of the engineer is to find the shape that is sufficient to all of the load cases [7].

Modern way: Form finding by computer software

Developments in computers and computer software have made it possible to calculate gridshells and use it as a form finding tool as well. Based on a method developed by Ritz in 1909, mathematician Richard Courant introduced the finite-element analysis (FEA) method in 1943. Since 1970, FEA programs started to spread widely as computers made it possible to solve the required big volume of computations. At the moment, the method is the most widely used method of engineering analysis at the moment [8]. An example of a FEA model of a gridshell is shown in Figure 7.

Due to the computer and software possibilities it is no longer necessary to use chain models. FEA programs make it possible to execute the form-finding and the structural analysis in the same environment which results in a much more flexible and faster design tool [9]. This development created the opportunity to design non-funicular structures, as it was only possible to design funicular forms and shapes by physical models [10]. Nowadays it is possible to sculpt any surface into a desired form by using a desktop computer.

Figure 6: Hanging chain model of Sagrada Familia by Antonio Gaudi. (Photo: Steve Baskin)
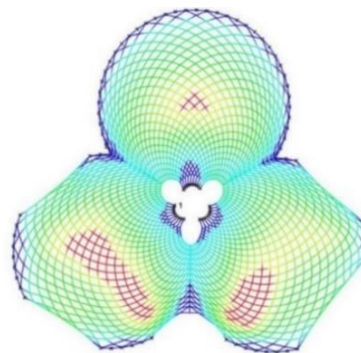
Figure 7: FEA model of a gridshell (example) [11].

2.1.3 STRUCTURAL PRINCIPLES

The unique structural principles of gridshells correspond to the structural principles of plane shells. By carrying the load with axial forces (membrane behaviour) instead of bending moments, gridshells can be very slender. These structures are extremely light and display elegance. Due to the application of double curvature, large spans can be achieved with a rather small thickness [12].

Shell theory

A shell is a generalization of an isotropic homogenous plate. The dimensions of the shell are in two directions much larger than in the third direction, i.e., the thickness. Plates and shells are defined by their *middle plane*, *thickness h* and *material properties*. While the middle plane of plates is flat, the middle plane of shells is curved. Because of the curvature it is possible for shells to carry out-of-plane loads by in-plane forces which is not possible for plates. More information about the curvature of surfaces is included in appendix A.2. This kind of membrane behaviour is described by the *membrane theory* [13].

In regions where the equilibrium and/or deformation requirements of all cases cannot be met by the membrane solution, bending moments are introduced to satisfy the specific equilibrium and deformation requirements. Typical examples are (Figure 8):

- At the supports where boundary conditions and deformation constraints are not compatible with the requirements of a pure membrane field;
- Concentrated loads acting on the shell;
- Abrupt changes in the geometry of the shell.

The introduced bending moments do not carry the applied load, but are compensating for the shortcoming of the membrane behaviour. These disturbances of the membrane field are locally. *Edge disturbances* are disturbances that are dealing with boundary conditions. Even when edge disturbances are occurring in a shell, the major part can still act like a true membrane. It is preferred to avoid bending moments as they could lead to large deformations in the shell. This is due to the fact that the flexural stiffness of the shell is rather small compared to the axial stiffness. The analysis of the behaviour by bending moments is called the *bending theory*.

The membrane theory combined with the bending theory creates the *shell theory* [13]. The solution of the shell equation can be found by the superposition of the membrane and bending equations which can be solved separately. The analytic relations of the membrane, bending and shell theory are fully elaborated in appendix A.3. Especially the membrane theory is recommended to the reader, as it explains how out-of-plane forces can be carried by in-plane forces.

Translation to gridshells

The most obvious difference between shells and gridshells is that gridshells are made of a grid instead of a solid surface. In fact, material is removed from a plain shell in order to create a grid pattern. In a solid shell the load can be transferred in all directions. This is not the case for a gridshell where it can direct the load into the direction of the elements/laths. This results in the fact that gridshells contain a limited number of load paths to carry the external load in contrast to plain shells which have an infinite number of load paths. Gridshells can be made of different kind of materials, e.g. steel, aluminium, wood or even cardboard tubes.

Membrane behaviour

In order to activate membrane behaviour it is necessary that the shell is able to transfer in-plane shear forces. In order to activate the membrane behaviour in a gridshell, the grid should be able to transfer shear forces. A triangular grid is built from rigid elements and will automatically be a rigid grid. Non-rigid grids like quadrangular, pentagonal or hexagonal grids will need to apply rigid joints or other options to stiffen the grid, for example cables in cross-direction, see Figure 10. Although opinions can vary about aesthetics of the type of grid, a triangular grid is the best solution from a structural point of view.

Bending behaviour

The bending behaviour of a gridshell corresponds to the bending behaviour of a continuous shell. In disturbed regions (Figure 8), the membrane behaviour cannot describe the equilibrium or the deformation requirements. Therefore bending moments will occur in the system. In gridshells the bending moments will concentrate in the structural members.
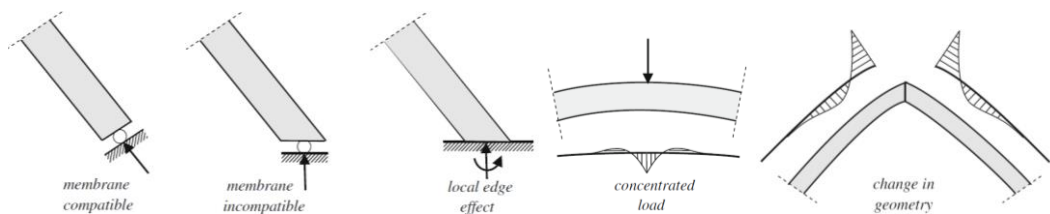

Figure 8: Bending moments are introduced in disturbed regions [13].

Figure 9: Gridshell made of cardboard tubes (Japanese pavilion EXPO 2000) [14].
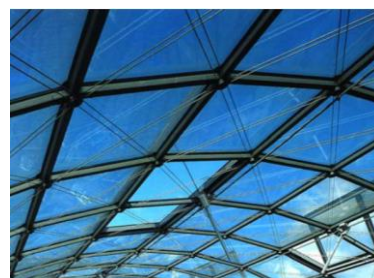

Figure 10: Quadrangular grid stiffened by cables [15].

2.2 JOINTS IN GRIDSHELLS

The previous paragraph addressed the structural principles of freeform gridshells. One of the most appealing structural advantage of well-designed gridshells is that they can activate membrane behaviour to carry out-of-plane loads by in-plane stresses. Subsequently, it is necessary to understand the role of the joints in gridshells and which requirements they need to satisfy.

This paragraph will start with a method to classify joints in gridshells. This method enables designers to quickly recognize if their design is correct. Taking the classification and the study about the flow of forces in gridshells into account it is possible to list all structural requirements. Along with additional requirements to the joints, an overview will be given which can be used in the design stage of this thesis. Also, three examples will be briefly be discussed to study the possible joints which have previously been used in completed gridshells.

2.2.1 JOINT CLASSIFICATION

Joints have a large influence on the behaviour of gridshell structures. They fulfil an important role in the local and global stability. The local stability, *snap-through* (see appendix A.4) of one or several joints, is directly influenced by the rigidity of the joints. In addition, the global stability, *global buckling*, is also influenced by the joint rigidity. This is due to the fact that gridshells, like continuous shells, are sensitive to imperfections. Different imperfections in gridshells can be distinguished as structural, loading and geometrical imperfections, but also imperfections of the structure. The latter implies the lack of joint rigidity like pinned joints [16].

Whereas beam-to-column joints in steel frames have been studied extensively and systematic classification systems are available (Eurocode 3, Part 1-8), little research has been carried out on a classification system for joints in gridshells. Therefore, Fan, Ma, Cao and Shen (2011) developed a joint classification system which can help designers in the design stage of the joints. The joint classification is based on joint stiffness and on the moment capacity. Both criteria should be considered simultaneously as a joint system may fall into a certain class in terms of stiffness, whereas this is not the case for the moment capacity. The following three classes will be considered:

1. Rigid: both high strength and bending stiffness;
2. Semi-rigid: both moderate strength and bending stiffness;
3. Pinned: either low strength and/or low bending stiffness.

Figure 11: Example of a mock-up joint for a gridshell [17].

Classification on stiffness

Studying the influence of the stiffness k of the joint, a structure composed of two members is considered. A structure with a rigid joint between the members (Figure 12) is compared to a structure with a flexible joint with stiffness k (Figure 13).

The structures are deformed by a vertical load P. The deformed shape of the structures is depicted in Figure 14. The relation between bending and the angle θ can be derived for both structures:

$$M_{zr} = \frac{4EI}{L_0}(\theta_0 - \theta) + \frac{6EI}{L_0}\cos\theta(\sin\theta_0 - \sin\theta) \tag{1}$$

$$M_{zs} = k \cdot 2(\theta_0 - \theta) \tag{2}$$

With M_{zr} is the bending moment in the rigid joint; M_{zs} the bending moment in the flexible joint; L_0 the length of the members, E the Young's modulus; I the moment of inertia of the members; θ_0 the initial angle between the members and the horizontal; θ the angle variable between the members and the horizontal.

By setting M_{zr} equal to M_{zs}, the stiffness k can be derived at which point a flexible joint behaves like a rigid joint:

$$\frac{4EI}{L_0}(\theta_0 - \theta) + \frac{6EI}{L_0}\cos\theta(\sin\theta_0 - \sin\theta) = k \cdot 2(\theta_0 - \theta) \tag{3}$$

Rewriting the equation:

$$k = \frac{2EI}{L_0} + \frac{3EI(\sin\theta_0 - \sin\theta)}{L_0(\theta_0 - \theta)}\cos\theta \tag{4}$$

By assuming small deformations it yields:

$$k = \frac{2EI}{L_0} + \frac{3EI}{L_0}\cos\theta \tag{5}$$

For this structure $\cos\theta_0 \approx 0.998$, $0 \leq \theta \leq \theta_0$; therefore $0.998 \leq \cos\theta \leq 1$, $\cos\theta \approx 1$. A flexible joint behaves like a rigid joint when the following stiffness is present:

$$k = \frac{5EI}{L_0} \tag{6}$$

A determination coefficient α can be introduced which indicates the ratio of the stiffness k to the stiffness of the members EI/L_0 connected to the joint in the structure:

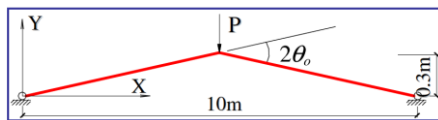$$\alpha = \frac{k}{EI/L_0} \tag{7}$$

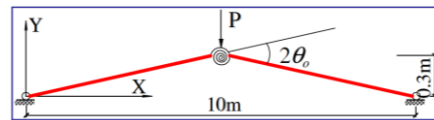Figure 12: Two-member structure with rigid joint [18].

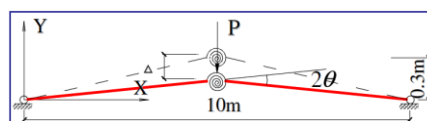Figure 13: Two member structure with flexible joint with stiffness k [18]

Figure 14: Deformed structure by load P [18].

Critical loads can be found with varying determination coefficients α. These critical loads can be plotted against the varying determination coefficients α. The effect of the different determination coefficients related to the stiffness on the behaviour of the structure (Figure 15) can therefore be used to categorize the earlier mentioned type of joints:

1. Rigid $\alpha \geq 5$
2. Semi-rigid $0{,}05 < \alpha < 5$
3. Pinned $\alpha \leq 0{,}05$

Classification on moment capacity

The mechanical behaviour is next to the stiffness of influence on the overall behaviour of the joint. A determination coefficient β, related to the moment capacity, can be defined. This coefficient takes the effect of the moment capacity of the joints on the mechanical behaviour of the gridshell into account:

$$\beta = \frac{M_{j,u}}{M_{e,u}} \tag{8}$$

With $M_{e,u}$ is the plastic moment capacity of the member connected to the joint; $M_{j,u}$ the moment capacity of the joint. Again, the effect of the different determination coefficients can be investigated. The critical loads of a two-member structure with flexible joints is determined with varying β in Figure 16. The three joint types can again be classified:

1. Rigid $\beta \geq 0{,}5$
2. Semi-rigid $0{,}5 < \beta < 0{,}01$
3. Pinned $\beta \leq 0{,}01$

Combined classification

By taking both the coefficients α and β for respectively the stiffness and the moment capacity of the joint into account, the classification of the joint types is determined by:

1. Rigid $\alpha \geq 5$ and $\beta \geq 0{,}5$
2. Semi-rigid $\alpha \geq 5$ and $0{,}5 < \beta < 0{,}01$ or $0{,}05 < \alpha < 5$ and $\beta \geq 0{,}01$
3. Pinned $\alpha \leq 0{,}05$ or $\beta \leq 0{,}01$

Note: a gridshell containing joints with $\alpha \gg 5$ and $\beta \gg 0{,}5$ and a gridshell containing joints with $\alpha = 5$ and $\beta = 0{,}5$ will behave in a similar way. Hence, it is advantageous to develop joints with $\alpha = 5$ and $\beta = 0{,}5$. These joints are not fully rigid, but behave in a rigid way. This can lead to a reduction of material and weight.
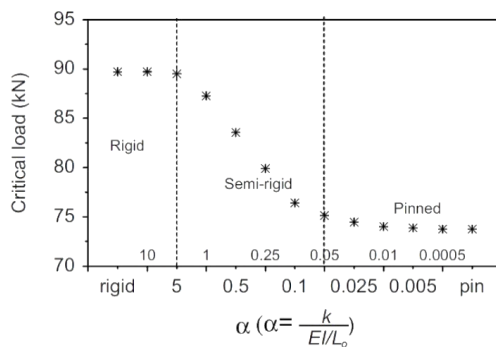

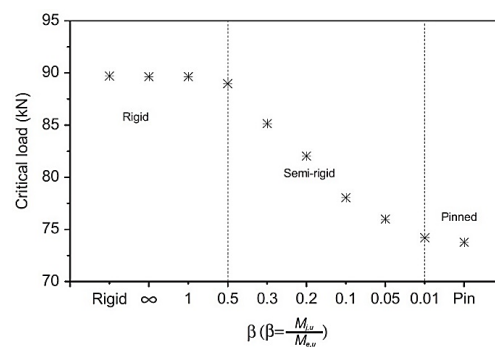Figure 15: Critical load with different determination coefficients α [18].

Figure 16: Critical load with different determination coefficients β [18].
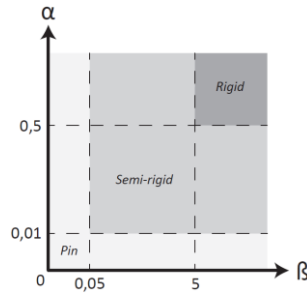
Figure 17: Classification of joints based on α and β.

2.2.2 REQUIREMENTS OF THE JOINTS

Knowledge of joints is essential to design an efficient gridshell. This paragraph lists all the requirements to joints in gridshells. This overview will be taken into account during the design (second) part of the thesis.

In-plane requirements

The in-plane joint requirements take the membrane behaviour of the gridshell into account. Therefore the joint should:

- Be able to transfer axial forces;
- Be able to transfer in-plane shear forces in case of non-rigid grid patterns, e.g., quadrangular, pentagonal, hexagonal patterns.

Out-of-plane requirements

The out-of-plane requirements address for the bending behaviour of the gridshell. Also relating to the stability of the gridshell the joints fulfil an important role, such as:

- Be able to transfer bending moments;
- Contain sufficient out-of-plane stiffness;
- Be able to transfer out-of-plane shear forces.

Additional requirements

There are also additional requirements to the joints with respect to:

- *Tolerances*. Gridshells are sensitive to imperfections, therefore it is important that the geometry of the joints is accurate and easily connectable to the members;
- *Weight*. The dead load is a substantial part of the total load on gridshells. Therefore, massive heavy steel blocks as joints should be avoided. Parts of hollow sections or CNC (Computer Numeric Control) produced parts can be welded together. However, this increases the complexity (and costs) of the joint;
- *Manufacturing*. The designed joint should be able to manufacture efficiently;
- *Costs*. As time is equal to money it is important that the erection speed is high. Therefore the joints should enable to be installed rapidly without further adjustments. Moreover, costs for manufacturing of the joints should be monitored;
- *Appearance*. Although architects have different visions, the goal of most architects is to design a smooth and elegant grid. Hence, it is important to blend the joints into the entire structure.

2.2.3 EXAMPLES

In the previous paragraphs attention is paid to joint classification and the requirements in respect to the design of the joint. It is also important to consider some example projects in order to study possible joint solutions.

1. Palacia de Comunicaciones
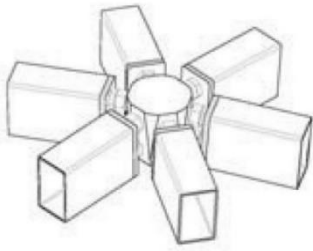
Figure 18: Single Layer Ortz joint [17].

Joint info	
Connection	Bolted
Aesthetics	Visible node detail
Labour intensity	Medium; assembly of joint existing of multiple parts
Erection	Quick; by bolts
Weight	Medium: ± 80 kg/joint, Joint weight per m² roof*: 18 kg (or: 12,3%)
Costs	Medium

2. Westfield shopping Centre
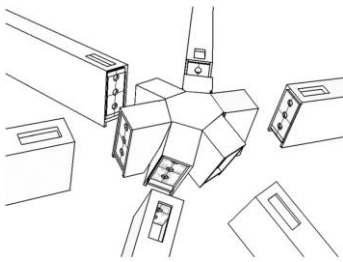
Figure 19: Connection between the joint and the beams [3].

Joint info	
Connection	Bolted
Aesthetics	Non-visible node detail
Labour intensity	High; assembly of 20 parts, geometry corrected by laser and preparation work beams required
Erection	Quick; by bolts
Weight	High: ± 110 kg/joint Joint weight per m² roof*: 25 kg (or 16,2%)
Costs	High

3. FrankfurtHochVier
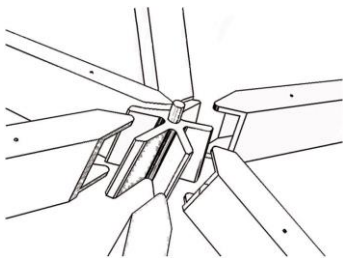
Figure 20: Connection between the joint and the beams [3].

Joint info	
Connection	Welded
Aesthetics	Non-visible node detail
Labour intensity	Medium; joints produced by CNC machine. However, welded on site and beams need weld preparation
Weight	Low: ± 40 kg/joint Joint weight per m² roof*: 9 kg (or 6,6%)
Erection	Medium; making use of ladders, but welded on site
Costs	High
Other	Difficulties with applying and inspecting the welds

*Estimation based on the roof weight of the Złoty Tarasy gridshell (introduced in paragraph 2.5).

2.3   TOPOLOGY OPTIMIZATION

Gridshells are light-weight structures and designers try to reduce the weight of the structure as the dead load is a large ratio of the entire load on the structure. In order to reduce the dead load of the gridshell, topology optimization can be used as a design tool to create light-weight structures.

The fact that nowadays freeform gridshells consist of complex 3D shapes lead to unique forces in each joints. Traditionally, the joints in gridshells are mostly designed on the critical forces in one of the joints. Therefore it is advantageous to design each joint on its unique forces. In this paragraph research is done on structural optimization and specifically topology optimization, which gives potentially the highest weight reduction. Topology optimization can be defined by:

> *Topological optimization involves the optimal distribution of material within the structure. It is used to find a preliminary structural configuration that meets predefined criteria* [19].

2.3.1   STRUCTURAL OPTIMIZATION

Designing optimal structures has become more important due to limited material resources, environmental impact and technological competition. Therefore, designers can apply *structural optimization* in order to obtain the best performance for structures while satisfying various constraints. Whereas the topic of structural optimization was formerly an academic research topic, it is nowadays widely used by engineers and architects. Software packages are available to end-users in an easy, reliable, efficient and inexpensive form. Three types of structural optimization (Figure 22) can be distinguished [20]:

- *Size optimization*: seeking for the optimal design by changing the size variables as cross-sectional dimensions.
- *Shape optimization:* changing the predetermined boundary in order to find the best possible solution.
- *Topology optimization:* searching for the optimal design by determining the best possible place for cavities within a stated domain.

The aim of the optimization is to minimise or maximise some kind of physical property. This can be either load dependent properties such as strain energy, deflection and stress, or load independent properties as volume, weight and perimeter area. Expressed in mathematical terms an optimization can have the following form [21]:

$$min_x f(x) \tag{9}$$

$$subject\ to: \begin{bmatrix} g(x) < c \\ x_i \in \phi \\ equilibrium\ condition \end{bmatrix}$$
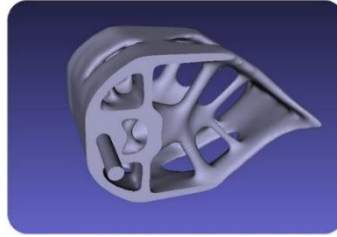
Figure 21: Example topology optimization [22].

With $f(x)$ the objective function that will be minimised, $g(x)$ the response that is limited by constraint c, $x_i = [x_1\ x_2\ ...\ x_n]$ are the design variables, ϕ the range of allowed values for the design variable. The optimized design needs to fulfil the equilibrium conditions. The optimization problem is solved by an iterative process.

Despite of the fact that topology optimization is technically the most challenging, it is the most rewarding economically as the designer is not limited to changes in size and shape. Topology optimization provides more freedom and designers are able to create totally new and highly efficient conceptual designs [20].

2.3.2   TOPOLOGY OPTIMIZATION

Topology optimization is the study on the topology of a structure. An answer is to be found to the discrete (0-1) problem where to apply material and voids. This takes place in a given domain with predefined loads, boundary conditions and possibly additional design restrictions such as the location and size of prescribed holes or solid areas. A mathematical approach is used to find a result which meets a prescribed set of design requirements [23].

Topology optimization can be used in the conceptual design stage. After having found the final optimized topology, the design will need to be fine-tuned for performance and manufacturability. There are several methods to carry out the topology optimization process. The following will be discussed in the following paragraphs [21]:

- Solid Isotropic Microstructure with Penalisation (SIMP) method;
- Evolutionary Structural Optimization (ESO) method;
- Bi-directional Evolutionary Structural Optimization (BESO) method;
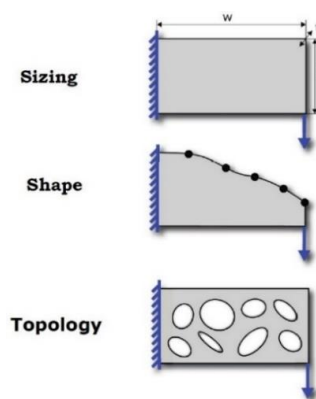- Homogenisation method;
- Level set method.

Figure 22: Different types of structural optimization [22].

Due to availability reasons, the BESO method is applied in the design part of the thesis and will be explained below. Information concerning other methods can be found in appendix B.1.

BESO method

The *Bi-directional Evolutionary Structural Optimization (BESO) method* is a combination of the mentioned ESO method and the Additive Evolutionary Structural Optimization (AESO) method. The BESO method allows material to be removed and added simultaneously. The rejection ratio (*RR*) and the inclusion ratio (*IR*) determine the number of elements that are removed or added. Both ratios need to be chosen carefully. If not, it is possible that the algorithm will not find an optimal solution [24].

An application of the BESO method, proposed by Huang & Xie, 2010, is using a volume constraint as an optimization criterion. Corresponding with the ESO method based on stiffness or displacement, sensitivity numbers are used to determine which elements should be removed or added. The BESO algorithm continues until the constraint volume and a convergence criterion are satisfied.

The ESO and BESO method are easily implemented and linked to finite element analysis (FEA) packages. However, the BESO method is much more efficient compared to the ESO method.

2.3.3 OPTIMIZATION PROCESS

A general BESO optimization process involves four steps. The first step is a linear static analysis of the initial design. The second step contains the set-up of the topology optimization, the evolutionary parameters and the indication of the design and non-design domain. The topology optimization includes the definition of the volume fraction, the mean compliance and the filter radius. The evolutionary parameters contain the evolutionary rate, the admission rate and the filter radius. The third step is running the optimization process. The fourth step consists of the post-processing of the optimization results; the derivation of the concept (CAD) design, evaluation of the results and if necessary carrying out a new analysis [20]. Figure 23 depicts the steps of the optimization process.

Step 1
- Lineair static analysis

Step 2
- Set-up of topology optimization problem
  - Volume fraction
  - Mean compliance
- Evolutionary parameters
  - Evolutionary (rejection) ratio
  - Admission (inclusion) ratio
  - Filter radius
- Indication of design and non-design domain

Step 3
- Optimization run

Step 4
- Post-processing of results
  - Derive concept (CAD) design
  - Evaluation of results
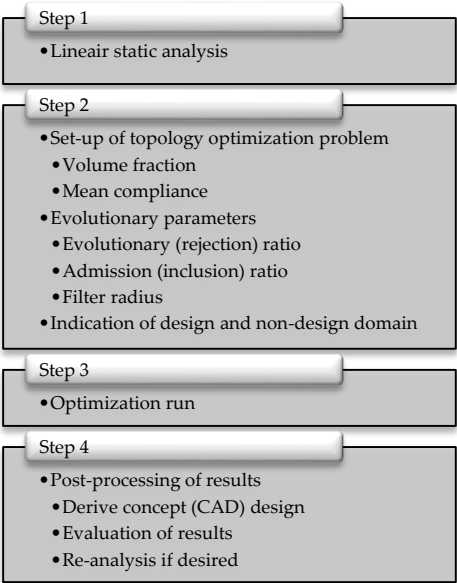 - Re-analysis if desired

Figure 23: Steps of a general BESO optimization process.

2.4 ADDITIVE MANUFACTURING

Results of topology optimization processes often result in complex geometries, see Figure 21 and Figure 24. Therefore the intended production method is additive manufacturing (AM) as Keulen, Langelaar, & Baars, 2013 state: "AM & topology optimization: 1 + 1 = 3". Also, a study performed by Galjaard, Hofman and Ren, shows that AM is an efficient way to produce an irregular set of complex shaped building components [26].

In this paragraph the possibilities, advantages and constraints of producing parts by AM will be discussed. Also, the AM technologies to print metal parts and different materials produced by AM machines will be introduced. Finally, parts need to be prepared for AM production. Therefore, points of attention, involved in this step, will be brought forward.

Additive Manufacturing, also referred to as 3D Printing, Additive Fabrication, Additive Processes, Additive Techniques, Additive Layer Manufacturing, Layer Manufacturing and Freeform Fabrication, is an upcoming production method in the building industry. Therefore, the following definition helps understanding the term A*dditive Manufacturing*:

> *"Additive Manufacturing is the process of joining materials to make objects from 3D model data, usually layer upon layer, as opposed to subtractive manufacturing methodologies."* [27]

2.4.1 IN GENERAL

Additive Manufacturing (*AM*), also called 3D printing, is an established production method in several industries, but only emerging in the building industry. Printing of a plastic canal house in Amsterdam by DUS architects has been a topic over the last months. Also attention was paid by the media to print full-scale concrete buildings. Less known is the opportunity of printing with metals. However, printed metal parts are already applied in military, aerospace and aircraft, automotive and medical industries. Concrete examples are printing of turbine rotor blades, fuel nozzles, airplane door hinges, seatbelt buckles personalised titanium teeth and artificial sculls.

2.4.2 PRINCIPLE

Additive Manufacturing (AM) incorporates different kind of techniques that are based on the same principle. Computer-Aided Design (CAD) is used to define and model a 3D object. The model is broken down by special software in layers called slicing. The sliced model can be send

Figure 24: Example of AM produced part (below) in contrast to the same part produced in a conventional way (top) [28].

to an AM output device, the printer. The printer, depending of the method, applies different kind of technologies to bond the layers together, e.g., by exposure, heating or bonding. The printer contains a specific build space or chamber. The building process can vary from hours to days depending on the method, the layer thickness and the size of the object. The printing process is followed by the subsequent processes. Post-processes can include removal of support fixings, surface cleaning and removal of uncured material. Powder which has not been sintered can be recycled. A simplified representation of the process is depicted in Figure 25 [29].

Advantages

The largest difference between conventional manufacturing methods and AM is the additive way of production instead of a subtractive way, such as milling and cutting. Restrictions because of moulding forms do not need to be taken into account. Because of these differences there are several advantages of using AM over conventional manufacturing [30]:

- Freedom of shape;
- Tool-less processing;
- Reduction of processing steps which could result in a shorter lead time;
- 'Batch size one' production, i.e., producing one-off products;
- Reduction of structurally irrelevant material;
- Reduction of waste.

Taking above mentioned advantages into account it is possible to conclude that with the application of AM a different design approach can be considered. *Design-driven* manufacturing processes make it possible to step away from the concept '*design for production*'. Engineers could directly start thinking from the perspective of the performance of the desired product. Therefore, this creates new opportunities in the building industry, such as [31]:

1. Production of highly complex objects;
2. Optimization and integration of functional features;
3. Manufacturing of small batch sizes at reasonable unit costs;
4. Production of metal objects in a sustainable way.

Constraints

Next to the advantages there are also constraints to AM. The following limiting factors can play a role in the consideration of the application of AM for steel objects [26]:

- High costs associated with machines, maintenance and materials;
- There is a limited range of available metals;
- Material properties of AM produced metal can differ from conventional produced metal;
- The printer contains a specific building space or chamber which limits the maximum dimensions of the object, approximately 400x400x400mm;

Figure 25: Left: 3D CAD model.   *Middle: slicing process.*   *Right: building process* [29].

- The accuracy of the printed object is determined by the layer thickness of the printing device;
- Additional support structure might be necessary to avoid deformations;
- The production time can vary from hours to days depending on the volume, layer thickness and AM method of the object.

The biggest barrier are the high costs associated with machines, maintenance and materials. Costs will drop until AM technologies become more standard and competition increases between suppliers [30].

2.4.3 METAL PRINTING

Direct Metal Fabrication (DMF) is used for the direct production of metal parts. The processes are either based on a 'powder bed process' or a 'powder feed process'. The material is heated during the building process by a laser or an electron beam. Attention should be paid to waste heat and should carefully be directed. Preferably by support structure to the base plate where the part is built on. If the heat is not properly exhausted this could result in adhesion of surrounding material to the part, but also warping, distortion and bending in Z-direction.

Powder bed process

The collective term for powder bed process technologies is Selective Laser Sintering (SLS). Metal particles are fused together by sintering, meaning that the particles are heated just below the point of liquefaction. Layers of powder are deposited and sintered subsequently. Most powder bed processes take place in a building space filled by an inert gas to form a protective atmosphere. Therefore reactive metal powders, such as aluminium and titanium, can be applied. Even though many different materials are available, they cannot be applied in the same building process. Unsintered material is removed after completion of the part. Figure 26 depicts schematically the SLS process [29]. Different SLS technologies can be distinguished, such as:

- Selective Laser Melting;
- LaserCusing;
- Electronic Beam Melting;
- Direct Metal Laser Sintering.

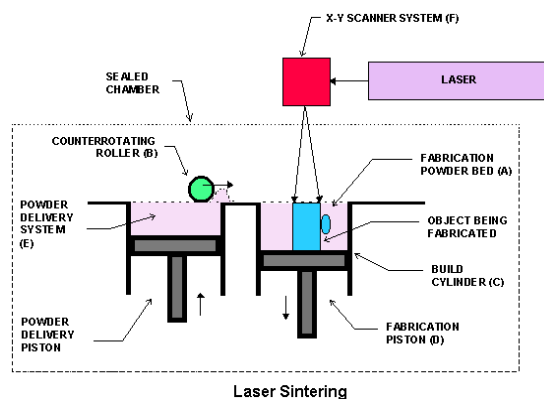The mentioned SLS technologies are discussed in appendix C.1.

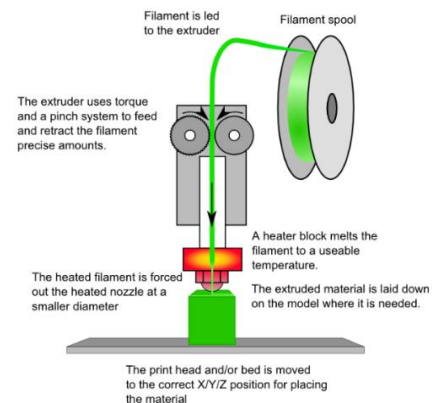Figure 26: Selective Laser Sintering (SLS) process. © Castle Island's Co.

Figure 27: Fused Deposition Modelling (FDM) process [32].

Powder feed process

The powder feed process, also called Fused Metal Deposition (FDM) method, deposits molten material by means of a nozzle. In order to build a 3D object, the nozzle is able to move in X- and Y-direction, while the base plate moves down in Z-direction. In order to obtain a proper cohesion between the layers, the building chamber is heated and maintained at a certain temperature. In powder fed processes, different materials in different quantities can be applied. Also, damaged or defect parts can be repaired by rebuilding layers. During post-processing, inaccurate surfaces need to be finished by conventional techniques.

Different FDM technologies can be distinguished, such as:

- Laser Engineered Net Scaping
- Direct Metal Deposition
- Construction Laser Additive Directe

The above mentioned FDM technologies are discussed in appendix C.1.

Materials

Different kind of metals can be distinguished which are developed for different kind of purposes. Once fully validated, any metal alloy can be used in AM machines. Table 1 lists different kind of metals which are developed and produced by EOS GmbH (Munich).

Table 2 presents the associated properties of metals that are applied in mechanical engineering purposes.

In addition, tests has been carried out on the material *EOS MaragingSteel MS1*. The test report is added in appendix C.2. The material data sheet is included in appendix C.3. Note: A limited amount of test pieces has been used in this test.

Table 1: Different kind of metals produced by EOS [31].

Product class	Product name	Material type*	Typical applications
Maraging steel	EOS MaragingSteel MS1	18 Mar 300 / 1.2709	Series injection-moulding tools; mechanical parts
Stainless steel	EOS StainlessSteel GP1	Stainless steel 17-4 / 1.4542	Functional prototypes and series-production parts; mechanical engineering and medical technology
	EOS StainlessSteel PH1	Hardenable stainless steel 15-5 / 1.4540	Functional prototypes and series-production parts; mechanical engineering and medical technology
	EOS StainlessSteel 316L	1.4404/UNS S31673	Lifestyle: jewellery, functional elements in yachts, spectacle frames, etc. Aerospace: supports, brackets, etc. Medical: functional prototypes and series-production parts in e.g. endoscopy and orthopedics
Nickel alloy	EOS NickelAlloy IN718	Inconel™ 718, UNS N07718, AMS 5662, mat. # 2.4668	Functional prototypes and series-production parts; high-temperature turbine components
	EOS NickelAlloy IN625	Inconel™ 625, UNS N06625, AMS 5666F, mat. # 2.4856 etc.	Functional prototypes and series-production parts; high-temperature turbine components
	EOS NickelAlloy HX	UNS N06002	Components with severe thermal conditions and high risk of oxidation, e.g. combustion chambers, burner components, fans, roller hearths and support members in industrial furnaces
Cobalt chrome	EOS CobaltChrome MP1	CoCrMo super alloy, UNS R31538, ASTM F75	Functional prototypes, series-production parts, mechanical engineering, medical technology, dental
	EOS CobaltChrome SP2	CoCrMo super alloy	Dental restorations (series-production)
Titanium	EOS Titanium Ti64	TiAl4V light metal	Functional prototypes and series-production parts; aerospace, motorsports etc.
	EOS Titanium Ti64ELI	TiAl4V ELI	Functional prototypes and series-production parts in medical technology
Aluminium	EOS Aluminium AlSi10Mg	AlSi10Mg light metal	Functional prototypes and series-production parts; mechanical engineering, motorsports etc.

Table 2: Mechanical properties of different kind of materials.

Material	Property	Value
EOS MaragingSteel MS1	Tensile strength	Min.[1] 1930 MPa
	Yield strength	Min. 1862 MPa
(after age hardening)	Elongation at break	Min. 2%
	E-modulus	Typ. 180 ± 20 GPa
	Density	8,0 – 8,1 g/cm³
EOS StainlessSteel GP1	Tensile strength	Typ.[2] 1100 MPa (XY-direction)
		Typ. 980 MPa (Z-direction)
(stress relieved)	Yield strength	Typ. 590 MPa (XY-direction)
		Typ. 590 MPa (Z-direction)
	Elongation at break	Typ. 29 % (XY-direction)
		Typ. 31 % (Z-direction)
	E-modulus	Typ. 180 GPa
	Density	7,8 g/cm³
EOS StainlessSteel PH1	Tensile strength	Min. 1310 MPa
	Yield strength	Min. 1170 MPa
(hardened)	Elongation at break	Min. 10%
	E-modulus	Typ. 180 GPa
	Density	7,8 g/cm³
EOS StainlessSteel 316L	Tensile strength	640 ± 50 MPa (XY-direction)
		540 ± 55 MPa (Z-direction)
(as built)	Yield strength	530 ± 60 MPa (XY-direction)
		470 ± 90 MPa (Z-direction)
	Elongation at break	Typ. 40 ± 15 % (XY-direction)
		Typ. 50 ± 20 % (Z-direction)
	E-modulus	Typ. 185 GPa (XY-direction)
		Typ. 180 GPa (Z-direction)
	Density	7,9 g/cm³
EOS CobaltChrome MP1	Tensile strength	1100 ± 100 MPa
	Yield strength	600 ± 50 MPa
(stress relieved)	Elongation at break	Min. 20 %
	E-modulus	220 ± 20 GPa
	Density	8,3 g/cm³
EOS Titanium Ti64	Tensile strength	Min. 930 MPa
	Yield strength	Min. 860 MPa
(heat treated)	Elongation at break	Min. 10 %
	E-modulus	Typ. 116 ± 10 GPa (XY-direction)
		Typ. 114 ± 10 GPa (Z-direction)
	Density	4,41 g/cm³
EOS Aluminium AlSi10Mg	Tensile strength	345 ± 10 MPa (XY-direction)
		350 ± 10 MPa (Z-direction)
(heat treated)	Yield strength	230 ± 15 MPa (XY-direction)
		230 ± 15 MPa (Z-direction)
	Elongation at break	12 ± 2 % (XY-direction)
		11 ± 2 % (Z-direction)
	E-modulus	70 ± 10　GPa (XY-direction)
		60 ± 10 GPa (Z-direction)
	Density	2,67 g/cm³

[1]Min. = minimal, [2]Typ. = typical

2.4.4 DESIGN FOR PRODUCTION

Once a design is developed, by means of topology optimization or any other methods, attention needs to be paid to prepare the design for production. When properly executed, the following advantages can be obtained:

- Reduction of build times and costs;
- Reduction of post-processing steps (machining or support removal);
- Reduction of scrap-rate;
- Proper accuracy and surface finish.

In order to obtain the above mentioned advantages, the following aspects need to be considered:

- Build orientation;
  - Vertically built parts have best quality;
  - Flat built parts can increase residual stresses;
  - Building multiple parts in the same building chamber will speed up the building process.
- Support structure;
  - The part needs to be built from support structure that is fixed to the base plate. When finished, they are separated by breaking away the support structure;
  - Overhangs with angles less than 45° need support structure (Figure 28);
  - Surfaces with 15° to 45° angle to the horizontal can be built, but with decreasing surface finish and accuracy.
  - Adding support structure increases time and costs to build and remove;
- Self-supporting features;
  - Holes up to 20 mm diameter can be produced without support structure, unsupported holes with larger diameters will decrease accuracy;
  - Using gothic arches instead of constant radius arches provides more accurate results;
  - Smooth steps by using chamfers.
- Residual stress reduction;
  - Large 2D surface areas can cause stress to parts;
  - Tilting the part will reduce the surface area (Figure 29);
  - Heat treatment can be applied in order to release residual stresses after the part is built.
- Wall thickness and gaps;
  - Wall thicknesses of 0,2 mm can be achieved;
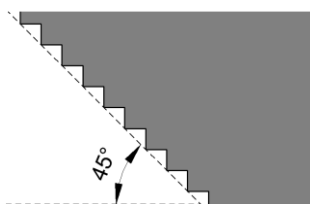 - Gaps of 0,1 mm can be achieved.
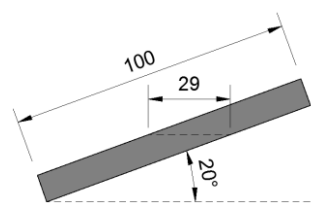

Figure 28: Overhang without support structure   *Figure 29: Tilted part to reduce surface area.*

2.5   CASE STUDY: ZŁOTE TARASY

To achieve the objective of the thesis, the design approach that makes use of topology optimization and additive manufacturing will be carried out. In order to be able to value this approach, a comparison will be made with an existing case; the freeform gridshell roof of Złote Tarasy in Warsaw, Poland, see Figure 30.

Since the structural engineering for the gridshell of Złote Tarasy was done by Arup, structural calculations, geometry of the gridshell and information concerning the joints were available. Although Arup had designed multiple gridshells, the case of Złote Tarasy was selected as the available information offered a good starting point for the design of the joints elaborated in chapter 3.

2.5.1   DESIGN OF GRIDSHELL – ATRIUM ROOF

The concept of the atrium roof was to form a symbiosis between nature and technology. The undulating form was developed by draping a virtual cloth over eleven spheres. The roof, consisting of a triangulated mesh of steel rectangular hollow sections (RHS), is supported by a large end beam and intermediate branching tree columns. The roof in combination with the tree columns represent a forest canopy. Figure 31, Figure 32 and Figure 33 are giving an impression of the design.

The undulating roof, with a total weight of 1400 tons and a weight of 130 kg/m², has an elliptical plan of 116m long and 100m wide. Design and engineering of the complex shape of the roof was made possible by increased power of computer-aided analysis. The structural calculations were performed by the structural software of Oasys GSA. Due to the complex roof shape, the structure consisted of unique structural elements and façade panels. Advanced computer-controlled manufacturing made it possible to produce all the 2300 nodes, 7123 RHS members and 4788 glass panels with a unique geometry [33].
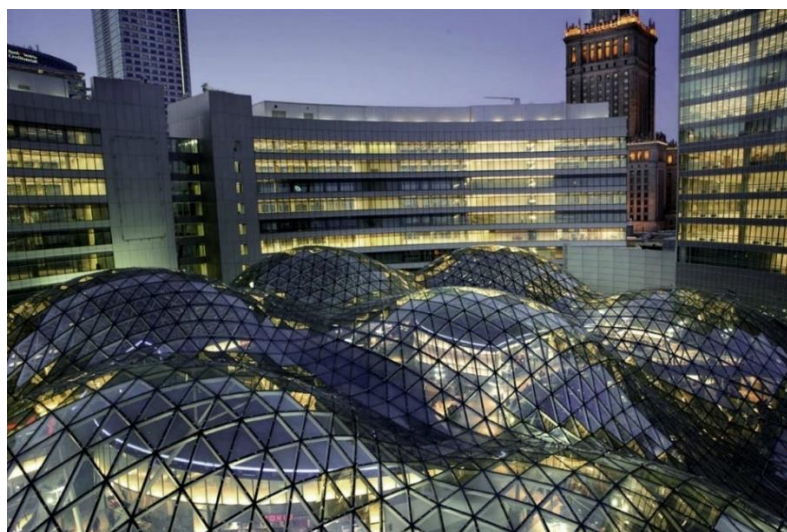

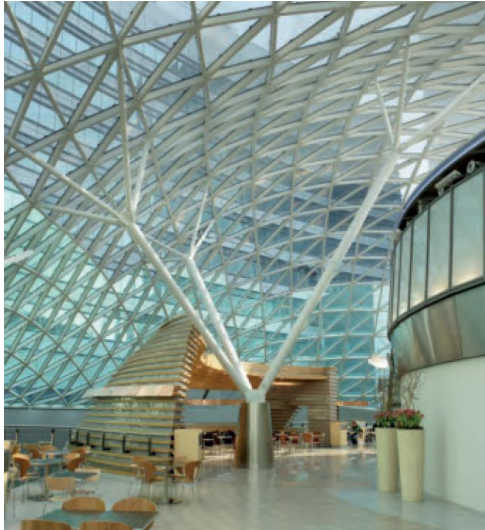*Figure 30: Złote Tarasy. © 2012 Waagner-Biro AG*

Figure 31: Interior view: tree column support [33].

Figure 32: Interior view: roof-like forest canopy [33].

Figure 33: Exterior view of the undulating roof [34].

2.5.2 JOINTS IN ATRIUM ROOF

Joint design

The design of the joints was extremely complicated due to several factors. An imported point was the freeform undulating shape of the roof. As it switches between convex and concave areas, it introduces a high degree of twist of the RHS members in respect to their neighbours connected to the same joint.

Moreover, due to local insufficient curvature it was impossible to develop a pure membrane field that could efficiently transfer the forces to the foundation by axial forces. Therefore, in parts of the mesh the joints were required to be able to resist large bending moments.

Also the deflection of the roof due to its self-weight had to be taken into account. After depropping the construction it would deform in its final position. By raising all the joints by the predicted deflection a new 'zero geometry' was obtained. After removing the scaffolding the roof would achieve the original geometry.

The result of the above mentioned aspects is a large set of nodes with complex 3-dimensional unique shapes which had to be manufactured.

In order to develop an economic joint, contractors got involved early in the design process. Both an option for a welded as a bolted connection were developed, which finally resulted in the design of the joint specified in the next paragraph.

Specifications

The final design consisted of a star shape metal joint (Figure 34) connecting six RHS members. The welded connection was preferred over the bolted connection as it resulted in a more 'invisible' connection, which was desired by the architect, see Figure 35. The six arms of the star bisect the angle between two adjacent members. By fully welding the RHS members to the joint a continuous structure is obtained. Although the gridshell is rigid enough to withstand the load, it is sufficiently flexible to allow thermal movements.

Five different principle node types with similar features, see Table 3, are applied in the gridshell structure of Złote Tarasy. The steel strength used for the joints is either S355 or S460, depending on the desired strength of the joint. The higher type joints are applied in the most heavy loaded areas of the roof. Also, the thickness of the lever arm and the radius at the root determine the strength of the joint. The lever arm thickness t and the radius R are indicated in Figure 36.

Table 3: Specifications of different node types.

Node type	Material	Lever arm thickness t (mm)	Radius at root R (mm)	Weight (kg)
1	S355	20	15	40
2	S355	30	15	60
3	S460	30	15	60
4	S460	30	30	65
5	S460	30	40	70

Mock-up

During the design process, mock-up joints were manufactured to check the visual appearance and additional production difficulties. While producing the mock-ups it became clear that it was difficult to weld the joints as angles between adjacent RHS members were rather small. Next to this, the inspection of the applied welds was limited or ineffective because of the same reason.

Problems such as porosity, lack of penetration, lack of fusion and cracking had to be overcome in the welding procedure. Incorrect use of welding consumables, failure to preheat prior to welding and additional problems of overhead welding were encountered. Approved welding procedures, qualified welders and supervision was of great importance in order to achieve the structural required standards.
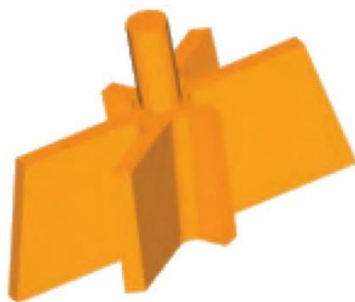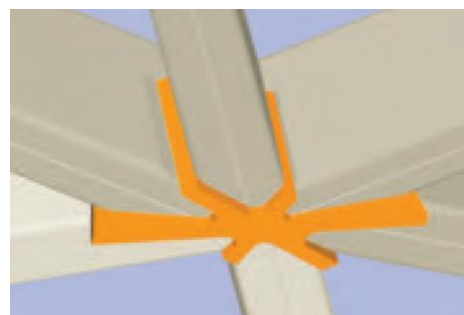

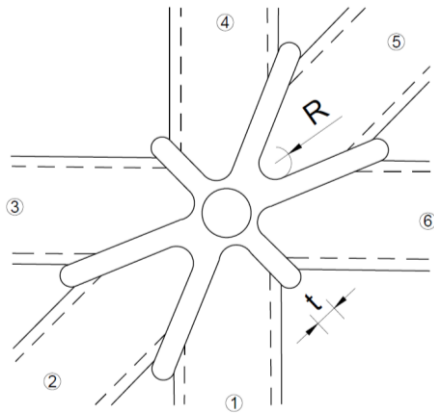*Figure 34: Metal star-shaped joint* [33].   *Figure 35: Six RHS members connected to the joint* [33].

Figure 36: Joint with lever arm thickness t and radius at the root R.

Figure 37: Mock-up of the joint. ©Arup

Manufacturing of the joint

The complex freeform geometry of the gridshell structure led to the fact that all the joints consisted of a unique shape. Therefore, digital fabrication was the only possibility to effectively produce joints with non-repeating angles and shapes as the amount of time for unique cuts is similar to repeated cuts.

Cutting machines were fed directly by data from a digital model, containing all the elements of the roof. As the joints were three dimensional objects, the cutting machinery had to be adjusted to be able to cut in three dimensions. A welding robot, which could work in three dimensions, was rebuilt to cut the steel. By using the digital input, human error was excluded as the steel elements were produced with a tolerance of less than one millimeter. This requirement made installation at later stages more easy.

2.6 CONCLUSION

This section provides answers to the following subquestions:

2.1   What is a gridshell structure and what are its structural principles?

2.2   What are the design requirements for joints in gridshell structures?

2.3   What is topology optimization and how can it be applied to design lightweight metal joints of a gridshell structure?

2.4   What is additive manufacturing and what are the advantages compared to traditional design and production techniques?

Gridshells

A gridshell is a lightweight structure consisting of straight members connected by joints. Gridshells perfectly showcase the lightness of the structure and are preferred over plain shells when daylight sources are preferred. The structure can be made of any kind of material, e.g., steel, aluminium, wood or even cardboard tubes.

A gridshell commonly contains the shape and strength of a double-curvature shell. Different kind of surfaces can influence the behaviour of gridshells. Because of the curvature, out-of-plane loads can be transferred to the supports by in-plane forces. This is possible by the membrane behaviour of the structure. Membrane behaviour can only develop in gridshells which are rigid enough to transfer in-plane shear forces. If shear stiffness is lacking, the gridshell will function as a system of combined arches instead of a shell. The preferred lay-out is a grid built of triangles.

As the out-of-plane stiffness of a gridshell is small compared to its axial stiffness, bending moments in the grid should as much as possible be avoided in order to reduce deformations. Factors affecting the gridshells structural behaviour are the overall shape of the gridshell, the lay-out and the width of the mesh, the cross-section of the members and the type of joints.

Concluding, a well-designed gridshell has sufficient curvature and in-plane rigidity in order to make full use of the membrane behaviour. Moreover, edge and other disturbances of the membrane field are avoided and different modes of instability are taken into account.

Joints

Joints play an important role in the structural behaviour of gridshell structures. The joints contribute to the structural behaviour and inadequately designed joints could lead to failure of the structure.

Both in-plane as out-of-plane requirements need to be met. Except for triangular grids, the joints (or additional measures such as transverse cables) need to be able to transfer in-plane shear forces to develop membrane behaviour. Moreover, the joints influence the out-of-plane behaviour. With regard to global and local stability semi-rigid or rigid classified joints need to be applied to create a stable structure. The class of the joint can be determined by carrying out

the classification system as presented in subsection 2.2.2. This system will be used to set up design criteria in subsection 3.1.5 for the topology optimized joints.

Additional requirements can be considered next to the requirements with respect to the structural behaviour. First of all, the joints should be able to make rapid erection possible. Studying the three described examples in subsection 2.2.3, bolted connections speed up the erection speed, however ladders prefabricated in the shop could also lead to a rapid erection process. Moreover, high accuracy of the geometry of the joints allows for quick erection because deviations are almost reduced to zero. Of course, costs and aesthetical appearance of the joint should be taken into account. The same holds for the production of the joints as this process is often complex due to the unique shapes of the joints.

Topology optimization

Topology optimization carries out a study on the topology of a structure in order to find the best possible lay-out of that structure. The optimization needs a given domain and predefined loads and boundary conditions. There are several developed methods to carry out topology optimization processes.

Topology optimization can be used for the preliminary design of joints. While applying a volume constraint as optimization criterion, the stiffness function can be maximised. The optimization will result in a light-weight joint that is as stiff as possible in order to resist the predetermined loads.

Additive manufacturing

AM offers new opportunities to designers who deal with manufacturing constraints. Taking the opportunities into account it is possible to tackle several difficulties in the production of joints of freeform gridshells as well.

Challenges faced are the production of unique joints, the corresponding high labour intensity when parts need to be cut and welded together with a high ratio of accuracy and the amount of waste material. Moreover, it is likely that organic results of topology optimization are impossible to produce by traditional manufacturing methods.

The opportunities AM is offering suit well with the posed challenges. Since AM offers the opportunity for mass-customisation, unique joints can be produced to the same unit costs. Also, the offered design freedom makes it possible to manufacture complex (internal) shapes. Moreover, preparations for the connection between joint and beam can be prevented when they are printed directly to the joint. This prevents costly and labour-intensive activities. Finally, topology optimized joints require less material and production by AM causes very little waste material.

Taking above into account, AM seems an efficient way to produce unique metal joints with a complex geometry.

3

JOINT DESIGN

"Everything is theoretically impossible, until it is done."

Robert A. Heinlein

This chapter describes the joint design process of the Złote Tarasy gridshell. Topology optimization (TO) and additive manufacturing (AM) for the design and production of the joints respectively. The process to design the joints, schematically depicted in Figure 38, is divided into three main parts:

- Shape development of the joint;
- Detailing of the joint;
- Preparation for production.

The following three sub-questions will be answered associated with the three main design parts:

3.1 What are the topology optimized shapes of representative structural joints?

3.2 What is the best option to connect the joints to the beams?

3.3 Which steps need to be taken to prepare the joint for AM production?
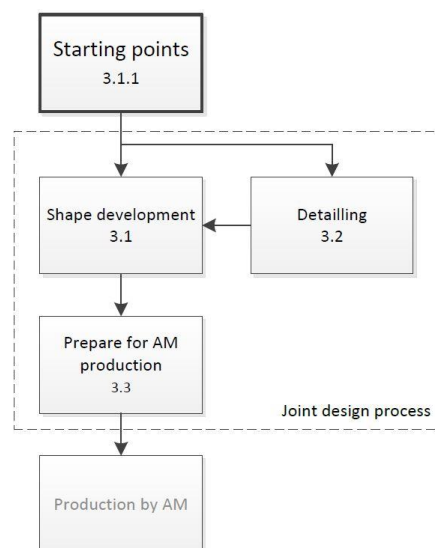
Figure 38: Joint design process.

Whereas it is not feasible to design 2300 joints, not all joints will be designed. In order to take different loading conditions into account, the gridshell is divided into three typical zones with similar loading conditions, see Figure 39. A representative joint, called *joint type*, in each zone is selected and optimized. The representative joints are highlighted in Figure 39 by the green circles and Table 4 indicates the number of joints in each typical zone. The loading conditions for the three joint types are:

- Type 1: joints located very close to end and intermediate supports: the membrane field is highly disturbed.
- Type 2: joints near end and intermediate supports or insufficient curvature of the gridshell: the membrane field is mediumly disturbed.
- Type 3: joints located in a pure membrane field: the gridshell follows perfect shell.

Note: the division of the zones of the gridshell is made by a visual inspection of the FEA model.

Table 4: Different types of representative joints.

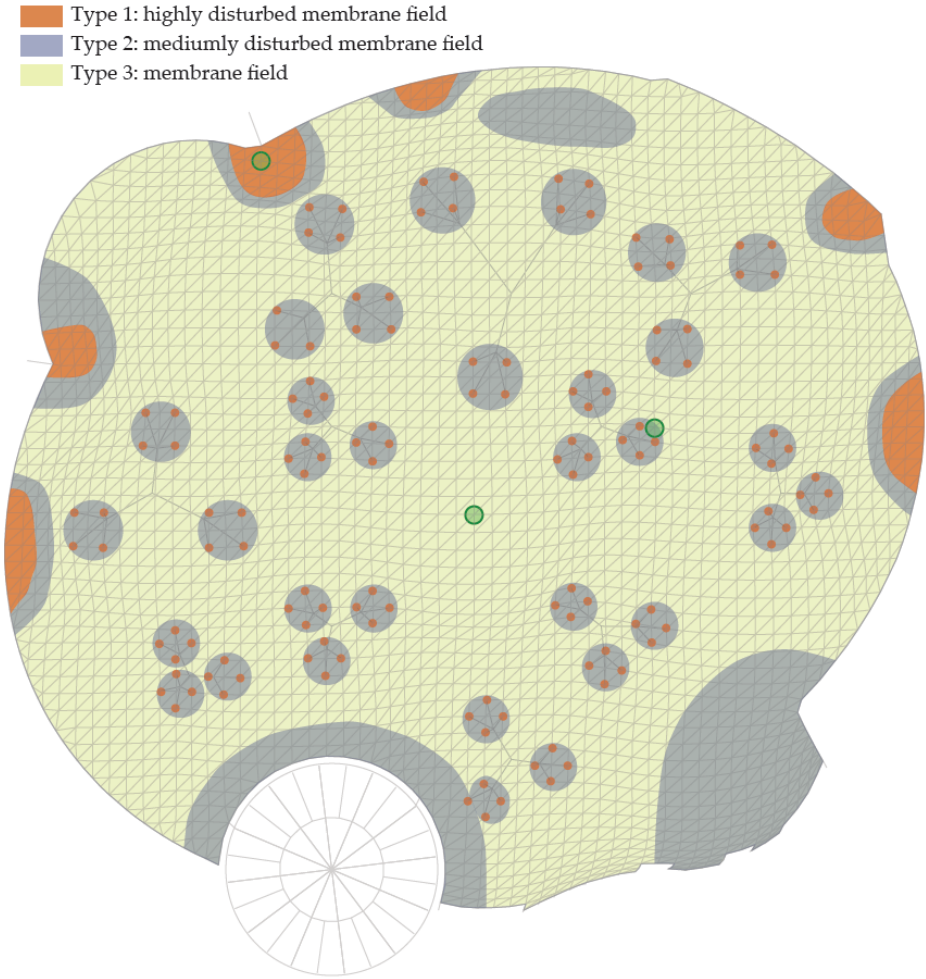| Type	Typical zone	Axial forces	Moments	Number
1	Highly disturbed membrane field	Medium/High	High	200
2	Mediumly disturbed membrane field	Low/Medium	Medium	300
3	Pure (non-disturbed) membrane field	Low/Medium	Low	1800

Figure 39: Overview typical zones of representative joint classification. The representative joints are highlighted with a green circle.

3.1 SHAPE DEVELOPMENT

This section focusses on the shape development of the joints by the application of TO. The followed process contains several steps, each influencing the final results, see Figure 40.

The first step consists of setting-up the geometry of the joint model in the 3D modelling environment of Rhinoceros by using the 3D wireframe model of the gridshell. This is directly influenced by the pre-defined starting points. In the second step, properties are assigned to the joint model in the finite element environment of Abaqus. The third step contains both entering the input settings for the TO in BESO3D, as well as the optimization run itself. In the last step, the obtained results are analysed and checked with predefined design criteria. When results are satisfying, the TO shape can proceed to be prepared for AM production.

The process is iteratively carried out. The following sections discuss the results of each individual step.
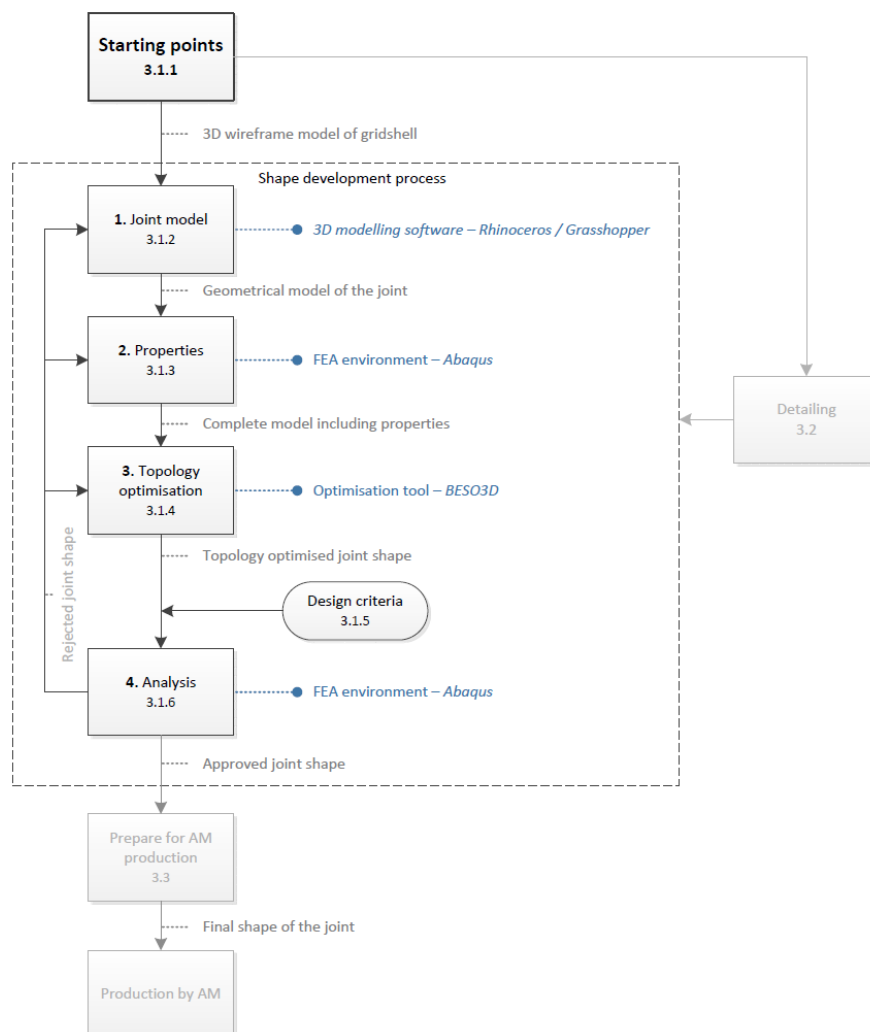
Figure 40: Shape development process: the steps of the analysis are shown together with the used programs and intermediate products.

3.1.1 STARTING POINTS

The shape development process is carried out by considering multiple starting points. Several assumptions are made in order to define a feasible scope for the research. The starting points and assumptions are explained below.

1. Weight reduction
The main goal is to minimise the weight of the joint while being able to perform its structural function.

2. Original 3D geometry
The joint has to fit the original 3D geometry of the Złote Tarasy gridshell. Therefore it is necessary to use the 3D wireframe model of the gridshell.

3. Loads
Four load cases, corresponding to the load cases used in the design of the gridshell, will be taken into account during the topology optimization of the joint. The following load cases in the ultimate limit state (ULS) will be taken into account:

1. $1,4DL + 1,6LL$
2. $1,4DL + 1,6LL + 1,6SL$
3. $1,4DL + 1,6LL + 1,2Tpos$
4. $1,4DL + 1,4WL$

With DL the dead load, LL the live load, SL the uniform snow load, $Tpos$ the extreme thermal expansion, and WL the maximum upward wind load.

4. Introduction of applied forces
The applied forces on the joints need to be introduced corresponding to the real situation. Since the loads are introduced by the RHS members, parts of these members need to be modelled as well.

5. Joint-beam connection
The type and geometry of the connection between the joints and the beams should allow for proper and rapid installation on site. When possible, complex and labour intensive work should be avoided on site in order to increase the quality of the work.

6. Production
The production will take place by the AM technique Direct Metal Laser Sintering (DMLS), see appendix C.1. The production restrictions by AM need to be taken into account (see subsection 2.4.2), especially:

- Production costs: (i) material costs are high and (ii) since building rates (volume of build material per h) are rather small, large building volumes are very costly;
- Maximum part size: volume of the building chamber equals 400x400x400 mm.

7. Material

The material *EOS Stainless Steel GP1* is selected to be applied for the joints. The material data sheet of the material is included in appendix C.3. The following considerations are decisive to select the material:

- High yield strength;
- High E-modulus;
- Ductile material;
- Weldable material;
- Corrosion resistant material.

8. Aesthetics

The fluent shape of the joint needs to be visible if desired. Opening up the shape of the joint would perfectly showcase new possibilities offered by the application of AM. This might add extra value to a building by applying innovative design, engineering and production methods.

3.1.2 JOINT MODEL

Joint models for the three representative joints (Figure 39) are developed by taking the starting points into account. The models consist of a *design domain* and the *adjacent beams*. The design domain will be optimized on topology. The adjacent beams will be used to introduce the loads on the joint.

By using the starting points, two types of models are developed:

1. Hybrid joint solution using partially bolts and partially welds (Figure 43), from now on called *bolted joint*;
2. *Welded joint (*Figure 44*).*

The main difference between the two types is the way of connecting the joints to the beams: welds vs bolts. This has mainly been influenced by the erection scheme. To be able to rapidly erect the structure, large parts (ladders) will be welded together in the shop. The beams between the ladders will be connected by bolts. The erection method is illustrated in subsection 3.2.1. More information on the detailing of the joint is given in section 0.

Design domain

Geometry

The 3D geometry of the gridshell is used to obtain the correct approaching angles of the adjacent beams (Figure 41). Moreover, the geometry of the design domain is developed by considering the advantage of integrating functions in the part that will be produced by additive manufacturing; the joint. Therefore preparation work for the connections is as much as possible integrated in the shape of the design domain, such as:

- The bolted joint contains the required space to apply the bolts during erection (vertical holes cut out of the design domain);
- The welded joint contains the required grooves for the welding process;
- For both joint types: the interfaces of the design domain are orientated perpendicular to the orientation of the beams. Hence, all the beams can be cut straight.
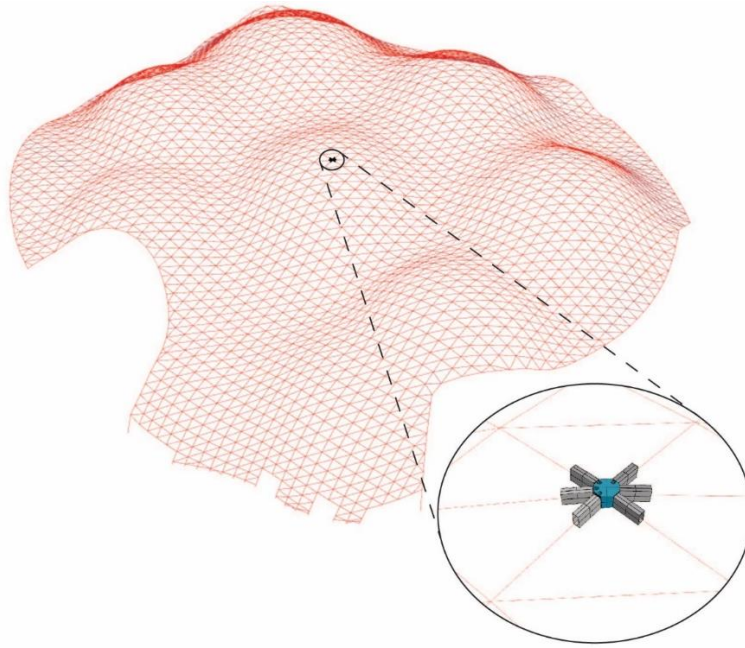
Figure 41: 3D geometry of the gridshell is used to find the correct approaching angles of adjacent beams.

Dimensions

The dimensions of the design domain for both types were defined by taking the following considerations into account:

- *Costs of production*: large fabrication volumes are expensive, therefore it is favourable to design a joint that is as small as possible. Hence a small design domain is favourable;
- *Weight reduction*: in almost all cases topology optimization leads to reduction in weight. From this perspective it is favourable to apply a large design domain is favourable;
- *Connection*: the design domain should be large enough to include the required space for the application of the welds and the bolts.

In consideration of the mentioned arguments, the applied dimensions of the design domain are shown in Figure 42 (blue: design domain). The dimensions offer the possibility to apply proper welds and enough space to apply the bolts. Moreover, the dimensions provide the challenge to obtain a satisfying weight reduction. Dependent on the amount of removed material, the costs of the joint will be determined.

Generative modelling

The geometry of the joints is defined with Computer Aided Design (CAD) software of Rhinoceros [35]. In order to generate different joint models that are all slightly different due to the different angles of the adjacent beams, a generative algorithm was defined in Grasshopper [36]. By setting up the joint model in a parametric way, the geometry of the joint could be adjusted to its desired shape by changing a set of input parameters. The input parameters are illustrated in Figure 45. The 3D geometry of the gridshell was selected by selecting the central point of the joint (the point of intersection of the center lines of the beams) and the other ends of the beams in the wireframe model (Figure 46).
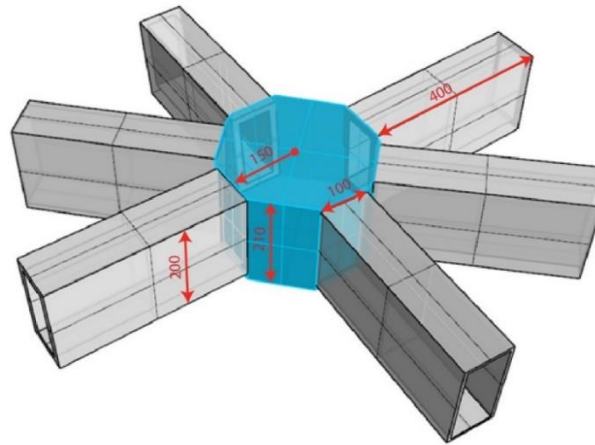
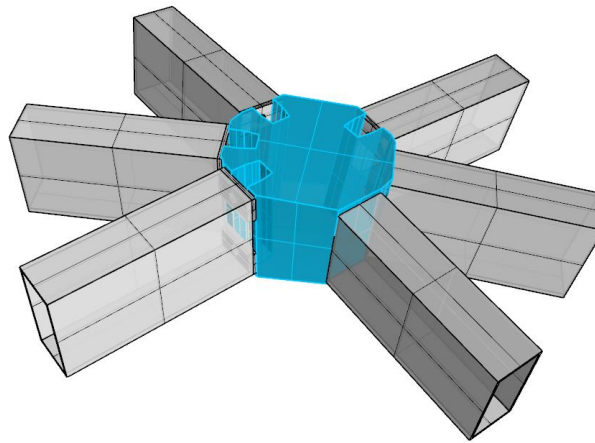*Figure 42: Dimensions of the joint model. (Blue: design domain)*

Figure 43: Type 1: Bolted joint, the required space in order to tighten the bolts by a torque wrench is cut out of the design domain. (Blue: design domain)
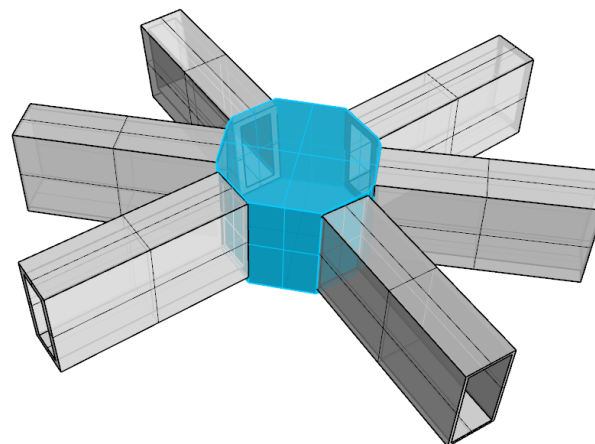

Figure 44: Type 2: Welded joint, because of the applied welds the design domain can remain as a solid block. (Blue: design domain)
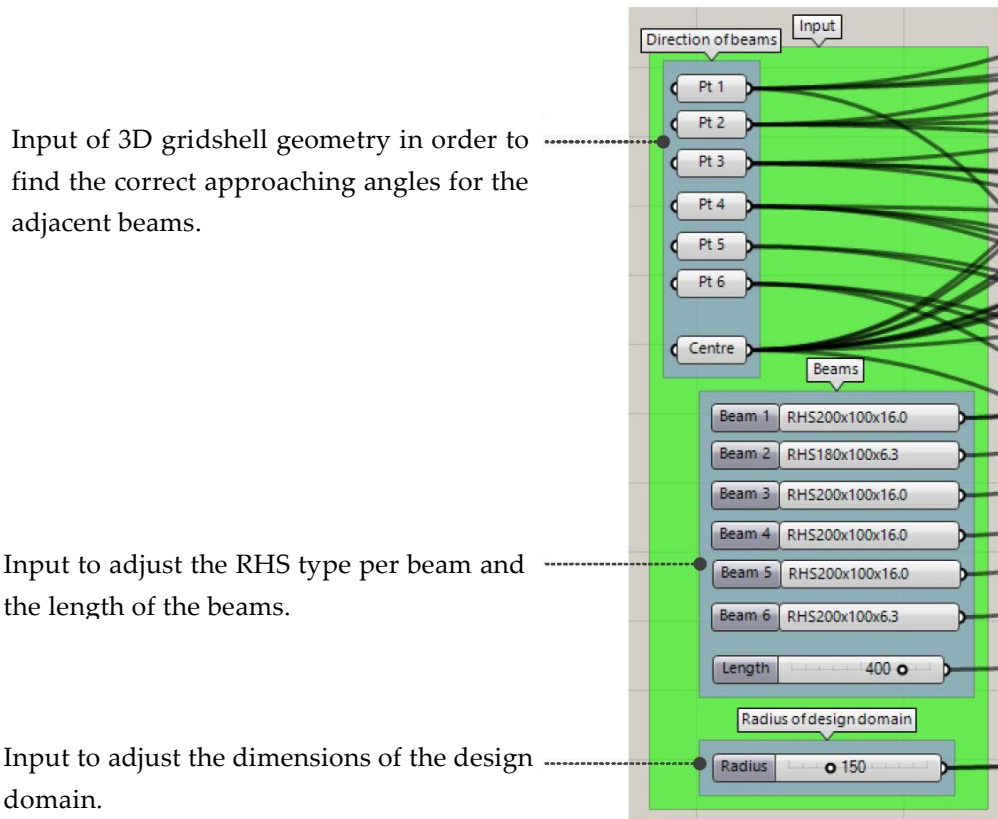
Input of 3D gridshell geometry in order to find the correct approaching angles for the adjacent beams.

Input to adjust the RHS type per beam and the length of the beams.

Input to adjust the dimensions of the design domain.

Figure 45: Input settings to vary the geometry of the joint model.
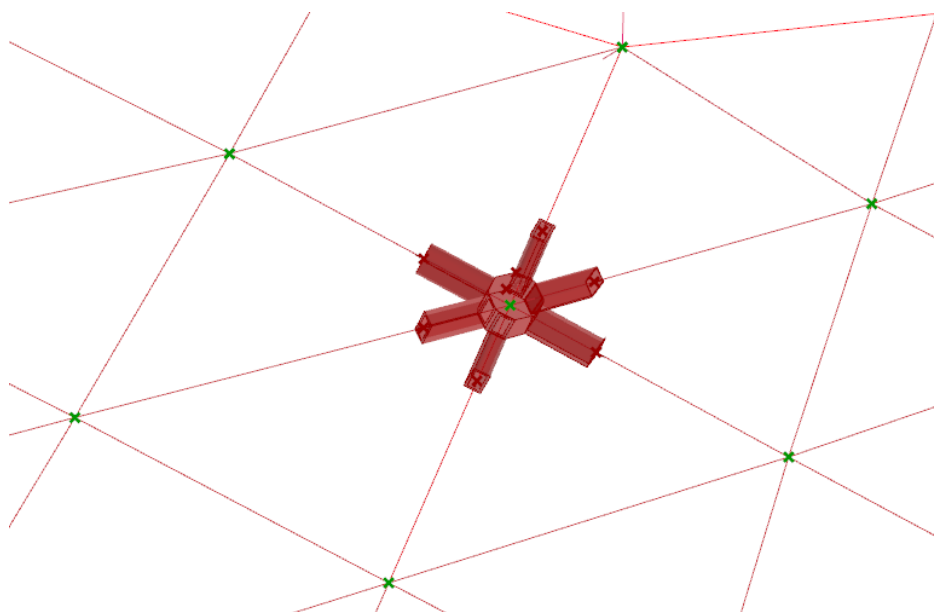
Figure 46: Selection of the central point and the ends of the beams to set up the geometry of the joint model.

Adjacent beams

The adjacent RHS beams in the joint model corresponded to the original applied RHS beams in the Złote Tarasy gridshell. Table 5 lists the applied RHS profiles with associated steel grade for each joint. The beams are numbered clock-wise as depicted in Figure 47.

Note: the numbers correspond to the applied loads in section 3.1.4 – Loads.

Table 5: The adjacent RHS profiles connected to the joint.

#	Joint 1 RHS profile	Joint 1 Steel grade	Joint 2 RHS profile	Joint 2 Steel grade	Joint 3 RHS profile	Joint 3 Steel grade
1	200x100x16	S455	200x100x8.0	S355	200x100x5.0	S355
2	200x100x6.3	S355	200x100x8.0	S355	200x100x5.0	S355
3	200x100x16	S455	200x100x8.0	S355	200x100x5.0	S355
4	200x100x16	S455	200x100x5.0	S355	200x100x5.0	S355
5	200x100x16	S455	200x100x5.0	S355	200x100x5.0	S355
6	200x100x6.3	S355	200x100x8.0	S355	200x100x5.0	S355

For all the model types, the loads are applied to the adjacent beams. In order to obtain a natural spreading of stresses over the cross-section of the beam, the beams need to have a sufficient length. As a reasonable length, two times the height of the beams is used. This implied that the length of the beams had to be 400 mm.

Introduction of the loads

The loads on the joint model are introduced at the ends that were not connected to the joint. They were directed in a local coordinate systems that correspond to the local coordinate systems of the FEA model from which the loads are extracted (see Figure 49). The model was calculated in the FEA program Oasys GSA [37]. Each beam was loaded by an axial force in x-direction, two shear forces in y- and z-direction, two bending moments around the y- and z-axis, and a torsion moment around the x-axis. The actual loads on the joints are given in section 3.1.4.
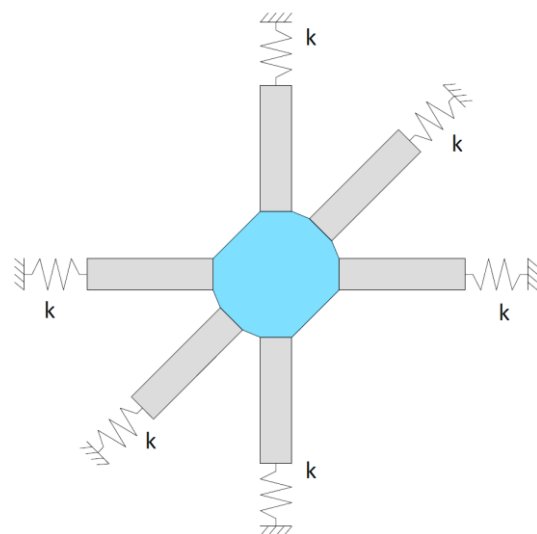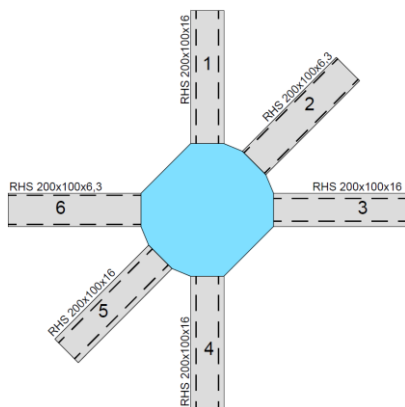

Figure 47: Number indication of the RHS-member (example given for joint 1).

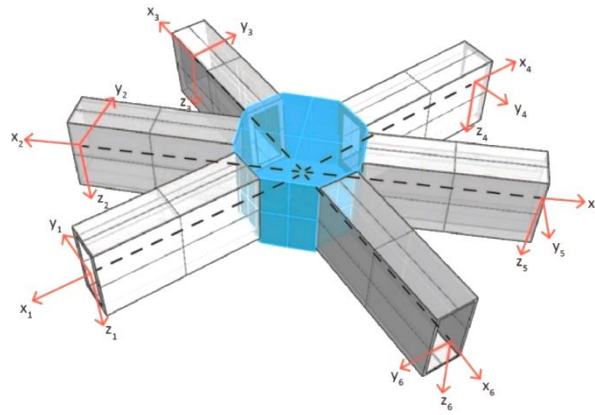Figure 48: Boundary conditions of the joint model.

Figure 49: Local coordinate systems located at the non-connecting ends of the beams.

Boundary conditions

Although the loads on the joint make equilibrium, FEA programs needs boundary conditions to obtain a solution. In case of a rigid boundary conditions, undesired forces and deformations will occur. Therefore, springs with low stiffness k are attached to the ends of the RHS beams (Figure 48). In this way, minimal disturbance will be encountered by the applied boundary conditions.

3.1.3   PROPERTIES

After setting up the geometry of the joint model, properties are assigned to the joint models in the same FEA environment. The FEA program Abaqus is used in this study [38]. The settings presented below are applied to define the properties of the joint models.

Material

Three different materials are assigned to different parts of the joint models. The design domains for all the joint models consist of the material *EOS Stainless steel GP1.* For extensive information on this material, see appendix C.3. The adjacent beams to the design domain consisted of either *S355* or *S435*, according to the real properties of the beams.

For additional data of the beams, reference is made to appendix E.1. The applied material settings are:

- Design domain: *EOS Stainless steel GP1*
  - E-modulus: $1,8E5$ N/mm²
  - Poisson ratio: 0,3
  - Yield strength: 530 N/mm²
- RHS members (S355):   *Steel S355*
  - E-modulus: $2,1E5$ N/mm²
  - Poisson ratio: 0,3
  - Yield strength: 355 N/mm²
- RHS members (S435):   *Steel S435*
  - E-modulus: $2,1E5$ N/mm²
  - Poisson ratio: 0,3
  - Yield strength: 435 N/mm²

Mesh data

The applied mesh (the representation of the finite elements) is almost similar for each of the three joint models. During the optimization run the following mesh elements is used: *linear hexahedron elements*, 8-node linear brick: *C3D8R.* These mesh elements consists of a *solid homogeneous section*. This followed from the fact that the used TO tool only accepts linear solid elements. In order to divide the design domain into a structured mesh, the *sweep* method is applied. The mesh width and the number of elements applied is:

- Design domain;
    - Mesh width: 4,0 mm;
    - Number of elements: ± 250.000;
- RHS members;
    - Mesh width: Equal to wall thickness of the member in mm (in case of RHS200x100x16: mesh width of 8,0 mm);
    - Number of elements: ± 500-1000.

3.1.4 TOPOLOGY OPTIMIZATION

The topology optimization (TO) of the three joints is carried out by BESO3D [39].

BESO3D

BESO3D is a standalone program that can solve 3D topology optimization problems. It applies the Bi-directional Evolutionary Structural Optimization (BESO) method (subsection 2.3.2). Within a certain domain, BESO3D develops the optimal material lay-out in order to maximise the stiffness of the structure with a reduced amount of material. In other words, a structure is developed that deflects as little as possible by the predefined loads and takes predefined boundary conditions into account.

BESO3D is controlled by the users input. Two types of input parameters can be distinguished (Figure 50):

- Parameter input for the optimized parts (*Part parameters*);
- Parameters to control the optimization run (*Overall control*).

Part parameters

The input for the part parameters is divided into four sections.

In the first section, the user defines the optimization problem. Either the volume fraction is reduced to a certain percentage while the mean compliance is minimised (stiffness maximised), or the volume of the initial domain is minimised while satisfying the predefined mean compliance.

The second section contains the input for the parameters concerning the evolutionary steps in the optimization process. The evolutionary ratio and the admission ratio determine the amount of elements that are removed and added respectively during the steps of the optimization. The filter radius determines to which extent mesh elements take neighbouring elements into account. By increasing the filter radius, stress values will be smoothed and slender structures

can be prevented by applying a proper filter radius. More information and an example concerning the filter radius is included in appendix D.3.

In the third section the user can make use of symmetry properties. This can reduce the size of the problem. Using symmetry, less mesh elements are applied resulting in a reduction of the computational time.

Finally, in the fourth section the user defines whether the problem needs to be topology or shape optimized.

Overall control

The overall control parameters include two sections. The first section controls the termination of the optimization run. Either the solution has converged with a given tolerance or a maximum amount of iterations has been reached.

The second section offers the possibility to apply multiple load cases during the optimization run. The first input parameter implies the number of applied load cases and the second input contains the weight of each load case during the analysis. Appendix D.2, provides more information about the possible application of multiple load cases.

Analysis type

The topology optimization is performed by using a linear analysis (*linear perturbation*). Non-linearity of the material and the geometry were not taken into account during the optimization runs. This was not possible as the computational time would explode (to be estimated to 300 days).
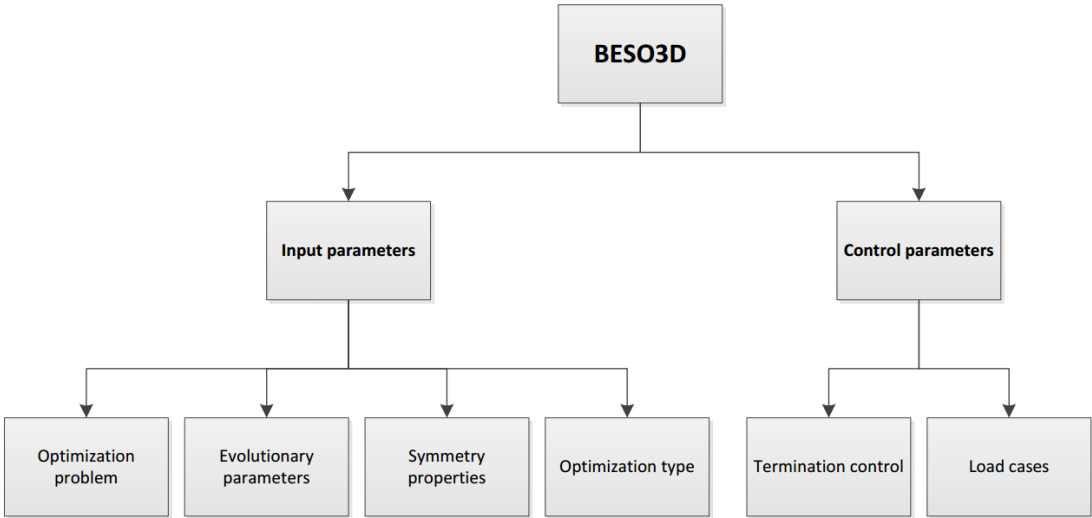
Figure 50: Input and control parameters of BESO3D.

Getting to know BESO3D

When a topology optimization tool is used to design structural parts for buildings the applied design (optimization) tool must be checked if the program does what is expected. BESO3D was tested by means of elementary optimization problems.

Simple optimization problems

For this test a simplified version of a joint was used: two beams are connected by a joint (Figure 51). The joint model consisted of three parts; the design domain and two non-design domains. Both non-design domains consisted of RHS200x100x16 members with a length of 400 mm. While the left RHS member was fully constraint at the left-hand side, the right RHS member introduced the load to the system. The design domain consisted of a solid cross-section of 200x100 mm and is 400 mm in length.

Optimization runs were carried out for the six different loads on the joint, i.e., an axial force, two shear forces in the direction of the strong and weak axis, a torsional moment and two moments around the strong and weak axis of the member.

Appendix D.1.1, includes all the different possible loads on the joint and more information about the complete test. For illustration purposes the example of a moment around the strong axis y-axis will be discussed, see Figure 52.

Result

The topology optimized result of the posed problem is shown in Figure 53 (the RHS members at the left- and right-hand side are not depicted). The material is situated in such a way that the moment of inertia is maximised. The largest deformations occur in the top and bottom fibres of the structure when applying a bending moment. Therefore, in order to minimise the deformation of the structure, material is placed at the other zones of the design domain by the optimization tool.

Conclusion

The results obtained for the simplified optimization problems are plausible and the shapes developed as expected. By means of these tests it is concluded that BESO3D acts as expected and could be used for design purposes in this thesis. Moreover, in appendix D.2, the application of multiple load cases during an optimization run is checked.
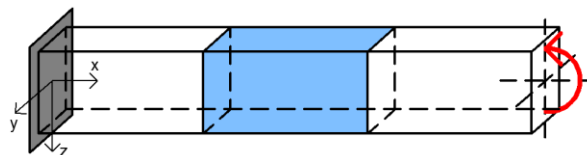

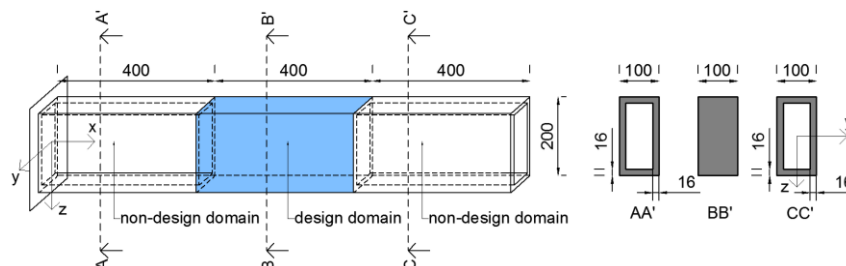*Figure 51: Moment around the strong y-axis of the member.*

Figure 52: Geometry of the test model.

Loads

The load cases that were taken into account during the optimization run are given in subsection 3.1.1. These load cases were applied in order to simulate the different behaviour of the gridshell under varying loading conditions. In this way the joint would be optimized by taken varying circumstances into account. The entire sets of loads on the three representative joints are presented in Table 6, Table 7 and Table 8.

The loads on the joint model were extracted from an available FEA model of the gridshell in Oasys GSA [37]. As the loads were introduced to the joint model at the ends of the adjacent beams (see Figure 42), the loads in each beam at 550 mm from the centre of the joint had to be extracted from the FEA model. An illustration of the described load extraction is given in Figure 56.

Simple stress check

In order to quickly check the results of the optimization for a moment around the strong y-axis of the member, the optimized joint in Figure 53 is loaded by a moment around the y-axis of $25\ kNm$. Taking the cross-section of the joint (Figure 54) into account, the section modulus can be derived:

$$W = \frac{h \cdot b^2}{6} = \frac{100 \cdot 200^2}{6} - \frac{100 \cdot 140^2}{6} = 3{,}4 \cdot 10^5\ mm^3$$

Which yields for the stresses in the other fibres:

$$\sigma = \frac{M}{W} = \frac{25 \cdot 10^6}{3{,}4 \cdot 10^5} = 73\ N/mm^2$$

Satisfactorily, the result of the stress calculation corresponds to the Von Mises stresses derived by Abaqus as presented in Figure 55.
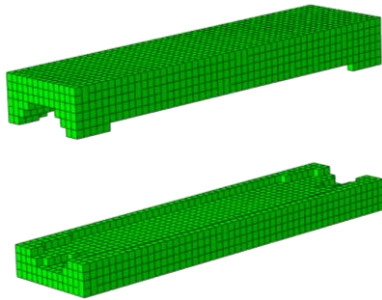

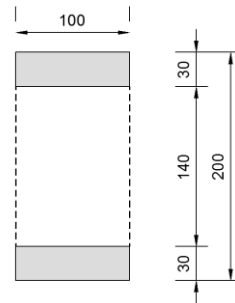Figure 53: Optimized result for a moment around the strong y-axis of the member.

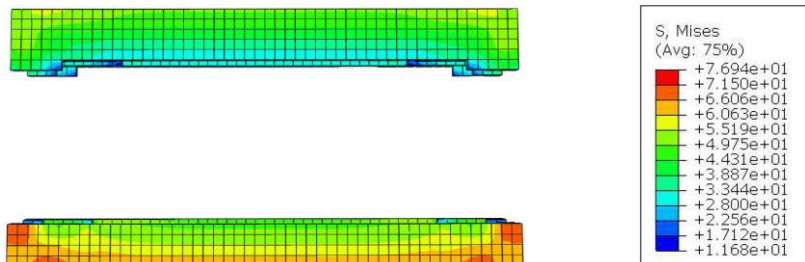Figure 54: Cross-section of optimized joint for a moment around the strong y-axis.

Figure 55: Von Mises stresses (N/mm²) in the optimized joint for a moment (25 kNm) around the strong y-axis.
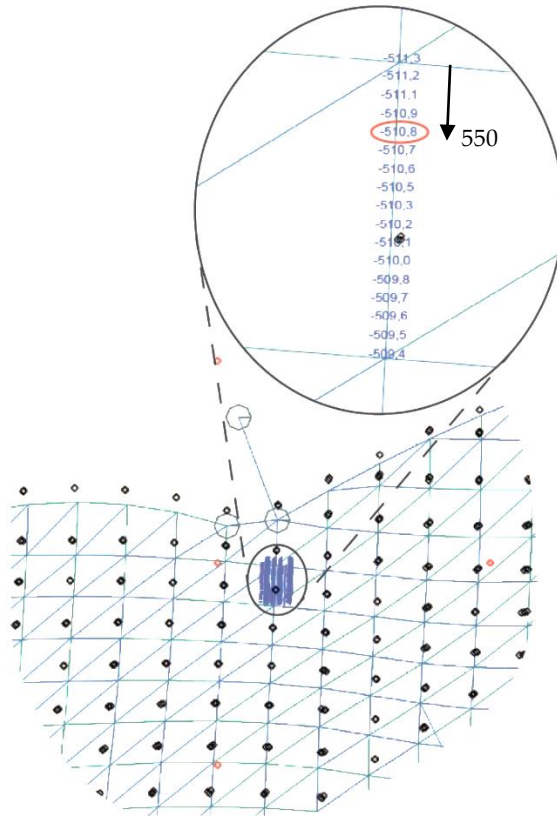
Figure 56: Extracting the loads from the Oasys GSA model.

Table 6: Applied forces on joint type 1.

Load case	Member number	Axial F_x (kN)	Shear F_y (kN)	Shear F_z (kN)	Torsion M_{xx} (kNm)	Moment M_{yy} (kNm)	Moment M_{zz} (kNm)
	1	-510,80	0,45	-2,99	4,60	19,25	-0,47
	2	-160,70	0,71	4,18	0,57	1,87	0,57
	3	355,90	1,29	-9,93	-1,56	8,73	0,71
1	4	-897,70	-0,09	-30,86	2,53	5,20	-0,18
	5	349,90	0,04	4,88	-2,38	-4,63	0,36
	6	-7,68	-2,05	0,93	-3,01	10,75	0,94
	1	-1063,00	2,22	-4,20	7,25	30,77	-1,37
	2	-158,30	1,02	6,44	0,15	5,27	0,99
	3	680,10	0,21	-15,49	-3,72	27,65	0,53
2	4	-1943,00	1,73	-42,29	5,98	6,19	0,49
	5	1013,00	0,31	12,88	-6,13	-0,29	0,87
	6	-153,60	-4,99	7,57	-4,32	22,90	2,49
	1	-788,70	0,60	-4,69	7,08	29,03	-0,67
	2	-257,90	1,14	6,52	0,83	2,77	0,89
	3	562,40	2,02	-15,33	-2,37	13,51	1,17
3	4	-1390,00	-0,22	-47,66	3,88	7,34	-0,32
	5	536,20	0,17	7,67	-3,80	-7,55	0,56
	6	-3,03	-3,17	1,33	-4,63	16,65	1,44
	1	-345,20	0,33	-1,33	2,88	12,47	-0,29
	2	-100,30	0,59	2,32	0,29	1,57	0,37
	3	234,60	0,91	-6,47	-1,05	6,78	0,42
4	4	-616,60	0,10	-18,29	1,66	3,85	-0,05
	5	256,30	-0,16	3,39	-1,50	-1,77	0,27
	6	-19,15	-1,55	1,37	-1,85	7,33	0,67

Table 7: Applied forces on joint type 2.

Load case	Member number	Axial F_x (kN)	Shear F_y (kN)	Shear F_z (kN)	Torsion M_{xx} (kNm)	Moment M_{yy} (kNm)	Moment M_{zz} (kNm)
	1	72,69	0,46	-0,50	0,66	11,07	0,02
	2	-31,46	-0,16	-2,13	0,94	6,38	0,07
	3	-54,83	0,92	6,48	0,40	6,60	-0,44
1	4	93,95	-0,52	4,94	-0,71	2,20	-0,11
	5	-67,87	-0,07	-3,83	-0,17	9,17	-1,08
	6	-32,95	0,26	2,65	-0,33	6,44	0,15
	1	70,76	1,02	0,18	1,01	13,42	0,23
	2	35,32	-0,21	-2,36	1,23	7,25	0,07
	3	-113,80	0,47	7,68	0,06	7,83	-0,20
2	4	89,17	0,34	5,71	-0,43	9,20	-0,01
	5	5,86	-0,07	-3,69	0,00	10,19	-0,13
	6	-97,69	-0,20	1,77	-0,66	7,80	-0,08
	1	113,80	0,10	-2,30	0,95	16,25	-0,38
	2	-57,01	-0,29	-3,23	1,56	10,39	0,09
	3	-90,40	1,53	10,32	0,77	10,00	-0,72
3	4	149,80	-0,20	6,92	-1,21	9,93	0,31
	5	-116,60	-0,12	-6,41	-0,37	14,60	-0,16
	6	-54,17	0,45	4,91	-0,44	9,95	0,27
	1	55,37	0,18	-0,10	0,51	7,79	-0,26
	2	-2,48	-0,15	-2,14	0,66	4,90	0,04
	3	-55,05	0,53	4,99	0,25	5,16	-0,23
4	4	59,62	0,23	3,06	-0,59	5,51	0,04
	5	-11,28	-0,02	-2,26	-0,13	7,46	-0,05
	6	-52,46	-0,05	2,55	-0,22	5,51	0,04

Table 8: Applied forces on joint type 3.

Load case	Member number	Axial F_x (kN)	Shear F_y (kN)	Shear F_z (kN)	Torsion M_{xx} (kNm)	Moment M_{yy} (kNm)	Moment M_{zz} (kNm)
	1	-34,13	0,24	-0,40	-0,10	-0,10	-0,11
	2	5,53	0,10	0,89	-0,10	0,41	0,00
	3	-46,53	-0,12	-0,51	0,11	0,42	0,10
1	4	-29,35	0,01	0,61	-0,09	-0,01	0,08
	5	-2,12	-0,12	-0,86	-0,56	0,41	0,02
	6	-40,83	-0,20	0,45	0,10	0,42	-0,07
	1	-53,15	0,25	-0,41	-0,13	0,03	-0,12
	2	11,18	0,12	1,05	-0,05	0,47	0,02
	3	-35,80	-0,17	-0,54	0,14	0,21	0,13
2	4	-46,18	0,13	0,62	-0,10	0,13	0,09
	5	0,40	-0,10	-0,82	0,00	0,38	0,00
	6	-28,04	-0,24	0,45	0,10	0,21	-0,09
	1	-57,46	0,37	-0,81	-0,15	-0,09	-0,16
	2	0,85	0,20	1,73	-0,16	0,66	0,00
	3	-78,02	-0,16	-1,00	0,18	0,73	0,15
3	4	-50,87	0,17	1,18	-0,15	0,06	0,13
	5	-10,06	-0,24	-1,73	-0,08	0,68	0,03
	6	-69,79	-0,33	0,88	0,15	0,73	-0,11
	1	-11,56	0,12	-0,18	-0,07	0,03	-0,04
	2	-0,96	0,10	0,41	-0,03	0,29	0,00
	3	-24,59	-0,01	-0,23	0,07	0,19	0,04
4	4	-10,57	0,03	0,32	-0,06	0,07	0,04
	5	-3,20	-0,12	-0,42	-0,01	0,30	0,02
	6	-22,59	-0,11	0,22	0,07	0,20	-0,02

Minimal stiffness

In order to satisfy the stiffness criterion as stated in the design criteria (to be introduced in subsection 3.1.5), the optimized joints need to contain a minimal out-of-plane stiffness. Due to the specific load combination of an axial force and a bending moment (Figure 57) it is possible that material is removed at 'undesired' locations (Figure 58 and Figure 59). To increase the effectiveness of the optimization, an additional load case (number 5) with out-of-plane bending moments is applied to improve the performance of the optimized joint. Table 9 lists the applied additional moments to increase the out-of-plane stiffness. The moments are adjusted to the different type of RHS member in order to introduce a similar stress level in each direction in the design domain. Note: the topology optimization tool situates material in such a way that the deformation of the structure is minimised. As there are only bending moments in this load case, the magnitude of the applied bending moments is in fact irrelevant.

Table 9: Applied additional moments to obtain a minimal out-of-plane bending stiffness.

Load case	Member number	M_{yy} (kNm)		
		Joint 1	Joint 2	Joint 3
	1	50,0	50,0	50,0
	2	24,2	50,0	50,0
	3	50,0	50,0	50,0
5	4	50,0	33,0	50,0
	5	50,0	33,0	50,0
	6	24,2	50,0	50,0
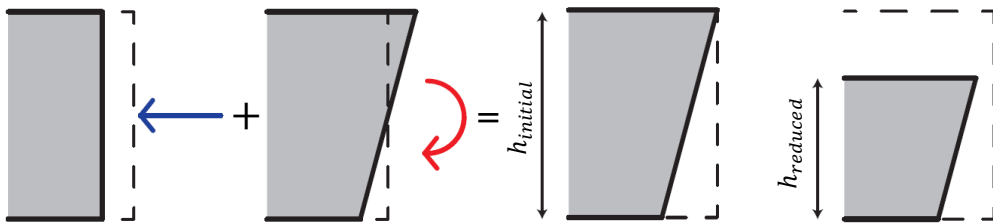
Figure 57: Displacements due to a normal force (left) and a bending moment (middle) result in a translated and rotated loading plane (right).

Figure 58: Reduced height after optimization.
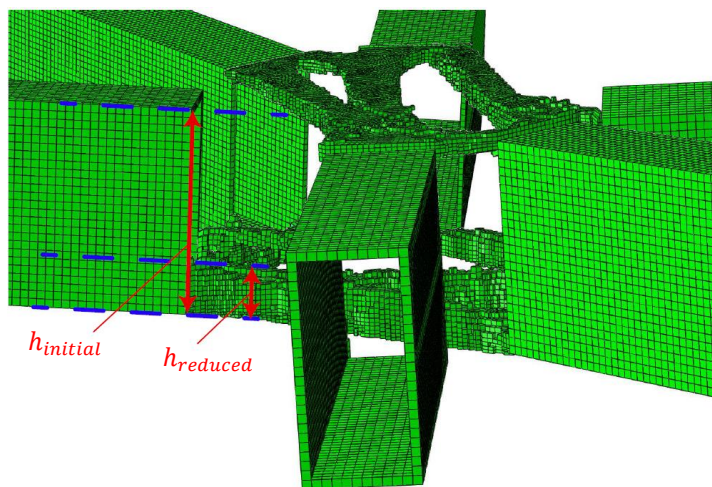
Figure 59: Example of undesired removal of material due to specific loading conditions.

BESO3D settings

In order to find the right topology optimization settings for BESO3D, several iterative steps are made by tuning the settings and inspection of the obtained results. The final settings for the volume fractions are found by carrying out the checks on the design criteria (subsection 3.1.5). The priority of the load cases (weights) are found by consideration of (i) giving the most critical load case a higher weight factor and (ii) satisfying criteria 1 and 2 of the design criteria. This leads to the following final settings:

- Volume fraction;
    - Joint 1:   24%
    - Joint 2:   14 %
    - Joint 3:   10%
- Mean compliance: MIN;
- Evolutionary ratio: 3.0;
- Admission ratio: 3.0;
- Filter radius: 17.0 mm;
- Symmetry properties: No symmetry;
- Multiple load cases: 5;
- Load case weight factors (sequence corresponding to the load cases 1, 2, 3, 4, 5);
    - Joint 1: 0,15; 0,25; 0,15; 0,15 ;0,30;
    - Joint 2: 0,15; 0,15; 0,25; 0,15; 0,30;
    - Joint 3: 0,15; 0,15; 0,15; 0,15; 0,40.

Topology optimized joints

With the presented settings for BESO3D, results are obtained for the shape of the joint. The topology optimized joints are depicted on the pages 49, 50 and 51.

Computational time

An important issue in finding the right settings for the topology optimization process is the computational time that is needed to complete the analyses. The computational time is influenced by several factors.

First, the number of applied elements in the joint model. The size of the calculation magnifies rapidly by an increase in applied elements. Although, better results are obtained by using as much elements as possible, the optimization should take a limited amount of time to complete. Second, the evolutionary and admission ratios were influencing factors. The computational time increases by reducing both ratios as there are more steps needed to find the solution. However, smaller steps of removal and adding elements increases the accuracy of the calculation. Third, the computational time is determined by the available computational power of the work station.

Finally, a workable process is created by limiting the amount of elements to 250.000 and applying 3% for the evolutionary and admission ratio. The computations are carried out on a Windows based computer (Intel Xeon W3690 @ 3.47 GHz, 24GB Ram), Finally, the computational time varied around 35 hours.

Joint 1

The results of the topology optimization for joint 1 are presented in Figure 60 and Figure 61. The geometry of the optimized joint is mainly formed in order to take up the large compression forces introduced by beam 1 and 4. In fact, a profile is formed as a coupling between two RHS members, see Figure 62. The material is divided over the top and the bottom of the joint. The top and bottom are connected by a 'column'-like structure. However, due to the slenderness of this structure, it seems that this column is not likely to significantly influence the behaviour of the joint.
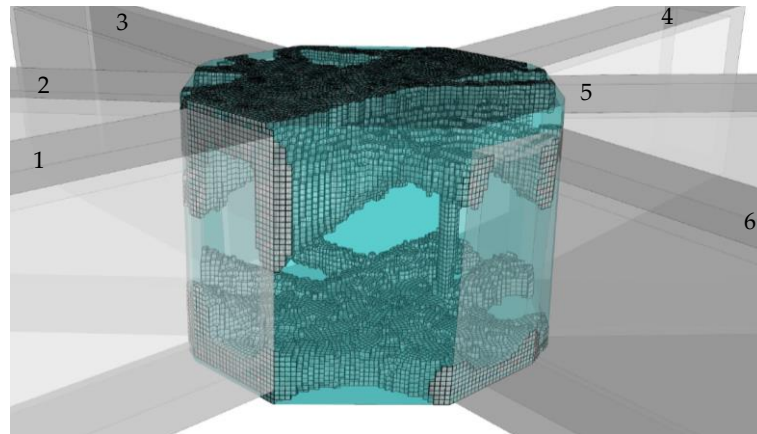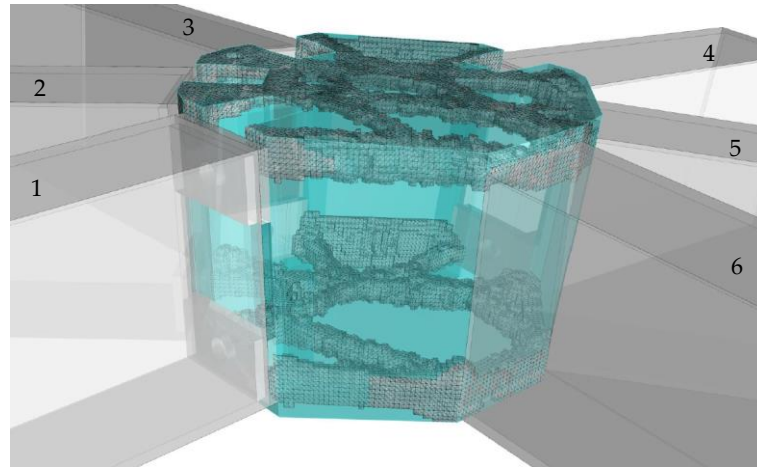

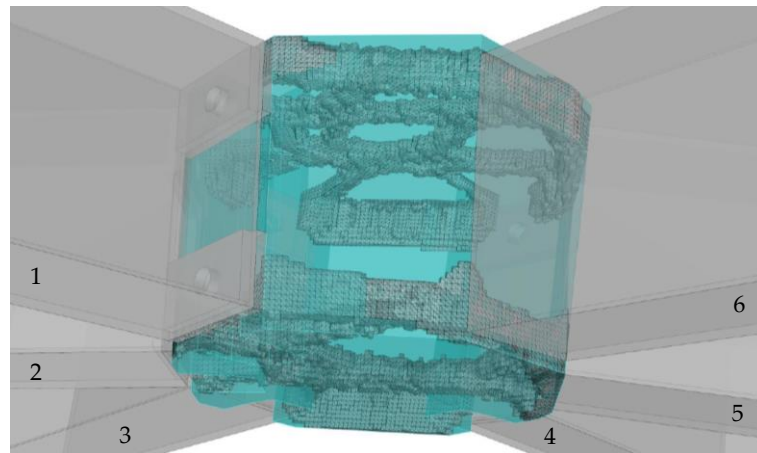*Figure 60: Optimized result for joint 1. Perspective view from the top. (Blue: original design domain)*
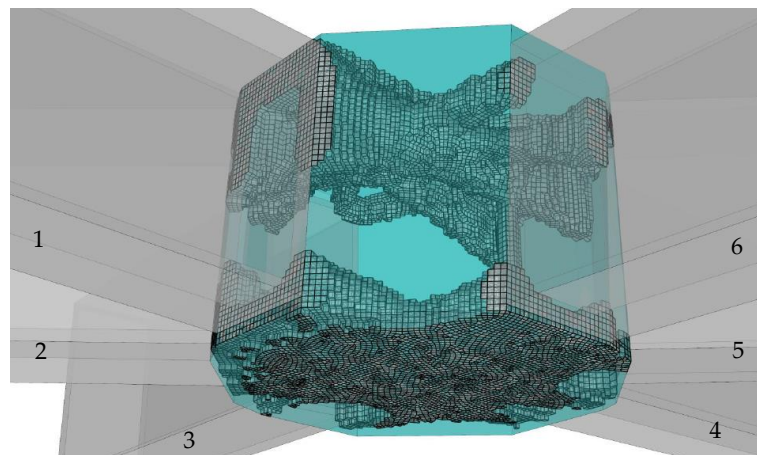
Figure 61: Optimized result for joint 1. Perspective view from the bottom. (Blue: original design domain)
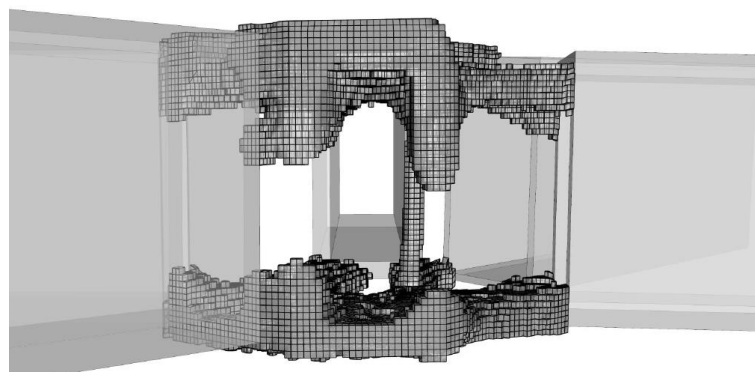

Figure 62: Formed RHS profile in the joint. (View from beam #1)

Joint 2

The results of the topology optimization for joint 2 are presented in Figure 63 and Figure 64. As joint 2, located in a mediumly disturbed membrane field, is loaded by out-of-plane bending moments that are dominant over the axial forces, material is required at the top and bottom of the joint. Therefore, two 'plates' are formed at the top and the bottom of the joint, see Figure 65 and Figure 66. In fact: the optimization tool ensures the best possible lay-out of the top and bottom plates.
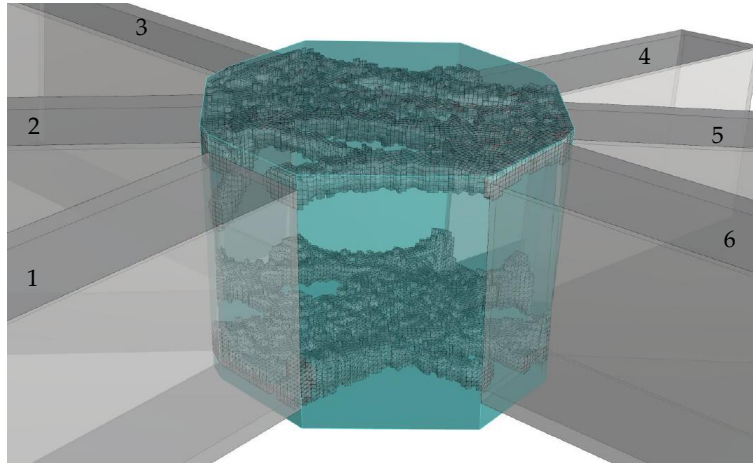
Figure 63: Optimized result for joint 2. Perspective view from the top. (Blue: original design domain)
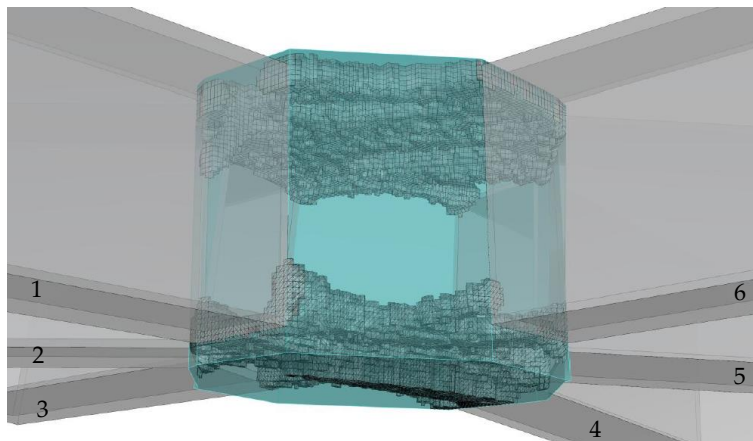
Figure 64: Optimized result for joint 2. Perspective view from the bottom. (Blue: original design domain)
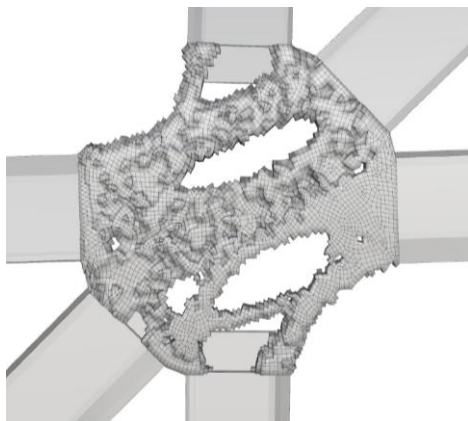
Figure 65: Lay-out of top plate.
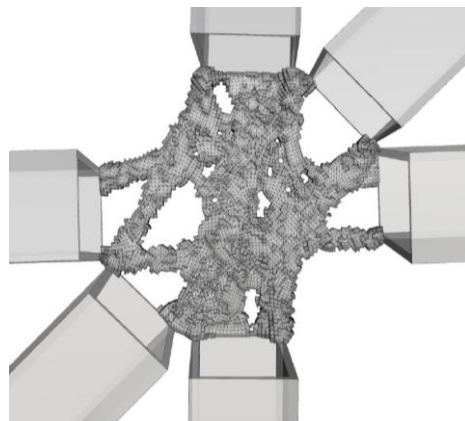
Figure 66: Lay-out of bottom plate.

Joint 3

The results of the topology optimization for joint 3 are presented in Figure 67 and Figure 68. Joint 3 is located in a pure membrane field, therefore the axial forces are dominant over the other loads. The most ideal lay-out of the material is to form two plates (similar to joint 2) to transmit the forces through the joint. Figure 69 shows the reserved space, which is remained by the optimization tool to apply the bolts in the holes during erection of the gridshell. However, as the optimization tool removed the material from the middle of the joint, space became available to tighten the bolts from the side of the joint. Therefore, in this case it was not necessary to reserve space in the design domain (Figure 43).

Figure 67: Optimized result for joint 3. Perspective view from the top. (Blue: original design domain)

Figure 68: Optimized result for joint 3. Perspective view from the bottom. (Blue: original design domain)
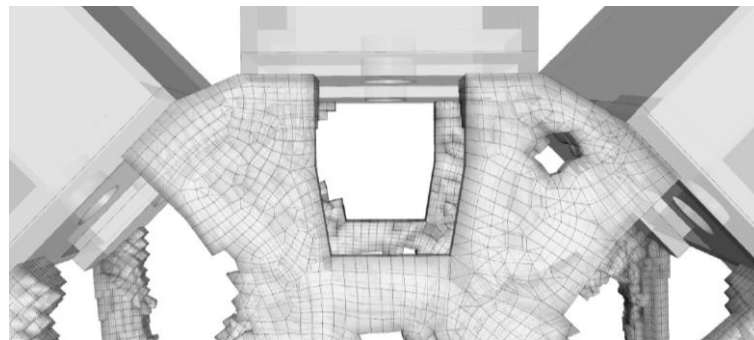
Figure 69: The pre-defined holes for the application of the bolts are remained.

3.1.5 DESIGN CRITERIA

Design criteria were defined in order to be able to check whether the optimized joints are considered as safe. Moreover, in order to prevent changing the behaviour of the gridshell, the newly designed joints had to behave in a similar way to the applied joints in the original FEA model of the gridshell. In the original model rigid joints were used, i.e., infinite stiff and strong. In order to verify whether the designed joints behave in a rigid way, the classification system by Fan, Ma, Cao and Shen (subsection 2.2.1) is used. Unless the joints are not completely stiff, the joints still behave rigidly when stiffness and strength criteria are met.

Joint classification system

Based on the joint classification system, the stiffness criterion (criterion 1) is defined as:

- *Criterion 1:* $\qquad \boldsymbol{\alpha = \dfrac{k}{EI/L_0} \geq 5}$

With k the out-of-plane stiffness of the joint, E the Young's modulus, I the moment of inertia of the members and L_0 the length of the members.

Based on the joint classification system, the strength criterion (criterion 2) is defined as:

- *Criterion 2:* $\qquad \boldsymbol{\beta = \dfrac{M_{j,u}}{M_{e,u}} \geq 0,5}$

With $M_{j,u}$ the plastic moment capacity of the joint and $M_{e,u}$ plastic moment capacity of the adjacent members.

Allowable maximum stress

Although properties of AM produced material are checked it is not yet applied in the and experience with the material is lacking. Therefore a material factor of 1,5 is applied. The maximum stress (criterion 3) in the applied *EOS Stainless Steel GP1* (see material datasheet in appendix C.3) is allowed to:

- *Criterion 3:* $\qquad \boldsymbol{f_{u,d} \leq \dfrac{f_u}{\gamma_M} = \dfrac{530}{1,5} = 350 \, N/mm^2}$

The shape and the design of the joint influence the stresses in the beams. Therefore the beams should not become critical and for the stresses in the beams (criterion 4) hold:

- *Criterion 4:* $\qquad \boldsymbol{f_{u,d} \leq f_y}$

Table 10: Overview of design criteria.

Joint classification system	1. Stiffness	$\alpha = \dfrac{k}{EI/L_0} \geq 5$
	2. Strength	$\beta = \dfrac{M_{j,u}}{M_{e,u}} \geq 0,5$
Allowable maximum stress	3. Joint*	$f_{u,d} \leq \dfrac{f_u}{\gamma_M} = \dfrac{530}{1,5} = 350 \, N/mm^2$
	4. Beams**	$f_{u,d} \leq f_y$

* Material EOS Stainless Steel GP1

** Either S355 of S435

3.1.6 ANALYSIS

The presented topology optimized results in 3.1.4 are checked on the design criteria as introduced in subsection 3.1.5. This section discusses the applied methods and the obtained results.

Joint classification system

To verify whether the joints are classified as rigid, the stiffness and the plastic moment capacity of the joint need to be determined. Although it is not possible to use *Eurocode 3 Design of steel structures – Part 1-8 Design of joints* to classify the joints of a gridshell (see subsection 2.2.1), it gives a clear indication on how the stiffness and plastic moment capacity can be derived. Both characteristics can be determined by the relation between an applied moment on the joint and the associated rotation between the joint and the attached beam. The values can be plotted in a moment-rotation diagram, see Figure 70. The characteristic values in the moment-rotation diagram apply for the design of the optimized joints:

- Design moment resistance $M_{j,Rd}$: the maximum moment in the moment-rotation diagram represents the plastic moment capacity of the joint; (Note: in subsection 3.1.5 $M_{j,u}$ is used for $M_{j,Rd}$)
- Initial stiffness $S_{j,ini}$: the slope of the characteristic in the elastic area represents the stiffness of the joint. (Note: in subsection 3.1.5 k is used for $S_{j,ini}$)

Generation of moment-rotation diagrams

The moment-rotation diagrams are generated by carrying out a finite element analysis on the topology optimized joints. Both the non-linear behaviour of the material as the geometry are taken into account. A *RIKS analysis* takes both non-linear behaviour into account.

RIKS analyses are performed on the obtained topology optimized results. In the RIKS analyses an increasing out-of-plane moment is applied on the interface of the joint with one of the RHS members while the other interfaces are restrained (see Figure 71). A nodal point, restrained to the interface of the beam, is used to introduce the moment to the joint. The rotation of the nodal point is plotted versus the applied moment to generate the moment-rotation diagrams.
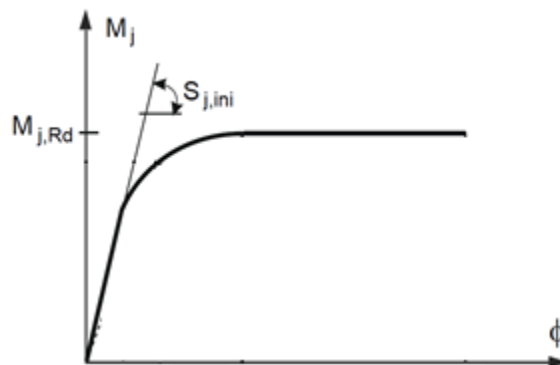
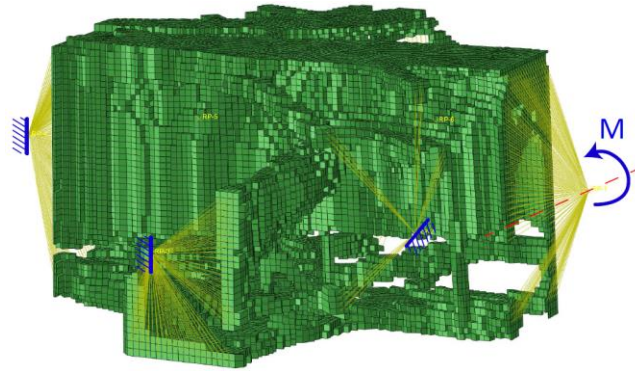*Figure 70: Moment-rotation diagram.* [40]

Figure 71: Set-up RIKS analysis

As illustrated in section 3.1.5, the geometries of the topology optimized joints are highly asymmetrical and so the properties of the joints (stiffness and plastic moment capacity) vary in different directions. Different values for the stiffness and the plastic moment capacity in each of the direction of the adjacent beams are found and therefore all the six directions are checked. Moreover, due asymmetry of the geometry of the joint, both positive and negative rotations of the out-of-plane bending moments need to be checked.

The moment-rotation diagrams of the optimized joints as depicted on the pages 49, 50 and 51 are presented in Figure 72 to Figure 77 for joint 1, Figure 78 to Figure 83 for joint 2 and Figure 84 to Figure 89 for joint 3.

Classification of the joints – check design criteria 1 and 2
By extracting the stiffness k and the plastic moment capacity $M_{j,u}$ for each of the six directions per joint out of the moment-rotation diagrams, the joints could eventually be classified. The classification of the joints is presented in Table 11, Table 12 and Table 13.

With the obtained classifications, the joints were verified on the design criteria number 1 and 2. An example calculation for the determination coefficients α and β is given in appendix E.2 of determination coefficients α and β.

Note: in the calculations to classify the joints, the properties (E, I, σ, $W_{p,l}$), the geometrical data (l_0) and the stiffness k of the adjacent beams to the three representative joints were used. Information with respect to these properties can be found in appendix E.1.

Joint 1

The classification for joint 1 is presented in Table 11.

Table 11: Classification of joint 1.

| Direction	Positive			Negative			Verification
	α [-]	β [-]	Class	α [-]	β [-]	Class	
1	10,94	0,88	Rigid	10,94	0,93	Rigid	
2	26,19	0,92	Rigid	26,19	0,93	Rigid	
3	7,48	0,70	Rigid	7,48	0,58	Rigid	✅
4	20,36	1,63	Rigid	20,36	1,72	Rigid	
5	24,44	1,26	Rigid	24,44	1,28	Rigid	
6	13,08	0,92	Rigid	13,08	0,95	Rigid	
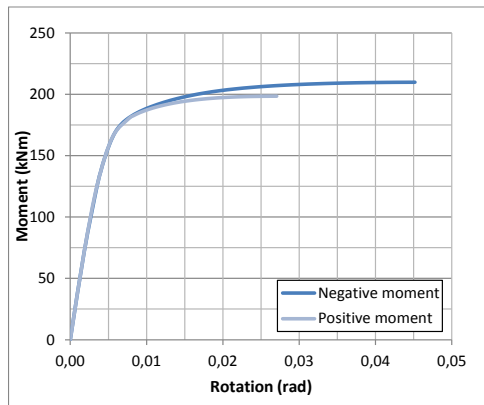
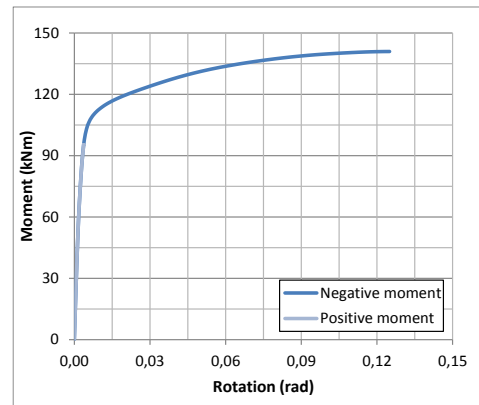*Figure 72: Moment-rotation diagram: direction 1.*
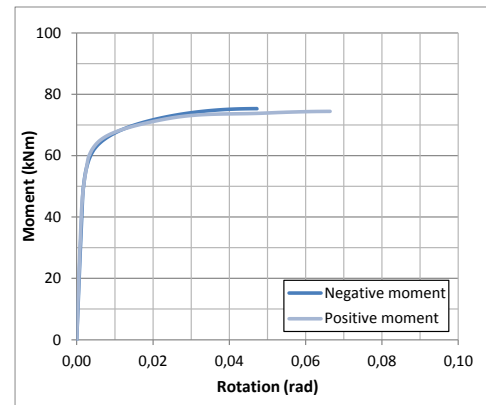
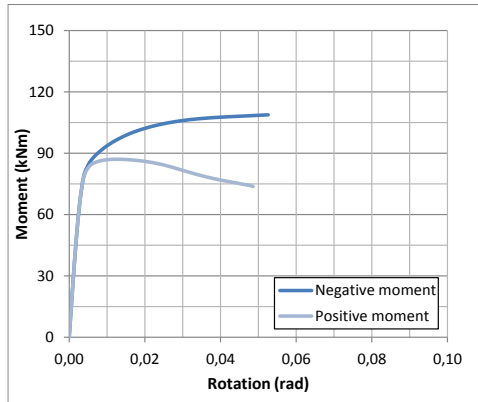*Figure 73: Moment-rotation diagram: direction 2.*
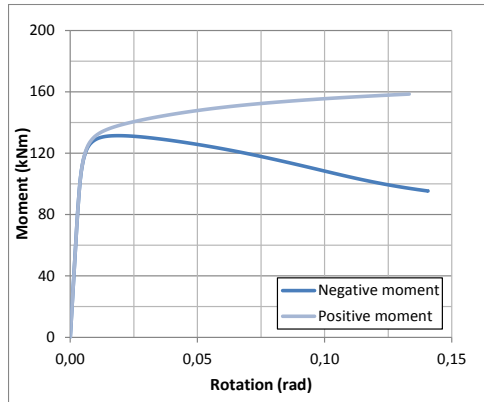
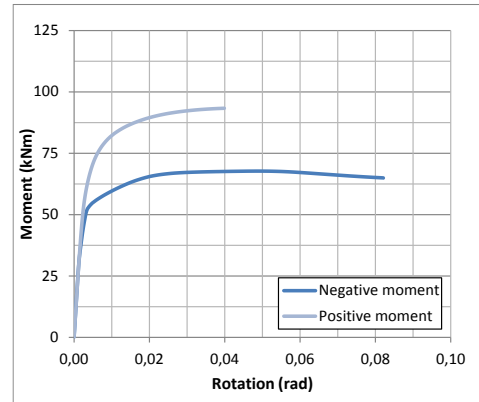*Figure 74: Moment-rotation diagram: direction 3.*
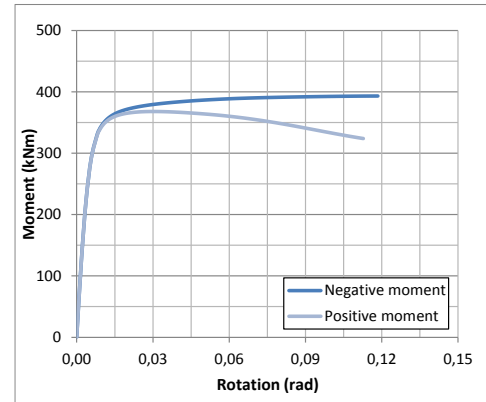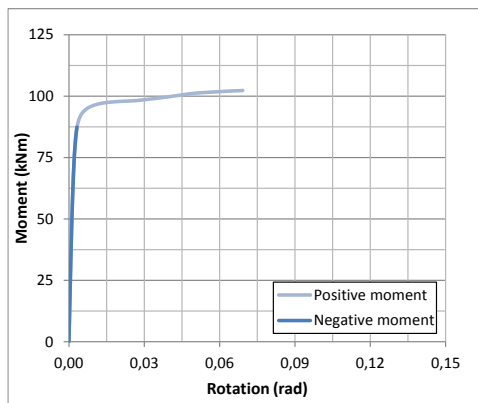

Figure 75: Moment-rotation diagram: direction 4.
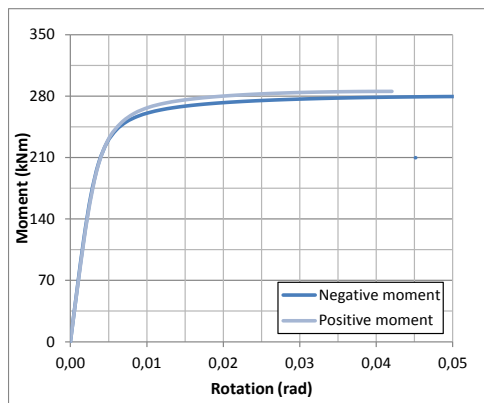
Figure 76: Moment-rotation diagram: direction 5.
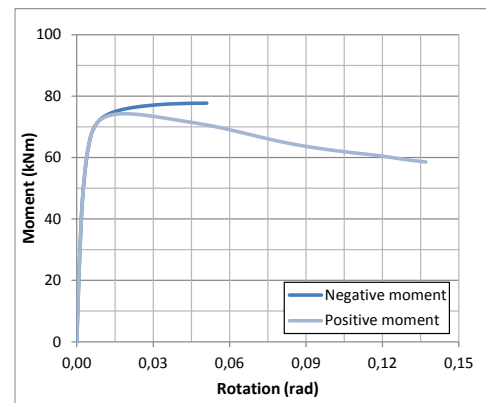
Figure 77: Moment-rotation diagram: direction 6.

Joint 2

The classification for joint 3 is presented in Table 12.

Table 12: Classification of joint 2.

Direction	Positive			Negative			Verification
	α [-]	β [-]	Class	α [-]	β [-]	Class	
1	10,39	0,93	Rigid	10,39	0,61	Rigid	
2	24,26	0,95	Rigid	24,26	1,41	Rigid	
3	11,15	0,87	Rigid	11,15	1,09	Rigid	✓
4	16,39	1,66	Rigid	16,39	1,03	Rigid	
5	42,98	1,55	Rigid	42,98	1,33	Rigid	
6	13,16	0,74	Rigid	13,16	0,99	Rigid	
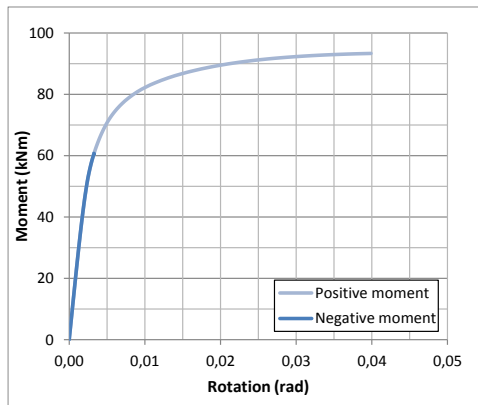
Figure 78: Moment-rotation diagram: direction 1.

Figure 79: Moment-rotation diagram: direction 2.

Figure 80: Moment-rotation diagram: direction 3.

Figure 81: Moment-rotation diagram: direction 4.

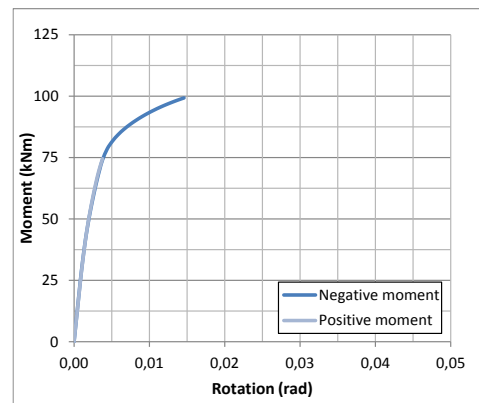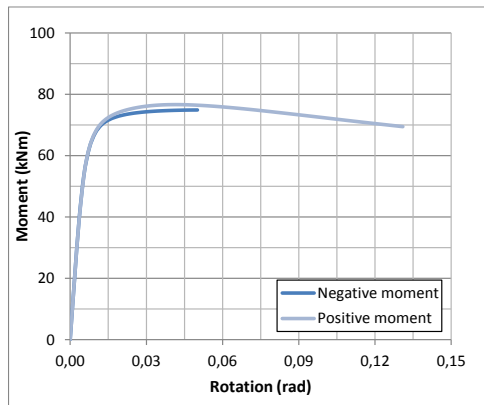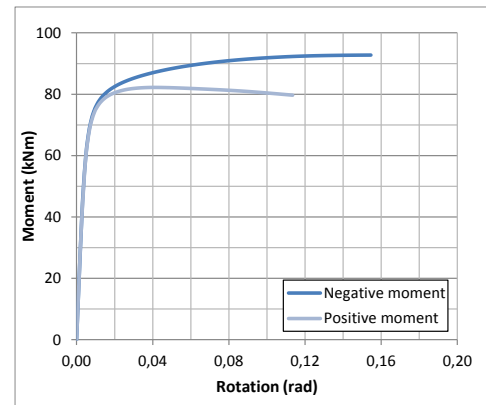*Figure 82: Moment-rotation diagram: direction 5.*

Figure 83: Moment-rotation diagram: direction 6.

Joint 3

The classification for joint 3 is presented in Table 13.

Table 13: Classification of joint 3.

Direction	Positive			Negative			Verification
	α [-]	β [-]	Class	α [-]	β [-]	Class	
1	8,08	1,17	Rigid	8,08	1,14	Rigid	
2	14,63	1,25	Rigid	14,63	1,41	Rigid	
3	8,39	1,41	Rigid	8,39	1,30	Rigid	
4	8,77	1,08	Rigid	8,77	1,14	Rigid	
5	20,49	1,33	Rigid	20,49	1,40	Rigid	
6	13,88	1,66	Rigid	13,26	1,48	Rigid	

Figure 84: Moment-rotation diagram: direction 1.

Figure 85: Moment-rotation diagram: direction 2.
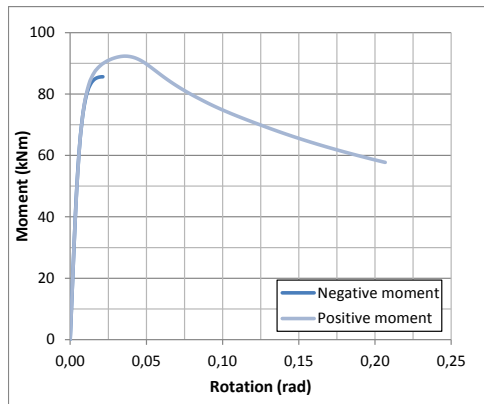

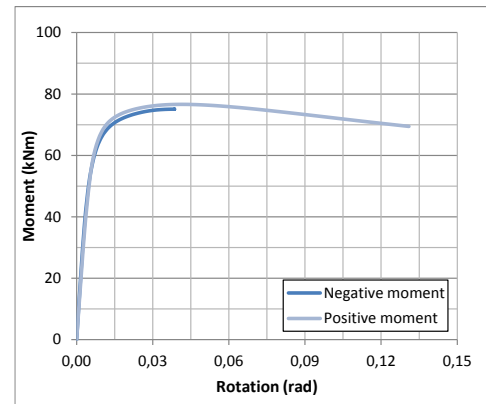*Figure 86: Moment-rotation diagram: direction 3.*

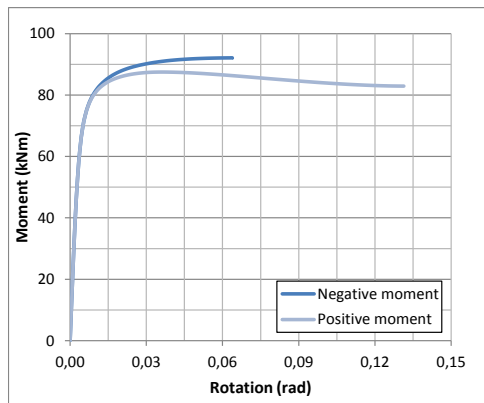*Figure 87: Moment-rotation diagram: direction 4.*

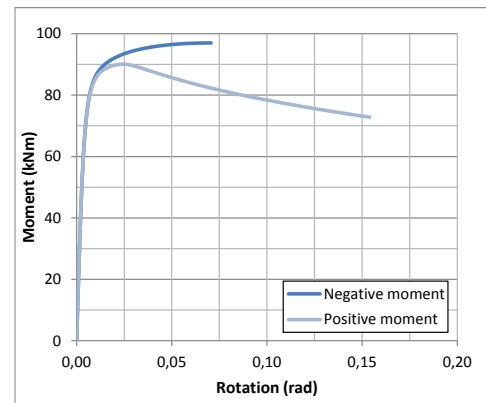*Figure 88: Moment-rotation diagram: direction 5.*

Figure 89: Moment-rotation diagram: direction 6.

Allowable maximum stress

In addition to the design criteria for the stiffness and plastic moment capacity, the joints need to satisfy the criteria for allowable maximum stress in the material. As the optimization of the joints gradually proceeds, the stresses in the joints are increasing as material is removed during each step.

Design criterion 3 controls the maximum allowable stresses in the material of the joint. When the stresses exceed the allowable stress the topology optimization needs to be terminated. Moreover, as material is locally removed in the neighbouring areas of the adjacent beams, local peak stresses can occur in the beams that exceed the maximum yielding strength of the beams. This should be avoided and is included in design criterion 4.

Check of allowable maximum stress – check design criterion 3 and 4

In order to check design criteria 3 and 4, linear elastic analyses are carried out on the geometry developed by the topology optimization run. The load cases causing the highest stresses in the joints and beams were used for the check on design criteria 3 and 4. The results are shown on the pages 59, 60 and 61. These results are derived from the critical load cases for the stresses in the joint and the for the stresses in the adjacent members. The number of the corresponding critical load cases are given in Table 14.

Table 14: Critical load cases per joint for the joints and the adjacent members.

Joint type	Joint	Adjacent members
1	2	2
2	2	3
3	3	3

Allowance of local stress concentrations

Stress concentrations are a common phenomenon when working with FEA programs. Especially when the geometry in the FEA model contains sharp corners, linear fine element analyses tend to find such 'hotspots'. In practice, the material would locally yield and the surrounding material would pick up the load. Stress concentrations can therefore be accepted to a certain extent. However, several conditions need to be met, such as:

- A ductile material is applied;
- The structure is loaded statically (cyclic loading is excluded (fatigue);
- The peak stresses occur only locally.

Note 1: whereas stress concentrations can be accepted, they cannot be ignored. They need to be examined individually and checked with the stated conditions.

Note 2: With regard to safety and the inexperience with the applied material *EOS Stainless Steel GP1*, peak stresses were not allowed in the joint.

Joint 1

The stress distribution for joint 1 is given in Figure 90. The largest stresses in the joint approaches the maximum allowable stress level of $f_{u,d} = 350\ N/mm^2$ leading to the termination of the topology optimization. It also shows that that the high strength of the printed material is utilized to a large extent.

Note: one mesh element contains a large stress of $487\ N/mm^2$ (see yellow circle). As this mesh element is surrounded by mesh elements containing significantly lower stresses, this stress is not classified as a stress concentration, but as a numerical error and is therefore ignored.
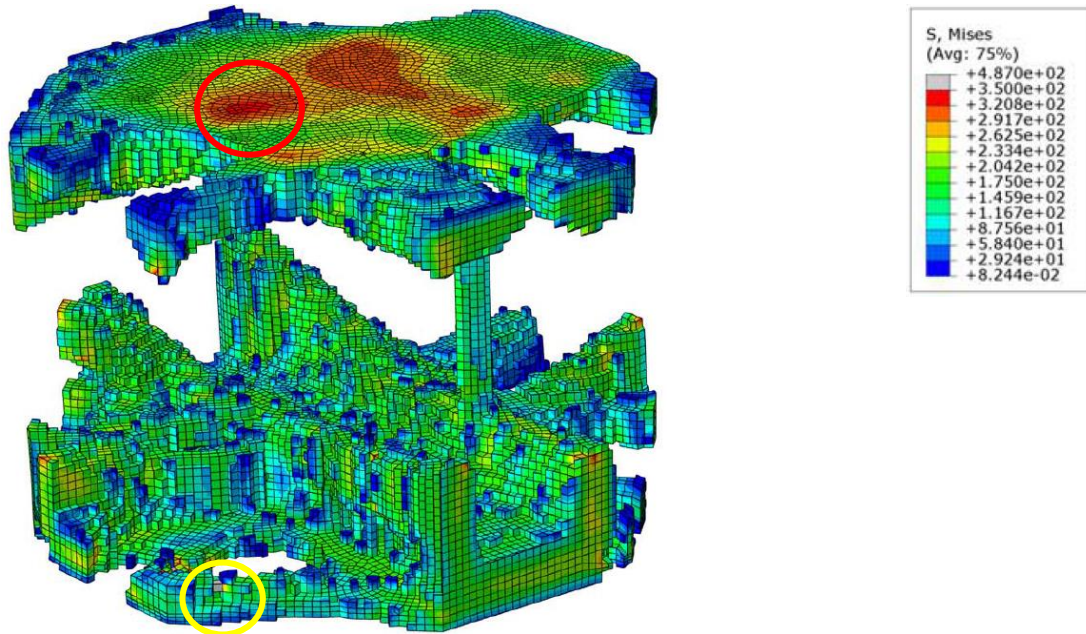

Figure 90: Von Mises stresses (N/mm²) in joint 1 (red circle: largest stress in joint and yellow circle indicates a numerical error in the analysis).

Along with the stresses in the joints, the stresses in the beams (Figure 91) increase to the maximum stress level. More than that, some peak stresses exceed the yield strength locally. The stress concentrations are examined and in consideration that steel S455 is applied (ductile material) and no cyclic loading will occur, these stress concentrations are acceptable.
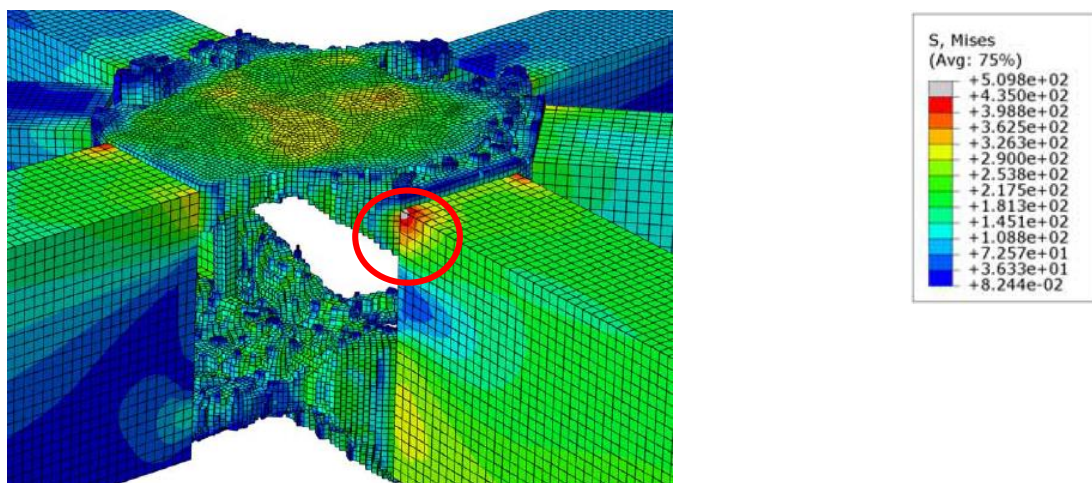

Figure 91: Von Mises stresses (N/mm²) in the beams of joint 1 (red circle: largest stress in member).

Joint 2

The stress distribution for joint 2 is given in Figure 92. With a maximum stress of $172 \, N/mm^2$ it is clear that the stresses remain well below the maximum stress level of $f_{u,d} = 350 \, N/mm^2$. The high strength of the material cannot fully be utilized as the topology optimization is terminated because of two parameters approaching the stated design criteria. This is related to the plastic moment capacity in direction 1 for a negative applied moment (see Table 12) and the stresses in the beams (see Figure 93).
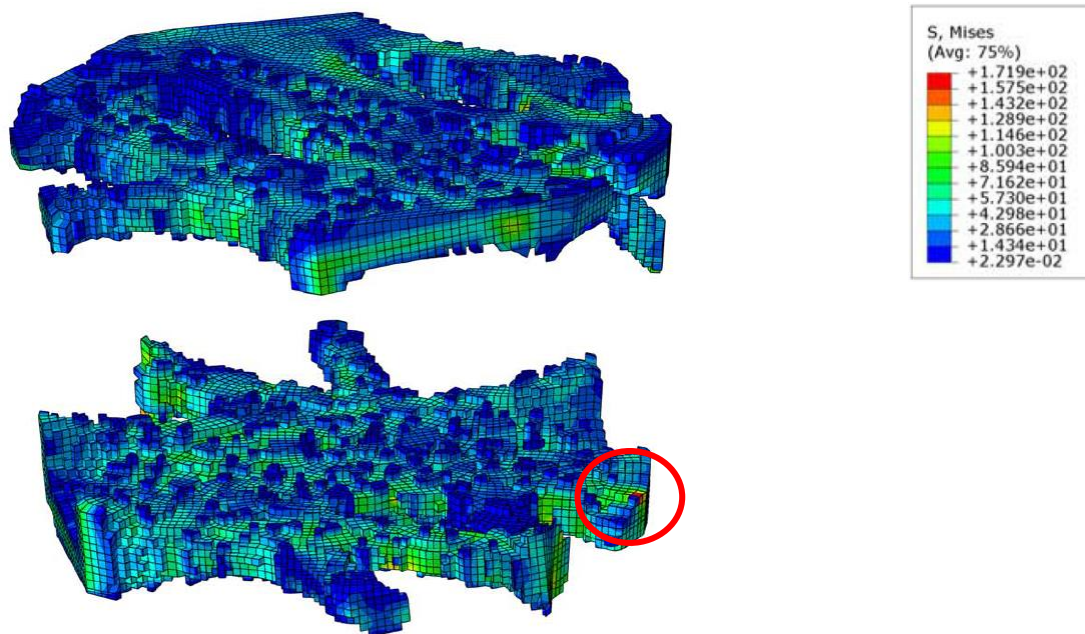

Figure 92: Von Mises stresses (N/mm²) in joint 2 (red circle: largest stress in joint).

The stresses in the attached beams, see Figure 93, remain below the yield strength of the members: $355 \, N/mm^2$. However, some peak stresses approach the yield strength.
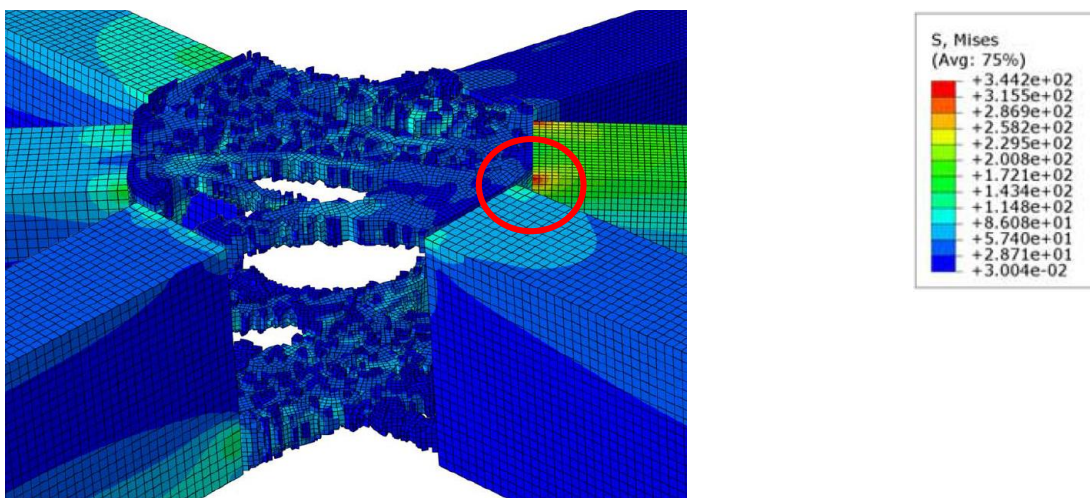

Figure 93: Von Mises stresses (N/mm²) in the beams of joint 2 (red circle: largest stress in member).

Joint 3

The stress distribution for joint 3 is given in Figure 94. Corresponding to joint 2, the stresses remain well below the maximum stress level. The high strength of the material cannot be utilized as termination of the topology optimization is caused by the reduction in stiffness.
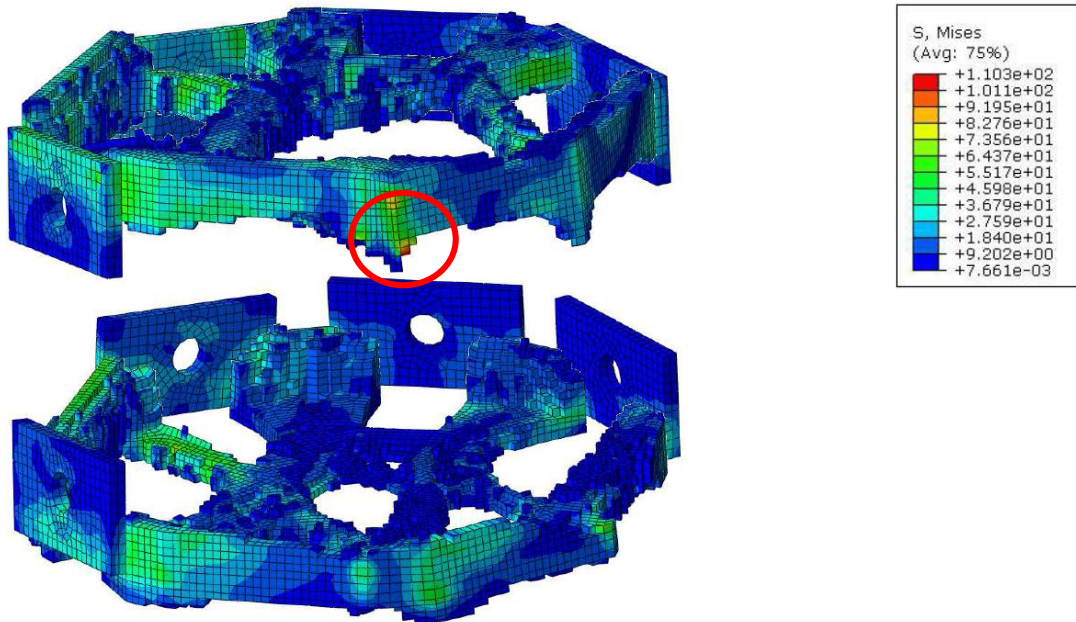

Figure 94: Von Mises stresses (N/mm²) in joint 3 (red circle: largest stress in joint).

The stresses in the attached beams to joint 3 also remains well below the yield strength 355 N/mm^2 for all the members.
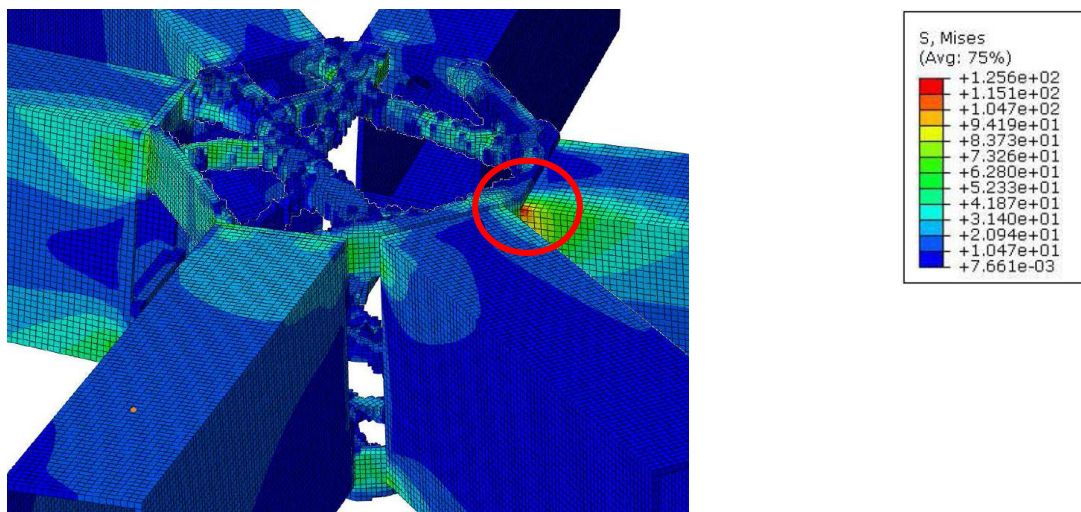

Figure 95: Von Mises stresses (N/mm²) in the beams of joint 3 (red circle: largest stress in member).

3.1.7 REFLECTION ON OBTAINED RESULTS

The shapes of the joints are developed by the topology optimization tool. Subsequently, the joints are checked on the design criteria that are based on the joint classification system, introduced in subsection 2.2.1. Since the design criteria on out-of-plane stiffness and moment capacity are satisfied, the joint is classified as rigid.

By studying the optimised shapes it becomes clear that the joints consist of what generally can be identified as a top and bottom 'plate'. With these two plates the joints are able to transfer bending moments, but it seems the joints are lacking adequate shear capacity. With engineering common sense it is identified that with the lack of significant shear resistance, the joints could potentially behave in a non-rigid way. Note that this is potentially undesired behaviour, which requires further research to fully determine the influence of shear deformation on the behaviour of the joint. This research is beyond the scope of this study.

In order to anticipate this potentially undesired behaviour, the development of the shape of the joint is reconstructed and the three main influencing aspects are reviewed in order to arrive at a possible solution.

First, the input for the optimization tool influences the outcome of the optimization. The main input variable is the load input; the shape of the optimized joint is highly depending on the applied loading conditions. This is demonstrated in the simple optimization problems in appendix D, section D.1. Considering the applied loads (see Table 6, Table 7 and Table 8), the axial forces and out-of-plane bending moments are dominant over the shear forces. Since the optimization tool gives priority to develop a structure to resist the dominant axial forces and out-of-plane bending moments, little shear capacity is required and developed.

Second, the optimization tool BESO3D is a critical factor. However, based on the results for simple optimization problems it is determined that the tool generates results that can reasonably be expected based on engineering principles. In case of shear forces, the optimization tool develops a structure that can transfer shear (see appendix D.1.3). This shows that in case of necessary shear capacity, this would have been developed in the joint.

Third, the design criteria approve the optimized shapes of the joints. Whereas the design criteria do not prescribe rules for the shear stiffness and strength, the lack of adequate shear stiffness is not detected during the verification of the joint. It is reasonable to assume that criteria in respect to shear capacity are not included in the joint classification system, because shear is normally not a critical factor in the design of joints for gridshells.

It is concluded that the final shapes for the joints are a direct result of the given input, the method of the design tool, and finally the design criteria. The joints will be able to transfer the present loads in the structure and will behave rigid in respect to the defined design criteria. However, considering the lack of shear stiffness of the joint it is assumed that the joint may not behave rigidly with regard to shear. Therefore the input of the optimization tool needs to be adjusted. Similar to the addition of a load case with bending moments to guarantee the out-of-plane stiffness, an extra load case with shear forces can be added. This make sure that the required shear capacity is developed by the optimization tool. Adding two extra design criteria with respect to (i) the shear stiffness and (ii) the shear capacity, it will be assured that the joints have sufficient shear capacity.

3.2 DETAILING

AM offers advantages (subsection 2.4.2) such as design freedom and the possibility to integrate functional features. These advantages have been used in the design process of the joints to offset the high costs related to the production of the joint by AM. During the design process, the following design goals were taken into account in order to increase the performance of the joint:

1. Maximise erection speed;
2. Minimise labour intensive work;
   a. Different kind of preparation work (weld preparation, CNC cutting);
   b. Welding;
3. Avoid quality work (welding) in uncontrolled environments;

It was strived for to convert these design goals into concrete solutions. The first goal was achieved by optimising the erection scheme, which is explained in subsection 3.2.1. Two types of joints, with different connection types, were designed to support the developed erection scheme. The first type consists of bolted connections (subsection 3.2.2) and the second type applies welded connections (subsection 3.2.3).

3.2.1 ERECTION SCHEME

In order to deliver the project as fast as possible and to reduce costs, the goal was to maximise the erection speed. Therefore the following erection scheme is proposed:

1. Large parts, *'ladders',* are prefabricated in the shop;
2. The ladders are transported to the site;
3. The ladders will be hoisted into place;
4. The missing members and joints are added by means of bolted connections.

Note: due to the fabrication accuracy of the joints by AM and the beams by CNC machines, it is expected that the missing members will fit. However, this will need to be checked for occurring temperature differences during erection.

Note 2: the ladders need to be propped temporarily until completion of the gridshell.

Ladders
The gridshell is divided into smaller segments (Figure 39), *ladders*, that are prefabricated in the shop. Two types of ladders can be distinguished:

1. Ladders containing heavily loaded parts of the gridshell;
2. Ladders containing parts of the gridshell in membrane action.

The maximum size of the ladders is determined by taking transport restrictions into account. The maximum allowable dimensions for road transport are [41], [42]:

- Length: 18 m;
- Width: 2,55 m, with a maximum up to 4,5 m with an acquired permit;
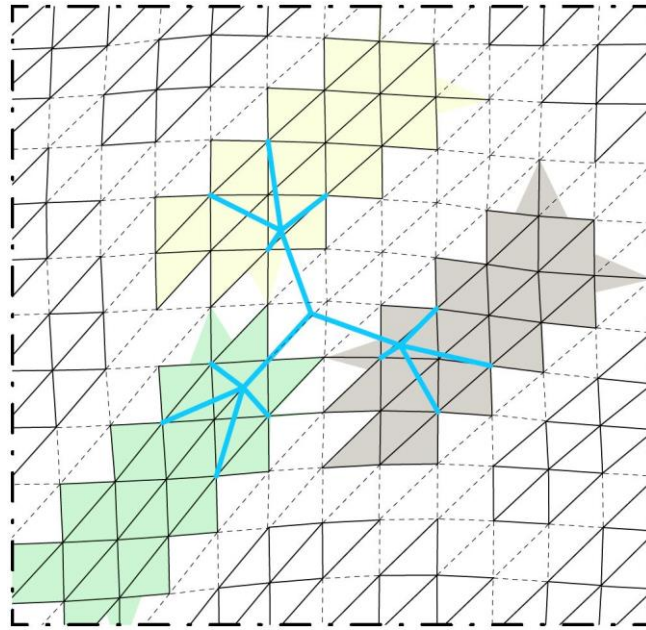- Height: 3,5 m.

Figure 96: Example of division of the gridshell at an intermediate tree support (blue).

Type 1 ladder: heavily loaded parts

The first type of ladders are the ladders that are heavily loaded (coloured in Figure 96). They are located in the zones of the highly disturbed membrane field (Figure 39). It is necessary that the joints and the members are connected by welds to satisfy the stiffness criterion (section 3.2.2).

The type 1 ladders will be prefabricated in the shop in a controlled environment in order to avoid welding on site. This will result in higher quality as the environment badly influences welded connections. An example ladder (yellow ladder in Figure 96) is depicted in Figure 97, the outer dimensions of the ladder are indicated. These type of ladders need to be transported with special transport and permits need to be acquired. During transport the ladder needs to be placed diagonally as the maximum transportable dimension (diagonally) is 5,7 m. As bolted joints at the outer perimeter suffice, they will not be installed in the shop to avoid the risk of getting damaged during transport.

The ladders are only allowed to be transported with a permit because of the large dimensions. However, the route from the shop to the building site needs to be checked for clashes; problems can rise with viaducts, bridges, small turning circles, etc. This needs to be done before the ladders will be fabricated. In case of restricted passages, either temporary measures need to be taken or the large dimensions need to be reduced. Smaller ladders will be welded on site before hoisting them in place. The latter is not preferred.

Type 2 ladder: parts in membrane action

The second type of ladders contain parts of the gridshell that are loaded in membrane action. The connections will be made by welding. In this way, adding extra weight (gusset plates and bolts) for a bolted connection is avoided (see section 3.2.2).
Similar to the first type of ladders, the ladders will be prefabricated in the shop. The dimensions of these ladders are smaller with respect to the first type of ladders (see Figure 98). In this way, the ladders can be transported without the need of any permit.
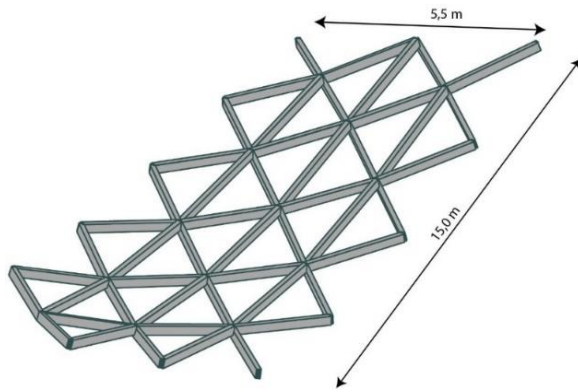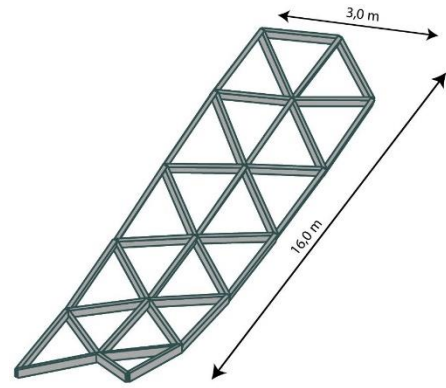
64

Figure 97: Dimensions of type 1 ladder.

Figure 98: Dimensions of type 2 ladder.

3.2.2 BOLTED CONNECTION

The first connection type applies bolts to connect the beams to the joints and is depicted in Figure 99. These bolted connections will be applied for the joints in a pure membrane field and in the mediumly disturbed membrane field (Figure 39). The connection is made by the application of two bolts of M24 x 50 – 12.9 that connect a lower and an upper gusset plate of the RHS member to the gusset plates of the joint. On site, the members need to be brought in position which is followed by the application of the bolts, see Figure 101. To satisfy the stiffness criterion (section 3.1.5) the connection had to act monolithic and therefore it is necessary to pretension the bolts.

Whereas the gusset plate of the joint will be printed directly as part of the joint, the gusset plates of the RHS members need to be fabricated and welded in the shop. The bolts are located as far as possible away from the centre line of the RHS member in order to take up larger out-of-plane bending moments.

Note: Although different aspects of this connection are important, focus has been put on the pretension in the bolts and less on the gusset plates and the welds of the gusset plates.

Pretension

The pretension in the bolts prevents the joint to give way from the RHS member when loaded. By means of applying pretension the clamping force per bolt equals $175 \, kN$ (see appendix E.3). A monolithic connection is obtained until the tension force exceeds the clamping force. This implies that the stiffness is remained in case of:

- An axial force:
$$F_x \leq 2 \cdot F_m = 2 \cdot 175 = 350 \, kN;$$

- An out-of-plane bending moment:
$$M_{max} \leq F_m \cdot r = 175 \cdot (0,134 + 0,33) = 29,2 \, kNm;$$

- A combination of an axial force with an out-of-plane bending moment under the estimation that other forces and moments are negligible.

The torque required to apply the desired pretension equals $1,4 \, kNm$ (see appendix E.4). An example of a torque wrench is depicted in Figure 100. With a length of 1,6 m, this type of wrench has a torque range of 150-1500 Nm.
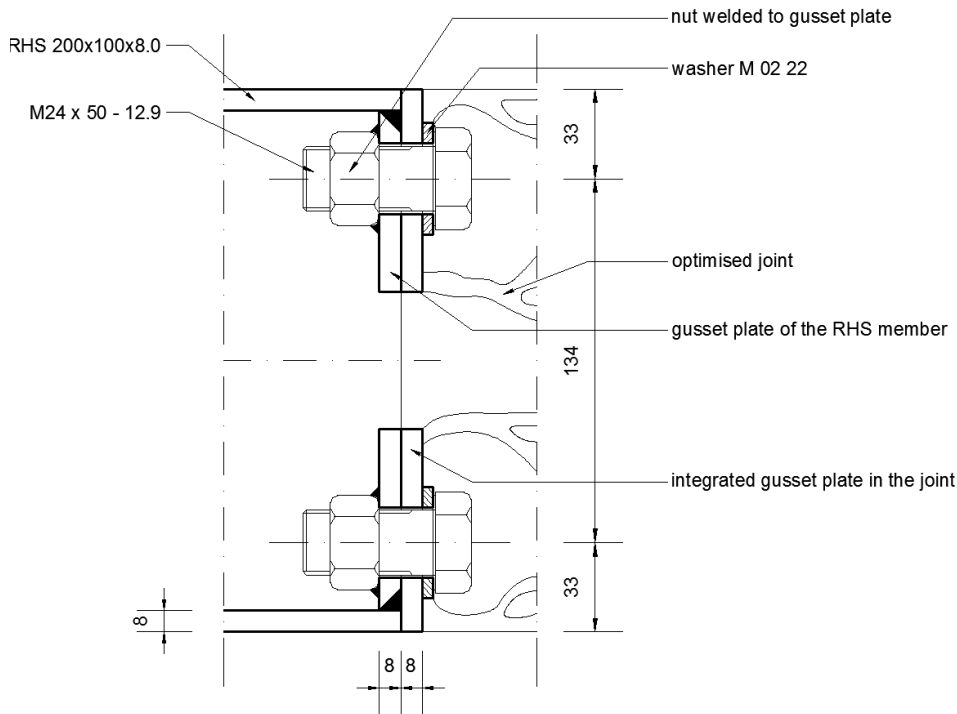
Figure 99: Bolted connection between an optimized joint and a RHS member.

Influence on the design domain

The placement of the bolts influences the design domain for the bolted connection. As the production of AM allows to integrate functional features, the best place to insert the bolts is from inside the joint. This avoids preparation work of the RHS member similar to the gridshell of the Westfield shopping centre (see subsection 2.2.3). The space, cut out of the design domain as shown in Figure 43, has been limited to the required space for the insertion of the bolt and the required torque wrench to pretension the bolts.

The bolts will connect the gusset plates of the RHS member to the gusset plates of the joint. The gusset plate is taken up in the design of the joint and will be printed as part of the joint. In the joint model the gusset plates are marked as non-design domain. In this way the optimization tool could not take away the material from this part.

Figure 100: Example torque wrench with a torque range of 150-1500 Nm. © 2013 BMS Ireland
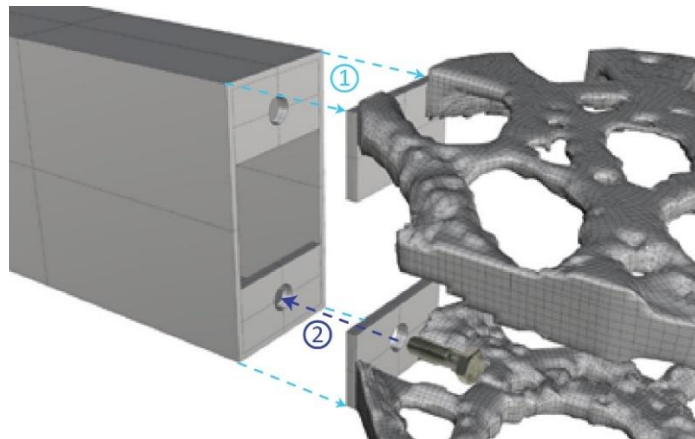
66

Figure 101: Connection method between joint and RHS member. 1: Bring member to the joint. 2: Apply the bolt and fasten it with required torque.

3.2.3 WELDED CONNECTION

The second type of connection applies welds to connect the beams to the joints. The welded connection was required for the joints in the highly disturbed zones (Figure 39) in order to satisfy the stiffness criterion (section 3.2.2). As the joint will be heavily loaded, the applied type of welds will be butt-welds, reliable in heavily loaded structures.

In order to create reliable and well-functioning welds, grooves need to be prepared prior to the welding process. These grooves are traditionally prepared by machining, grinding, forging, casting or shearing which is labour intensive and thus expensive [43]. Therefore, the weld preparations are integrated in the design of the joint. Due to the design freedom the grooves can be designed in the best possible way, which is normally very expensive. Therefore J-grooves will be printed directly to the joint (see Figure 102) that makes welding over the entire cross-section possible, even in case of 16 mm thick RHS members. An example is depicted in Figure 103.
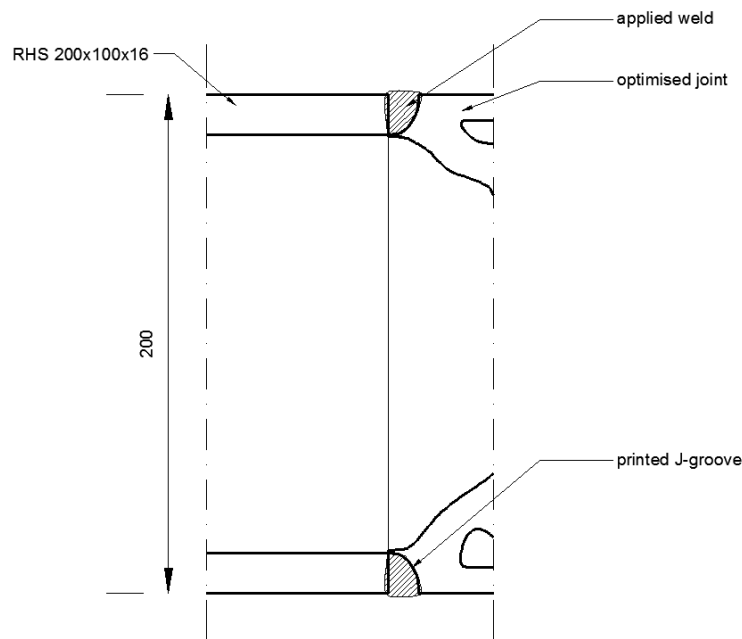

Figure 102: Welded connection between a RHS member and an optimized joint.

Influence on the design domain

The application of welds mainly influences the dimensions of the design domain. In order to save costs with regard to AM production, the design domain needs to be as small as possible (subsection 3.1.2). However, in order to avoid the problems as faced during the application and inspection of the welds of the Złote Tarasy gridshell (subsection 2.5.2), the angle between neighbouring members should not become too small.

In order to apply proper welds, angles between two parts had to be at least 60° and the welder should be able to have access to the welds. It was possible to avoid the mentioned problems by applying a sufficient large design domain, see Figure 104.

Note: the dimensions in Figure 104 were checked by experienced welders of the Delft University of Technology, faculty of Civil Engineering.
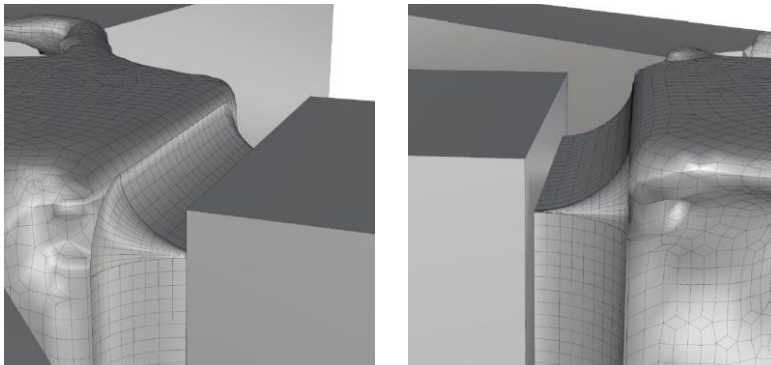

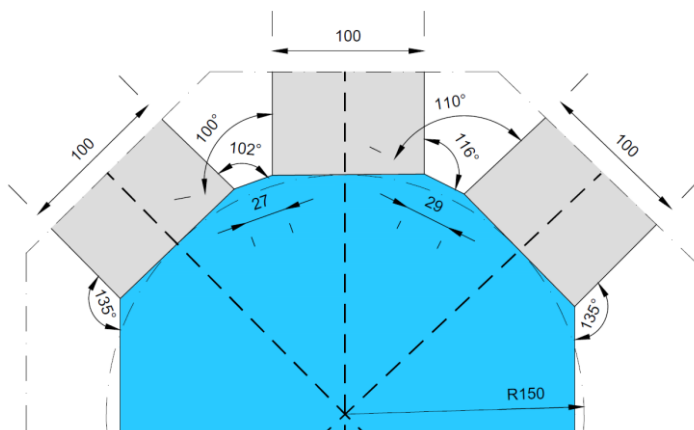*Figure 103: Examples of the printed J-grooves to the joints.*

Figure 104: Angles and space to apply the joints.

3.3 PREPARE FOR AM PRODUCTION

The topology optimization provides the preliminary designs for the joints. In order to create a detailed design, several steps are carried out to prepare the joint for AM production. One of the most important steps in this process involves the smoothing of the geometry of the optimized joints. Next to this, additional steps are carried out to prepare the design for the joints for production (see also section 2.4.4). Illustrations of these steps are presented in appendix C.4.

3.3.1 SMOOTHING

Working with sharp-edged mesh elements in the topology optimization process results in a rough surface as shown in the results on page 49, 50 and 51. The surface is smoothed in order to avoid stress concentrations, remove superfluous material and improve aesthetics. Whereas Abaqus does not contain an automatic smoothing function, the smoothing is done by hand in Rhinoceros resulting in the models shown in Figure 105, Figure 106 and Figure 107.
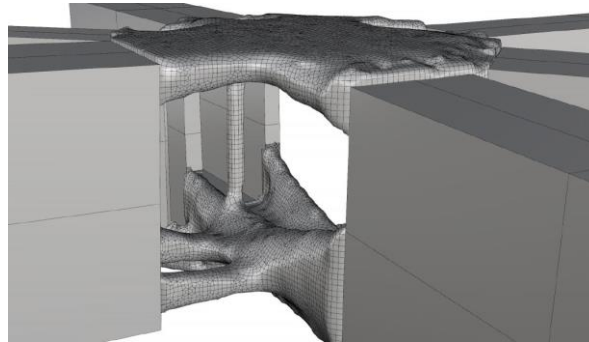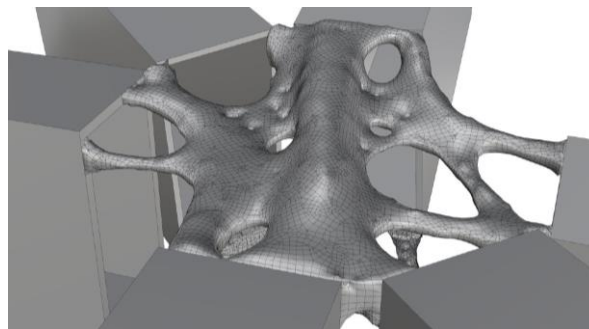

Figure 105: Smoothed joint type 1.
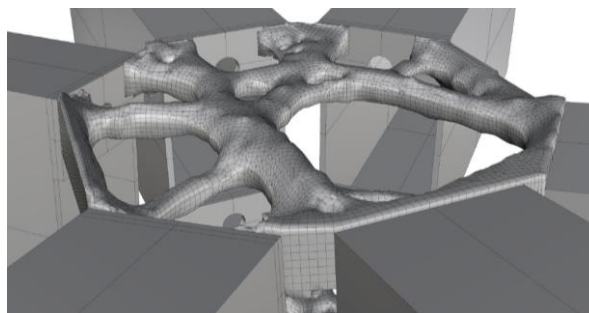

Figure 106: Smoothed joint type 2.

Figure 107: Smoothed joint type 3.

3.4 CONCLUSION

This section provides answers to the following subquestions:

- What are the topology optimized shapes of representative structural joints?
- What is the best option to connect the joints to the beams?
- Which steps need to be taken to prepare the joint for AM production?

Shape development

The shapes of the three developed joints are unique in terms of geometry and in amount of required material. This follows from the fact that the joints are developed by the topology optimization tool while applying varying loading conditions. Identified in subsection 3.1.7 is that the joints seem to lack adequate shear capacity. Whereas little shear capacity is required to withstand the loads, shear capacity is required in order to assure the rigid behaviour of the joints.

Detailing

A hybrid solution for the joint-beam connection is developed; a type that applies partly bolted and partly welds and a fully welded connection type. This resulted in an improved erection scheme. With the application of this type of erection scheme, the three stated design goals are achieved: the erection speed is maximised, labour intensive work is minimised and, quality work, such as welding, is avoided in uncontrolled environments. The erection speed of the gridshell is maximised by the use of large prefabricated parts (ladders). The ladders are installed on site by members that are connected by bolts. Moreover, labour intensive work for detailing is integrated in the joint such as grooves for welding and printing a gusset plate to the joint. Next to this, welding can take place in a controlled environment in the shop leading to a high quality result.

With the application of two connection types it is concluded that there is no optimal joint connection type. However, with the design freedom offered by AM, optimal solutions can be found to different design challenges. Furthermore, it seems advantageous to integrate the detailing in the joint as much as possible in order to increase the quality of the structure and reduce labour intensive on-site work.

Prepare for AM production

When using a topology optimization tool to design the joints, several steps need to be carried out to prepare the joint for AM production. However, the most important step to prepare topology optimized results for AM production is the smoothing of the joint.

4

COMPARISON

In chapter 3 the applied method of topology optimization and additive manufacturing for respectively the design and production of light-weight structural joints for the Złote Tarasy gridshell in Warsaw (Poland) have been discussed. The results and findings of this process are discussed in this chapter.

The chapter is divided into two sections:

1. Quantitative comparison;
2. Qualitative comparison.

Quantitative comparison

The main result of the topology optimization are the joints developed by the optimization tool BESO3D with the least amount of material possible. In the quantitative comparison the results of the applied design method will be compared with the reference case of Złote Tarasy.

Qualitative comparison

The differences between the applied method for the design and production of the topology optimized joints and a traditional method will be identified and discussed in this section.

The following two subquestions will be answered in the two sections:

4.1 What are the quantitative results by the applied design method compared with a traditional design approach?

4.2 What qualitative opportunities and pitfalls exist for the application of additive manufacturing in order to produce joints for gridshells?

4.1 QUANTITATIVE COMPARISON

The quantitative comparison will focus on two main points. First of all, the weight reduction that is obtained by the topology optimization of the joints will be discussed. Secondly, the costs of the printed joints will be estimated and compared with the original applied joints. In addition to the research on the weight reduction of the joints, the influence of this weight reduction on the behaviour of the gridshell will be examined.

4.1.1 WEIGHT OF THE JOINTS

The design of the joints by topology optimization lead to the weight of the joints as presented in Table 15. Moreover, the weight of the traditional applied joints is included. In order to calculate the total weight of the joints, the weight of the optimized joints is assumed to be an average for the total group of joints of each joint type.

Table 15: Weight of the topology optimized joints.

Joint type*	Topology optimized joints		Traditional applied joints	
	Weight (kg)	Total weight (ton)	Weight** (kg)	Total weight (ton)
1	26,7	5,3	63,1	12,6
2	13,8	4,1	47,9	14,4
3	10,6	19,0	34,4	61,9

*The number of joints for joint type 1, 2 and 3 is 200, 300 and 1800 respectively.

**Since parts of the beams are not applied anymore, this is included in the weight of the joints.

Comparing the weight of the topology optimized joints with the weight of the traditional applied joints, the weight reductions are presented in Table 16.

Table 16: Weight reduction per joint type.

Joint type	Weight reduction (kg)	Weight reduction (%)	Total weight reduction (ton)
1	36,4	57,7	7,3
2	34,2	71,3	10,2
3	23,8	69,3	42,9
Average*	26,3	68,5	
Total**			60,4

*The number of joints in each joint type (200; 300; 1800) had been used to calculate the average values.
**The total weight reduction is calculated by multiplying the weight reduction of the designed joints by the number of joints in the joint type.

In perspective, the weight reduction of the joints led to the following weight reductions on the steel structure and the entire gridshell roof:

Table 17: Weight reduction of the gridshell.

	Total weight (ton)	New weight (ton)	Total weight reduction (%)
Steel structure	630	570	9,6
Total gridshell*	1400	1340	4,3

*including steel structure, glass facade plates, gaskets, etc.

Discussion of the results

As indicated in Table 16, a large weight reduction of the joints of almost 70% has been achieved. Although the values for the weight reductions in percentage are different for the three designed joints, it is clear that quite some material can be saved. In cases where the joint is not loaded with extreme forces and moment (joint type 2 and 3), the most material can be saved.

Assuming that the weight reduction of the designed joints are an average value for the whole group of joints in each joint type, the total weight reduction of the gridshell is estimated to 60 tons (see Table 17). This implies that the weight of the steel structure has been decreased by 10% and the total weight of the structure by 4,3%.

Future consequences

In gridshells with a high joint to roof weight ratio, the influence of the weight reduction on the internal forces and moments is significant. The reference projects in subsection 2.2.3 can be used to illustrate this principle. Whereas the roofs of the reference projects consist of similar components; RHS beams, steel joints and glass panels, the ratio of the joint weight to the roof weight varies as the joints vary in weight. When assuming that topology optimizing the joints of the other projects would lead to the same weight reduction of 68,5% as for the Złoty Tarasy gridshell, the estimation for the results for the total weight reduction of the reference gridshells is presented in the following table:

Table 18: Weight reduction of other gridshell projects.

Reference project*	Joint weight (kg)	Ratio joint to roof weight (%)	Total weight reduction (%)
Palacia de Comunicaciones	70	11,0	7,5
Westfield shopping Centre	100	15,0	10,2
FrankfurtHochVier	40	6,6	4,5

*For more information concerning the joints in the reference projects, see subsection 2.3.3

As shown in Table 18, the total weight of gridshells can be reduced by applying topology optimized joints. Even up to 10% can be reduced. As the dead load of the structure is a large part of the total load on the gridshell, it is likely that for gridshells with a high joint to roof weight ratio it is possible to also optimize the gridshell resulting in smaller wall thicknesses for the beams. This again would reduce the total weight and on their terms reduces the loads on the joints even further. The following subsection will exemplify the influence of lighter joints and beams for the Złoty Tarasy gridshell.

4.1.2 GRIDSHELL OPTIMIZATION

Since the weight of the joints is reduced, the gridshell has become a lighter structure and as the designed joints behave in a similar way as the applied joints, the forces and moments in the structure are reduced. Whereas the dead load of the gridshell is a large part of the total load, the weight reduction could have a significant impact on the internal forces and moments. In the best possible scenario, this would lead to the application of smaller wall thicknesses of the RHS members. This would lead to a reduction of the loads on the joints which could again be optimized.

Small study

In order to verify the hypothesis of optimizing the RHS beams of the gridshell, a small study has been carried out. The behaviour of the Złoty Tarasy gridshell is analysed for the following two cases:

1. *Original gridshell*:   original loading conditions;
2. *Optimized gridshell*:   topology optimized joints and beams with reduced wall thickness.

In case of the *original gridshell*, no adjustments are made to the loading conditions. In case of the *optimized gridshell*, the weight of the topology optimized joints is applied. Upward directed point loads of $0,25\ kN$ are placed at the nodes to indicate the weight reduction of the joints as the average weight reduction of the joints was $26\ kg$ (Table 16).

In order to decide whether it is assumable that the wall thickness of the beams can safely be reduced, the following design assumption is used:

> *If the relative reduction of the forces in the beams is larger than the relative reduction of the cross-section of the beams, then it is possible to reduce the wall thickness of the RHS members.*

The behaviour of the gridshell is compared at three locations. The three locations correspond to the members adjacent to the representative joints that are optimized in section 3.1 (Figure 39). The applied RHS members can be found in Table 5 and the new applied RHS members in Table 19.

In this comparison the two dominant loads are examined: (i) axial force and (ii) the out-of-plane bending moment. The critical load case of the applied load cases (subsection 3.1.4) are used for the analysis of the loads:

- Joint 1: *thermal expansion;*
- Joint 2: *snow load;*
- Joint 3: *snow load.*

Table 19: Reduced wall thicknesses of the RHS members.

Member number	Joint 1	Joint 2	Joint 3
1	200x100x14,2	200x100x6,3	200x100x4,0
2	200x100x5,0	200x100x6,3	200x100x4,0
3	200x100x14,2	200x100x6,3	200x100x4,0
4	200x100x14,2	200x100x4,0	200x100x4,0
5	200x100x14,2	200x100x4,0	200x100x4,0
6	200x100x5,0	200x100x6,3	200x100x4,0

Joint 1

Figure 108 and Figure 109 depict respectively the present axial force and bending moment in the gridshell near joint 1.
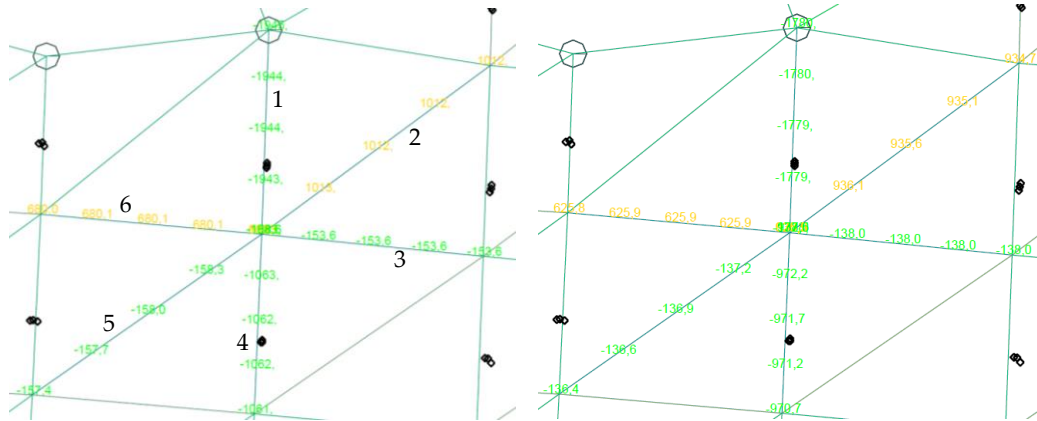

Figure 108: Joint 1 – axial force. Left: original gridshell, right: after optimization.
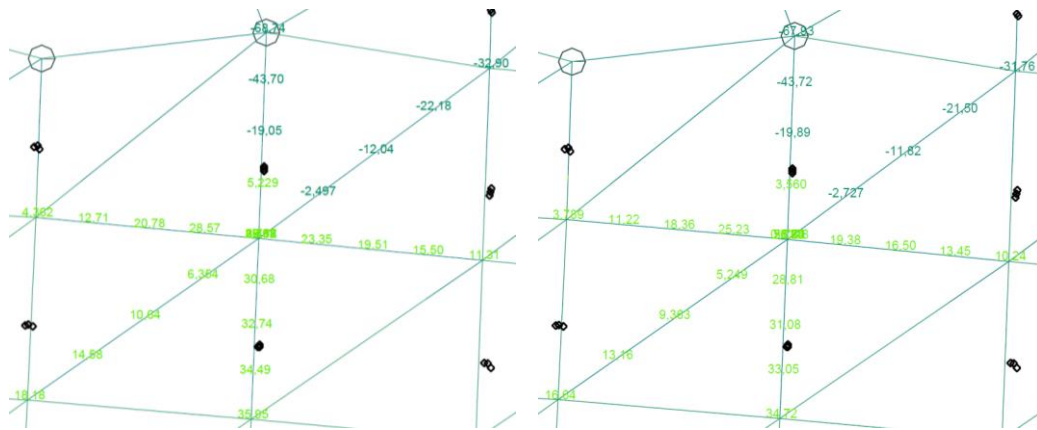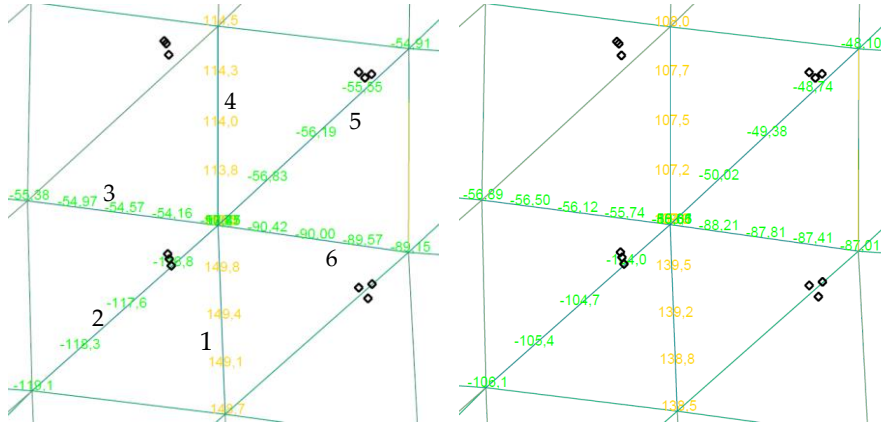

Figure 109: Joint 1 - bending moment. Left: original gridshell, right: after optimization.

The checks for joint 1 are carried out by means of comparing the different behaviour. The results are presented in Table 20 and Table 21. The reduction of the cross-section is indicated with A_{red}. F_{red} and M_{red} indicate the reduction in axial force and moment respectively.

Table 20: Joint 1 – Axial force check.

Member number	$A_{original}$ (mm²)	$A_{optimized}$ (mm²)	$F_{x,original}$ (kN)	$F_{x,optimized}$ (kN)	A_{red} (%)	F_{red} (%)	Check $F_{red} > A_{red}$
1	83,0	75,0	-1944,0	-1779,0	9,6	8,5	X
2	35,8	28,7	1012,0	935,6	19,8	7,5	X
3	83,0	75,0	-153,6	-138,0	9,6	10,2	OK
4	83,0	75,0	-1062,0	-971,7	9,6	8,5	X
5	83,0	75,0	-159,0	-136,9	9,6	13,9	OK
6	35,8	28,7	680,1	625,9	19,8	8,0	X

Table 21: Joint 1 – Bending moment check.

Member number	$A_{original}$ (mm²)	$A_{optimized}$ (mm²)	$M_{y,original}$ (kN)	$M_{y,optimized}$ (kN)	A_{red} (%)	M_{red} (%)	Check $F_{red} > A_{red}$
1	83,0	75,0	-19,1	-19,9	9,6	-4,4	X
2	35,8	28,7	-12,0	-11,8	19,8	1,8	X
3	83,0	75,0	19,5	16,5	9,6	15,4	OK
4	83,0	75,0	32,7	31,1	9,6	5,1	X
5	83,0	75,0	10,8	9,4	9,6	13,3	OK
6	35,8	28,7	20,8	18,4	19,8	11,6	X

Joint 2

Figure 110 and Figure 111 depict respectively the present axial force and bending moment in the gridshell near joint 2.

Figure 110: Joint 2 – axial force. Left: original gridshell, right: after optimization.
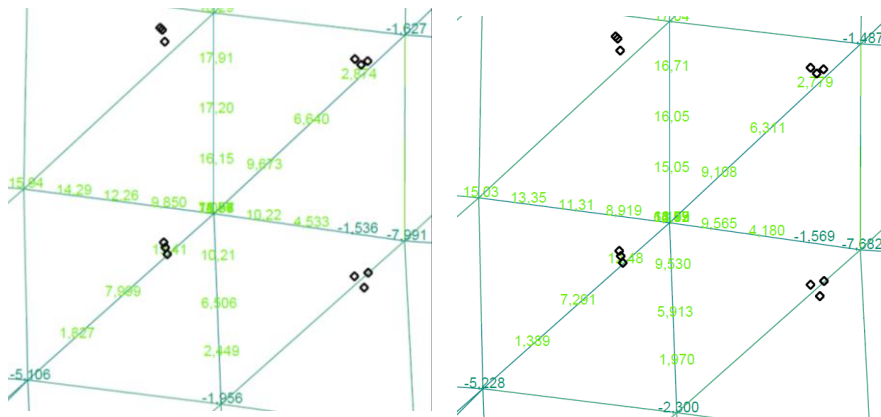

Figure 111: Joint 2 – bending moment. Left: original gridshell, right: after optimization.

The checks for joint 2 are carried out by means of comparing the different behaviour. The results are presented in Table 22 and Table 23. The reduction in cross-section, axial force and moment are indicated by A_{dec}, F_{dec} and M_{dec} respectively.

Table 22: Joint 2 – Axial force check.

Member number	$A_{original}$ (mm²)	$A_{optimized}$ (mm²)	$F_{x,original}$ (kN)	$F_{x,optimized}$ (kN)	A_{red} (%)	F_{red} (%)	Check $F_{red} > A_{red}$
1	44,8	40,0	149,4	139,2	10,7	6,8	X
2	44,8	40,0	-117,6	-104,7	10,7	11,0	OK
3	44,8	40,0	-54,6	-56,1	10,7	-2,8	X
4	28,7	23,2	114,0	107,5	19,2	5,7	X
5	28,7	23,2	-56,2	-49,4	19,2	12,1	X
6	44,8	40,0	-90,0	-87,8	10,7	2,4	X

Table 23: Joint 2 – Bending moment check.

Member number	$A_{original}$ (mm²)	$A_{optimized}$ (mm²)	$M_{y,original}$ (kN)	$M_{y,optimized}$ (kN)	A_{red} (%)	M_{red} (%)	Check $F_{red} > A_{red}$
1	44,8	40,0	6,5	5,9	11,3	9,1	X
2	44,8	40,0	8,0	7,3	10,7	9,0	X
3	44,8	40,0	12,3	11,3	10,7	7,7	X
4	28,7	23,2	17,2	16,1	19,2	6,7	X
5	28,7	23,2	6,6	6,3	19,2	5,0	X
6	44,8	40,0	4,5	4,1	10,7	9,6	X

Joint 3

Whereas bending is not present in the joint 3, only the axial forces are examined. Figure 112 depict the present axial force in the gridshell near joint 3.
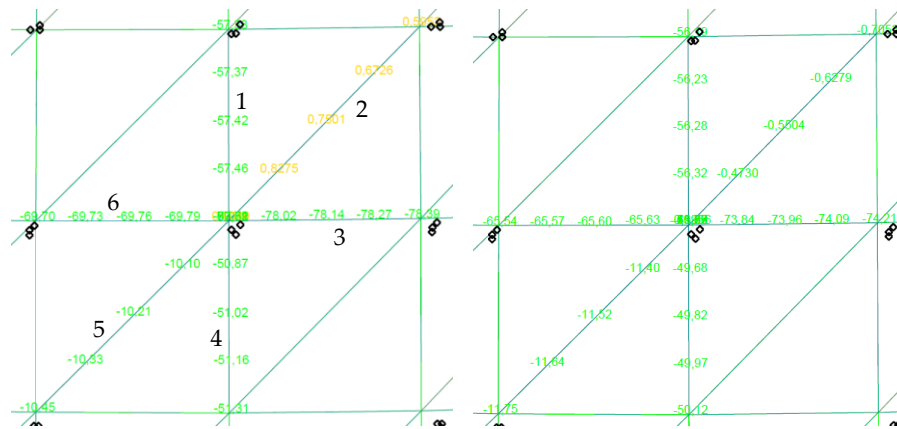

Figure 112: Joint 3 – axial force. Left: original gridshell, right: after optimization.

The checks for joint 3 are carried out by means of comparing the different behaviour. The results are presented in Table 24. The reduction in cross-section and axial force and moment are indicated by A_{dec} and F_{dec} respectively.

Table 24: Joint 3 – Axial force check.

Member number	$A_{original}$ (mm²)	$A_{optimized}$ (mm²)	$F_{x,original}$ (kN)	$F_{x,optimized}$ (kN)	A_{red} (%)	F_{red} (%)	Check $F_{red} > A_{red}$
1	28,7	23,2	-57,4	-56,3	19,2	2,0	X
2	28,7	23,2	0,8	(-)0,6	19,2	26,6	OK
3	28,7	23,2	-78,1	-74,0	19,2	5,3	X
4	28,7	23,2	-51,0	-49,8	19,2	2,4	X
5	28,7	23,2	-10,2	-11,5	19,2	-12,8	X
6	28,7	23,2	-69,8	-65,6	19,2	6,0	X

Discussion of the results

The study demonstrates that the internal forces and moments are reduced as a result of the optimization of the joints and the beams. However, in case of the Złoty Tarasy it is not possible to reduce the wall thickness of the beams.

Future consequences

The results of this study implies that due to the application and development of light-weight joints in gridshells it might be possible to optimize the beams in the grid of the gridshells. However, this will need more extensive research and simulations of the behaviour of the gridshell.

4.1.3 COSTS

In this subsection the costs of traditional designed and yet applied joints (called *traditional joint*) in the Złoty Tarasy gridshell are compared to the current costs for the joints designed by topology optimization and produced by additive manufacturing (called *AM produced joint today)*. The costs of the joints include different cost items. Not only the fabrication costs are taken into account, but additional costs that are related to the joints are included.

Since it is prospected that the costs of the production by AM will drop in the coming years due to further developments it is interesting to imply these costs (*AM produced joint in 5 years*) in the comparison as well [44]. The costs of the following three joints are compared:

1. A traditional designed joint that is applied in the gridshell of Złoty Tarasy;
2. A joint designed by topology optimization and produced by AM today;
3. The same designed joint by topology optimization and produced by AM, but in five years from now.

The results are presented in Table 25:

Table 25: Cost comparison of the three joints per cost item.

	Traditional joint	AM produced joint today	AM produced joint in 5 years
Material	€ 80	€ 1.320	€ 240
Waste material	€ 140	€ 70	€ 10
Fabrication	€ 110	€ 3.640	€ 670
Preparation beams	€ 300	€ 50	€ 50
Connection	€ 740	€ 180	€ 180
Transport	€ 50	€ 0	€ 0
Scaffolding	€ 160	€ 130	€ 130
Engineering/Inspection	€ 85	€ 110	€ 60
Totaal	*€ 1.650*	*€ 5.500*	*€ 1.350*

Appendix F.1 provides more detailed information on the different cost items. The presented cost estimation is an order of magnitude with limited information and supplier input. For the traditional joint, the costs comparison serves as a rough cost estimation. The costs for the AM produced joint today and the AM produced joint in 5 years are composed by shared information provided by the developer of AM devices Arcam. Arcam mentions that this is dependent on different aspects. Although influencing aspects are beyond perspective at this moment, it is possible to identify presumed developments with respect to AM techniques:

- AM techniques will evolve, with developments such as:
  - Increasing print speed (estimated to increase by a factor 10) because of:
    - Application of multiple lasers in the same building chamber;
    - Application of higher power lasers beams;
  - Larger building chamber which;
  - Improved application of different materials in the same product;
  - New materials will become available;
- Growing interest in AM produced products;
- The number of suppliers on the market will increase.

Erection speed

An aspect that is not included in the cost comparison of the joints is the difference in erection speed when applying the newly designed joints instead of the traditional applied joints. As complex and time-consuming welding on site (limited welding access due to small angles, overhead welding and working at a large height) is avoided, the newly designed joints make it possible to shorten the construction period. By creating a faster erection scheme, the structure is earlier completed. This implies that higher initial expenditure (printing of the joints) can be offset by earlier cashing of revenues and a reduction in labour, equipment, and overhead costs. This is illustrated in Figure 113 that schematically shows the cash flow CF and it gives an indication of the cash balance CB (the costs that are not directly related to the joints are not taken into account). It is clear that the cash balance will become positive in an earlier stadium resulting in a higher net present value of the project, i.e., the difference between the present value (corrected for time) of incoming and the present value of outgoing cash flows.

The erection of the steelwork of the Złoty Tarasy gridshell with the traditional joints was finished in 7 months. This period was partly used for hoisting in the ladders and partly for the welding of the beams to the joints. Due to encountered difficulties during installation, it is estimated that a large part of the erection time was required for the application of the welds. It is expected that 5 months were required to apply all the welds.

In case of bolted connections, the erection speed is much faster and the expected time to complete the steelwork of the gridshell will be reduced to 4 months. The time to install the connecting beams between the ladders is reduced to 2 months while the time to lift the ladders into place remains the same.

Extra revenue

By assuming that the erection and completion of the gridshell is on the critical path of the project, it implies that areas under the gridshell roof and adjacent areas can earlier be put into service. Therefore revenues can earlier be cashed as shown in Figure 113. To give an estimation for these revenue R the following calculation is made:

- The amount of lettable floor area in Złoty Tarasy is: 78000 m^2;
- The rental price in Złoty Tarasy is 30 $€/m^2$ [45].

With the maximum amount m^2 rented, the revenue R per month can be calculated:

$$R = 78.000 \cdot 30 = 2.340.000 \text{ €}$$

Since the complex can be put into service up to three months earlier, the total revenue becomes significant. Assuming that 50% of the revenue can be considered as a benefit B that could be attributed to the joint design, the total benefit per joint becomes:

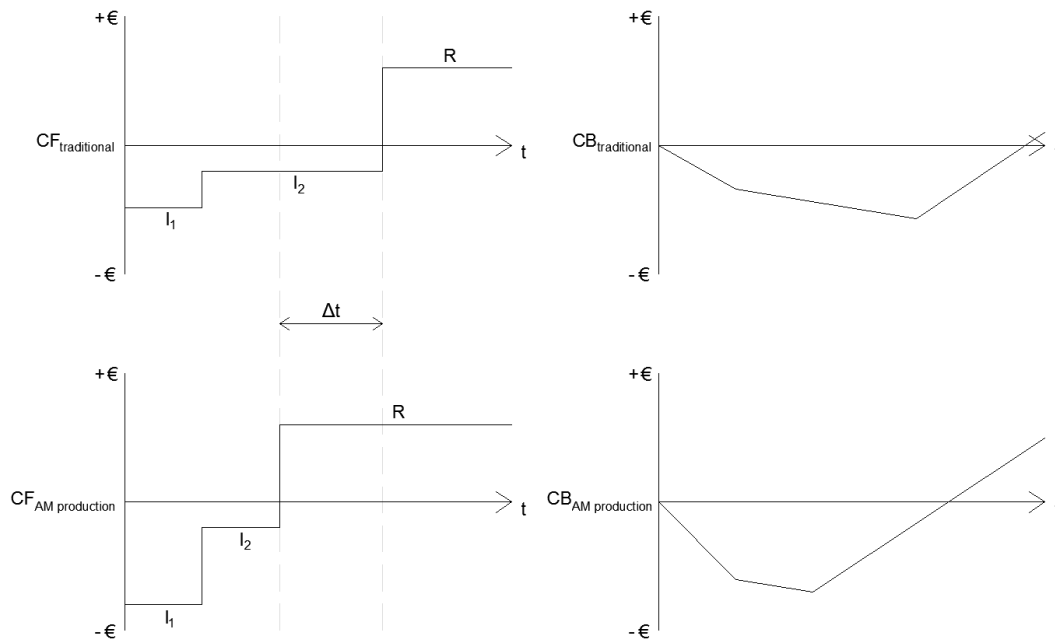$$B_{total} = 2.340.000 \cdot 3 \cdot 0,5/2300 \approx 1500 \text{ €}$$

+€

R

$CF_{traditional}$ ⟶ t

I_2

I_1

-€

+€

$CB_{traditional}$ ⟶ t

-€

Δt

+€

R

$CF_{AM\ production}$ ⟶ t

I_2

I_1

-€

+€

$CB_{AM\ production}$ ⟶ t

-€

Figure 113: The diagrams at the left schematically indicate the cash flow (top: traditional joints, bottom: AM produced joints. The diagrams at the right schematically indicate the corresponding cash balance for the two cases (top: traditional joint, bottom: AM produced joints. (Note: discount rate is not taken into account)

Discussion of the results

Compared to the costs for the traditional joints, the costs to produce the joints by the AM technique DMLS are high. This is mainly caused by the long printing time and the expensive material. However, considering the rapid developments it is reasonable to assume that these costs are expected to drop to a level that the costs for the joint are even lower than traditionally produced joints.

Also, it is demonstrated that improving the erection scheme could lead to reasonable benefits. In this study the joints are improved with respect to the traditional joints in the applied situation. However, this could certainly be further improved by developing new kind of connections such as click-connections, applied in high voltage towers. These can be designed in a custom-made manner, which is now possible due to the design-freedom that is offered by AM.

Future consequences

As a future consequence to the presented cost comparison it is likely that 3D printing of specialised building elements in steel or other metal, such as joints for gridshells, will become cost advantageous in the near future. It is not expected that linear building elements such as standard profiles will be produced by AM techniques as the current techniques to manufacture such products are more efficient.

Moreover, in case of projects were only a gridshell is built, such as the renovation projects as British Museum, Palacia de Comunicaciones, the erection time can significantly be reduced leading to profitable situations.

4.2 QUALITATIVE COMPARISON

In the qualitative comparison multiple topics in the design and manufacturing process of joints in free-form gridshells will be discussed and compared. This qualitative analysis is based on the findings discovered during the research of the thesis subject. The qualitative comparison is added with other relevant topics. These added topics were not possible to quantify and are therefore only qualitatively explained.

4.2.1 DESIGN

This subsection discusses different aspects in the design stage of the joints.

Design opportunities

Possible design solutions for the joints are increased when AM is applied for the production of the joints. This is due to the design freedom offered by AM. The perfect example is the production of the topology optimized joints. Unique light-weight geometrically complex structures are developed by the topology optimization tool. Such structures are difficult or impossible to be produced by conventional production techniques.

Although the topology optimization tool is used to obtain the required shape of the joint, the main design challenges remain with the detailing of the joint. This is similar for traditional produced joints as well as AM produced joints. For these purposes the advantage of AM is that multiple design solutions can be applied on different locations in the same structure. As showcased, an improved erection scheme can be achieved because of the application of a hybrid solution (bolts and welds). Although this would normally increase the complexity and the costs of the production, the two types of connections can be manufactured without increasing the costs of the joints.

An additional advantage of production by AM over traditional production methods is the possibility to integrate functions and thereby reduce the labour-intensive assembly of different parts. An example is the weld preparations and gusset plates that are part of the design and would directly be printed to the joint. This advantage could give a complete new dimension to structural elements by integrating functions of other building disciplines, such as the integration of ducts, lighting and connections for façade elements.

On the other hand, the AM design opportunities are restricted by the high costs related to the production of one kilogram metal by AM today. Therefore large objects are not likely to be fabricated. Even for small objects, it is wise to reduce the volume of the object as much as possible. Hence, in most cases it is beneficial to combine AM with topology optimization in order to avoid superfluous material. Another design restriction is the size of the building chamber. The dimensions of the produced parts are limited to around $400x400x400\ mm$ at the moment.

Design approach

A consequence of the offered design opportunities is that a new mindset should be applied during the design of structural elements. Compared to the traditional design approach, designers and engineers can focus on the answer to the design. The advantages of AM can now fully been utilized to develop parts with increased performances that could offset the relatively high costs of printing.

Although freedom of shape is offered by AM, designers should be aware of the fact that most designs cannot directly be manufactured as created initially by design software. In most cases post-processing of the design is required to prepare for actual manufacturing, including the addition of a support structure as part of the design to support overhang and dissipate heat to prevent the part from warping. Well-designed parts are developed when such rules are taken into account during the design process.

Costs

Comparing the costs of a solid metal block produced by traditional production techniques to the same metal block produced by AM, the costs for the AM produced block are relatively high. However, when an object with a highly complex geometrical structure assembled from many traditionally produced parts is compared with an AM produced part that could be printed in one go, the costs may be in favour of the AM produced part. Moreover, an AM produced part that is designed by topology optimization could save costs through its entire lifetime which is therefore able to offset higher initial expenditure.

Engineering

Joints designed by topology optimization tools are customized and need individual analysis. In contrast to a traditional approach where only a critical joint are designed, more calculations need to be performed. The optimization process will need to be carried out repeatedly and although computational power has increased enormously in the last years, the required computational time for all the joints is considerably higher than in traditional methods.

Robustness

By optimizing the topology of the joints, based on a unique set of loads, all 'unnecessary' material will be removed. With TO, the unity check for the applied material is below, but close to 1. This implies that the redundancy of the structure is reduced.

A result of the TO is that highly accurate calculations are performed and the internal forces and moments are well known. On the other hand, uncertainties with respect to the behaviour of the joint or the produced material by AM, could lead to issues. Hence, by assuming that the used model has correct set-up, the result of the optimization process will be safe when applying the right load cases.

Secondly, when the structural redundancy is reduced, the structure is often less suitable for a change in function of the building. This is the case as a prescribed set of load cases, related to a specified function of the building, has been used. Therefore, structural optimization seems to

be suitable in cases where the prescribed set of load cases do not change during the life span of the structure. However, gridshells are often intended as transparent covers or roofs. If the function of the building changes, this will likely not affect the loads on the roof structure.

Automated processes

Compared to a traditional approach, a lot more attention should be paid to setting up a well-functioning automated process when applying topology optimization. In comparison, in the design process of the Westfield shopping centre (subsection 2.2.3) the geometry of the joint is set up by extracting geometrical data from the structural model of the gridshell. However, the process to develop the final shapes of the joints in case of the application of topology optimization is much more complex. Next to the higher work load, more steps have to be linked and multiple computer software will be involved such as 3D modelling, FEA and topology optimization software. Therefore computational software experts with a structural background will become more important and need to be more intensively involved in the design process than in traditional cases.

Aesthetics

Topology optimized joints could provide a special aesthetical experience since the application is not used in any other building project before. Architects might prefer to show such details of the structure. In some architectural trends free-form topology optimized shapes could contribute to the architecture of the building.

Sustainability

Compared to traditional joints, several advantages can be distinguished. First, the topology optimized joints require less material. Second, there is hardly any waste material produced by the production of AM. Only the powder that creates the final part will be melted with the exemption of a little amount for support structures. Unused powder is filtered and returned to the AM machine that can use this powder for new parts. Third, transport and storage of building elements can be reduced because AM machines can easily be shipped to a desired location (shop or building site), reducing emissions.

On the other hand, in contrast to conventional manufacturing techniques, extra energy is required to produce the metal powder for the AM machines and to melt the material. As the pros and cons concerning sustainability needs to be weighted it is recommended to conduct further research on this topic.

4.2.2 PRODUCTION

This subsection discusses different aspects in the production stage of the joints.

Material

For the production of the traditional joint steel is used. This is due to the fact that there is a lot of experience with this material and the costs of the material are relatively low. Applying other metals would become too expensive.

In case of design and production by topology optimization and additive manufacturing, the material with the best suiting properties can be selected. It might even be possible to cooperate with material suppliers to develop a specific material for a specific design purpose [46]. However, this would increase costs.

Tools

In most production processes tools are necessary. In case of the traditional joints, an applied tool is the developed cutting robot to produce the set of unique joints. In case of AM produced joints no tools are necessary. In fact, the AM machine can be considered as the tool that can perform any kind of functions.

Lead time

The lead time for the joints produced by AM can be very short as no tools (such as the cutting robot) need to be prepared or developed. Assuming that the desired material is readily available, a prepared model can be send to an AM device and production can start instantly.

However, the actual printing is rather slow. Multiple AM machines are required to produce a large number of joints. In contrast to the production of the traditional joints, only one cutting robot is required.

Replacement

Since the lead time for a joint produced by AM is very short, missing, damaged or defected joints can very quickly be replaced. This might be more difficult for the traditional produced joints. The cutting robot is needed to produce new joints, which can be difficult in the case that the robot is defect, removed or used for other purposes.

Indication of parts

For both the methods, unique joints are produced which need to be registered and indicated in order to know the exact place and orientation of each particular part. In case of the conventional production methods these indications are done by hand. Due to the large amount of unique joints, joints can by mistake get indicated with the wrong indication leading to problems at the site. In contrast, the joints produced by AM, can directly be indicated by a number and orientation by means of printing letters or signs on the joints. In this way, human errors are reduced when indicating and installing the joints.

4.3 CONCLUSION

This section provides answers to the following subquestions:

4.1 What are the quantitative results by the applied design method compared with a traditional design approach?

4.2 What qualitative opportunities and pitfalls exist for the application of additive manufacturing in order to produce joints for gridshells?

Quantitative comparison

A comparison of the weight of the joints shows that it is possible to apply topology optimized joints that are significantly lighter than traditional joints. The weight of the joints was reduced by an average of almost 70%. This weight reduction could even lead to a reduction of the wall thicknesses of the RHS members for gridshells with high joint to roof weight ratios.

By comparing the costs of the production of topology optimized joints by additive manufacturing with the traditionally produced joints, it became clear that the costs for AM produced joints are higher today. However, for purposes in the near future, AM produced joints seem to be advantageous and the costs might become lower than traditionally produced joints.

The main reason for the high costs of the AM produced joints is that the production of the joints is currently time consuming. Nevertheless, it is interesting to note that many benefits can be obtained today, e.g., reduced labour for the preparations of the beams, an improved connection method between the joints and the beams, and a reduction of waste material and scaffolding.

Qualitative comparison

The quantitative comparison of the costs of the AM produced joints is supplemented by a qualitative comparison. Concluded is that the main opportunity is the offered design freedom. The design freedom can fully be utilized in order to reduce costs of different items in the production, preparation and installation of the joints. Moreover, the offered design freedom enables the possibility to produce such highly complex shapes that outperform current production techniques.

Important is to indicate that designers need to be aware of the design rules for AM production. Also, using topology optimization for the design of the joints will require high computational times. Setting up a an automated process is therefore recommendable.

5

DISCUSSION

5.1 ANSWER TO THE RESEARCH QUESTION

Anticipating the potential benefits that additive manufacturing offers for the production of structural joints for gridshells, this study is concerned with the following research question:

What opportunities are created by additive manufacturing in the design and production process of structural joints in gridshells?

Based on this work, the research question can be answered:

The opportunity of additive manufacturing is that lighter joints for gridshells can be developed and improved solutions for detailing can be found. This reduces the weight of the structure, labour intensity and it speeds up the erection process. Although the use of additive manufacturing of structural joints for gridshells is not cost efficient yet, it can be in the near future when printing speed goes up and material costs go down.

5.2 CONCLUSIONS

More specifically the following is concluded:

- With the use of additive manufacturing, the design of structural joints is no longer limited by current production restrictions. AM enables the production of highly complex shapes. The required material of the joint can be minimized by using topology optimization. This results in lighter joints for gridshells. In case of the Złoty Tarasy gridshell, an average weight reduction of almost 70% can be obtained.

- With the use of AM, designers and engineers can develop innovative solutions for design problems. Detailing can easily be adjusted to different requirements. To this extent, a hybrid solution was developed that used welded and bolted connections. The result is an improved erection scheme with a shorter construction period.

- In case of large joint-to-roof weight ratios, it seems feasible that the wall thicknesses of the applied RHS members of the gridshell can be reduced, as a result of the application of topology optimized joints. In this way, loads on the joints are reduced, which enables to further reduce the weight of the joints.

- The high costs associated with the AM production of joints is not yet compensated by the reduction of labour costs. It is expected that new generation AM machines will have higher printing speeds, which will reduce costs of printing.

Regarding the applied method with the topology optimization tool BESO3D and the used classification system, the following is concluded:

- BESO3D can be used to develop topology optimized shapes for joints in gridshells. However, additional input is required to improve the effectiveness of the results.

- To improve the accuracy of the numerical models of the optimized joints, BESO3D needs to accept higher order mesh element types to prevent numerical errors.

- With the applied method it is not feasible to optimize a large set of joints, since the verification of the joints in an iterative process. Checking results after the optimization process was time-consuming.

- The joint classification system is a useful way to determine the behaviour of topology optimized joints in gridshells. However, certain approved optimized shapes seem to lack shear capacity. Therefore, it seems reasonable to assume that extra criteria, with regard to the shear stiffness and strength of the joint, should be added to the classification system to guarantee the behaviour of the joint.

5.3 RECOMMENDATIONS

Recommendations can be made for the building industry, educational institutions and software developers.

Engineers and designers in the building industry

It would be recommended to:

- Consider the use of AM for the design and production of structural joints in gridshells. In this way light-weight joints can be developed that could reduce the wall thickness of the applied members in the gridshell. Also, labour costs can be reduced and erection schemes improved.

- Expand the joint classification method in order to obtain a general set of design rules for joints in gridshells.

- Cooperate with suppliers of AM technologies. In this way an AM machine can be developed that is specialized for needs in the building industry. This could result in lower costs for the production of metal objects.

- Inspire clients and investors to realise a prototype project with AM produced structural elements. A successful prototype project will increase the confidence in AM for purposes in the building industry.

- Start a dialogue with parties in the aviation industry. Applied design rules for critical components in airplanes could lead to approved design rules for structural elements produced by AM in building structures.

- Be aware of the fact that computer models are still a means in the design process. Verification of numerical results by applying engineering sense and rules of thumb is in every situation highly recommendable.

Educational institutions

It would be recommended to:

- Implement the subject of AM production in education programme. It is reasonable to assume that the future generation of engineers will work with AM techniques.

- Purchase an AM machine in order to explore and obtain practical knowledge.

Software developers

It would be recommended to:

- Implement geometrical and physical non-linear behaviour in optimization software;

- Set-up links between: 3D modelling space – FEM environment – optimization tool.

5.4 PROPOSED APPLICATION

Buildings containing canopies over their courtyards are often well-known (British Museum in London, Maritime Museum in Amsterdam) and contain a special architectural value.

Taking the obtained results of this study into account, a recommendation is given for the best possible application of topology optimized joints produced by AM in the near future:

Apply AM produced joints in a renovation project to cover a courtyard because:

- The weight reduction of the gridshell is of vital importance to limit loads on the existing foundation and superstructure;
- The erection time, and so the shut-down time of the building, will be shortened due to an optimized erection scheme;
- Innovative structural elements can contribute to the publicity of the building;

5.5 FUTURE OUTLINE AND RESEARCH

Different steps will be required to eventually realise buildings with structural elements produced by additive manufacturing. At the moment, this is an innovative production technique that has not yet been applied for structural purposes in the building industry. Experience with this technique is lacking and precedents are not available.

According to the Dutch codes (Bouwbesluit) a building requires to reach a sufficient level of safety. The Bouwbesluit is setting out requirements and refers to the Eurocode for verification. However, the Eurocode does not yet contain any rules with respect to AM produced building elements. Therefore, in order to realise a building with AM produced elements, the equal level of safety of the structure needs to be proven. In order to do so, extensive additional tests on the material and on prototype joints will need to be performed.

Future studies will contribute to the feasibility and reliability of the design and production of structural elements by AM. The following topics require future research:

- Calibration of used computer models by performing tests on prototypes;
- Development of a specific topology optimization tool for gridshell structures;
- Research on the influence of shear deformation for joints in gridshells with limited shear resistance;
- Determine the influence of the weight reduction of the joints on the optimization of the beams in the gridshell;
- Extensive cost analysis and monitoring of future developments and influencing factors of AM techniques focussed on the building industry;
- Extensive testing of AM produced materials;
- Analysis of risks concerning AM production methods;
- Optimization of the connection between the joint and the beam;
- Comparison of different AM techniques and investigation on next generation AM machines.

6

BIBLIOGRAPHY

6.1 MAIN REPORT

[1]   Avio   Aero,   "Additive   Manufacturing,"   2015.   [Online].   Available:
        https://www.avioaero.com/What/Additive-Manufacturing.

[2]   S.   Nathan,   "Printing   Parts,"   2011.   [Online].   Available:
        http://www.technologyreview.com/demo/425133/printing-parts/.

[3]   P. J. Knippers and T. Helbig, "Recent Developments in the Design of Glazed Grid
        Shells," *Intern. J. Sp. Struct.*, vol. 24, no. 2, 2009.

[4]   Eindhoven University of Technology, "Optimization Form and Grid Gridshell," 2014.
        [Online].   Available: http://www.tue.nl/en/university/departments/built-
        environment/the-department-of-the-built-environment/organization/units/structural-
        design/education/final-thesis/projects/isd/optimization-form-and-grid-gridshell/.

[5]   M. Beckh and R. Barthel, "The First Doubly Curved Gridshell Structure - Shukhovs
        Building for the Plate Rolling Workshop in Vyksa," no. May, Munich, 2009.

[6]   M. Rinaldi, "Joe and Rika Mansueto library by Murphy / Jahn," 2013. [Online].
        Available: http://aasarchitecture.com/2012/11/joe-and-rika-mansueto-library-by-
        murphy-jahn.html.

[7]   J. Hennicke, J. Matsushita, and F. Otto, *Gitterschalen Gridshells*. Stuttgart: Institut für
        Leichte Flächentragwerke, 1974.

[8]   E. Barkanov, "Introduction the finite element method," Riga, 2001.

[9]   M. Bechtold, *Innovative Surface Strutures - Technologies and Applications*. Taylor & Francis,
        2008.

[10]   C. Paoli, "Past and Future of Grid Shell Structures," Ecole Spéciale des Travaux Publics,
        Paris, 2007.

[11]   KARAMBA3D, "How virtual becomes real in gridshell design," 2015. [Online].
        Available: http://www.karamba3d.com/how-virtual-becomes-real-in-gridshell-design/.

[12]   M. Schlaich, "Conceptual design of light-weight structures," in *LSAA*, 2011.

[13]   J. Blaauwendraad and J. H. Hoefakker, *Structural Shell Analysis*, vol. 200. Dordrecht: Springer Netherlands, 2014.

[14]   New York Architecture, "Shigeru Ban." [Online]. Available: http://www.nyc-architecture.com/ARCH/ARCH-Shigero.htm.

[15]   S. Brell-cokcan, H. Schmiedhofer, and A. Schiftner, "Structurize – Planarize - Materialize," *Innov. Des. Constr. Technol. - Build. complex shapes beyeond*, 2009.

[16]   T. Bulenda and J. Knippers, "Stability of grid shells," *Comput. Struct.*, vol. 79, no. 12, pp. 1161–1174, May 2001.

[17]   M. Schlaich, U. Burkhardt, L. Irisarri, and J. Goñi, "Palacio de Comunicaciones – a single layer glass grid shell over the courtyard of the future town hall of Madrid," *Int. Assoc. Shell Spat. Struct. Symp. 2009, Val.*, no. October, pp. 1338–1348, 2009.

[18]   F. Fan, H. Ma, Z. Cao, and S. Shen, "A new classification system for the joints used in lattice shells," *Thin-Walled Struct.*, vol. 49, no. 12, pp. 1544–1553, Dec. 2011.

[19]   M. Kalanchiam and B. Mannai, "Topology Optimization of Aircraft Fuselage Structure," *World Acad. Sci. Eng. Technol.*, vol. 7, pp. 133–136, 2013.

[20]   X. Huang and Y. M. Xie, *Evolutionary Topology Optimization of Continuum Structures*. Wiley, 2010.

[21]   J. Lundgren and C. Palmqvist, "Structural Form Optimisation," Chalmers University of Technology, 2012.

[22]   M. Langelaar, F. Van Keulen, N. Van Dijk, E. Hooijkamp, A. Verbart, and F. Van Kempen, "Topology Optimization - A natural counterpart of additive manufacturing," 2013.

[23]   M. P. Bendsøe and O. Sigmund, *Topology Optimization - Theory, Methods and Applications*. Springer-Verlag, 2003.

[24]   G. I. N. Rozvany, "A critical review of established methods of structural topology optimization," *Struct. Multidiscip. Optim.*, vol. 37, no. 3, pp. 217–237, Feb. 2008.

[25]   F. Van Keulen, M. Langelaar, and G. E. Van Baars, "TOPOLOGY OPTIMIZATION AND ADDITIVE MANUFACTURING , State-of-the-Art and Challenges," in *28th Annual Meeting of the American Society for Precision Engineering*, 2013, pp. 2–3.

[26]   S. Galjaard, S. Hofman, and S. Ren, "New Opportunities to Optimize Structural Designs in Metal by Using Additive Manufacturing," in *AAG 2014*, 2014.

[27]   T. Wohlers, *Wohlers Report 2010*. Wohlers Associates, 2010.

[28]   THRE3D, "How direct metal laser sintering (DMLS) works." [Online]. Available: https://thre3d.com/how-it-works/powder-bed-fusion/direct-metal-laser-sintering-dmls.

[29]   H. Strauß, "AM Envelope - The potential of Additive Manufacturing for façade construction," Delft University of Technology, 2013.

[30]   N. Hopkinson and P. Dickens, "Analysis of rapid manufacturing — using layer," *Mech. Eng. Sci.*, vol. 217, pp. 31–39, 2003.

[31]   EOS, "Additive Manufacturing - For Technology-Interested." [Online]. Available: http://www.eos.info/additive_manufacturing/for_technology_interested.

[32]   RepRap, "Fused filament fabrication." [Online]. Available: http://reprap.org/wiki/Fused_filament_fabrication.

[33]   D. Anderson, Z. Czajewski, S. Clarke, I. Feltham, P. Geeson, M. Karczmarczyk, R. Kent, D. Killion, Z. Kotynia, M. Lewonowski, R. Lindsay, P. Monypenny, C. Murgatroyd, J. Ojeil, R. Orlowski, A. Sitko, and D. Woolf, "Zlote Tarasy, Warsaw , Poland," *Arup J.*, vol. 1, 2008.

[34]   Retail Info Poland Sp., "Zloty Tarasy," 2015. [Online]. Available: http://zlote-tarasy.promoceny.pl/.

[35]   Robert McNeel & Associates, "Rhinoceros." 2014.

[36]   Robert McNeel & Associates, "Grasshopper." 2014.

[37]   Oasys, "Oasys GSA suite." 2014.

[38]   Dassault Systèmes, "Abaqus/CAE 6.13-1." Providence, RI, USA, 2013.

[39]   Y. M. Xie, "BESO3D." 2014.

[40]   European committee for standardization, *Eurocode 3: Design of steel structures - Part 1-8: Design of joints*, vol. 8, no. 2005. 2011.

[41]   Martens Transport Oosterhout b.v., "Vergunning en ontheffingen," 2015. [Online]. Available: http://martenstransport.nl/exceptioneel_transport/vergunningen.

[42]   M.J. van Riel, "Breedte transporten," 2013. [Online]. Available: http://www.mjvanriel.nl/vanriel/19-Breedte-transport---pagina-12.aspx.

[43]   W. H. Minnick, *Gas Metal Arc Welding Handbook*, 5th ed. Goodheart-Willcox Publisher, 2008.

[44]   Goed PolHome O.G., "INHOUD :"

6.2 APPENDICES

[1] G. Croci, "Seismic behaviour of masonry domes and vaults Hagia Sophia in Istanbul and St. Francis in Assisi," Geneva, Sep-2006.

[2] Somastruct, "Arches of the Foot," 2015. [Online]. Available: http://www.somastruct.com/wp-content/uploads/2012/06/archload1.jpg.

[3] Crystalinks, "The Roman Pantheon." [Online]. Available: http://www.crystalinks.com/romepantheon.html.

[4] Tesla Memorial Society of New York, "Hagia Sophia." [Online]. Available: http://www.teslasociety.com/hagiasophia.htm.

[5] Tectónica-online, "Les estructuras de edificación de Eduardo Torroja Miret," 2012. [Online]. Available: http://tectonicablog.com/?p=43146.

[6] B. Peerdeman, "Analysis of Thin Concrete Shells Revisited: Opportunities due to Innovations in Materials and Analysis Methods," Delft University of Technology, 2008.

[7] M. Beckh and R. Barthel, "The First Doubly Curved Gridshell Structure - Shukhovs Building for the Plate Rolling Workshop in Vyksa," no. May, Munich, 2009.

[8] R. Graefe, *Netzdächer, Hängedächer und Gitterschalen*. 1990, p. 48.

[9] C. Paoli, "Past and Future of Grid Shell Structures," Ecole Spéciale des Travaux Publics, Paris, 2007.

[10] M. Bechtold, *Innovative Surface Strutures - Technologies and Applications*. Taylor & Francis, 2008.

[11] J. Blaauwendraad and J. H. Hoefakker, *Structural Shell Analysis*, vol. 200. Dordrecht: Springer Netherlands, 2014.

[12] M. Y. H. Bangash and T. Bangash, *Elements of spatial structures*. Thomas Telford, 2003.

[13] T. Bulenda and J. Knippers, "Stability of grid shells," *Comput. Struct.*, vol. 79, no. 12, pp. 1161–1174, May 2001.

[14] A. López, I. Puente, and M. a. Serna, "Numerical model and experimental tests on single-layer latticed domes with semi-rigid joints," *Comput. Struct.*, vol. 85, no. 7–8, pp. 360–374, Apr. 2007.

[15] J. Cai, Y. Xu, J. Feng, and J. Zhang, "Nonlinear stability of a single-layer hybrid grid shell," *J. Civ. Eng. Manag.*, vol. 18, no. 5, pp. 752–760, Oct. 2012.

[16] M. P. Bendsøe and O. Sigmund, *Topology Optimization - Theory, Methods and Applications*. Springer-Verlag, 2003.

[17] J. Lundgren and C. Palmqvist, "Structural Form Optimization," Chalmers University of Technology, 2012.

[18] X. Huang and Y. M. Xie, *Evolutionary Topology Optimization of Continuum Structures*. Wiley, 2010.

[19] K. Suzuki and N. Kikuchi, "A homogenization method for shape and topology optimization," *Comput. Methods Appl. Mech. Eng.*, vol. 93, pp. 291–318, 1991.

[20] M. Y. Wang, X. Wang, and D. Guo, "A level set method for structural topology optimization," *Comput. Methods Appl. Mech. Eng.*, vol. 192, no. 1–2, pp. 227–246, Jan. 2003.

[21] H. Strauß, "AM Envelope - The potential of Additive Manufacturing for façade construction," Delft University of Technology, 2013.

[22] J. P. Kruth, L. Froyen, J. Van Vaerenbergh, P. Mercelis, M. Rombouts, and B. Lauwers, "Selective laser melting of iron-based powder," *J. Mater. Process. Technol.*, vol. 149, no. 1–3, pp. 616–622, Jun. 2004.

[23] RepRap, "Fused filament fabrication." [Online]. Available: http://reprap.org/wiki/Fused_filament_fabrication.

[24] Y. Kaya, "popular3Dprinters.com," 2013. [Online]. Available: http://www.popular3dprinters.com/electron-beam-freeform-fabrication/.

[25] BeAM, "Industrialise your manufacturing & repair processes with our CLAD systems," 2013. [Online]. Available: http://www.beam-machines.fr/uk/en/innovation/techology.html.

[26] Ultimaker, "Cura." 2015.

[27] S. Fiebig and J. K. Axmann, "Using a binary material model for stress constraints and nonlinearities up to crash in topology optimization," in *10th World Congress on Structural and Multidisciplinary Optimization*, 2013.

[28] Z. H. Zuo, "BESO2D." 2014.

[29] A. Van Beek, "Schroefverbinding met bedrijfslast," 2015. [Online]. Available: http://www.tribologie.nl/calculators/e3_6c.htm.

[30] A. Van Beek, "Joint stiffness factor," 2015. [Online]. Available: http://www.tribologie.nl/calculators/e3_6h.htm.

APPENDICES

<div style="text-align: right">

A

</div>

GRIDSHELLS

A.1 HISTORY

A.1.1 SHELLS

The first shell type structures are dating back to 3000 BC. In Spain and Portugal beehive tombs (Figure 1) were used for burial rituals. They were followed by beehive houses in Ireland and Scotland from around 2000 BC. Both types of structures were built by piling up blocks of stone.

In the Roman period, the construction of many arches for aqueducts and amphitheatres brought the Romans the knowledge of transferring out-of-plane forces by normal forces to the foundation (Figure 2). This resulted in the construction of the oldest known concrete shell structure: the Roman Pantheon (Figure 3). With a span of 43 meters it is an incredible piece of engineering considering the moment of construction in ± 125 AC.

In Istanbul another example of outstanding classical engineering can be found. With its 32 m span, the Haga Sophia dome (Figure 4) is still an impressive structure. Started in the 6th century, the construction of the dome is different to the Roman Pantheon as it is supported by hemidomes, abutments and pendentives. This is due to the fact that the dome of the Haga Sophia is supported on four large columns instead of a solid base of the Roman Pantheon [1].
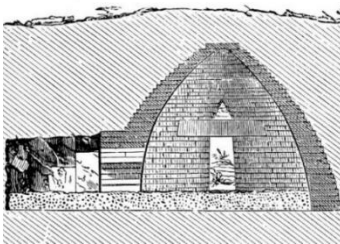
Figure 1: Beehive tombs (±3000 BC).
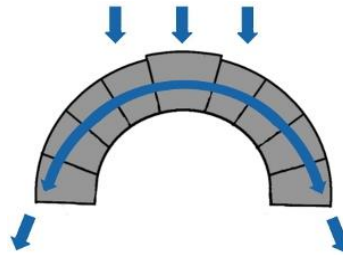
Figure 2: Structural principle of an arch [2].

Figure 3: The Roman Pantheon (±125 AC) [3].

Figure 4: Interior of the Haga Sophia (6th century) [4].

Figure 5: Hangar by Nervi in Orbetello (1935). Photo: Eche Martinez
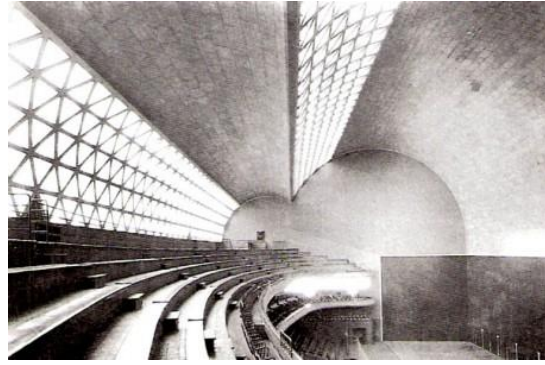
Figure 6: Frontón Recoletos by Torroja in Madrid (1935) [5].

Figure 7: L'Oceanogràfic by Candela in Valencia (2003). Photo: Felipe Gabaldón

Figure 8: Garden center Wyss by Isler in Zuchwil (1962). © Chriusha

The use of vaults and domes continued during the Byzantium empire, the Romanesque and Gothic period, the Renaissance and the Baroque era. The invention of reinforced concrete eventually led to a new period in the early 20th century. The development of theoretical understanding and improved computational possibilities were also of great influence. This resulted in longer spans and thinner shells, but also in the possibility to design free-form and BLOB architecture. Some famous engineer architects explored the design freedom they were offered. Examples are Pier Luigi Nervi (1891-1979), Eduardo Torroja (1899-1961), Felix Candela (1910-1997) and Heinz Isler (1926-2009) who designed and constructed advanced concrete shells [6].

A.1.2 GRIDSHELLS

In the second half of the 19th century the first gridshell structures appeared. When daylight sources are desired, it is obvious that a gridshell is preferred over a closed concrete shell. In 1890, Vladimir Shukhov constructed two steel single curved gridshells with a span of approximately 9 m to cover two pump stations in Grozny. In 1897, Shukhov was able to build the first steel doubly curved gridshell (Figure 9) in the world. The footprint of this production hall for a steelwork company in Vyksa was 73,0x38,4 m and consisted of five 14.6 m wide bays [7].

Although Shukhov introduced the double curved gridshell he did not yet make fully use of the structural advantage of the double curvature as he neglected the positive impact of the curvature in cross-direction. In contrast to Shukhovs gridshell in Vyksa, the Mannheim Multihalle (Figure 10), designed by Frei Otto, made perfectly use of its double curvature.

97
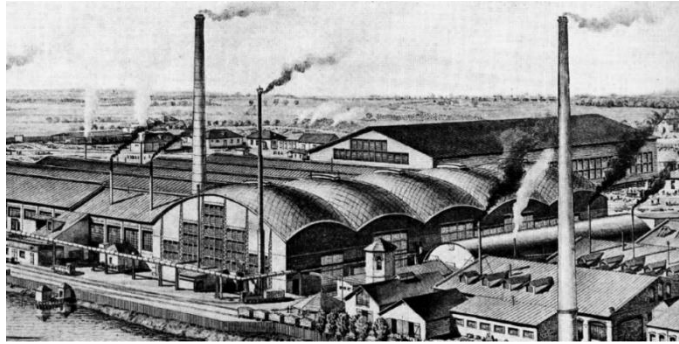
Figure 9: The first doubly curved gridshell by Vladimir Shukhov in Vyksa (1897) [8].

This was achieved by using scale models during the form finding process in order to find the optimal shape. Otto developed models with different forms and shapes to study the behaviour of the grid of the structure. He used small loads which represented the weight of the structure (Figure 11). In contrast to steel gridshells, wooden gridshells can be assembled to a flat math on the ground. By pushing the boundaries into place of the supports the gridshell can take its tri-dimensional shape [9].

Having found the desired shape of the structure of the Multihalle, Otto worked together with the consultancy firm Arup to study the behaviour of the gridshell by computer analysis. Over the last decades computer software gained momentum and physical scale models are no longer necessary. Today, free-form gridshells are very popular and without a doubt a way to create attractive (public) spaces. Examples are the well-known Queen Elizabeth II Great Court (Figure 12), covering the court of the British Museum in London and the Kogod Courtyard (Figure 13) at the Smithsonian American Art Museum in Washington.

Figure 10: Mannheim Multihalle by Frei Otto (1975). © SMD Arquitectes
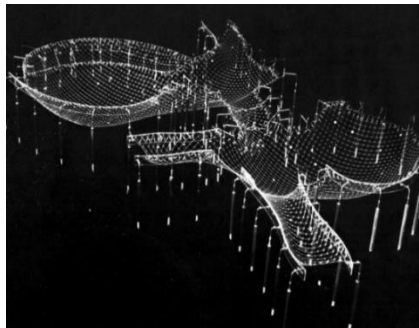
Figure 11: Hanging scale model of the Mannheim Multihalle. © SMD Arquitectes

Figure 12: British Museum in London (2000). (Photo: Andrew Dunn)

Figure 13: Smithsonian's Kogod Courtyard in Washington (2007). (Photo: Timothy Hursley)

A.2 SURFACE CLASSIFICATION

Surfaces of free-form gridshells can have any kind of geometry. Despite of the fact that free-form gridshells are most likely composed of different kind of surfaces, it is possible to classify the different surface geometries. With the understanding of surface geometries, understanding of structural surfaces is obtained as the surface curvature is directly related to the stiffness of the surface [10].

Surface curvatures can be measured by determining the curvature in different points on the surface. In any point P on the surface there is exactly one line that is perpendicular to the surface. An infinite number of planes can be placed, containing the perpendicular line and intersecting in P. In a complex surface the curvatures will be of different magnitude which are related to the radius R by $k = \frac{1}{R}$. There are two orthogonal normal sections oriented such that one radius of curvature R_1 is the maximum of all possible, whereas the other radius of curvature R_2 is the minimal of all possible. The intersecting curves are called *curves of principle section*. The associated curvatures, k_1 and k_2, are called the *principle curvatures* in P [10].

In 1827, Karl Friedrich Gauss published a theory on the specification of surfaces. He called the multiplication of the principle curvatures the *Gaussian curvature k_G*:

$$k_G = \frac{1}{R_1} \cdot \frac{1}{R_2} = k_1 \cdot k_2$$

Gauss defined the following types of surfaces (Figure 14):

- $k_G > 0$, a positive Gaussian curvature. The principle curvatures are in the same direction and the surface is called *synclastic*;
- $k_G = 0$, a Gaussian curvature of zero. The surface is curved in one direction, i.e., one of the principle curvatures is infinite and the surface is called *monoclastic*;
- $k_G < 0$, a negative Gaussian curvature. The principle curvatures are in opposite direction and the surface is called *anticlastic*.

Remarkably, monoclastic surfaces can be changed into a plane form and are therefore called *developable surfaces.* This is not the case for *non-developable surfaces* as synclastic and anticlastic surfaces which will need cutting and/or stretching of the middle plane to be changed into a plane form. This characteristic of non-developable surfaces has an interesting structural consequence. As there is more external energy required to deform a non-developable surface, they are usually stronger and more stable than developable surfaces [11].

Moreover, synclastic and anticlastic surfaces can be compared. Synclastic surfaces carry loads by meridional (compression or tension) and circumferential stresses. Anticlastic surfaces however, make use of a combination between compression in one direction and tension in the other direction. The result of this equilibrium between compression and tension is a stiffer behaviour of the surface.

For all the surfaces hold that the degree of curvature affects the stiffness of the surface. When a surface is more curved it implies that it is a stiffer surface. Therefore, loads on flat or slightly curved surfaces could lead to large deformations.
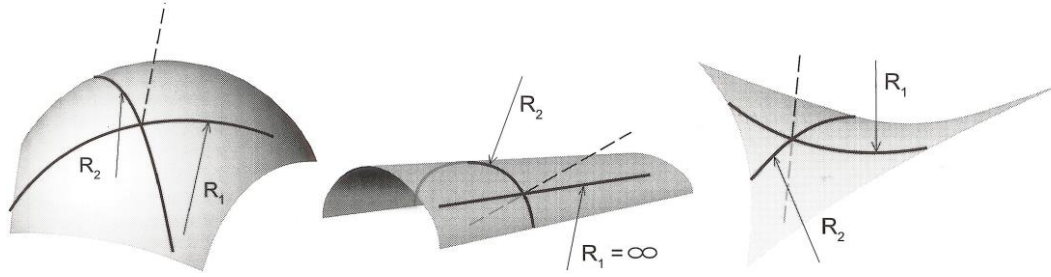
Figure 14: Types of Gaussian curvature [10].
Left: $k_G > 0$; synclastic.   *Middle: $k_G = 0$; monoclastic.*   *Right: $k_G < 0$; anticlastic.*

A.3   ANALYTIC RELATIONS

The following sections discuss the analytic relations of the membrane, bending and shell theory. Below one can find a list with notations and sign conventions which are applied in the theories.

A.3.1   NOTATION AND SIGN CONVENTIONS

For stresses and forces holds:

- For the stresses and forces two indices are used. The direction of the face on which the stress or force acts is the first indicator. The second indicator belongs to the direction in which the stress is acting;
- When a stress or force acts in the positive direction on a plane with the normal vector in the positive coordinate direction, it is positive;
- When a stress or force acts in the negative direction on a plane with the normal vector in the negative coordinate direction, it is also positive.

For moments and shear forces holds:

- The same notation is applied to moments and shear forces as for stresses and forces;
- For the transverse shear forces one indicator is used. The normal to the face on which the shear force acts is indicated by the subscript.
- When a bending moment causes bending stress at the positive z-side of the middle plane, it is positive;
- When a twisting moment causes shear stress at the positive z-side of the middle plane, it is positive;
- When a transverse shear force acts in the positive z-direction on a face with positive normal, it is positive.

The positive forces and moments on a shell element are given in Figure 15.
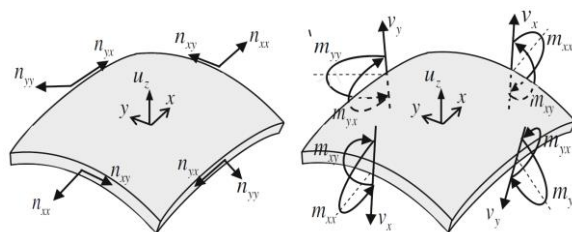
Figure 15: Forces and moments in a shell element [11].

100

A.3.2 MEMBRANE THEORY

In a smoothly curved shell it is possible to develop a pure membrane stress field when certain loading and boundary conditions are met. The presence of such a pure membrane stress field is the basic assumption of the membrane theory, i.e., only normal and in-plane forces are present. Furthermore, the following assumptions are made [12]:

1. Points lying on a normal of the middle surface before the deformation will be on a straight line after the deformation has taken place.
2. This line will remain perpendicular to the deformed middle surface.
3. Displacements are small compared to the thickness of the shell

A shell element with arbitrary curvatures, k_x and k_y, will be considered. The curvatures, k_x and k_y, are taken in the x- and y-direction of the reference system respectively. They are related to the radius of curvature in x-direction k_x and y-direction k_y. The twist of the shell element is defined as k_{xy}. The x-axis and y-axis are tangent to the middle surface. The z-axis is normal to the middle surface of the shell element. The loads are defined in x-, y- and z-direction as p_x, p_y and p_z. Deformations of the middle surface are defined by u_x, u_y and u_z. Where p_x, u_x and p_y, u_y are in-plane loads/displacements, p_z and u_z are an out-of-plane load/displacement. When the shell is loaded, normal stresses σ_{xx}, σ_{yy} and shear stresses σ_{xy}, σ_{yx} occur in the shell element. The stresses are integrated over the thickness yield n_{xx}, n_{yy}, n_{xy}, n_{yx} and generate corresponding strains ε_{xx}, ε_{yy}, γ_{xy}. The notation and sign conventions are listed in the previous paragraph.

The above mentioned quantities can be summarized into four vectors which lay down the membrane behaviour of shell structures by three basic relations:

$$u = \begin{bmatrix} u_x & u_y & u_z \end{bmatrix}^T \qquad (1)$$

$$p = \begin{bmatrix} p_x & p_y & p_z \end{bmatrix}^T \qquad (2)$$

$$e = \begin{bmatrix} \varepsilon_{xx} & \varepsilon_{yy} & \gamma_{xy} \end{bmatrix}^T \qquad (3)$$

$$s = \begin{bmatrix} n_{xx} & n_{yy} & n_{xy} \end{bmatrix}^T \qquad (4)$$

The first of three basic relations is the *kinematic relation* which relates the strains ε to displacements u. Secondly, the *constitutive relation* connects membrane forces s to strains ε. Thirdly, the *equilibrium relation* describes the relation between the intern membrane forces s to the extern load components p.
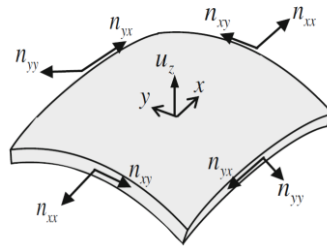
Figure 16: Membrane forces in an infinite shell element [11].

Kinematic relation

The kinematic relation is the relation between the strains ε and the displacements u, which can symbolically written as:

$$e = Bu \qquad (5)$$

Due to the tangential displacements u_x and u_y, and the normal displacement u_z we can derive the associated strains.

Similar to in-plane loaded plates, the terms for the strains due to the tangential displacements can quickly be found by:

$$\varepsilon_{xx} = \frac{\partial u_x}{\partial x}, \quad \varepsilon_{yy} = \frac{\partial u_y}{\partial y}, \quad \gamma_{xy} = \frac{\partial u_x}{\partial y} + \frac{\partial u_y}{\partial x} \qquad (6)$$

To investigate the influence of the normal deflection u_z we will consider an infinitesimal shell element which can be found when we take the normal plane through the x-axis and the shell, Figure 17. The shell element has unit width and length $2d_x$.

Due to the displacement u_z, length dx increases to $dx + de_x$. The curve/inclination of the shell element in the x, z-plane is defined as $\varphi_x = -\partial z/\delta x$. For the incremental change of inclination over the distance dx we can find the following expressions:

$$d\varphi_x = -\frac{\partial^2 z}{\partial x^2} dx \qquad (7)$$

The change of length is $de_x = u_z d\varphi_x$, which leads to:

$$de_x = -\frac{\partial^2 z}{\partial x^2} dx \cdot u_z \qquad (8)$$

Now we have find the change of length of the shell element we can find the strain of the middle service:

$$\varepsilon_{xx} = \frac{de_x}{dx} = -\frac{\partial^2 z}{\partial x^2} \cdot u_z \qquad (9)$$

In combination with the curvature $k_x = \frac{\partial^2 z}{\partial x^2}$ equation (9) yields:

$$\varepsilon_{xx} = -k_x u_z \qquad (10)$$

Whereas the derivations are related to a shell element which has been specified by the normal plane through the x-axis, the same can be done by the normal plane through the y-axis. Following the same steps as equations (7, 8, 9, 10) it is possible to find the following to equations:

$$\varepsilon_{yy} = -k_y u_z \qquad (11)$$

$$d\varphi_y = -\frac{\partial^2 z}{\partial y^2} dy \qquad (12)$$
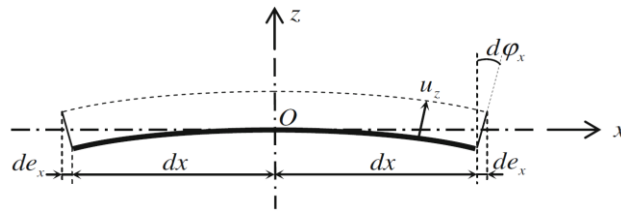
Figure 17: Effect of normal displacement u_z on an infinitesimal curved shell element [11].

To study the influence of the normal displacement u_z on the shear strain we will consider an infinitesimal twisted shell element, Figure 18. Corresponding to the curved shell element, the inclinations of the twisted shell element are $\varphi_x = -\delta z/\delta x$ and $\varphi_y = -\delta z/\delta y$ in x- and y-direction respectively. For the change of the inclination φ_x in y-direction we can find and the inclination φ_y in x-direction:

$$d\varphi_x = -\frac{\partial^2 z}{\partial y \partial x} dy, \quad d\varphi_x = -\frac{\partial^2 z}{\partial x \partial y} dx \qquad (13)$$

Figure 18 shows the deformations de_x and de_y of the edges of the shell element, which is caused by the normal displacement u_z. The deformation of the edges lead to deform the rectangular middle surface of the shell element into a rhombus. The shear strains can be derived by:

$$\varepsilon_{xy} = \frac{de_x}{dy}, \quad \varepsilon_{yx} = \frac{de_y}{dx} \qquad (14)$$

With

$$de_x = d\varphi_x\, u_z, \quad de_y = d\varphi_y\, u_z \qquad (15)$$

With equation (13, 14, 15) we can prove that $\varepsilon_{xy} = \varepsilon_{yx}$, which yields for the strain $\gamma_{xy} = \varepsilon_{xy} + \varepsilon_{yx}$. With $k_{xy} = \frac{\partial^2 z}{\partial x \partial y}$ we find:

$$\gamma_{xy} = -2k_{xy}u_z \qquad (16)$$
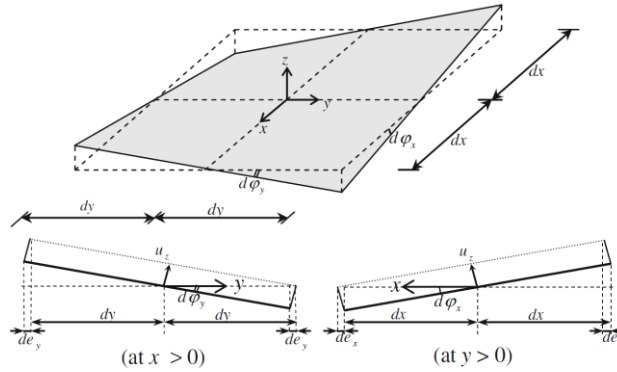
Figure 18: Effect of normal displacement u_z on an infinitesimal twisted shell element [11].
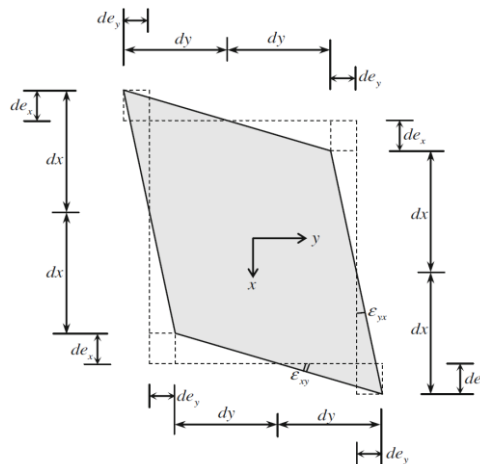
Figure 19: Normal displacement u_z leading to shear deformation of the middle surface [11].

The *kinematic relation* $\boldsymbol{e} = \boldsymbol{Bu}$ is defined by the equations (6, 10, 11, 16):

$$\begin{bmatrix} \varepsilon_{xx} \\ \varepsilon_{yy} \\ \gamma_{xy} \end{bmatrix} = \begin{bmatrix} \dfrac{\partial}{\partial x} & 0 & -k_x \\ 0 & \dfrac{\partial}{\partial y} & -k_y \\ \dfrac{\partial}{\partial y} & \dfrac{\partial}{\partial x} & -2k_{xy} \end{bmatrix} \begin{bmatrix} u_x \\ u_y \\ u_z \end{bmatrix} \tag{17}$$

With

$$k_x = \frac{\partial^2 z}{\partial x^2}, \quad k_y = \frac{\partial^2 z}{\partial y^2}, \quad k_{xy} = \frac{\partial^2 z}{\partial x \partial y} \tag{18}$$

Constitutive relation

The *constitutive relation* is symbolically expressed as:

$$\boldsymbol{s} = \boldsymbol{De} \tag{19}$$

The assumption is made that the shell material behaves according to Hooke's law. Hooke's law lays down the relation between the membrane stresses and the strains ε. When the membrane stresses are multiplied over the thickness we find:

$$\begin{bmatrix} n_{xx} \\ n_{yy} \\ n_{xy} \end{bmatrix} = \frac{Et}{1-v^2} \begin{bmatrix} 1 & v & 0 \\ v & 1 & 0 \\ 0 & 0 & \dfrac{1-v}{2} \end{bmatrix} \begin{bmatrix} \varepsilon_{xx} \\ \varepsilon_{yy} \\ \gamma_{xy} \end{bmatrix} \tag{20}$$

Equilibrium relation

The equilibrium relation between the intern membrane forces s and the external load components p is symbolically written as:

$$\boldsymbol{B}^* \boldsymbol{s} = \boldsymbol{p} \tag{21}$$

For the load components p_x and p_y we can set up the equilibrium equations:

$$\frac{\partial n_{xx}}{\partial x} + \frac{\partial n_{yx}}{\partial y} + p_x = 0, \quad \frac{\partial n_{xy}}{\partial x} + \frac{\partial n_{yy}}{\partial y} + p_y = 0 \tag{22}$$

For the load component in z-direction, the influence of the curvatures k_x and k_y, and the twist k_{xy} will be considered.

For the influence of the curvature we will consider Figure 20. The membrane forces n_{xx} in a shell part with unit width and length d_x cause a downward resultant $n_{xx}d\varphi_x$. This resultant is in equilibrium with the upward force p_z acting over d_x:

$$p_z dx - n_{xx} d\varphi_x = 0 \tag{23}$$

With equation (7) and the expression for k_x in equation (18) we find:

$$k_x n_{xx} + p_z = 0 \tag{24}$$

Following the same steps for a shell strip with unit width in y-direction we can obtain:

$$k_y n_{yy} + p_z = 0 \tag{25}$$

When taking a shell part with dimensions d_x and d_y we notice that the downward resultant $n_{xx}d\varphi_x$ works over a width d_y and $n_{yy}d\varphi_y$ over d_x. The equilibrium of the shell part is:

$$p_z dx dy + n_{xx} \varphi_x dy + n_{yy} d\varphi_y dx = 0 \qquad (26)$$

With equations (7, 12) and the expression for k_x and k_y in equation (18) we find:

$$k_x n_{xx} + k_y n_{yy} + p_z = 0 \qquad (27)$$

To investigate the influence of the shear membrane forces in a twisted shell part we consider Figure 21. The two forces n_{xy} at $x = 0$ and at $x = dx$ have a downward resultant $n_{xy}\varphi_y$ which act over a width dx. Similarly, in y-direction $n_{yx}\varphi_x$ occurs over a width dy. We can set up the equilibrium relation for the twisted shell part:

$$p_z dx dy + (n_{xy}\varphi_y)dx + (n_{yx}d\varphi_x)dy = 0 \qquad (28)$$

With equation (13) and the expression for k_{xy} in equation (18) we can derive:

$$2k_{xy}n_{xy} + p_z = 0 \qquad (29)$$

The *equilibrium relation* $\boldsymbol{B}^*\boldsymbol{s} = \boldsymbol{p}$ is defined by the equations (22, 27, 29):

$$\begin{bmatrix} -\dfrac{\partial}{\partial x} & 0 & -\dfrac{\partial}{\partial y} \\ 0 & -\dfrac{\partial}{\partial y} & -\dfrac{\partial}{\partial x} \\ -k_x & -k_y & -2k_{xy} \end{bmatrix} \begin{bmatrix} n_{xx} \\ n_{yy} \\ n_{xy} \end{bmatrix} = \begin{bmatrix} p_x \\ p_y \\ p_z \end{bmatrix} \qquad \boldsymbol{B}^*\boldsymbol{s} = \boldsymbol{p} \qquad (30)$$

Note: the matrix $\boldsymbol{B}^*$ is the adjoint of matrix $\boldsymbol{B}$ in equation (17).
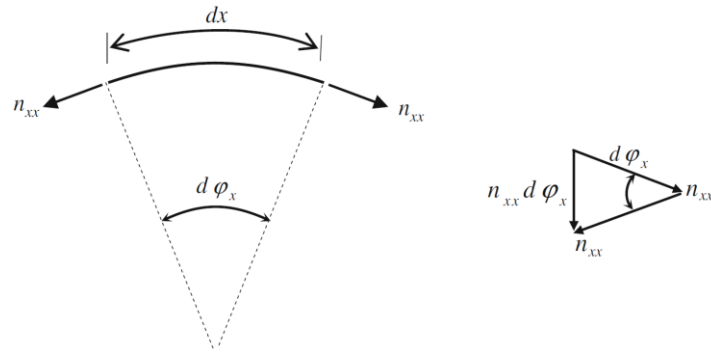
Figure 20: Membrane forces caused by the curvature of the shell [11].
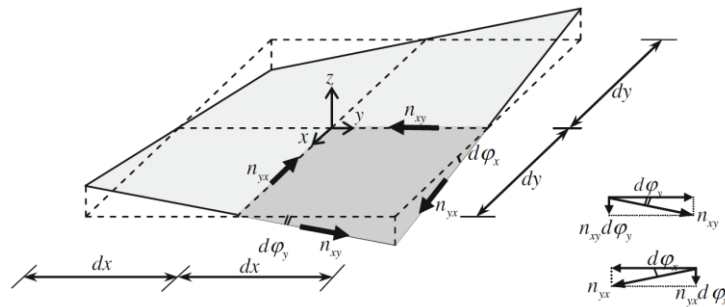
Figure 21: Shear membrane forces in a twisted shell part [11].

A.3.3 BENDING THEORY

Bending moments do not carry the applied load, but are compensating for the shortcoming of the membrane behaviour. These disturbances of the membrane field are locally. They can be caused by deformation constraints and boundary conditions which are incompatible with the requirements of a pure membrane field. Also concentrated forces, changes in geometry and abrupt changes in curvature are leading to bending moments [11].

A shell element with arbitrary curvatures, k_x and k_y, will be considered. The curvatures, k_x and k_y, are taken in the x- and y-direction of the reference system respectively. They are related to the radius of curvature in x-direction k_x and y-direction k_y. The twist of the shell element is defined as k_{xy}. The x-axis and y-axis are tangent to the middle surface. The z-axis is normal to the middle surface of the shell element. The loads are defined in x-, y- and z-direction as p_x, p_y and p_z, whereas the loads p_x and p_y are equal to zero. Deformations of the middle surface are defined by u_x, u_y and u_z. Where u_x and u_y are in-plane displacements, p_z and u_z are an out-of-plane load/displacement. When the shell is loaded, bending moments m_{xx}, m_{yy}, torsion moments m_{xy}, m_{yx} and lateral shear forces v_x, v_y occur in the shell element. The deformations are presented by κ_{xx}, κ_{yy}, ρ_{xy}. The notation and sign conventions are listed in section 'Analytic relations' in this appendix.

The above mentioned quantities can be summarized into four vectors which lay down the bending behaviour of shell structures by three basic relations.

$$u = \begin{bmatrix} u_x & u_y & u_z \end{bmatrix}^T \qquad (31)$$

$$p = \begin{bmatrix} p_x & p_y & p_z \end{bmatrix}^T \qquad (32)$$

$$e = \begin{bmatrix} \kappa_{xx} & \kappa_{yy} & \rho_{xy} \end{bmatrix}^T \qquad (33)$$

$$s = \begin{bmatrix} m_{xx} & m_{yy} & m_{xy} \end{bmatrix}^T \qquad (34)$$
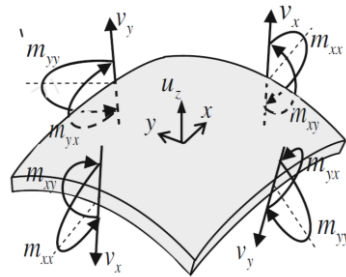
Figure 22: Moments and shear forces in an infinite shell element [11].

Kinematic relation

The kinematic relation is the relation between the strains ε and the displacements u, which can symbolically written as:

$$e = Bu \qquad (35)$$

The kinematic relation of the bending theory of shells resembles the bending theory of plates. For a curved shell element, like in Figure 17, it is possible to derive that the curvature κ is equal to minus the second derivative of the displacement u_z. For the curvatures in x- and y-direction we can derive respectively:

$$\kappa_{xx} = \frac{\partial \varphi_x}{\partial x} = -\frac{\partial^2 u_z}{\partial x^2} \qquad (36)$$

$$\kappa_{yy} = \frac{\partial \varphi_y}{\partial y} = -\frac{\partial^2 u_z}{\partial y^2} \qquad (37)$$

The twist due to the torsional moments is equal to:

$$\rho_{xy} = \frac{\partial \varphi_x}{\partial x} + \frac{\partial \varphi_y}{\partial y} = -2\frac{\partial^2 u_z}{\partial x \partial y} \qquad (38)$$

The kinematic relation yields:

$$\begin{bmatrix} \kappa_{xx} \\ \kappa_{yy} \\ \rho_{xy} \end{bmatrix} = \begin{bmatrix} 0 & 0 & -\dfrac{\partial^2}{\partial x^2} \\ 0 & 0 & -\dfrac{\partial^2}{\partial x^2} \\ 0 & 0 & -2\dfrac{\partial^2}{\partial x \partial y} \end{bmatrix} \begin{bmatrix} u_x \\ u_y \\ u_z \end{bmatrix} \qquad e = Bu \qquad (39)$$

Constitutive relation

The *constitutive relation* is symbolically expressed as:

$$s = De \qquad (40)$$

The assumption is made that the shell material behaves according to Hooke's law. Hooke's law lays down the relation between the stresses and the strains ε. When the stresses are multiplied over the thickness, we find a constitutive relation which is equal to the plate bending constitutive relation:

$$\begin{bmatrix} m_{xx} \\ m_{yy} \\ m_{xy} \end{bmatrix} = \begin{bmatrix} D_b & \nu D_b & 0 \\ \nu D_b & D_b & 0 \\ 0 & 0 & D_b\left(\dfrac{1-\nu}{2}\right) \end{bmatrix} \begin{bmatrix} \kappa_{xx} \\ \kappa_{yy} \\ \rho_{xy} \end{bmatrix} \qquad s = De \qquad (41)$$

With the flexural rigidity D_b:

$$D_b = \frac{Et^3}{12(1-\nu^2)} \qquad (42)$$

Equilibrium relation

The equilibrium relation describes the relation between the moments, out-of-plane shear stresses s and to the external load components p:

$$B^*s = p \qquad (43)$$

An infinite shell element, shown in Figure 22, will be considered to set up the equilibrium relation.

The applied load p_z makes equilibrium with the out-of-plane shear forces:

$$\frac{\partial v_x}{\partial x} + \frac{\partial v_y}{\partial y} + p_z = 0 \tag{44}$$

The equilibrium of moments in respectively x- and y-direction can be derived:

$$\frac{\partial m_{xx}}{\partial x} + \frac{\partial m_{yx}}{\partial y} - v_x = 0 \tag{45}$$

$$\frac{\partial m_{yy}}{\partial y} + \frac{\partial m_{xy}}{\partial x} - v_y = 0 \tag{46}$$

By replacing the terms of the shear forces in equation 5 by the equilibrium equations for the moments we find the total equilibrium relation for a shell in bending:

$$\begin{bmatrix} 0 & 0 & 0 \\ 0 & 0 & 0 \\ -\dfrac{\partial^2}{\partial x^2} & -\dfrac{\partial^2}{\partial y^2} & -2\dfrac{\partial^2}{\partial x \partial y} \end{bmatrix} \begin{bmatrix} m_{xx} \\ m_{yy} \\ m_{xy} \end{bmatrix} = \begin{bmatrix} p_x \\ p_y \\ p_z \end{bmatrix} \qquad \boldsymbol{B^* s = p} \tag{47}$$

A.3.4 SHELL THEORY

The shell theory consist of three basic relations (Figure 23). Firstly, the *kinematic relation* which relates the strains e to displacements u. Secondly, the *constitutive relation* connects the internal membrane forces s to strains e. Thirdly, the *equilibrium relation* describes the relation between the internal membrane forces s to the extern load components p. The vectors of the displacements, strains, membrane forces and external loads are:

$$u = \begin{bmatrix} u_x & u_y & u_z \end{bmatrix}^T \tag{49}$$

$$p = \begin{bmatrix} p_x & p_y & p_z \end{bmatrix}^T \tag{50}$$

$$e = \begin{bmatrix} \varepsilon_{xx} & \varepsilon_{yy} & \gamma_{xy} & \kappa_{xx} & \kappa_{yy} & \rho_{xy} \end{bmatrix}^T \tag{51}$$

$$s = \begin{bmatrix} n_{xx} & n_{yy} & n_{xy} & m_{xx} & m_{yy} & m_{xy} \end{bmatrix}^T \tag{52}$$

An infinite shell element will be considered. The shell element has arbitrary curvatures and dimensions d_x, d_y. This implies that change of curvature κ_{xx} and κ_{yy}, and change of twist ρ_{xy} are present. Due to the external load components p_x, p_y and p_z, the shell will deform in x-, y- and z-direction: u_x, u_y and u_z. The deformations cause in-plane normal and shear forces n_{xx}, n_{yy}, n_{xy} and out-of-plane bending and twisting moments m_{xx}, m_{yy}, m_{xy}. Figure 24 shows the infinite shell element with positive direction of forces and moments. The complete explanation of the notations and sign conventions is included in paragraph 'Analytic relations' in this appendix.
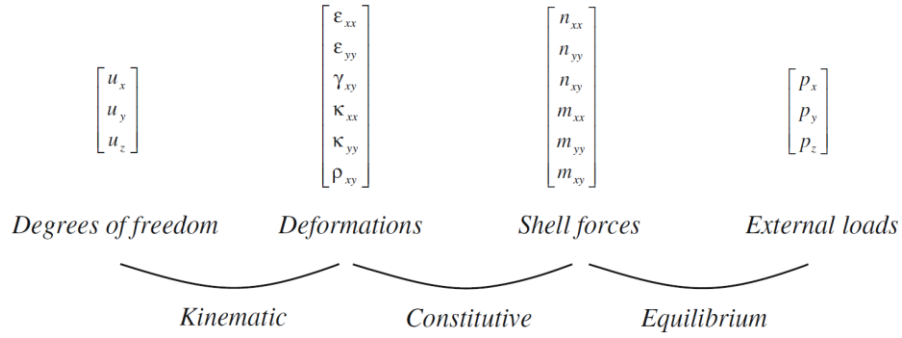
Figure 23: Relations in shell theory [11].
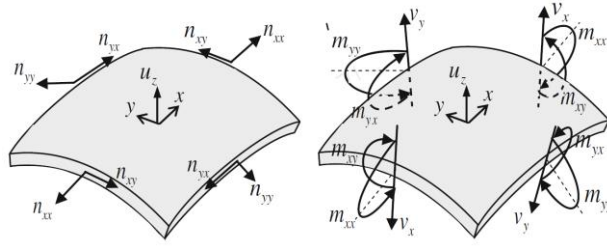
Figure 24: Internal forces and moments on a shell element [11].

Kinematic relation

The kinematic relation is the relation between the strains ε and the displacements u, which can symbolically written as:

$$e = Bu \qquad (53)$$

The membrane behaviour is described by:

$$\varepsilon_{xx} = \frac{\partial u_x}{\partial x} - \kappa_x u_z \qquad (54)$$

$$\varepsilon_{yy} = \frac{\partial u_y}{\partial y} - \kappa_y u_z \qquad (55)$$

$$\gamma_{xy} = \frac{\partial u_x}{\partial y} + \frac{\partial u_y}{\partial x} - 2\kappa_{xy} u_z \qquad (56)$$

The curvatures of the shell element

$$\varphi_x = -\frac{\delta u_z}{\delta x} \qquad (57)$$

$$\varphi_y = -\frac{\delta u_z}{\delta y} \qquad (58)$$

are used to derive the bending deformations:

$$\kappa_{xx} = \frac{\partial \varphi_x}{\partial x} = -\frac{\partial^2 u_z}{\partial x^2} \qquad (59)$$

$$\kappa_{yy} = \frac{\partial u_y}{\partial y} - k_y u_z \qquad (60)$$

$$\gamma_{xy} = \frac{\partial u_x}{\partial y} + \frac{\partial u_y}{\partial x} - 2k_{xy} u_z \qquad (61)$$

With the equations for the membrane and the bending behaviour the kinematic relation can be written as follows:

109

$$
\begin{bmatrix} \varepsilon_{xx} \\ \varepsilon_{yy} \\ \gamma_{xy} \\ \kappa_{xx} \\ \kappa_{yy} \\ \rho_{xy} \end{bmatrix} = \begin{bmatrix} \dfrac{\partial}{\partial x} & 0 & -k_x \\[2mm] 0 & \dfrac{\partial}{\partial y} & -k_y \\[2mm] \dfrac{\partial}{\partial y} & \dfrac{\partial}{\partial x} & -2k_{xy} \\[2mm] 0 & 0 & -\dfrac{\partial^2}{\partial x^2} \\[2mm] 0 & 0 & -\dfrac{\partial^2}{\partial y^2} \\[2mm] 0 & 0 & -2\dfrac{\partial^2}{\partial x \partial y} \end{bmatrix} \begin{bmatrix} u_x \\ u_y \\ u_z \end{bmatrix} \qquad \boldsymbol{e = Bu} \qquad\qquad (\,62\,)
$$

Constitutive relation

The *constitutive relation* is symbolically expressed as:

$$
\boldsymbol{s = De} \qquad\qquad (\,63\,)
$$

The assumption is made that the shell material behaves according to Hooke's law. Hooke's law lays down the relation between the stresses and the strains ε. When the stresses are multiplied over the thickness we find:

$$
\begin{bmatrix} n_{xx} \\ n_{yy} \\ n_{xy} \\ m_{xx} \\ m_{yy} \\ m_{xy} \end{bmatrix} = \begin{bmatrix} D_m & \nu D_m & 0 & 0 & 0 & 0 \\[1mm] \nu D_m & D_m & 0 & 0 & 0 & 0 \\[1mm] 0 & 0 & D_m\left(\dfrac{1-\nu}{2}\right) & 0 & 0 & 0 \\[1mm] 0 & 0 & 0 & D_b & \nu D_b & 0 \\[1mm] 0 & 0 & 0 & \nu D_b & D_b & 0 \\[1mm] 0 & 0 & 0 & 0 & 0 & D_b\left(\dfrac{1-\nu}{2}\right) \end{bmatrix} \begin{bmatrix} \varepsilon_{xx} \\ \varepsilon_{yy} \\ \gamma_{xy} \\ \kappa_{xx} \\ \kappa_{yy} \\ \rho_{xy} \end{bmatrix} \qquad \boldsymbol{s = De} \quad (\,64\,)
$$

With the membrane rigidity D_m and the flexural rigidity D_b:

$$
D_m = \frac{Et}{(1-\nu^2)}, \quad D_b = \frac{Et^3}{12(1-\nu^2)} \qquad\qquad (\,65\,)
$$

Equilibrium relation

The equilibrium relation describes the relation between the internal membrane forces s to the extern load components p:

$$
\boldsymbol{B^* s = p} \qquad\qquad (\,66\,)
$$

In tangential direction only membrane forces are providing equilibrium. In normal direction the out-of-plane shear forces, the bending moments and the contribution of the in-plane shear forces lead to equilibrium. This lead to the following equations:

$$
\frac{\partial n_{xx}}{\partial x} + \frac{\partial n_{xy}}{\partial y} + p_x = 0 \qquad\qquad (\,67\,)
$$

$$
\frac{\partial n_{yy}}{\partial y} + \frac{\partial n_{xy}}{\partial x} + p_y = 0 \qquad\qquad (\,68\,)
$$

$$
\frac{\partial v_x}{\partial x} + \frac{\partial v_y}{\partial y} + k_x n_{xx} + k_y n_{yy} + 2k_{xy} n_{xy} + p_z = 0 \qquad (\,69\,)
$$

For the equilibrium of moments in x- and y-direction holds:

$$v_x = \frac{\partial m_{xx}}{\partial x} + \frac{\partial m_{xy}}{\partial y} \qquad (\,70\,)$$

$$v_x = \frac{\partial m_{yy}}{\partial y} + \frac{\partial m_{xy}}{\partial x} \qquad (\,71\,)$$

We can now find the equilibrium relation by substitution of equation (21, 22) into (20):

$$\begin{bmatrix} -\dfrac{\partial}{\partial x} & 0 & -\dfrac{\partial}{\partial y} & 0 & 0 & 0 \\[2mm] 0 & -\dfrac{\partial}{\partial y} & -\dfrac{\partial}{\partial x} & 0 & 0 & 0 \\[2mm] -k_x & -k_y & -2k_{xy} & -\dfrac{\partial^2}{\partial x^2} & -\dfrac{\partial^2}{\partial y^2} & -\dfrac{\partial^2}{\partial x \partial y} \end{bmatrix} \begin{bmatrix} n_{xx} \\ n_{yy} \\ n_{xy} \\ m_{xx} \\ m_{yy} \\ m_{yx} \end{bmatrix} = \begin{bmatrix} p_x \\ p_y \\ p_z \end{bmatrix} \qquad \boldsymbol{B}^* \boldsymbol{s} = \boldsymbol{p} \quad (\,69\,)$$

Note: the matrix $\boldsymbol{B}^*$ is the adjoint of matrix $\boldsymbol{B}$ in equation (62).

A.4 FAILURE

Failure of gridshells is in many cases due to instability. Different types of stability failure for gridshells are [13]:

- Member buckling; a single member buckles without affecting the rest of the structure (Figure 25);
- Local instability; snap-through of one or several joints (Figure 26);
- Global instability; the structure buckles as a whole (Figure 27);
- A combination of the above mentioned modes.

Although single member buckling can simply be considered as a column in compression, investigating local instability takes more complex FE calculations. Also the rigidity of the joints play a role.

Figure 25: Local member buckling [14].
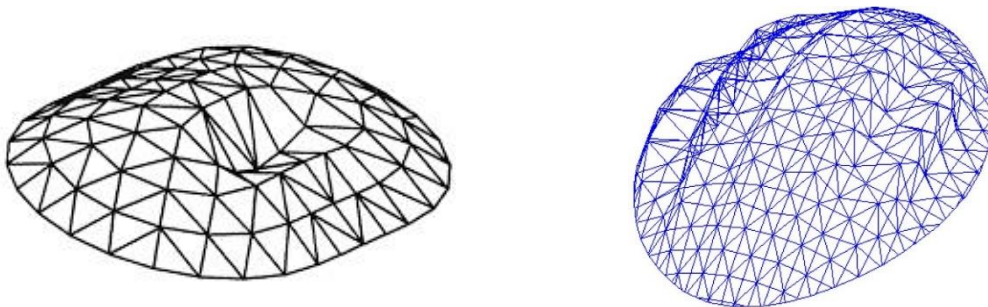
Figure 26: Local instability; snap-through of several joints. *Figure 27: Global instability* [15].
http://www.oit.ac.jp/english/engineering/res_architecture.html

111

B

TOPOLOGY OPTIMIZATION

B.1 TOPOLOGY OPTIMIZATION

Topology optimization is the study on the topology of a structure. An answer is to be found to the discrete (0-1) problem where to apply material and voids. This takes place in a given domain with predefined loads, boundary conditions and possibly additional design restrictions such as the location and size of prescribed holes or solid areas. A mathematical approach is used to find a result which meets a prescribed set of design requirements [16].

Topology optimization can be used in the conceptual design stage. After having found the final optimized topology, the design will need to be fine-tuned for performance and manufacturability. There are several methods to carry out the topology optimization process. The following will be discussed in the following paragraphs [17]:

- Solid Isotropic Microstructure with Penalisation (SIMP) method;
- Evolutionary Structural Optimization (ESO) method;
- Bi-directional Evolutionary Structural Optimization (BESO) method;
- Homogenisation method;
- Level set method.

B.1.1 SIMP METHOD

The *Solid Isotropic Microstructure with Penalisation method for intermediate densities*, or *SIMP method*, is developed in the late eighties. In the SIMP method, also called *density method*, a continuous design variable, a pseudo material density, is used. Prior to the optimization process a design domain Ω is defined. The design domain contains elements with a stiffness between 0 and 1. The density of the elements can be visualised by black, white or grey, respectively a full density of 1, zero density or an intermediate density. Zero density in fact implies a removal of the element. However, the requirement is that the optimization results in designs consisting of material or no material. Therefore, in the SIMP method the intermediate densities are penalised in order to push densities towards 0 or 1. This is done by a *power law* used by Bendsøe & Sigmund, 2003:

$$E_{ijkl}(x) = f(x)^p E_{ijkl}^0, \quad p > 1 \qquad (70)$$
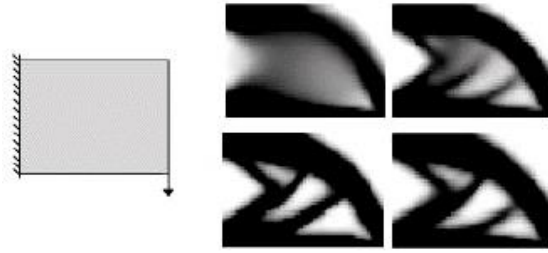
Figure 28: Example of topology optimization using the SIMP method [16].

With $E_{ijkl}(x)$ as the element stiffness, E^0_{ijkl} the material property of the base material, e.g., the stiffness, p the penalisation exponent and $f(x)$ the design function. By using penalisation values of $p > 1$, intermediate densities get penalised. In volume constraint problems, $p \geq 3$ is required to create a discrete result with a black-and-white visualisation [16].

Single load cases are in general easily adjusted to a situation with multiple load conditions. The situation for multiple load conditions is formulated as a weighted average for each of the load cases.

B.1.2 ESO METHOD

The *Evolutionary Structural Optimization (ESO) method* is based on the concept of removing inefficient material within a stated design domain. The process is resulting in a structure which is gradually evolving towards an optimal shape and topology. The optimization process can be based on [18]:

- Stress level. The von Mises stress of each element σ_e^{vm} is compared to the maximum von Mises stress of the whole structure σ_{max}^{vm}. Elements are removed when the ratio of element stress to maximum stress drops below a current rejection ratio (RR).
- Stiffness or displacement. The sensitivity number to the mean compliance is determined, i.e., the influence of an element on the overall stiffness of the structure. To maximize the stiffness of the structure, the mean compliance needs to be minimized. Elements with the least contribution to the stiffness, depending on the element removal ratio (ERR), will be removed.

B.1.3 HOMOGENIZATION METHOD

The *homogenization method* makes use of infinitely many micro scale voids forming a porous medium which creates a linearly elastic structure, see Figure 29. Optimization of the generalised lay-out contains solving the optimal porosity of the medium identified within a design domain. Solid structure is placed where no porosity is realized and if a portion of porous medium consists of only voids, structure is not placed. Porous medium is generated if the porosity is not the limit value. An example of an optimal distribution problems is [19]:

$$\text{Minimize the objective function such as the mean compliance} \qquad (71)$$

$$\text{subject to:} \begin{bmatrix} \text{equilibrium equations} \\ \text{void volume} \\ \text{stress / displacement constraints} \end{bmatrix}$$
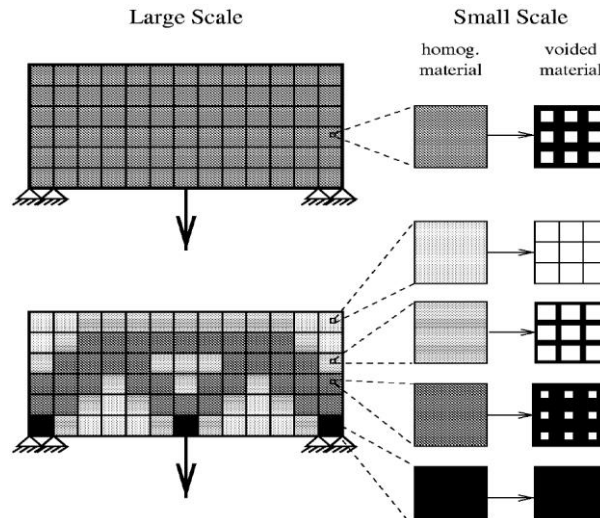
Figure 29: Porous material of homogenisation method.

http://www.herrera.unt.edu.ar/iest/stropt/stopttopopt@unt.pdf

B.1.4 LEVEL SET METHOD

The *level set method* is based on the ability to move the boundaries of the design domain. The movement of the boundaries depends on the stresses on the boundaries. Material is removed in regions of low stress and material is added in regions of high stress. Removal of material occurs when the stress is below a certain percentage of the maximal initial stress. Also, material is added when the stress is above a certain percentage. The closed stress contours, the new holes cut and the velocity of the boundary motion are determined by the removal rate. The evolutionary process can be characterized by the disappearance of holes which are initially positioned at the wrong places, see Figure 30.
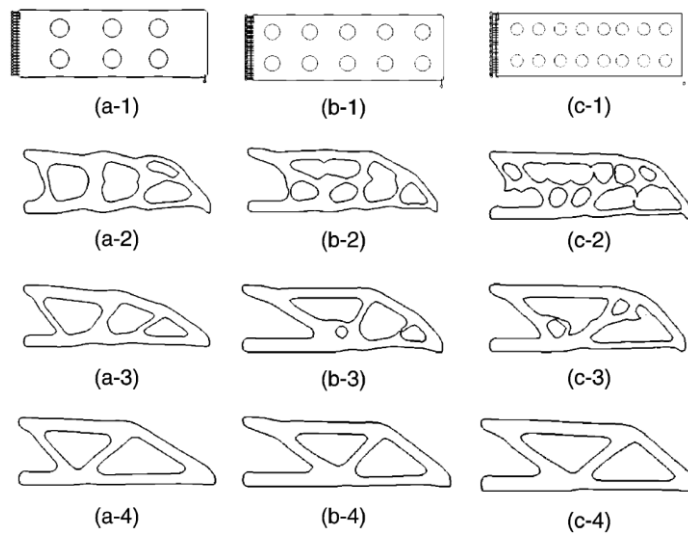
Figure 30: Examples of let set method process [20].

114

C

ADDITIVE MANUFACTURING

C.1 METAL PRINTING TECHNOLOGIES

Direct Metal Fabrication (DMF) is used for the direct production of metal parts. The processes are either based on a 'powder bed process' or a 'powder feed process'. Some technologies will be discussed below:

Powder bed process

The collective term for powder bed process technologies is Selective Laser Sintering (SLS). Metal particles are fused together by sintering, meaning that the particles are heated just below the point of liquefaction. Layers of powder are deposited and sintered subsequently. Most powder bed processes take place in a building space filled by an inert gas to form a protective atmosphere. Therefore reactive metal powders, such as aluminium and titanium, can be applied. Even though many different materials are available, they cannot be applied in the same building process. Unsintered material is removed after completion of the part. Figure 31 depicts schematically the SLS process [21]. Different SLS technologies can be distinguished, such as:

- Selective Laser Melting;
- LaserCusing;
- Electronic Beam Melting;
- Direct Metal Laser Sintering.

Selective Laser Melting

Selective Laser Melting (SLM) is developed in order to generate high density parts. This is obtained by fully melting the metallic powder particles are fully molten. Whereas high temperatures are required for this process, it is accompanied with residual stresses. This should be taken into account in order to prevent part failure, distortion, delaminating or cracking. An example SLM machine is depicted in Figure 32 [22].
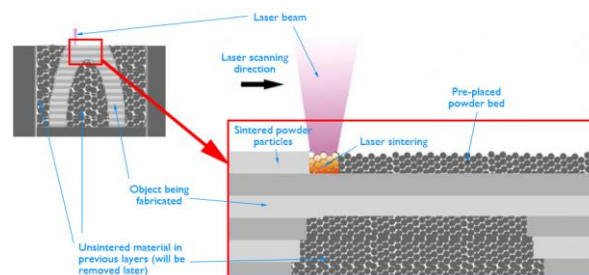
Figure 31: Selective Laser Sintering (SLS) process. ©Quill & Pad
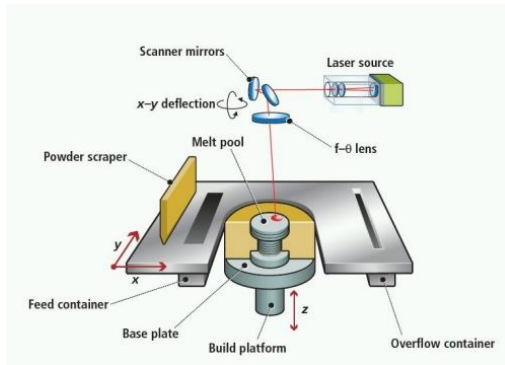
Figure 32: Principle of Selective Laser Melting (SLM). ©Popular 3D Printers

Figure 33: LaserCusing makes use of substrate plates which can be mounted in CNC machines [21].

LaserCusing

LaserCusing makes use of laser-melted powder to obtain a relative part density of 100%. The system uses a substrate plate with an industrial standard fixation system, see Figure 33. This makes it possible to mount the part in different CNC machines [21].

Electronic Beam Melting

Electronic Beam Melting (EBM) applies an electronic beam to generate an electric arc to melt the metal powder (Figure 34). The melting process is carried out under vacuum at approximately 1000° Celcius. The cooling process is controlled to achieve accurate cooling of the metal parts. While the relative density of the part is 100%, post-processing is often required to obtain desired surface finish quality [21].

Direct Metal Laser Sintering

Direct Metal Laser Sintering (DMLS) is directly evolved from SLS. The method uses a laser beam in order to selectively sinter metal particles. Lower relative densities are obtained in comparison to methods that make use of melting of the powder [21].
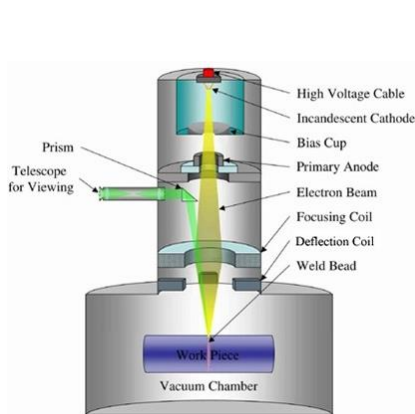
Figure 34: Principle of Electronic Beam Melting (EBM). ©Popular 3D Printers
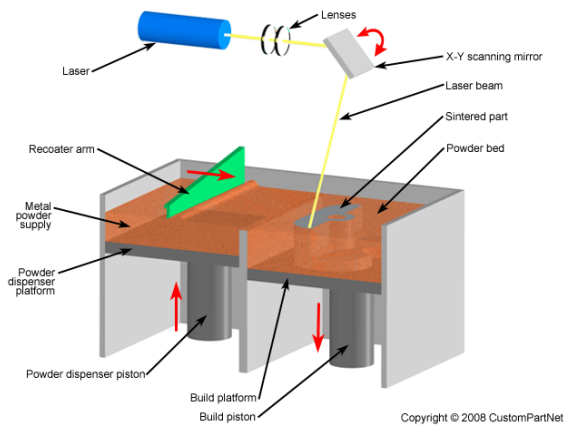
Figure 35: Principle of Direct Metal Laser Sintering (DMLS). ©2008 Custom PartNet

116

Powder feed process

The powder feed process, also called Fused Metal Deposition (FDM) method, deposits molten material by means of a nozzle. In order to build a 3D object, the nozzle is able to move in X- and Y-direction, while the base plate moves down in Z-direction. In order to obtain a proper cohesion between the layers, the building chamber is heated and maintained at a certain temperature. In powder fed processes, different materials in different quantities can be applied. Also, damaged or defect parts can be repaired by rebuilding layers. During post-processing, inaccurate surfaces need to be finished by conventional techniques.

Different FDM technologies can be distinguished, such as:

- Laser Engineered Net Scaping;
- Direct Metal Deposition;
- Electron Beam Free Form Fabrication;
- Construction Laser Additive Directe.

Laser Engineered Net Scaping

Laser Engineered Net Scaping (LENS) contains a printhead with a central nozzle and secondary powder delivery nozzles, which are positioned around the central nozzle. The central nozzle is used for the energy source; a focussed laser beam. The secondary nozzles spray powder into the meld bath created by the laser beam [21].

Direct Metal Deposition

Direct Metal Deposition (DMD) is derived from build-up welding. A melting bath is created by a CO2 laser beam and pure metal powder is sprayed into the melting bath to obtain a material density of 100%, see Figure 38. The printhead is attached to a five axial CNC robot to be able to deposit in three dimensions [21]. An example is the MX3D-robot developed by the Joris Laarman Lab, see Figure 39.
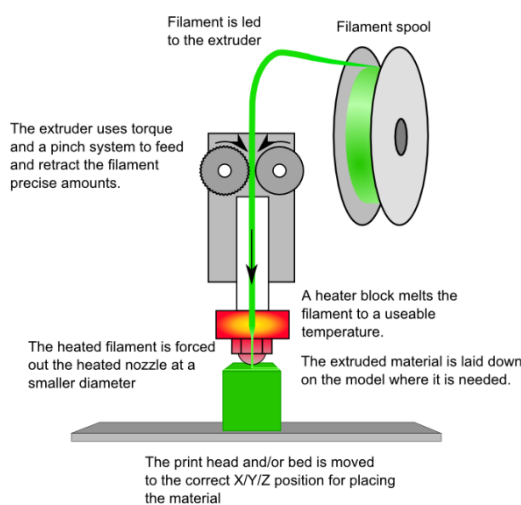
Figure 36: Fused Deposition Modelling (FDM) process [23].
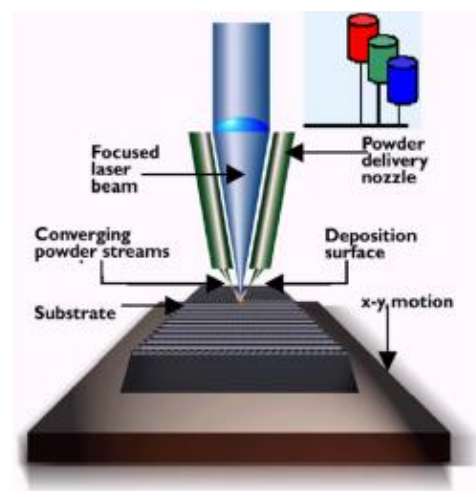
Figure 37: Principle of Laser Engineered Net Shaping (LENS). © 2015 RPM Innovations
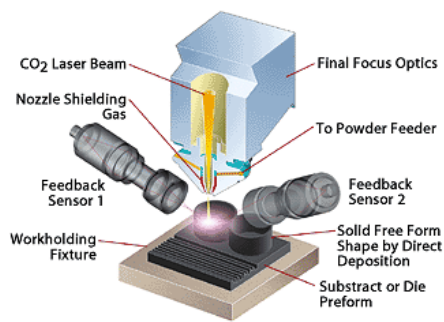
Figure 38: Principle of Direct Metal Deposition (DMD). ©Gardner Business Media, Inc. 2014

Figure 39: MX3D-Metal developed by Joris Laarman Lab. ©2014 Joris Laarman Lab

Electron Beam Free Form Fabrication

Electron Beam Free Form Fabrication (EBF3) uses an electron beam and a stock of solid wire to fabricate parts, see Figure 40. The material is melted by the electron beam in a vacuum chamber. Patented by NASA, the method is developed to operate in zero gravity environments [24].

Construction Laser Additive Directe

Construction Laser Additive Directe (CLAD) applies metal powder injected in a nozzle to create a uniform jet. A laser beam melts the powder when it moves across the beam. A local gas is used to protect the deposited material against oxidation. Figure 41 shows a CLAD machine [25].
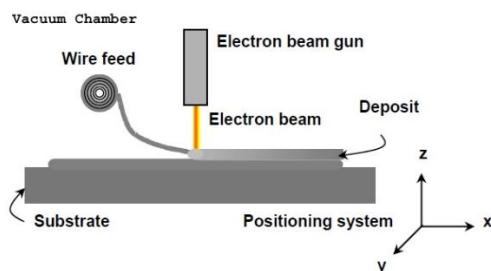
Figure 40: Principle of Electron Beam Free Form Fabrication (EBF3) ©Popular 3D Printers

Figure 41: A CLAD machine building up an object. ©Réalisation 2013

C.2 TEST REPORT

C.2.1 INTRODUCTION

Simple tensile tests have been carried out on 24 March 2014. The goal of the tensile tests was to gain knowledge and understanding for the tested material. Three test pieces (dogbones) were tested to check the material properties of *EOS MaragingSteel MS1* specified by the manufacturer.

C.2.2 TEST PIECES

Dimensions
The dogbones were printed by a SLS machine at CRDM (High Wycombe, UK) and had the shape as presented in Figure 42.

Original diameter d_0
In order to determine the stress in the cross-section, the original diameter of the parallel length was measured in advance of the testing, see Table 1.

Table 1: Original diameter d_0.

Test piece	d_0 (mm)
1	1,99
2	1,99
3	2,00

Material
The material used for the printed dogbones was *EOS MaragingSteel MS1* and built on EOSINT M 270 Installation mode Standard with PSW 3.3 or 3.4 (MS1_Surface 1.0 20 µm layer thickness). The material was not heat treated and tested in z-direction. The material datasheet can be found at page 125.

C.2.3 TESTING MACHINE

The tensile tests were carried out in the Stevin II laboratory of the faculty of Civil Engineering at the Delft University of Technology. The tensile capacity of the tensile machine is 5 kN. Figure 43 depicts the tensile machine.

Measurement elongation
To avoid inaccuracy in the data because of uncertainties in the machine, an external device was used to measure the elongation of the test pieces. A strain gauge was the best option, but because of size matters it was not possible to attach it to the test pieces. Therefore, an external sensor has been used which was attached to the clamps of the tensile machine by magnets, see Figure 44.
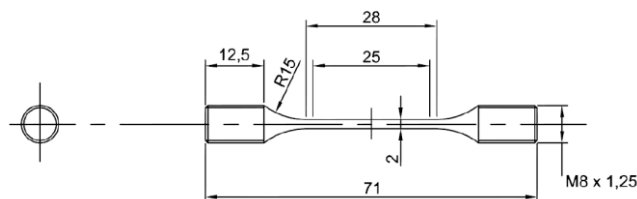
Figure 42: Dimensions of dogbone.

Figure 43: Tensile machine.

Figure 44: External sensor to measure the elongation.

Note: The external sensor had a limited range of 2 mm. It turned out that the elongation of the test pieces was slightly larger than 2 mm and therefore some data about the elongation at rupture is lacking.

Testing rate

The testing rate of the machine was set to 0,5 mm/min.

C.2.4 TEST RESULTS

Stress-strain curve

The stress-strain curve, as displayed in Figure 45, is derived from the data of the tensile machine. The result of Test 1 is not displayed in the stress-strain curve as the strain was not measured correctly during the test.
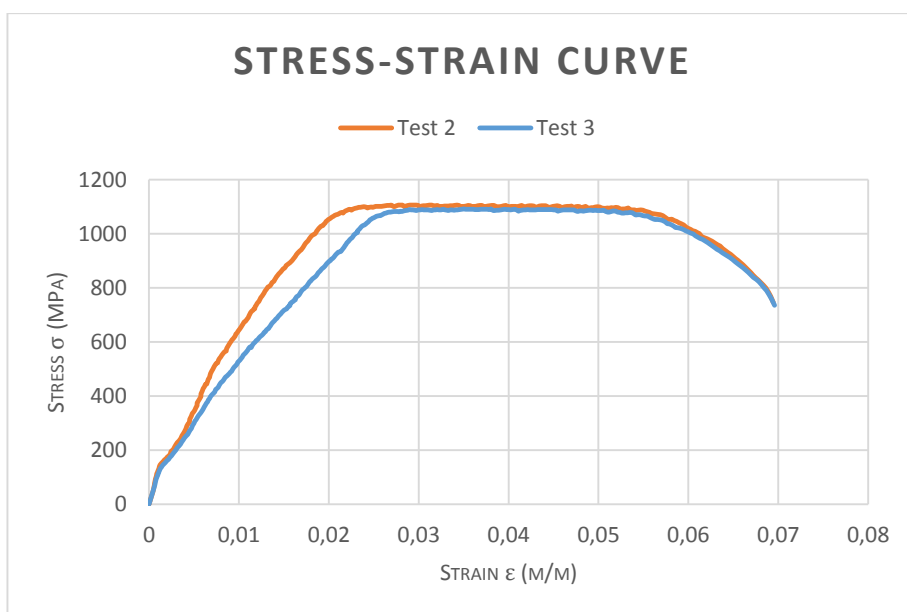
Figure 45: Stress-strain curve.

Ultimate tensile strength

The ultimate tensile strength (UTS) is the maximum stress that a material can withstand. The UTS can be determined as follows:

$$UTS = \frac{F}{A}$$

<div align="right">(1)</div>

With F the tensile force in N and A the cross-section of the test piece in mm², determined in Table 1. The results of the UTS test are listed in Table 2.

Table 2: Results ultimate tensile strength.

Test	UTS (MPa)
1	1115,7
2	1106,4
3	1091,5
Average	**1104,5**

Young's modulus

The Young's modulus (E-modulus) is the ratio of stress over strain measured along an axis. It can be determined from the stress-strain curve by:

$$E = \frac{\sigma}{\varepsilon}$$

<div align="right">(2)</div>

When analysing the results of the tensile tests it became clear that the data about the strain is not reliable. After a certain stress (±150 MPa) the steepness of the line in the stress strain curve decreases suddenly. This can be explained by the fact that the grip of the tensile machine was slipping when the stress increased. The result of slipping is shown in Figure 46.

Although a part of the data is not reliable when the data of the strain is involved, the Young's modulus can be determined from the first part of the stress-strain curve. This part contains reliable data as slipping did not occur in this part of the curve, Figure 47.

Figure 46: Result of slipping.
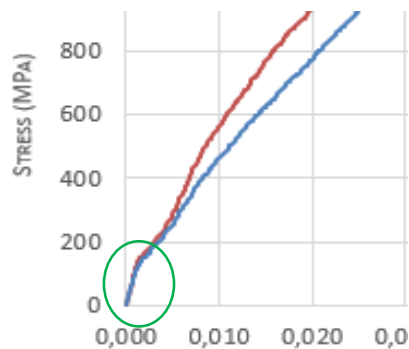
Figure 47: Reliable data.

The results are shown in Table 3:

Table 3: Results Young's modulus.

Test	Young's modulus (GPa)
1	-
2	153
3	129
Average	**141**

Yield strength

Because the information about the strain is not reliable it is hard to determine the yield strength out of the stress-strain curve. Although the data is not reliable it is known that the yield strength can be found right at the location the material starts to deform plastically. Therefore it is possible, considering the obtained stress-strain curve, to roughly estimate the yield strength at 1050 MPa, Figure 48.
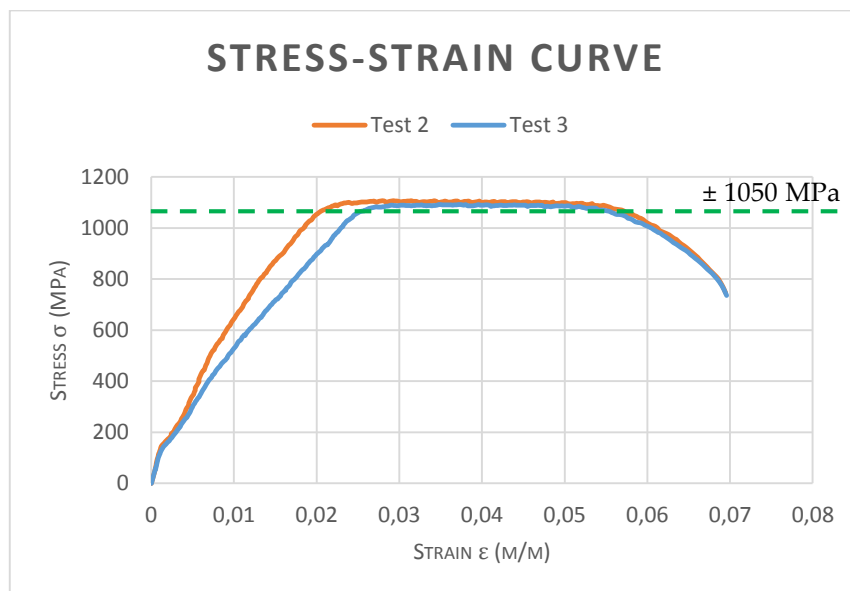
Figure 48: Estimation of yield strength.

Elongation at break

The elongation at break could not be measured throughout the entire tensile test due to the relative small range of the measuring instrument. Therefore, the stress-strain curve is extrapolated and the elongation at break could be approached. This led to a strain of 6,9% at the point of rupture.

Post testing

The physical result of the testing is shown in Figure 50. It is remarkable that all the test pieces have been broken at the same place. This might probably point to the fact that the grips of the testile machine were not exactly placed in a vertical line. This might have resulted in a moment in the test piece and so disturbing the results.
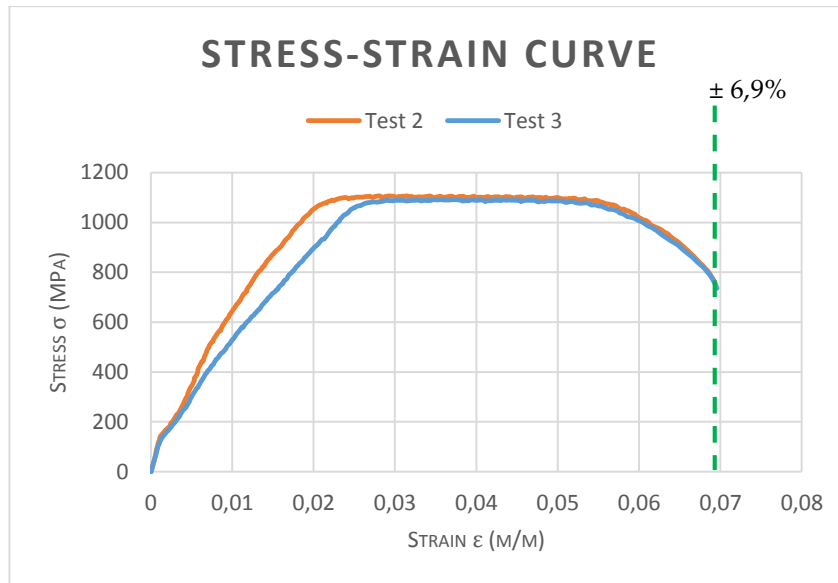
Figure 49: Estimation of elongation at break.

Figure 50: Ruptured test pieces.

C.2.5 FURTHER TESTING

The way forward is to identify materials for which are used in structural engineering with well-established design rules and which may be produced in powders for AM. This would represent a more known starting position and remove large variables compared to a material with no design code, unknown material properties and unproven manufacturing routes.

Established design codes and materials limit, rather than eliminate, possible variables. In particular it should be noted that design codes, such as EC3, are based on assumptions regarding materials including:

- Base materials for use in fabrication are produced to and meet the requirements of the relevant EN materials standards;
- The material properties assumed in the design code are founded on large historic data sets;
- The design assumes a level of workmanship and tolerance assumed typical of conventional manufacturing routes.

123

None of these assumptions can be taken as valid for a new manufacturing route such as Metal AM; this needs to be reflected in assumptions made in the engineering design and will influence any test programme for produced parts.

Material test programme

The test programme for Metal AM components should be run in parallel to a component made by conventional production methods for the same material, i.e., a cast or fabricated part.

Mechanical and physical testing

The base tests would be undertaken on or removed from production pieces and would include:

- Dimensional measurement for compliance with required tolerances on size, shape, etc.;
- Full tensile tests to include reported data on yield strength (or proof stress), ultimate tensile and elongation;
- Hardness testing;
- Facture toughness by Charpy impact test and CTOD testing at an appropriate temperature;
- Full chemical analysis and microstructural analysis (metallography) from different parts of the component prior to and post any heat treatment.

Additional, but not optional, tests for weldability of the produced piece:

- Welding procedure trials on production pieces;
- Post weld mechanical testing, as per the base materials, of the welded joints.

Non-destructive testing and inspection

Both production pieces and welded production pieces require non-destructive testing to validate the quality of the parts in the same manner as would occur for welded fabrications, casting or forgings. In the case of AM parts, there are no established acceptance criteria for deflects, flaws or discontinuities inspected by commonly used methods in the construction industry, i.e., Ultrasonic testing, Magnetic Particle, Dye Penetrant, etc. Procedures and methodologies for this testing will therefore require development and be specific to the parts produced.

Note that all the tests, destructive and non-destructive, would be taken on samples from different parts of the production test piece.

C.2.6 CONCLUSION

Although the data were gathered out of a small number of test pieces, the results which has been found are basically corresponding with the material data sheet. Because of the small number of tests and measurement uncertainties it is recommended to carry out further tests.

Table 4 summarizes the results of the tests.

Table 4: Results of tensile tests.

	Data sheet	Result of testing
Ultimate tensile strength	1100±100 MPa	1104,5 MPa
Young's modulus	150±20 GPa	141 GPa
Yield strength	1000±100 MPa	1050 MPa
Elongation at break	10±4 %	6,9 %

C.3 MATERIAL DATA SHEETS

C.3.1 EOS MARAGINGSTEEL MS1

Material data sheet

EOS MaragingSteel MS1

EOS MaragingSteel MS1 is a steel powder which has been optimized especially for processing on EOSINT M systems.

This document provides information and data for parts built using EOS MaragingSteel MS1 powder (EOS art.-no. 9011-0016) on the following system specifications:

- EOSINT M 270 Installation Mode *Standard*
  with PSW 3.3 or 3.4 and default job MS1_020_default.job or MS1_040_default.job

- EOSINT M 270 Dual Mode
  with PSW 3.5 and EOS Original Parameter Set MS1_Surface 1.0 or MS1_Performance 2.0

- EOSINT M 280
  with PSW 3.5 and EOS Original Parameter Set MS1_Performance 1.0 or MS1_Speed 1.0

Description

Parts built in EOS MaragingSteel MS1 have a chemical composition corresponding to US classification 18% Ni Maraging 300, European 1.2709 and German X3NiCoMoTi 18-9-5. This kind of steel is characterized by having very good mechanical properties, and being easily heat-treatable using a simple thermal age-hardening process to obtain excellent hardness and strength.

Parts built from EOS MaragingSteel MS1 are easily machinable after the building process and can be easily post-hardened to more then 50 HRC by age-hardening at 490 °C (914 °F) for 6 hours. In both as-built and age-hardened states the parts can be machined, spark-eroded, welded, micro shot-peened, polished and coated if required. Due to the layerwise building method, the parts have a certain anisotropy, which can be reduced or removed by appropriate heat treatment - see Technical Data for examples.

Material data sheet

Technical data

General process data

Typical achievable part accuracy [1]	
– small parts (< 80 x 80 mm)	approx. $\pm$ 20 µm approx. $\pm$ 0.8 x 10^{-3} inch
– large parts	approx. $\pm$ 50 µm approx. $\pm$ 0.002 inch
Age hardening shrinkage [2]	approx. 0.08 %
Min. wall thickness [3]	approx. 0.3 - 0.4 mm approx. 0.012 - 0.016 inch
Surface roughness (approx.) [4]	
– as manufactured	
MS1 Surface (20 µm)	R_a 4 µm; Rz 20 µm R_a 0.16 x 10^{-3} inch, R_z 0.78 x 10^{-3} inch
MS1 Performance (40 µm)	R_a 5 µm; Rz 28 µm R_a 0.19 x 10^{-3} inch, R_z 1.10 x 10^{-3} inch
MS1 Speed (50 µm)	R_a 9 µm; Rz 50 µm R_a 0.47 x 10^{-3} inch, R_z 2.36 x 10^{-3} inch
– after shot-peening	R_a 4 – 6.5 µm; R_z 20 – 50 µm R_a 0.16 – 0.26 x 10^{-3} inch R_z 0.78 – 1.97 x 10^{-3} inch
– after polishing	R_z up to < 0.5 µm R_z up to < 0.02 x 10^{-3} inch (can be very finely polished)

Material data sheet

Volume rate [5]	
– Parameter set MS1_Surface 1.0 / default job MS1_020_default.job (20 µm layer thickness)	1.6 mm³/s (5.8 cm³/h) 0.35 in³/h
– Parameter set MS1_Performance 2.0 / default job MS1_040_default.job (40 µm layer thickness)	3 mm³/s (10.8 cm³/h) 0.66 in³/h
– Parameter set MS1_Performance 1.0 / for M 280 / 400 W (40 µm layer thickness)	4.2 mm³/s (15.1 cm³/h) 0.92 in³/h
– Parameter set MS1_Speed 1.0 / for M 280 / 400 W (50 µm layer thickness)	5.5 mm³/s (19.8 cm³/h) 1.21 in³/h

[1] Based on users' experience of dimensional accuracy for typical geometries, as built. Part accuracy is subject to appropriate data preparation and post-processing, in accordance with EOS training.

[2] Ageing temperature 490 °C (914 °F), 6 hours, air cooling

[3] Mechanical stability is dependent on geometry (wall height etc.) and application

[4] Due to the layerwise building, the surface structure depends strongly on the orientation of the surface, for example sloping and curved surfaces exhibit a stair-step effect. The values also depend on the measurement method used. The values quoted here given an indication of what can be expected for horizontal (up-facing) or vertical surfaces.

[5] Volume rate is a measure of build speed during laser exposure of hatched areas. The total build speed depends on the average volume rate, the recoating time (related to the number of layers) and other geometry- and machine setting-related factors.

Material data sheet

Physical and chemical properties of parts

Material composition	Fe (balance) Ni (17 - 19 wt-%) Co (8.5 - 9.5 wt-%) Mo (4.5 - 5.2 wt-%) Ti (0.6 - 0.8 wt-%) Al (0.05 - 0.15 wt-%) Cr, Cu (each ≤ 0.5 wt-%) C (≤ 0.03 wt-%) Mn, Si (each ≤ 0.1 wt-%) P, S (each ≤ 0.01 wt-%)
Relative density	approx. 100 %
Density	8.0 - 8.1 g/cm³ 0.289 - 0.293 lb/in³

Material data sheet

Mechanical properties of parts at 20 °C (68°F)

	As built	After age hardening [2]
Tensile strength [6]		min. 1930 MPa min. 280 ksi
– in horizontal direction (XY)	typ. 1100 ± 100 MPa typ. 160 ± 15 ksi	typ. 2050 ± 100 MPa typ. 297 ± 15 ksi
– in vertical direction (Z)	typ. 1100 ± 100 MPa typ. 160 ± 15 ksi	
Yield strength (Rp 0.2 %) [6]		min. 1862 MPa min. 270 ksi
– in horizontal direction (XY)	typ. 1050 ± 100 MPa typ. 152 ± 15 ksi	typ. 1990 ± 100 MPa typ. 289 ± 15 ksi
– in vertical direction (Z)	typ. 1000 ± 100 MPa typ. 145 ± 15 ksi	
Elongation at break [6]		min. 2 %
– in horizontal direction (XY)	typ. (10 ± 4) %	typ. (4 ± 2) %
– in vertical direction (Z)	typ. (10 ± 4) %	
Modulus of elasticity [6]		
– in horizontal direction (XY)	typ. 160 ± 25 GPa typ. 23 ± 4 Msi	typ. 180 ± 20 GPa typ. 26 ± 3 Msi
– in vertical direction (Z)	typ. 150 ± 20 GPa typ. 22 ± 3 Msi	
Hardness [7]	typ. 33 - 37 HRC	typ. 50 - 56 HRC
Ductility (Notched Charpy impact test)	typ. 45 ± 10 J	typ. 11 ± 4 J

[6]   Tensile testing according to ISO 6892-1:2009 (B) Annex D, proportional test pieces, diameter of the neck area 5mm (0.2 inch), original gauge length 25mm (1 inch).

[7]   Rockwell C (HRC) hardness measurement according to EN ISO 6508-1 on polished surface. Note that measured hardness can vary significantly depending on how the specimen has been prepared.

Material data sheet

Thermal properties of parts

	As built	After age hardening [2]
Thermal conductivity	typ. 15 ± 0.8 W/m°C typ. 104 ± 6 Btu in/(h ft² °F)	typ. 20 ± 1 W/m°C typ. 139 ± 7 Btu in/(h ft² °F)
Specific heat capacity	typ. 450 ± 20 J/kg°C typ. 0.108 ± 0.005 Btu/(lb °F)	typ. 450 ± 20 J/kg°C typ. 0.108 ± 0.005 Btu/(lb °F)
Maximum operating temperature		approx. 400 °C approx. 750 °F

Abbreviations

typ.	typical
min.	minimum
approx.	approximately
wt	weight

Notes

The data are valid for the combinations of powder material, machine and parameter sets referred to on page 1, when used in accordance with the relevant Operating Instructions (including Installation Requirements and Maintenance) and Parameter Sheet. Part properties are measured using defined test procedures. Further details of the test procedures used by EOS are available on request. Unless otherwise specified, the data refer to the default job MS1_040_default.job or the equivalent parameter set MS1_Performance 2.0. The corresponding data for the default job MS1_020_default.job or the equivalent parameter set MS1_Surface 1.0 are approximately the same except where otherwise specified.

The data correspond to our knowledge and experience at the time of publication. They do not on their own provide a sufficient basis for designing parts. Neither do they provide any agreement or guarantee about the specific properties of a part or the suitability of a part for a specific application. The producer or the purchaser of a part is responsible for checking the properties and the suitability of a part for a particular application. This also applies regarding any rights of protection as well as laws and regulations. The data are subject to change without notice as part of EOS' continuous development and improvement processes.

EOS®, EOSINT® and DMLS® are registered trademarks of EOS GmbH.

© 2011 EOS GmbH – Electro Optical Systems. All rights reserved.

EOS GmbH – Electro Optical Systems

EOS MaragingSteel MS1
TMS, WEIL / 10.2011

6 / 6

Robert-Stirling-Ring 1
D–82152 Krailling / München

C.3.2 EOS S<small>TAINLESS</small>S<small>TEEL</small> GP1

Material data sheet

EOS StainlessSteel GP1 for EOSINT M 270

A number of different materials are available for use with EOSINT M systems, offering a broad range of e-Manufacturing applications. EOS StainlessSteel GP1 is a stainless steel powder which has been optimized especially for EOSINT M 270 systems. Other materials are also available for EOSINT M systems, and further materials are continuously being developed – please refer to the relevant material data sheets for details.

This document provides a brief description of the principle applications, and a table of technical data. For details of the system requirements please refer to the relevant information quote.

Description, application

EOS StainlessSteel GP1 is a pre-alloyed stainless steel in fine powder form. Its composition corresponds to US classification 17-4 and European 1.4542. This kind of steel is characterized by having good corrosion resistance and mechanical properties, especially excellent ductility in laser processed state, and is widely used in a variety of engineering applications.

This material is ideal for many part-building applications (DirectPart) such as functional metal prototypes, small series products, individualised products or spare parts. Standard processing parameters use full melting of the entire geometry with 20 µm layer thickness, but it is also possible to use Skin & Core building style to increase the build speed. Using standard parameters the mechanical properties are fairly uniform in all directions. Parts made from EOS StainlessSteel GP1 can be machined, spark-eroded, welded, micro shot-peened, polished and coated if required. Unexposed powder can be reused.

Typical applications:

- engineering applications including functional prototypes, small series products, individualised products or spare parts.

- parts requiring high corrosion resistance, sterilisability, etc.

- parts requiring particularly high toughness and ductility.

Material data sheet

Technical data

General process and geometric data

Minimum recommended layer thickness	20 µm 0.8 mil
Typical achievable part accuracy [1]	
– small parts	± 20 – 50 µm 0.8 – 2.0 mil
– large parts [2]	± 0.2 %
Min. wall thickness [3]	0.3 - 0.4 mm 0.012 - 0.016 in
Surface roughness	
– after shot-peening	R_a 2.5 - 4.5 µm, R_y 15 - 40 µm R_a 0.1 - 0.2 , R_y 0.6 - 1.6 mil
– after polishing	R_z up to < 0.5 µm (can be very finely polished)
Volume rate [4]	
– standard parameters (20 µm layers, full density)	2 mm³/s 0.44 in³/h
– Inner core parameters (Skin & Core style, full density)	4 mm³/s 0.88 - 1.1 in³/h

[1] Based on users' experience of dimensional accuracy for typical geometries, e.g. ± 20 µm when parameters can be optimized for a certain class of parts or ± 50 µm when building a new kind of geometry for the first time.

[2] For larger parts the accuracy can be improved by post-process stress-relieving at 650 °C for 1 hour.

[3] Mechanical stability is dependent on geometry (wall height etc.) and application

[4] Volume rate is a measure of build speed during laser exposure. The total build speed depends on the average volume rate, the recoating time (related to the number of layers) and other factors such as DMLS-Start settings.

Material data sheet

Physical and chemical properties of parts

Material composition	steel including alloying elements Cr (15 – 17.5 wt-%) Ni (3 - 5 wt-%) Cu (3 - 5 wt-%) Mn (max. 1 wt-%) Si (max. 1 wt-%) Mo (max. 0.5 wt-%) Nb (0.15 - 0.45 wt-%) C (max. 0.07 wt-%)
Relative density with standard parameters	approx. 100 %
Density with standard parameters	7.8 g/cm³ 0.28 lb/in³

Mechanical properties of parts [5]

	As manufactured	Stress relieved (1 hour at 650 °C)
Ultimate tensile strength		
– in horizontal direction (XY)	min 850 MPa (123 ksi) typical 930 $\pm$ 50 MPa (135 $\pm$ 7 ksi)	typical 1100 MPa (160 ksi)
– in vertical direction (Z)	min 850 MPa (123 ksi) typical 960 $\pm$ 50 MPa (139 $\pm$ 7 ksi)	typical 980 MPa (142 ksi)
Yield strength		
(R_{eL}, Lower yield strength)		
– in horizontal direction (XY)	min 530 MPa (77 ksi) typical 586 $\pm$ 50 MPa (85 $\pm$ 7 ksi)	typical 590 Mpa (86 ksi)
– in vertical direction (Z)	min 530 MPa (77 ksi) typical 570 $\pm$ 50 MPa (83 $\pm$ 7 ksi)	typical 550 MPa (80 ksi)
(R_{eH}, Upper yield strength)		
– in horizontal direction (XY)	min 595 MPa (86 ksi) typical 645 $\pm$ 50 MPa (94 $\pm$ 7 ksi)	typical 634 MPa (92 ksi)
– in vertical direction (Z)	min 580 MPa (84 ksi) typical 630 $\pm$ 50 MPa (91 $\pm$ 7 ksi)	typical 595 MPa (86 ksi)

EOS GmbH – Electro Optical Systems

EOS StainlessSteel GP1
MMI / 04.09

3 / 5

Robert–Stirling–Ring 1
D–82152 Krailling / München

Material data sheet

Young's modulus	170 ± 30 GPa (25 ± 4 msi)	typical 180 GPa (26 msi)
Elongation at break		
– in horizontal direction (XY)	min 25 % typical 31 ± 5 %	typical 29 %
– in vertical direction (Z)	min 25 % typical 35 ± 5 %	typical 31 %
Hardness [6]		
– as built	approx. 230 ± 20 HV1	
– ground & polished [7]	approx. 250 – 400 HV1	

[5]   Mechanical testing according to ISO 6892:1998(E) Annex C, proportional test pieces, Diameter of the neck area 5 mm, original gauge length 25 mm

[6]   Vickers hardness measurement (HV) according to DIN EN ISO 6507-1. Note that depending on the measurement method used, the measured hardness value can be dependent on the surface roughness and can be lower than the real hardness. To avoid inaccurate results, hardness should be measured on a polished surface.

[7]   Due to work-hardening effect

Thermal properties of parts

Coefficient of thermal expansion	
– over 20 – 600 °C (68 – 1080 °F)	14×10^{-6} m/m °C 7.8×10^{-6} in/in °F
Thermal conductivity	
– at 20 °C (68 °F)	13 W/m °C 90 Btu/(h ft² °F/in)
– at 100 °C (212 °F)	14 W/m °C 97 Btu/(h ft² °F/in)
– at 200 °C (392 °F)	15 W/m °C 104 Btu/(h ft² °F/in)
– at 300 °C (572 °F)	16 W/m °C 111 Btu/(h ft² °F/in)
Maximum operating temperature	550 °C 1022 °F

EOS GmbH – Electro Optical Systems

Material data sheet

The quoted values refer to the use of these materials with EOSINT M 270 systems according to current specifications (including the latest released process software PSW and any hardware specified for the relevant material) and operating instructions. All values are approximate. Unless otherwise stated, the quoted mechanical and physical properties refer to standard building parameters and test samples built in horizontal orientation. They depend on the building parameters and strategies used, which can be varied by the user according to the application. Measurements of the same properties using different test methods (e.g. specimen geometries) can give different results. The data are based on our latest knowledge and are subject to changes without notice. They are provided as an indication and not as a guarantee of suitability for any specific application.

EOS®, EOSINT®, DMLS® and DirectPart® are registered trademarks of EOS GmbH.

C.4 PREPARE FOR AM PRODUCTION

Next to smoothing the geometry of the joint, additional steps need to be carried out in order to prepare the designs for AM production. These steps are illustrated in this paragraph.

Build orientation

The most optimal orientation of the joints in the AM machine is to place them in that way that the printed cross-sections are as small as possible (Figure 51). In this way the residual stresses will not become problematic. Additionally, more joints can be placed in the building chamber, which will speed up the building process.

An example of the orientation of joint 1 in the building chamber is given in Figure 51. Figure 52 depicts an example placement of the joints in the building chamber. Placing as many joints as possible in the building chamber will increase the production speed.
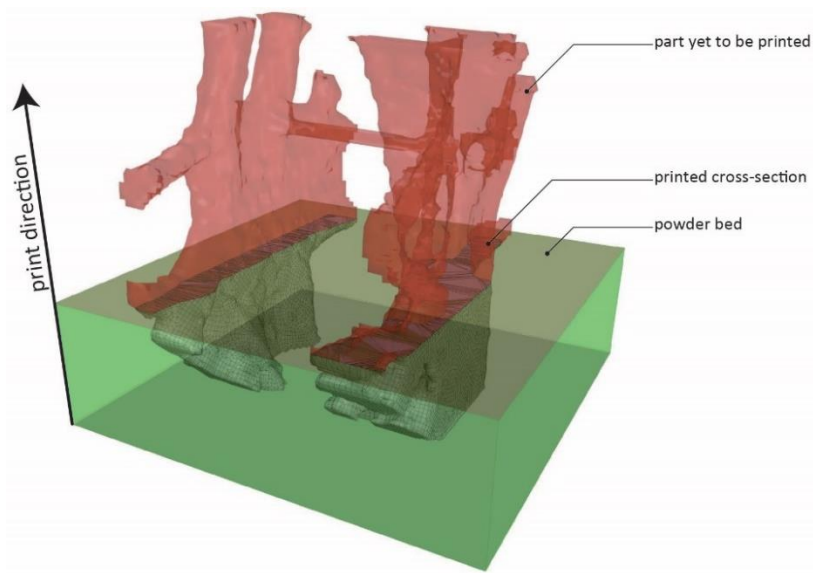
Figure 51: Optimal build orientation (example: joint 1).
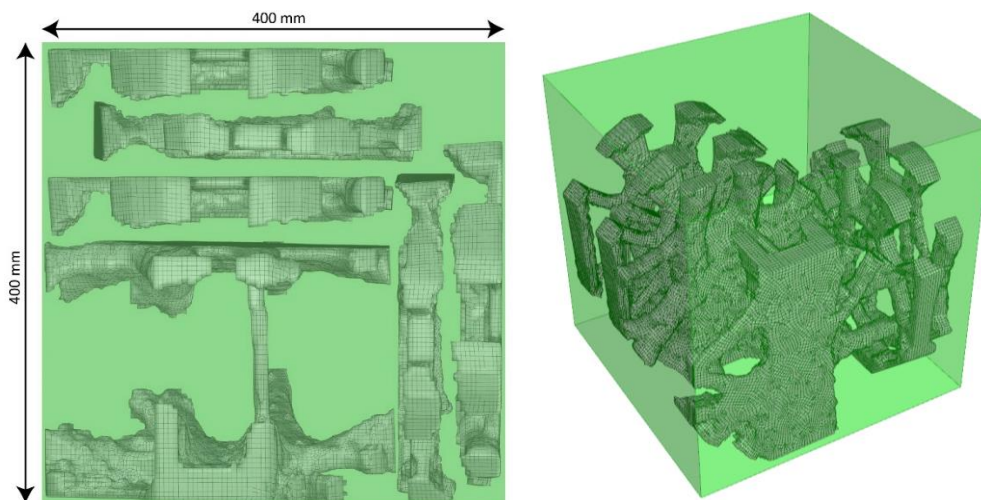
Figure 52: Example placement of joints in the building chamber (left): fit as many as possible joints and parts. The right picture shows a 3D view of the same building chamber.

Support structure

Figure 53shows where support structure is required (areas indicated by a red colour). For illustration purposes, joint 3 is taken as an example. The joint will be connected to the base plate by support structure. When printing is finished, the joint can be taken away by breaking the support structure.

Support structure is required in case of overhangs larger than 45° or in case Moreover, the joint will be connected to the base plate with support structure.

Note: support structure is also necessary to dissipate the heat that is developed during printing. This will avoid warping of the structure. This phenomenon has been taken into account, but not fully elaborated in this work.

Figure 54 shows the required support structure for joint 3. The support structure is generated with the free software of Cura [26].
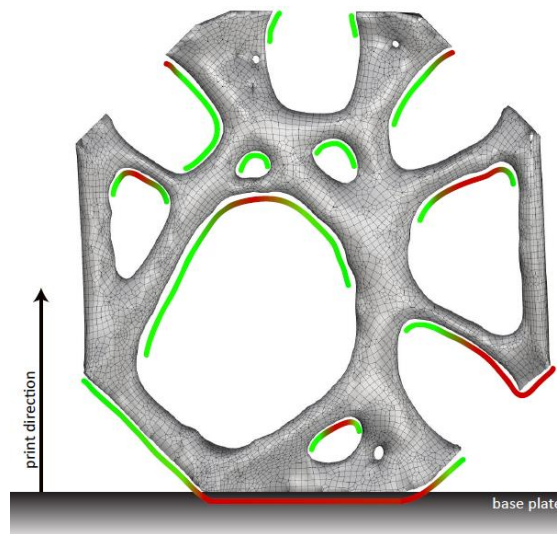
Figure 53: Locations where support structure is required (for example: joint 3). Red: support structure required; green: no support structure required.
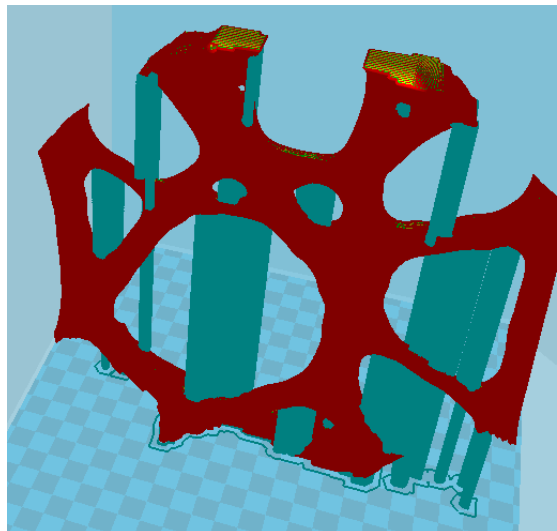
Figure 54: Generated (blue) support structure (for example joint 3).

Self-supporting features

Reducing the amount of support structure would reduce the building time, required material and time for post-processing. Most areas of the joint can be printed without the need of support structure. However, some areas can be improved by adding self-supporting features, like gothic arches, to avoid support structure. By slightly changing the geometry of the joint, support structure is not necessary anymore (Figure 56). It is not recommended to change the geometry of the joint on a larger scale, as the flow of forces might drastically change.

Whereas the topology optimization provided an ideal lay-out for the geometry of the structure. When changing the geometry a less effective structure is developed that needs to be checked by a structural analysis.

Residual stress reduction

By orienting the joints vertically in the building chamber, the printed cross-sections will be smaller than horizontally oriented (Figure 56). This will result in less residual stresses in the produced joint.

Note: it is recommended to post-process the joints by heat treatment in order to remove all residual stresses in the joint.

Wall thickness and gaps

The joints consists of solid structures, the thickness of the structures are controlled by applying a large filter radius.
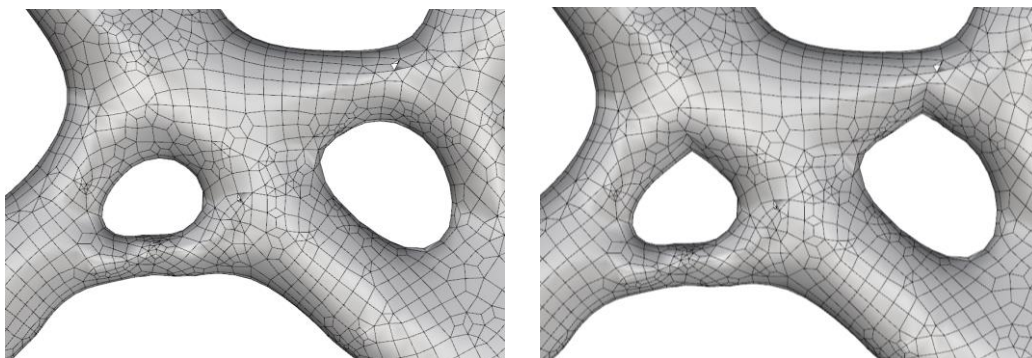
Figure 55: Holes with flat overhangs before transformation (left) and after transformation (right) with gothic arches.
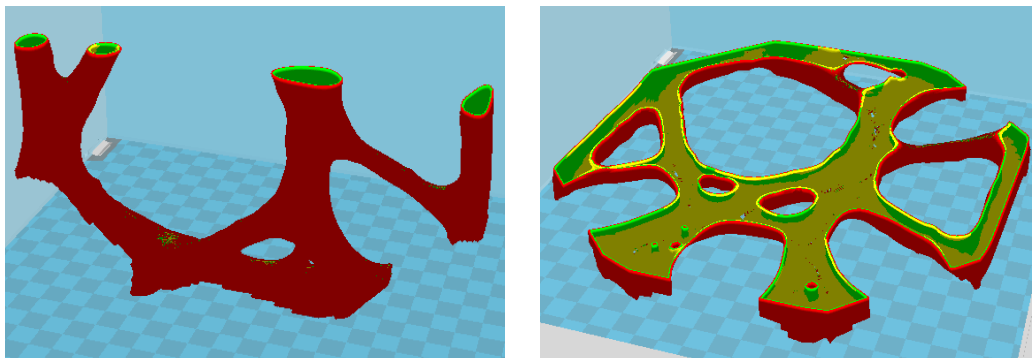
Figure 56: Cross-section vertically oriented (left) and horizontally oriented (right).

D

BESO3D

The topology optimization of the joints is carried out by the software *BESO3D*. BESO3D is developed by prof. Mike Xie of RMIT Univeristy (Australia) and made available for usage during this thesis. The software is a plug-in for Abaqus and is able to solve topology optimization problems by using the FEA engine of Abaqus.

The purpose of this appendix is to verify the application and different input settings of BESO3D in order to be able to understand the software. In this way, BESO3D is not just a black box, but a tool which can be trusted on. As simple optimization problems can be solved as expected, confidence is gained that BESO3D can handle complex problems as well.

The optimization function will be tested by using a simplified representation of a joint in a gridshell. Different cases will be split and analysed separately. Moreover, the ability to apply multiple load cases and adjust the filter radius will be explained and illustrated by examples.
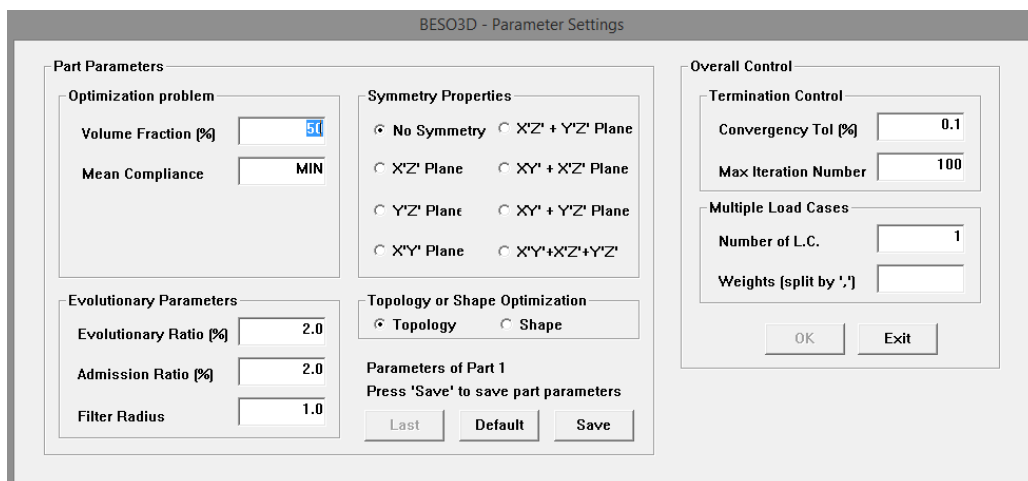
Figure 57: Interface of BESO3D plug-in for Abaqus.

D.1 TESTING BESO3D

D.1.1 SET-UP OF OPTIMIZATION MODEL

Geometry

The used model consists of three parts; the design domain and two non-design domains. By means of attaching two RHS members to the sides of the design domain, the same situation corresponding to the complex joints is created. Both non-design domains consist of RHS200x100x16 members with a length of 400 mm. While the left RHS member is fully constraint at the left-hand side, the right RHS member will introduce the load to the system. The design domain consists of a solid cross-section of 200x100 mm and is 400 mm in length. The model is schematically depicted in Figure 58.

Design domain

The design domain is the part of the model which is optimized by the BESO3D optimization tool. The design domain has the following properties:

- Material   Material with Young's modulus of $2,1*10^5$ N/mm² (steel);
- Mesh element   Linear hexahedron elements, 8-node linear brick: C3D8R;
- Section   Solid homogeneous;
- Step   Linear perturbation;
- Mesh width   8 mm;
- Cross-section   200x100 mm.
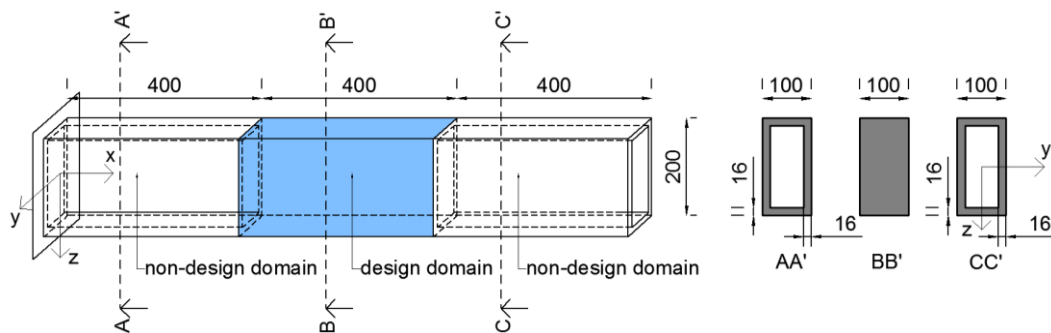
Figure 58: Geometry of the test model.

Loads and boundary conditions

The loads on the joint consist of three forces and three moments, which are applied separately. When only a single force or moment is working on the system, there is no influence on the result by the magnitude of the force or moment as it is when multiple forces or moments are applied. Hence, an arbitrary force and moment has been used.

Normal force in direction of members **x-axis**
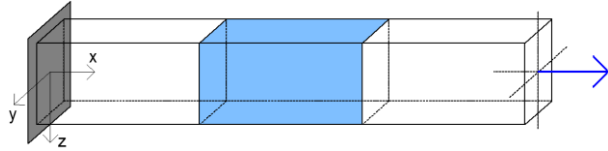
Shear force in direction of members **strong z-axis**
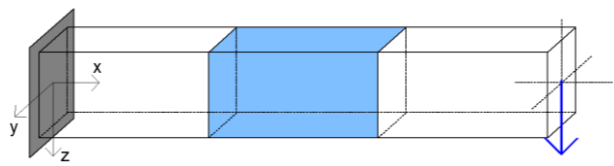
Shear force in direction of members **weak y-axis**
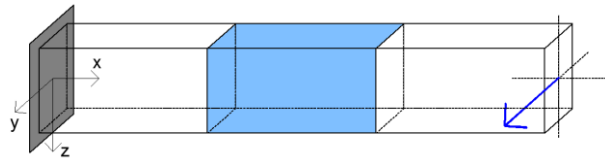
Moment around members **strong y-axis**
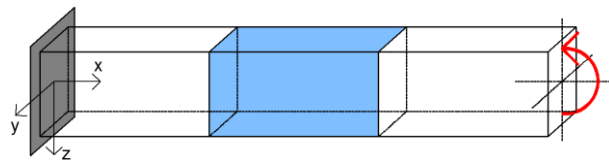
Moment around members **weak z-axis**
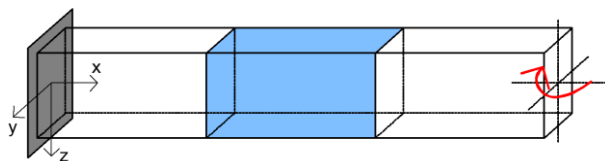
Moment around members axial x-axis: **torsion moment**
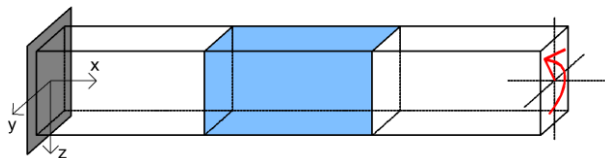
A typical load combination in joint 1 is a normal force with a moment around the members strong y-axis. Therefore, also this combination is analysed in the simple set-up as schematically depicted below. The situation in the heaviest loaded direction of the joint is chosen.

143

Normal force (1500 kN) and **moment** (35 kNm) around members **strong y-axis.**
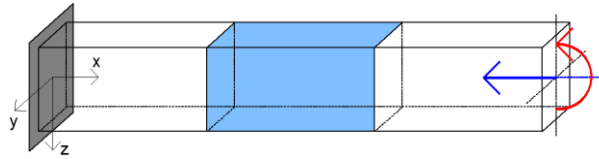
Remark 1: the forces are applied on an adjacent RHS member at the right-hand side of the design domain. This has been done in order to avoid local influences by the applied force. For the same reason the left-hand side of the design domain is connected to a RHS member as well.

Remark 2: as the applied shear forces are not directly applied on the right-hand side of the design domain, in fact an extra moment is introduced. Therefore a moment turning in the opposite direction is added for compensation. In this way, the desired problem with a shear force working at the right-hand side of the design domain is obtained.

Remark 3: positive forces and moments are applied for the chosen coordinate system. Excluding for the normal force problem, the results of negative applied forces and moments will correspond to the results of the positive forces and moments, except for the fact that they are mirrored.

Optimization settings

The different cases are optimized by using the following settings as depicted in Figure 59. The green highlighted boxes are adjusted and the grey boxes are set to default. While the mean compliance was minimised, the volume fraction was brought back to 30%. The results are depending on the volume fraction, but the specific percentage of 30% is chosen in order to create typical optimization patters which are obtained by removing 70% of the initial material of the design domain. Finally, the evolutionary ratio and admission ratio were set to 2,0% and the filter radius was set to 16,0 mm.

D.1.2 OPTIMIZATION RESULTS

In order to visualise the results as clear as possible, views of the top (XY-plane), front (YZ-plane) and side (ZX-plane) are presented alongside a perspective view. The RHS members on both sides of the design domain are not displayed in order to avoid visual hindrance on the optimized result of the design domain.
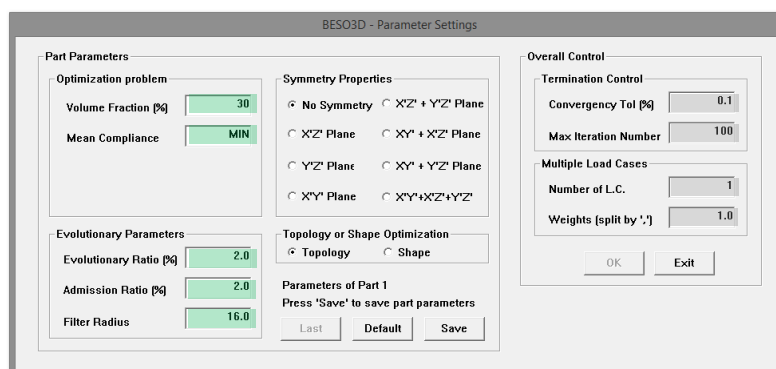
Figure 59: Optimization settings.

Starting point

Before the optimization starts, the design domain looks as follows:
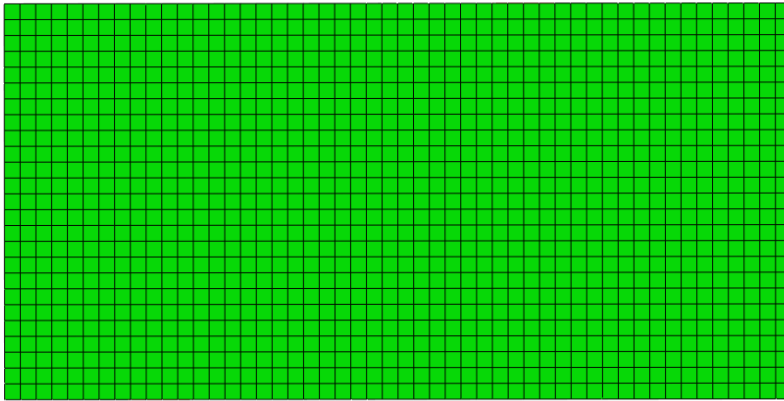
Figure 60: Front view (YZ-plane).
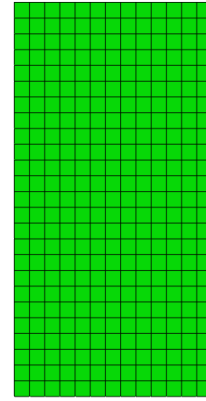
Figure 61: Side view (ZX-plane).
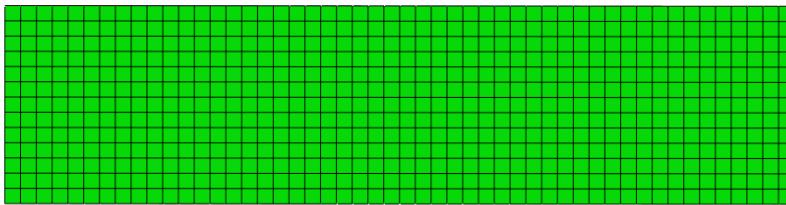
Figure 62: Top view (XY-plane).
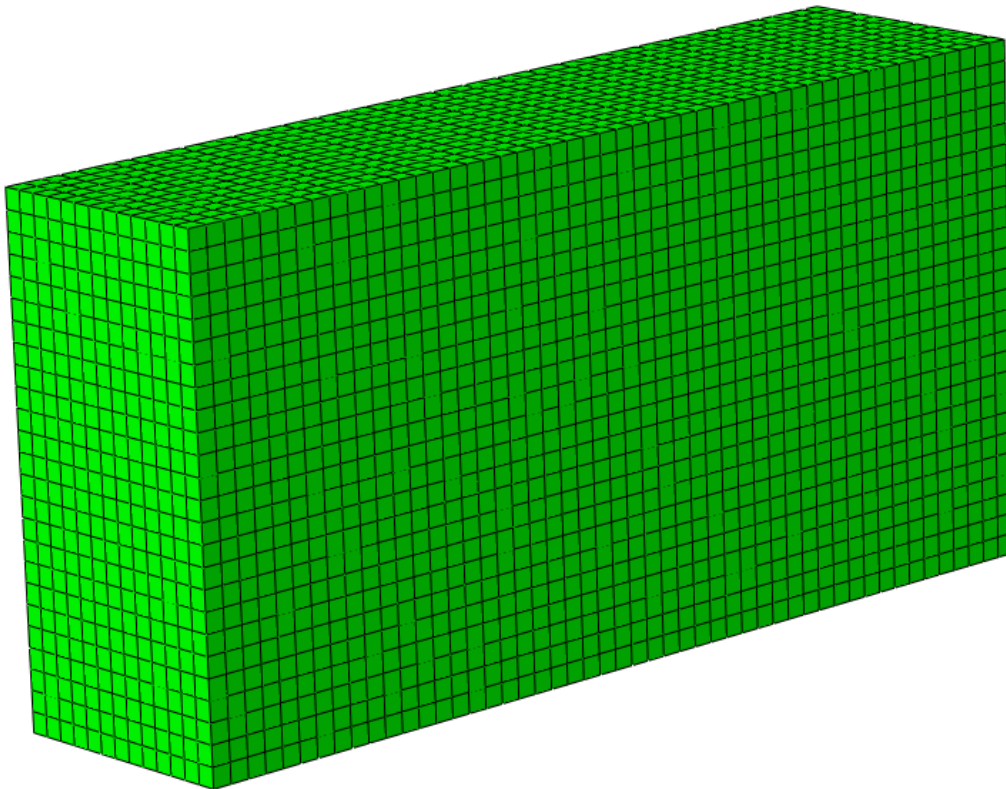
Figure 63: Perspective view.

145

Normal force

The optimization results by applying a normal force:
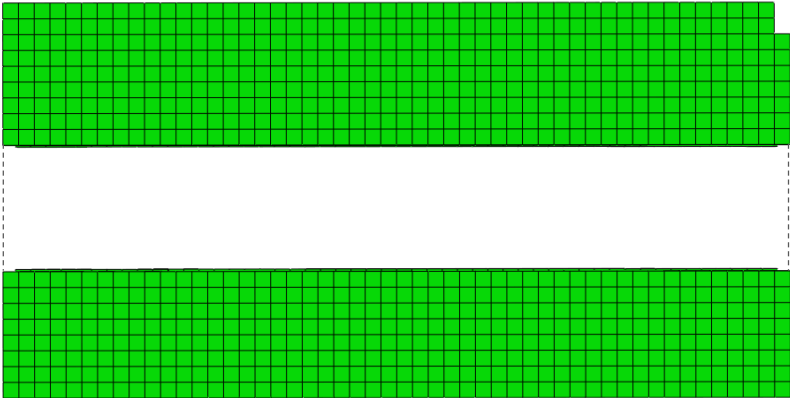
Figure 64: Front view (YZ-plane).
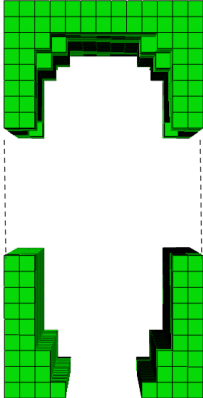
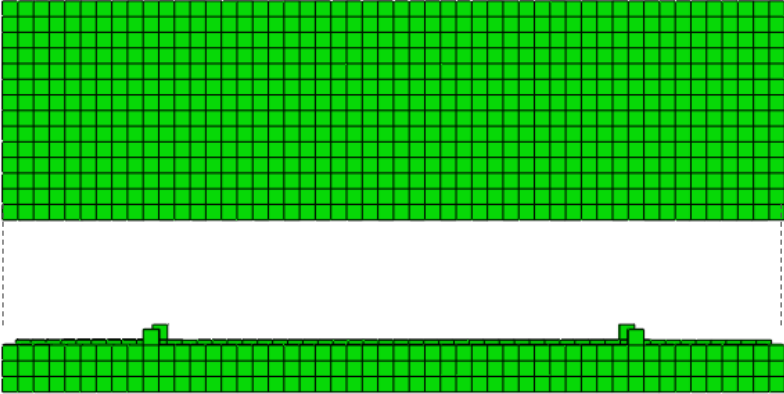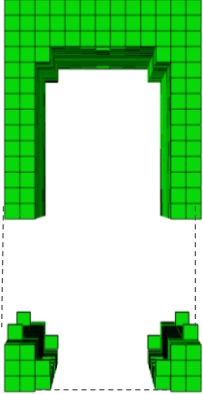*Figure 65: Side view (ZX-plane).*
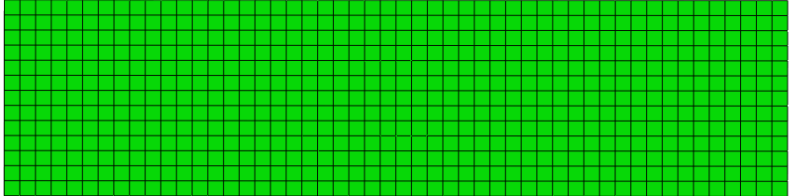
Figure 66: Top view (XY-plane).
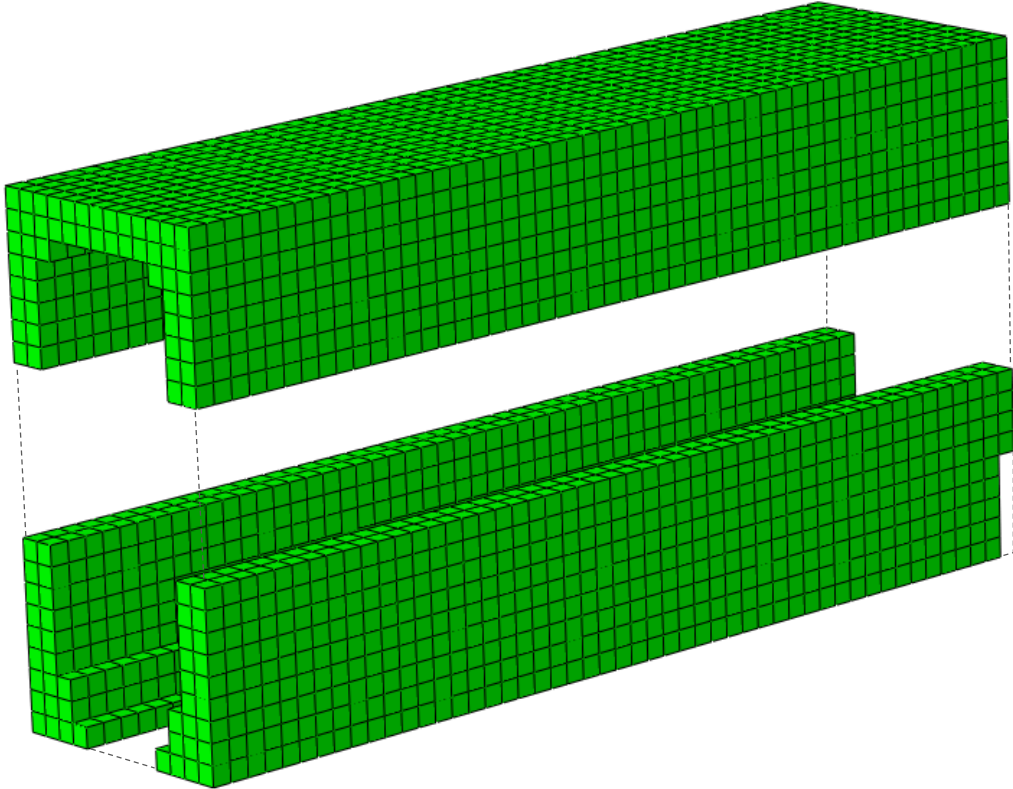
Figure 67: Perspective view.

Shear force – strong z-axis

The optimization results by applying a shear force In the direction of the strong axis:
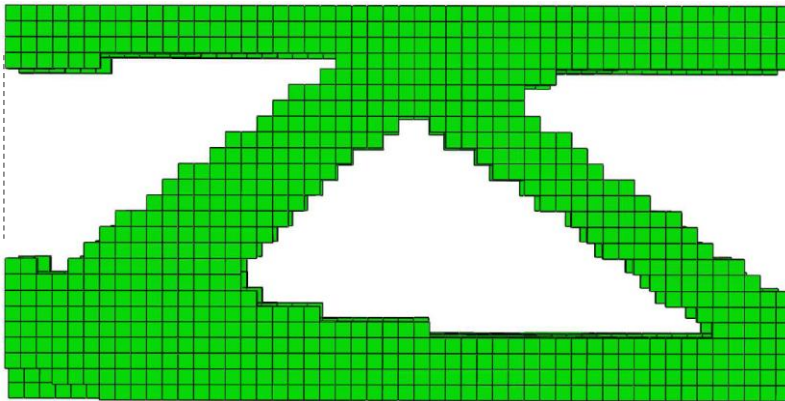
Figure 68: Front view (YZ-plane).
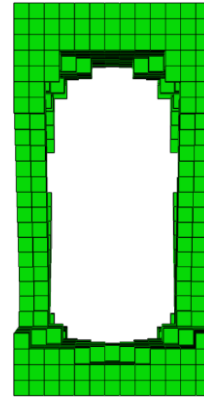
Figure 69: Side view (ZX-plane).
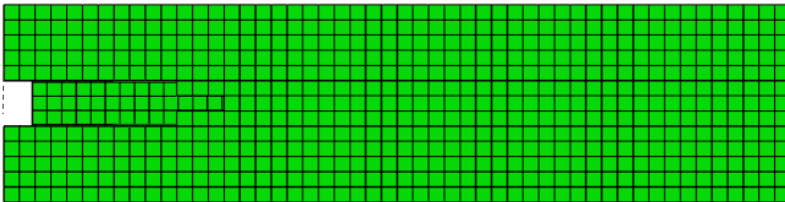
Figure 70: Top view (XY-plane).
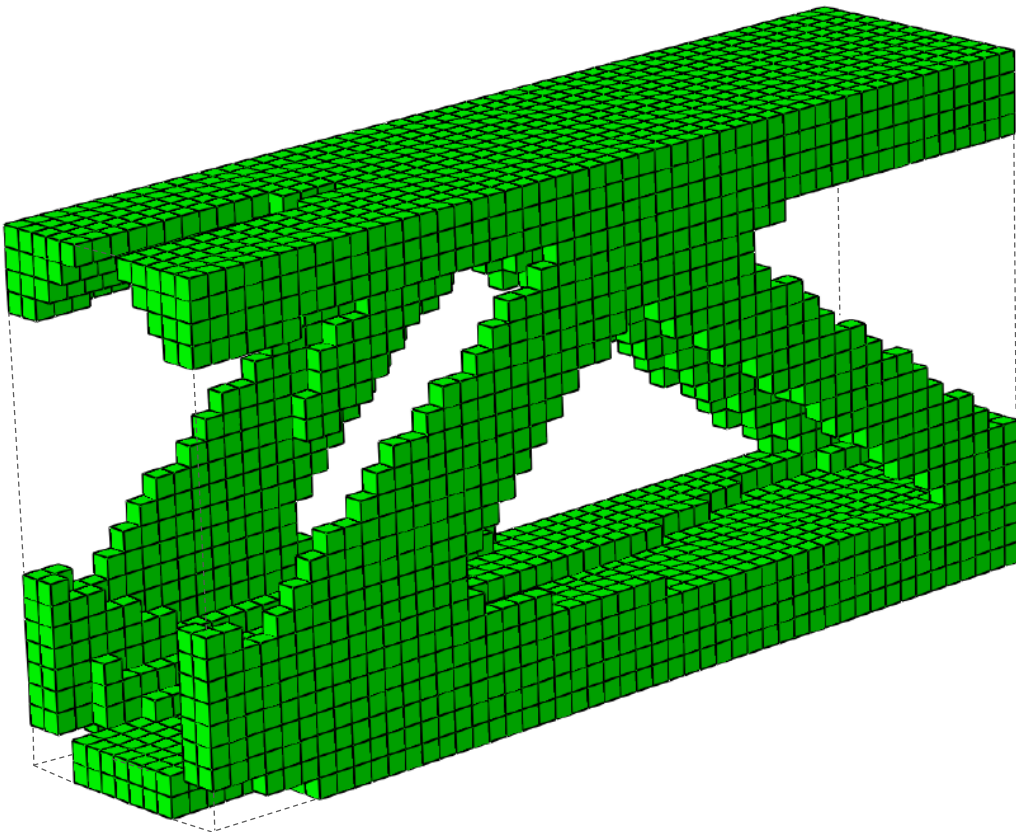
Figure 71: Perspective view.

147

Shear force – weak y-axis

The optimization results by applying a shear force In the direction of the weak axis:
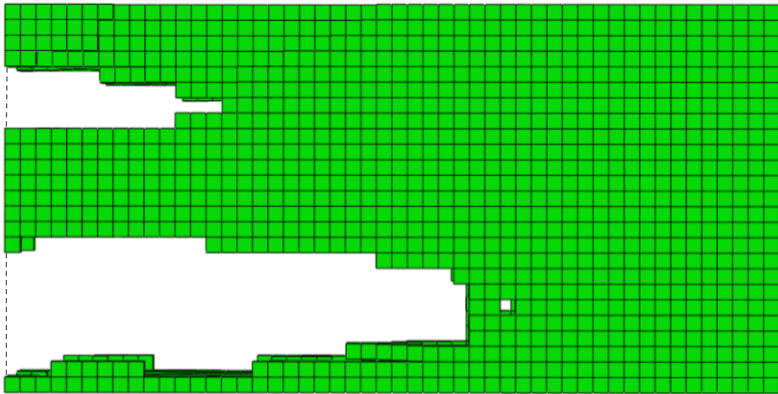
Figure 72: Front view (YZ-plane).
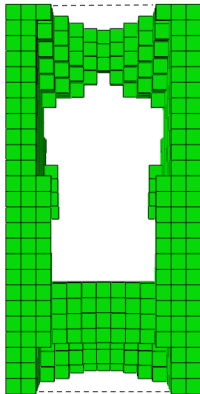
Figure 73: Side view (ZX-plane).
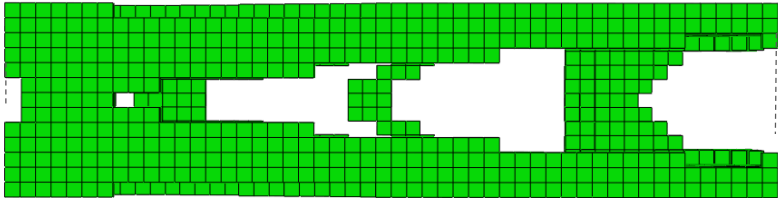
Figure 74: Top view (XY-plane).
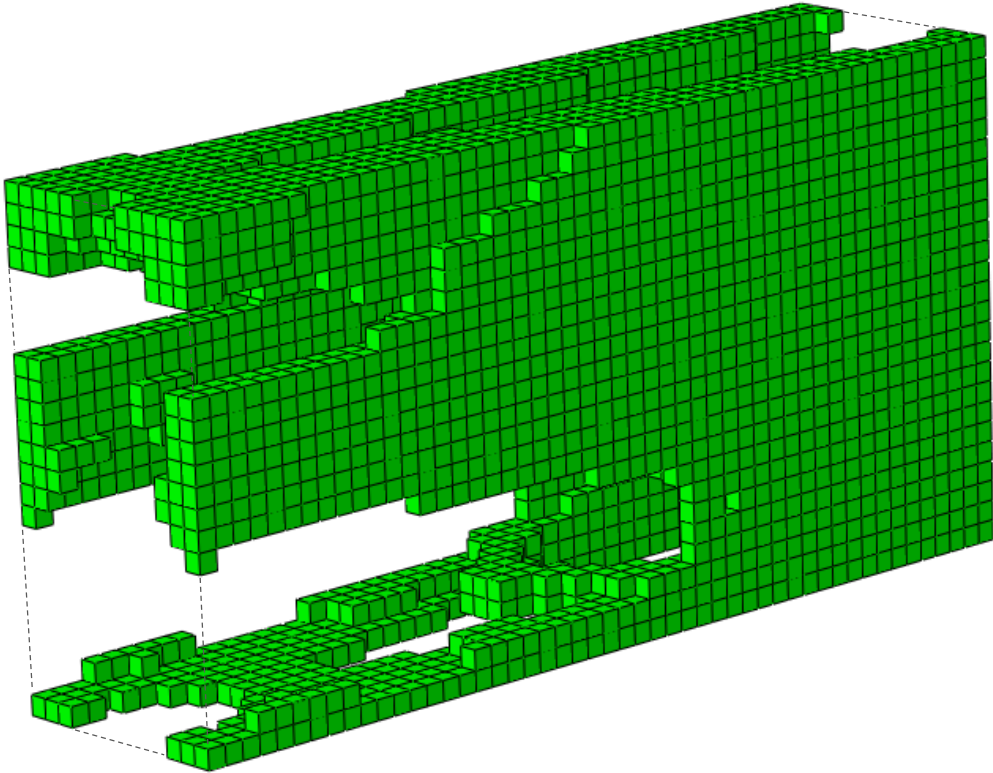
Figure 75: Perspective view.

Moment – strong y-axis

The optimization results by applying a moment around the strong axis.
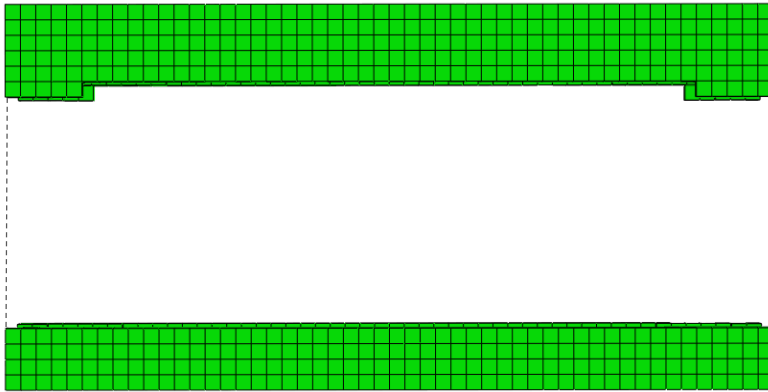
Figure 76: Front view (YZ-plane).
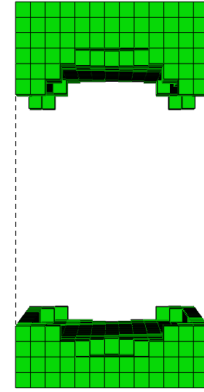
Figure 77: Side view (ZX-plane).
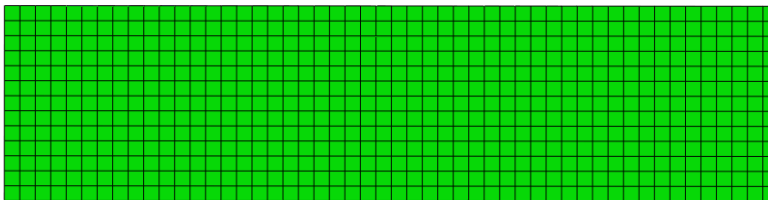
Figure 78: Top view (XY-plane).
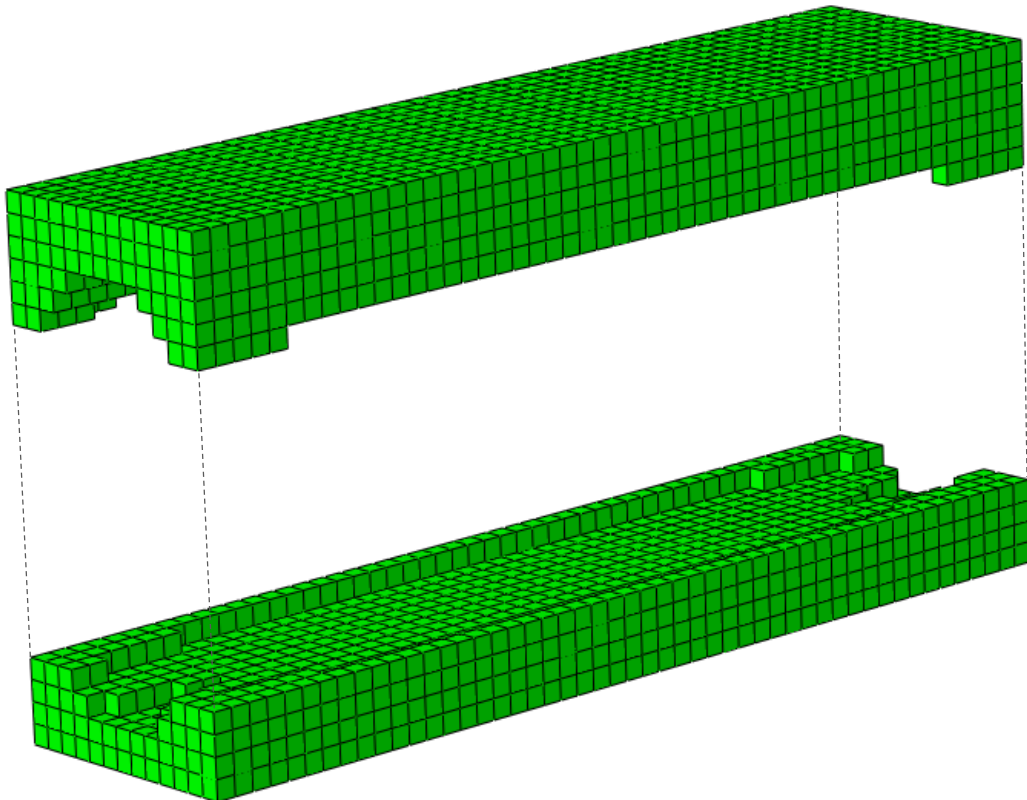
Figure 79: Perspective view.

Moment – weak z-axis

The optimization results by applying a moment around the weak axis.
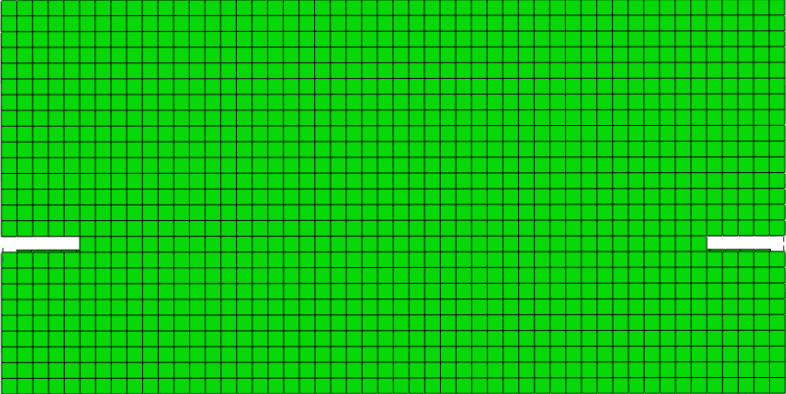
Figure 80: Front view (YZ-plane).
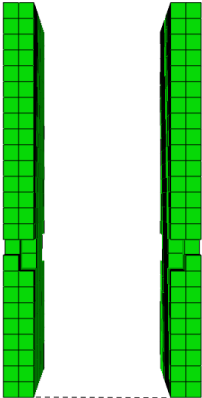
Figure 81: Side view (ZX-plane).
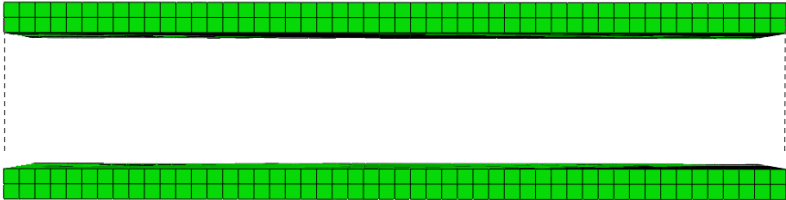
Figure 82: Top view (XY-plane).
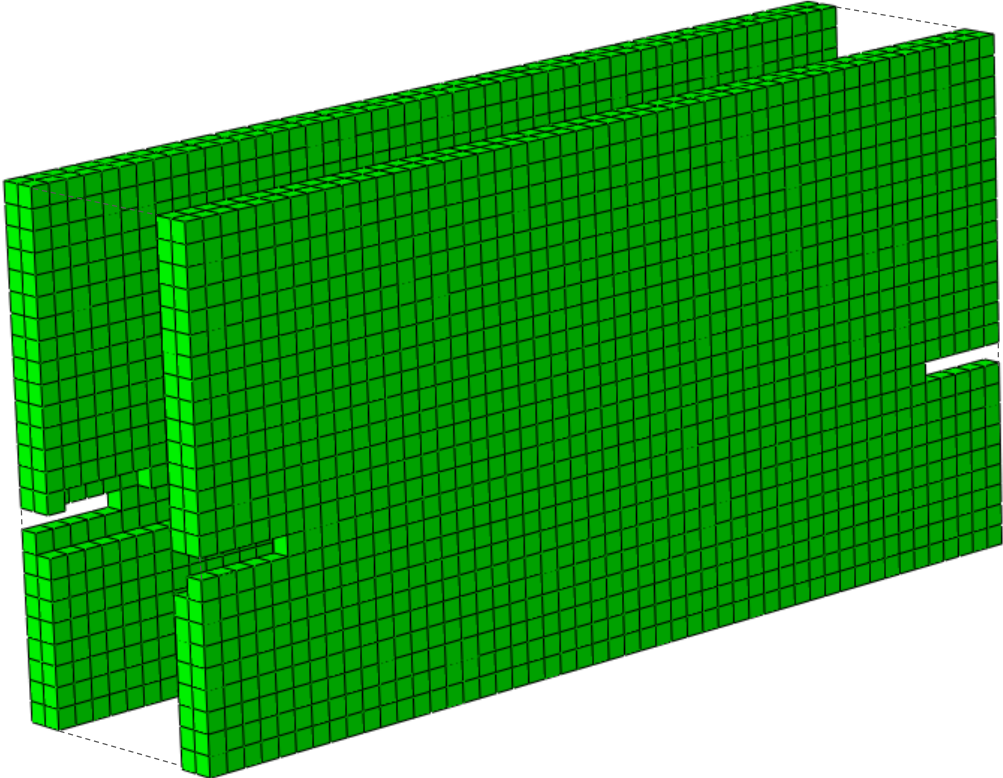
Figure 83: Perspective view.

Moment – torsion

The optimization results by applying a torsional moment.
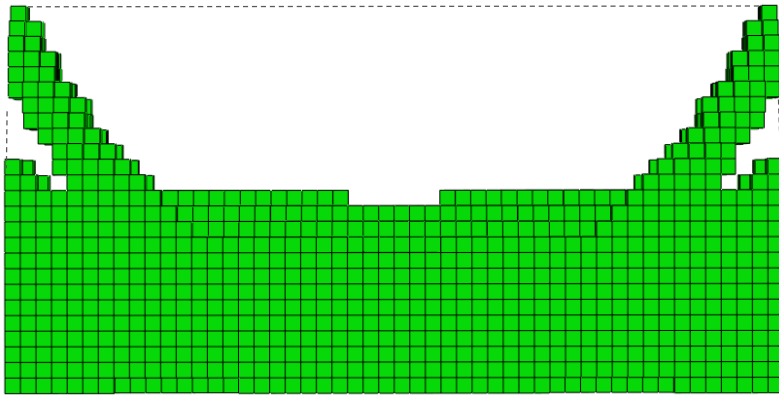
Figure 84: Front view (YZ-plane).
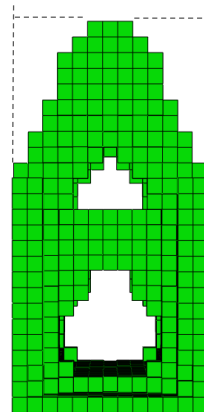
Figure 85: Side view (ZX-plane).
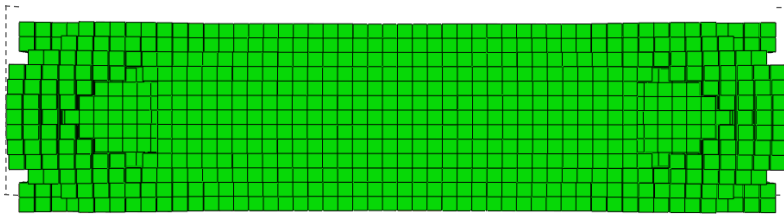
Figure 86: Top view (XY-plane).
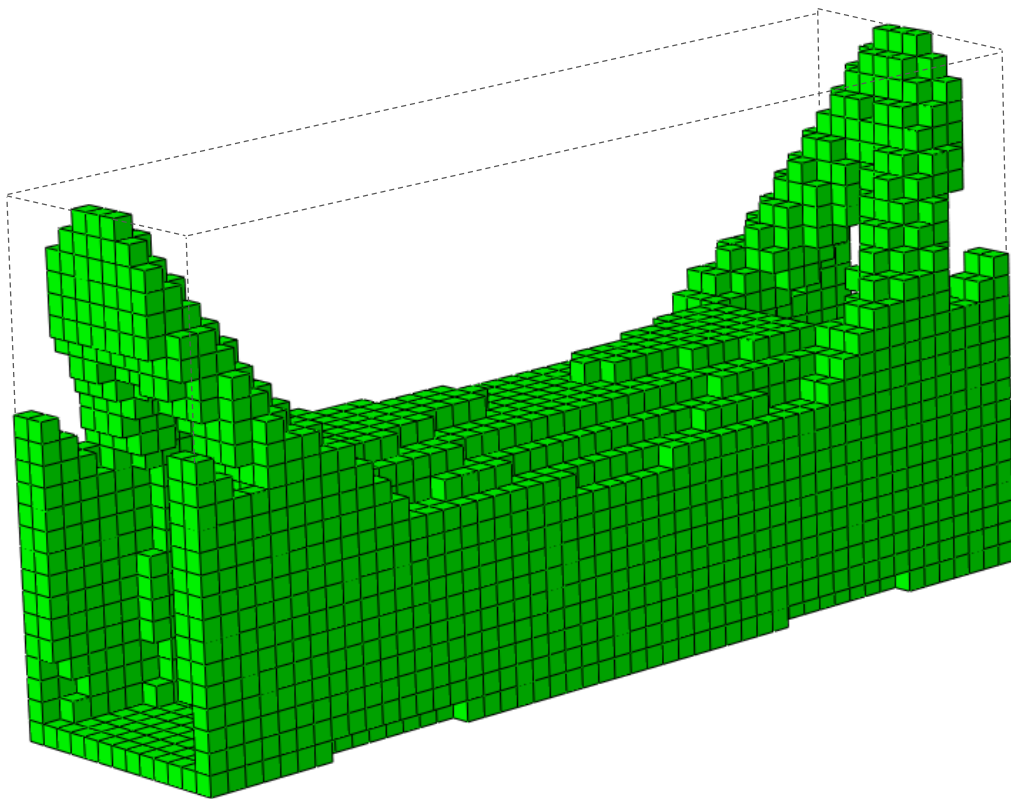
Figure 87: Perspective view.

Load combination: normal force – moment around strong y-axis

The optimization results by applying a normal force and a moment around the strong axis.

Figure 88: Front view (YZ-plane).

Figure 89: Side view (ZX-plane).
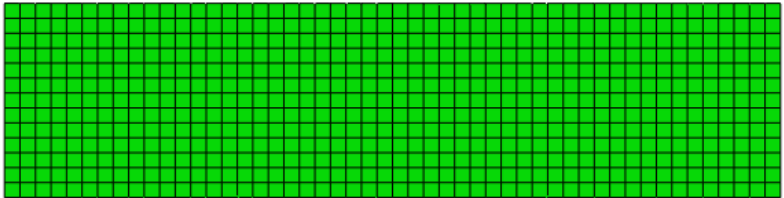
Figure 90: Top view (XY-plane).
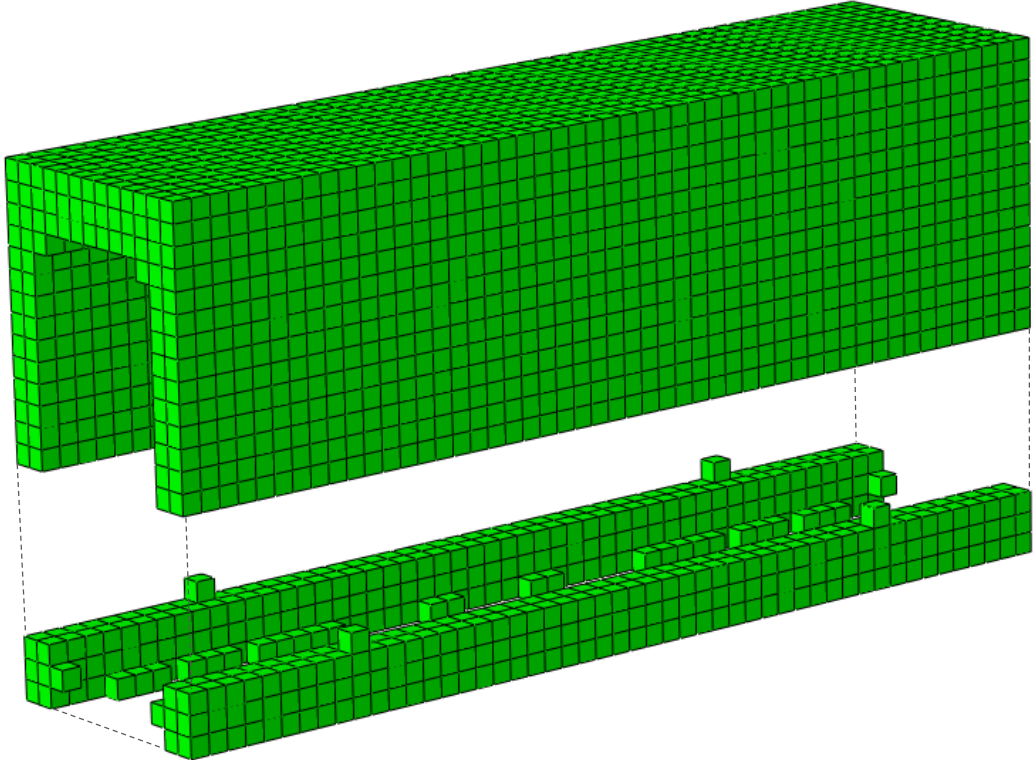
Figure 91: Perspective view.

D.1.3 OVERVIEW OF RESULTS

The results of the optimization of the separated cases make it clear that different kind of patterns and structures appear when loaded by loads or moments. The typical patterns belonging to the specific loads will be discussed in this overview. These results are used in order to clarify optimization results of complex problems.

Normal force

The developed structure is in fact an extension of the RHS members and it forms a tube. Depending on the amount of removed material, the remaining material will mostly be situated in line with the stiffest parts. These are in this case the corners of the RHS member.
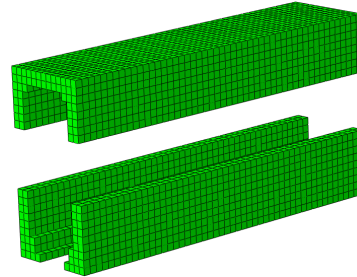
Shear force – strong z-axis

The optimized form consist of two truss structures. As the shear force at the right hand side introduces a moment in the structure, the optimization tool situates the material as far away as possible from the central axis. Moreover, the shear force needs to be transferred from one side to the other. Therefore, the truss structures is developed to create cohesion between the upper and lower structure. The trusses are located in line with the upright walls of the RHS member.
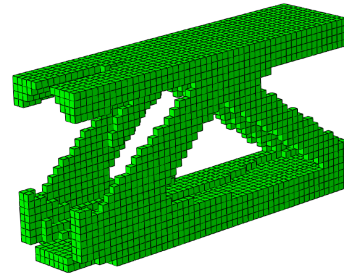
Shear force – weak y-axis

The optimized result corresponds with the result in case of a shear force in the direction of the members strong axis. However, the result is now rotated by 90 degrees around the members axis. Truss structures are formed at the top and the bottom walls.
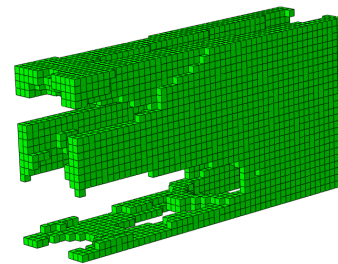
Moment – strong y-axis

The material is situated in such a way that as much as possible 'height' is created. The outer fibres of the structure are the most stressed when applying a bending moment. Therefore, the material is placed at the other zones of the design domain. As the top and bottom fibres are loaded by mere tension and pressure, they do not need to work together and thus no truss structures need to be developed.
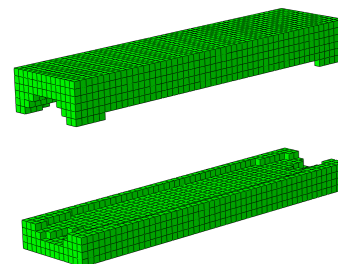
Moment – weak z-axis

The optimized result corresponds with the result in case of a shear force in the direction of the members strong axis. However, the result is now rotated by 90 degrees around the members axis. The material is now situated at the left and right walls of the RHS members.
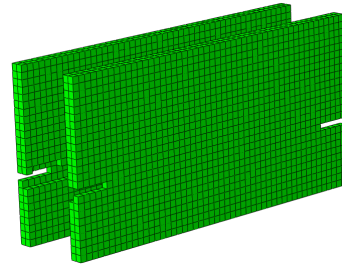

Torsion

The result of the optimization can be considered as a circular hollow section. This can be seen as a logic result as CHS profiles are well-known for their ability to resist torsion. The developed CHS profile can both be placed at the bottom or top of the RHS member.
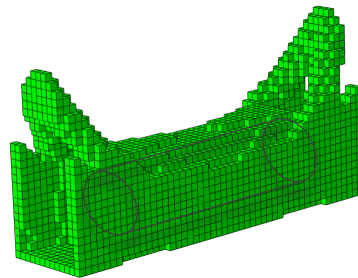
Normal force and moment – strong y-axis

Applying a normal force and a moment around the strong axis results in a combination of the separate optimization results. However, the result depends on the ratio between the normal force and the moment.

Taking a look at the derived result, at the sides of the design domain the pressure developed by the normal force is equal to the tension developed by the moment in the area. Therefore, the material is taken away at this spot. In this case, the result is neither dominated by the normal force nor the moment. It might also be possible that all material is taken away at the top or bottom when the stress in the fibres is equal to zero.
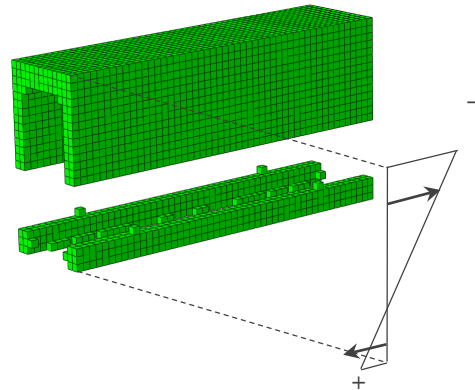
D.2   MULTIPLE LOAD CASES

BESO3D provides the possibility to apply multiple load cases during optimization runs (Figure 92). The possibility of applying multiple load cases will result in a structural joints with a higher capability of dealing with different kind of load cases. The different load cases are the result of different kind of loads on the gridshell, e.g. snow load, wind load, ponding or loads by maintenance work. Here, a load case consists of an entire set of loads on a joint, i.e.; an axial force, two shear forces, a torsional moment and two bending moments.

Applying multiple load cases can also be helpful in order to guide the optimization towards a satisfying result. To satisfy the stiffness condition, see subsection 3.1.5, the joint requires a certain height to resist out-of-plane moments. However, optimization tools are able to remove material at undesired locations which could reduce the initial height of the structure. This is illustrated by the following example.

Consider the following situation: a structure is loaded by a normal force and a bending moment (Figure 93). Due to the normal force and the bending moment, the structure will translate and rotate respectively. In case of equal displacements due to translation and rotation, the outer fibres will not move, see Figure 93.

During the optimization, the optimization tool maximises the stiffness while removing a certain amount of material. In order words: the optimization tool seeks the optimal structure to minimise the displacements due to the applied loads. In the example, material will be removed at the top of the structure and the initial height will be reduced (see Figure 94 and Figure 96 for a concrete example). It can occur that even though stresses are well below limits, the optimized structure (joint) might fail on the stiffness criterion. An example of this kind of 'undesired' material removal is depicted in Figure 96.

A solution to this phenomenon is to add an additional load case containing only out-of-plane bending moments. By taking the additional load case into account during the optimization run, material will remain at the top and the bottom of the structure which remains a large part of its initial stiffness, see Figure 95.
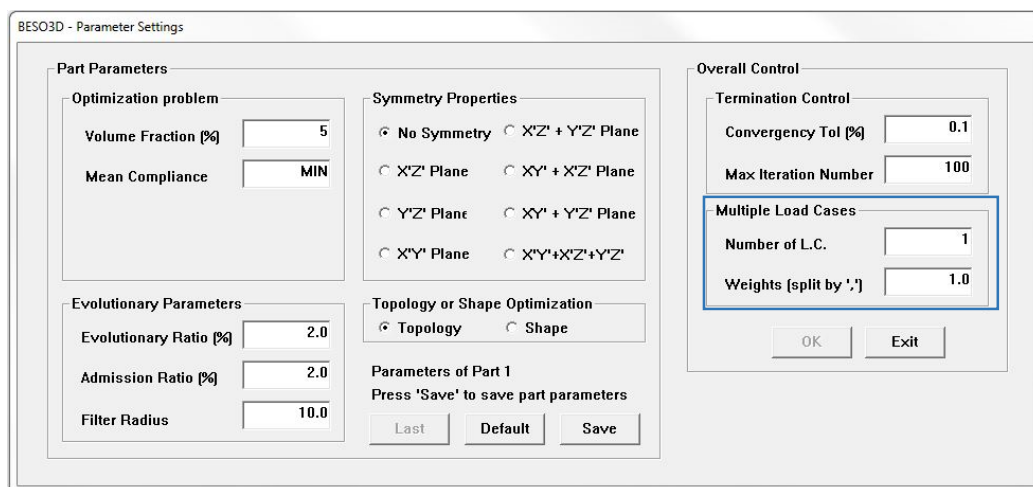

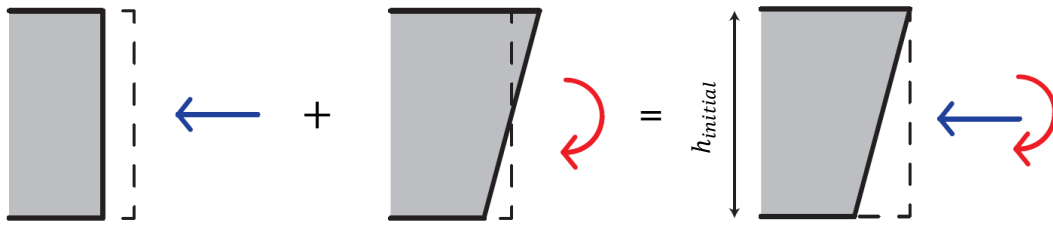*Figure 92: Option to apply multiple loadcases in BESO3D.*

Figure 93: Displacements due to a normal force (left) and a bending moment (middle) result in a translated and rotated loading plane (right).
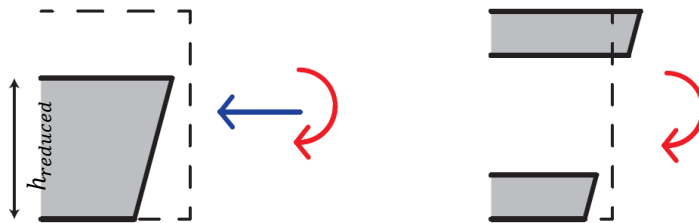

Figure 94: Reduced height due to removal of material.

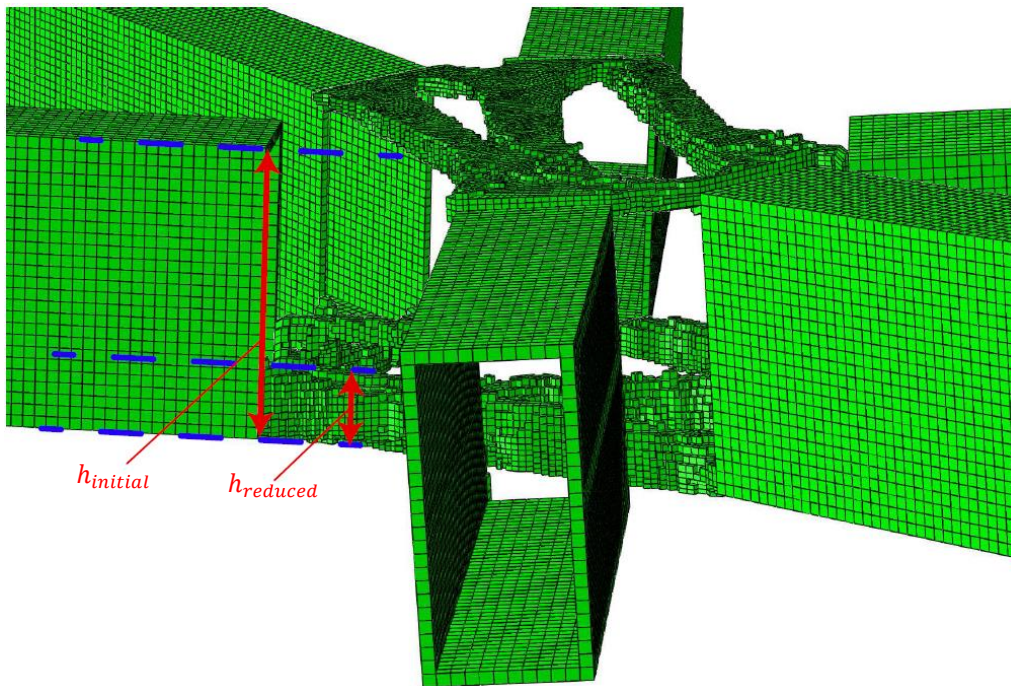*Figure 95: Initial stiffness due to additional load case.*

Figure 96: Example of undesired removal of material due to specific loading conditions.

D.2.1 APPLICATION

When applying multiple load cases it is possible to distinguish the importance of each load case by a pre-determined *weight*, see Figure 92. In this way, specific load cases can be emphasized in order to improve or influence the results. The pre-determined weight factors $X_1, X_2 \ldots X_n$ with $X_i \leq 1.0$ and $X_1 + X_2 + \cdots + X_n = 1.0$ define the object function as:

$$obj = X_1 C_1 + X_2 C_2 + \cdots + X_n C_n \qquad (3)$$

With C_i as the mean compliance.

D.2.2 TESTING OPTION OF MULTIPLE LOAD CASES IN BESO3D

The following example is carried out in order to provide insight in, but also to check the option to apply multiple load cases with BESO3D. In the example, the same FEA model with the same settings is used as in previous section. Moreover, the same optimization settings are used as in the case of the simple models; the volume fraction is brought back to 30% while the stiffness is maximised (minimisation of the mean compliance). The main difference is the application of multiple load during the optimization run. This example makes use of the following two load cases:

Load case 1:

Upward bending moment around members **strong y-axis**
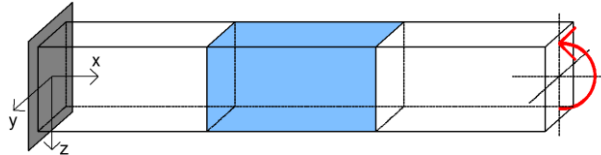
Load case 2:

Upward shear force in direction of members **strong z-axis**
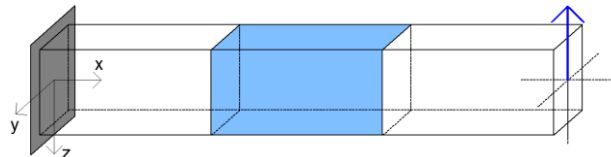
Three cases will be examined with the same above mentioned applied load cases:

1. Equally weighted load case 1 and 2 $obj = 0{,}5C_1 + 0{,}5C_2$
2. Dominant load case 1 $obj = 0{,}99C_1 + 0{,}01C_2$
3. Dominant load case 2 $obj = 0{,}01C_1 + 0{,}99C_2$

The first case demonstrates the result of taking multiple load cases into account during the optimization run. The result is used to show the difference between an optimized structure for multiple load cases versus a structure optimized for a single load case.

The second and third case are used as check for the use of multiple load cases. In case of a proper working multiple load cases function, the results would correspond to the following expectation:

- When applying a large weight factor of 0,99 to load 1 (bending moment) and a small factor of 0,01 to load 2 (shear force), the result will approach the optimized result for a mere bending moment, see Figure 79.
- When applying a large weight factor of 0,99 to load 2 (shear force) and a small factor of 0,01 to load 1 (bending moment), the result will approach the optimized result for a mere shear force, see Figure 71.

Note: in contrast to the optimization of the joints where a load case consists of a set of forces and moments on the joint, this example makes use of a single load or moment in each load case in order to create an understandable problem.

D.2.3 OPTIMIZATION RESULTS

Similar to the visualisation method for the simple optimization problems has been used; views of the top, front, side and a perspective view are presented. The RHS members are not displayed.

Equally weighted load case 1 (bending moment) and 2 (shear force)

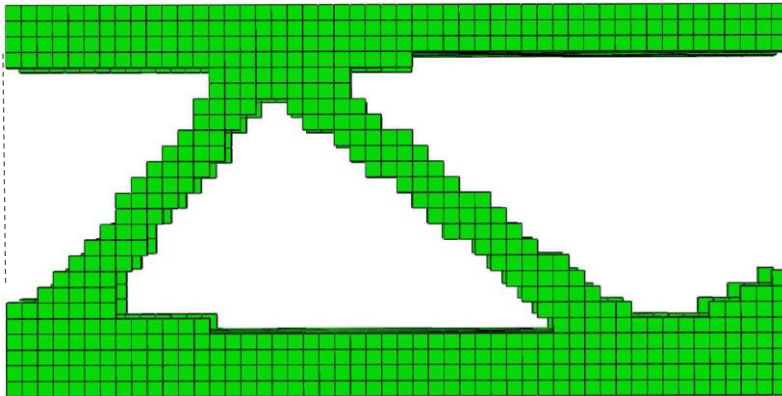The optimization results for the following objective function: $obj = 0{,}5C1 + 0{,}5C2$:
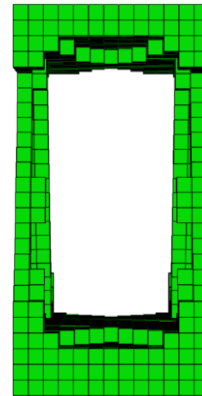

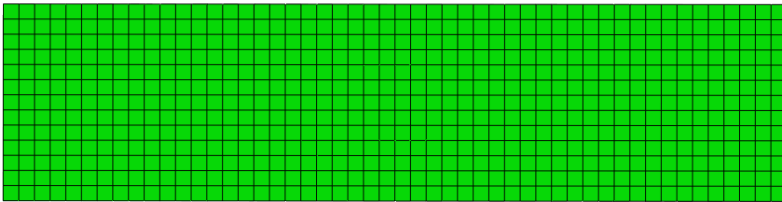*Figure 97: Front view (YZ-plane).*

Figure 98: Side view (ZX-plane).

Figure 99: Top view (XY-plane).
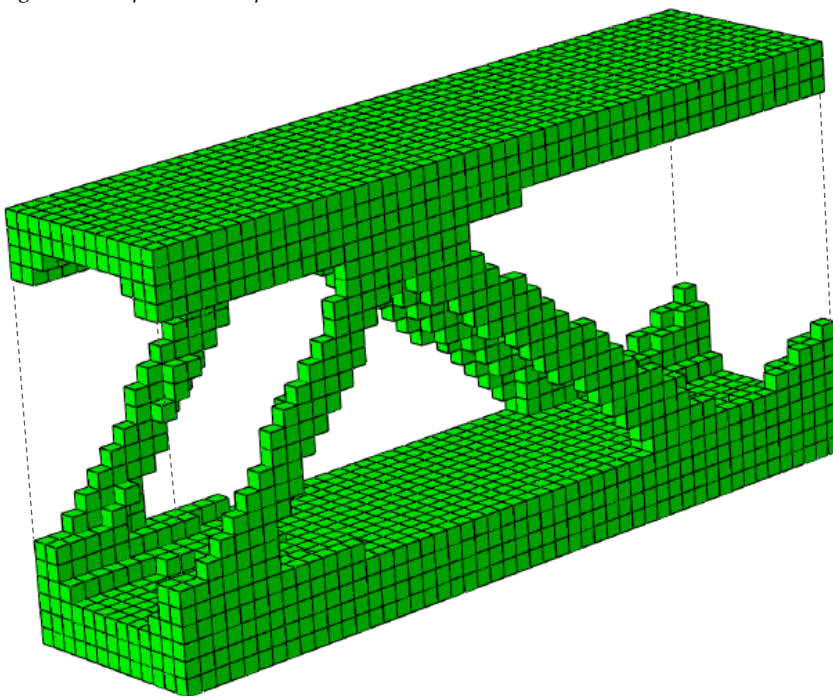
Figure 100: Perspective view.

D.2.4 MULTIPLE LOAD CASES VERSUS SINGLE LOAD CASE

The optimized structure for a single load case will be the optimal structure for that specific load case. However, the optimized structure taking multiple load cases into account, will not be optimal for a specific load case. This is illustrated by the following comparison.

Consider a structure as in the previous example that has been optimized for (i) a shear force and a bending moment with weight factors 0,5 and 0,5 (Figure 97 to Figure 100) and (ii) a single shear force (Figure 71). Loading both structure with a single shear force will result in a stress distribution within the structures as presented in Figure 101 and Figure 102. The result for the structure optimized for both load cases shows an unequal stress distribution whereas the stress distribution is equal for the structure optimized for the single shear force.

In fact, optimising a structure for a single load case results in an 'ideal' structure which could potentially utilize the full strength of the material (disregarding geometrical non-linearity). However, the practical situation always consists of multiple load cases and therefore the optimized structure will be a mixed result of all the load cases which has been taken into account.
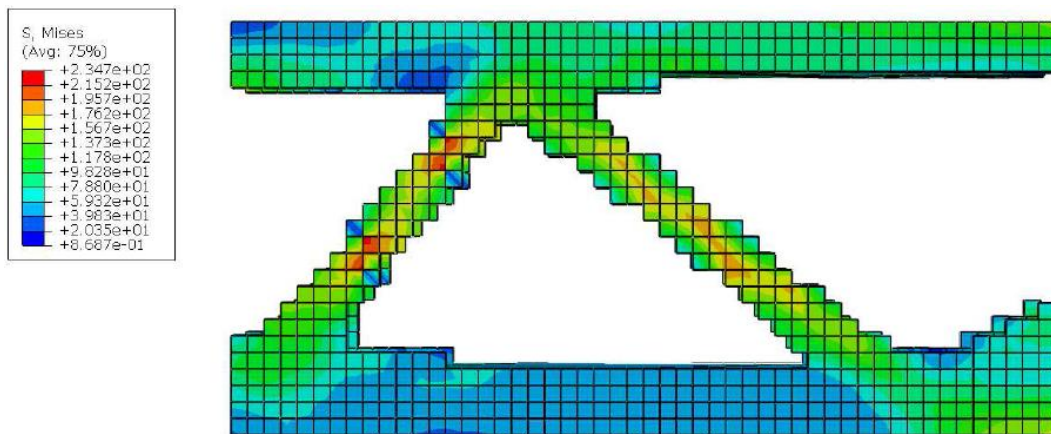

Figure 101: Stress distribution in a structure optimized for both a bending moment and a shear force loaded by a shear force.
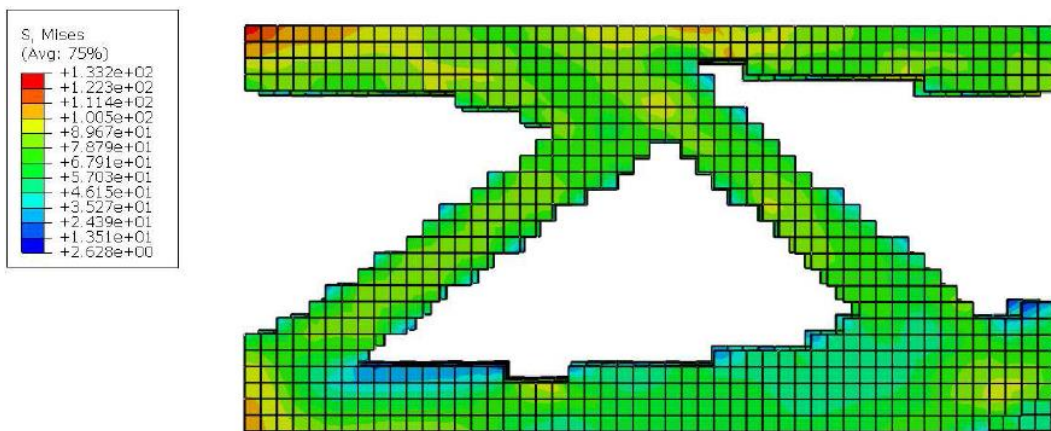

Figure 102: Equal stress distribution for a structure optimized for only a shear force and loaded by a shear force.

159

Dominant load case 1 (bending moment)

The optimization results for the following objective function: $obj = 0,99C1 + 0,01C2$:
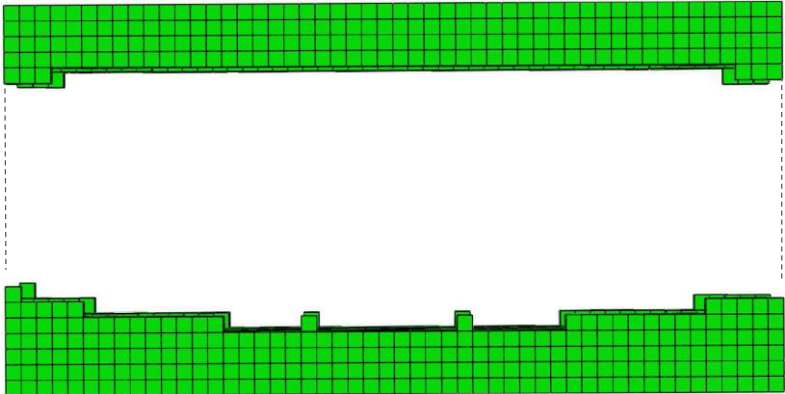

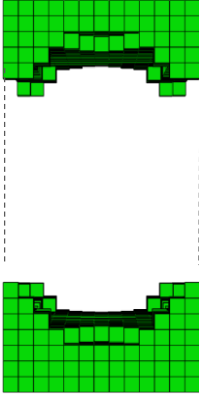*Figure 103: Front view (YZ-plane).*
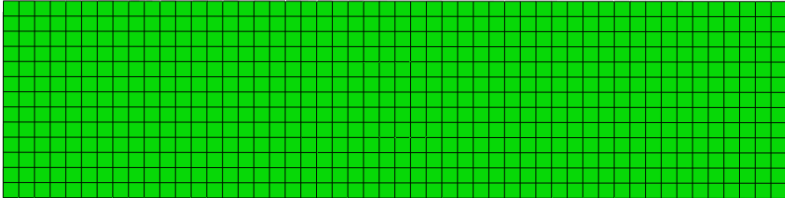

Figure 104: Side view (ZX-plane).
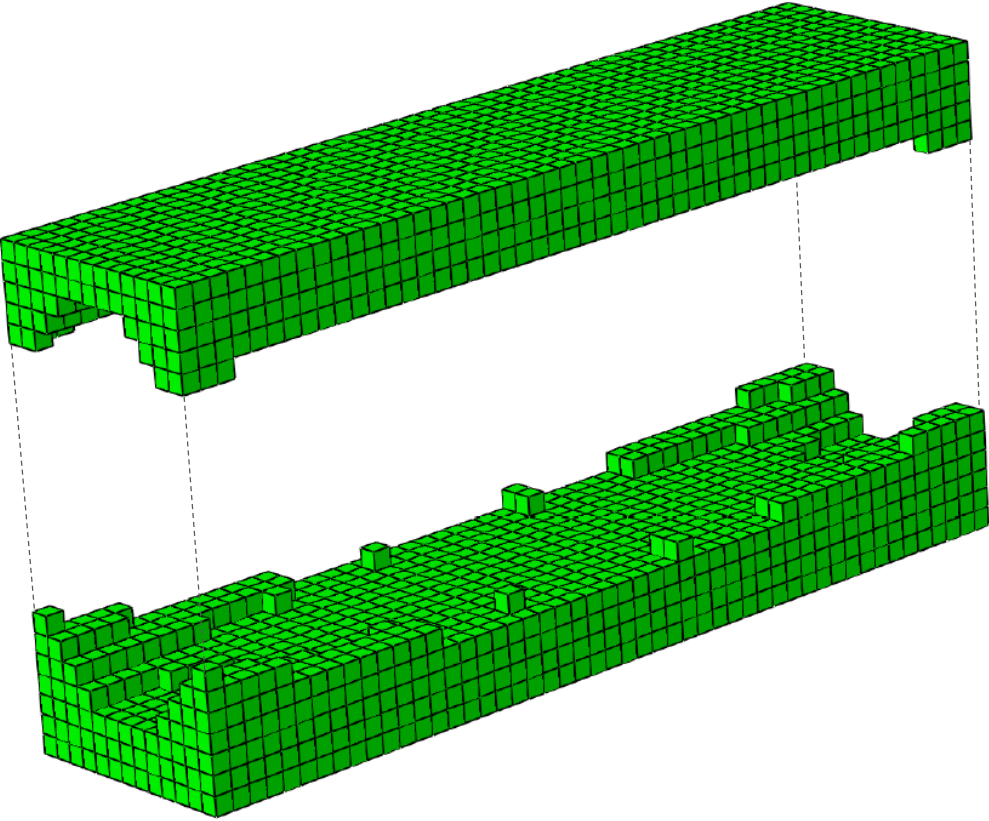

Figure 105: Top view (XY-plane).

Figure 106: Perspective view.

Dominant load case 2 (shear force)

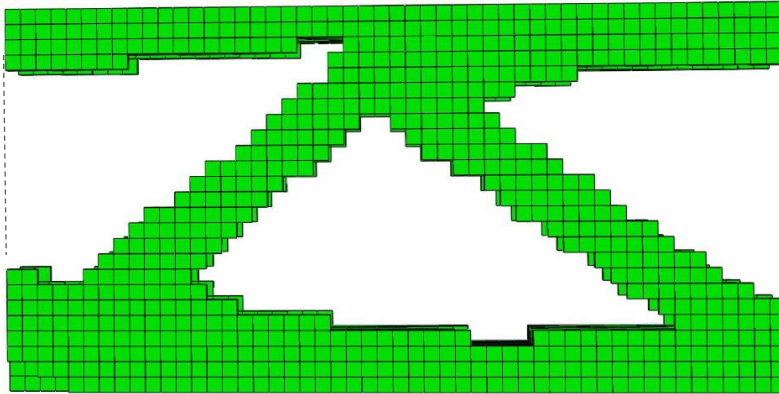The optimization results for the following objective function: $obj = 0,01C1 + 0,99C2$:
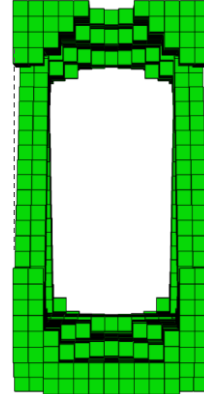

Figure 107: Front view (YZ-plane).
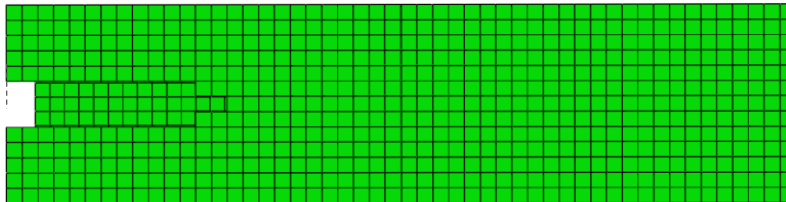

Figure 108: Side view (ZX-plane).

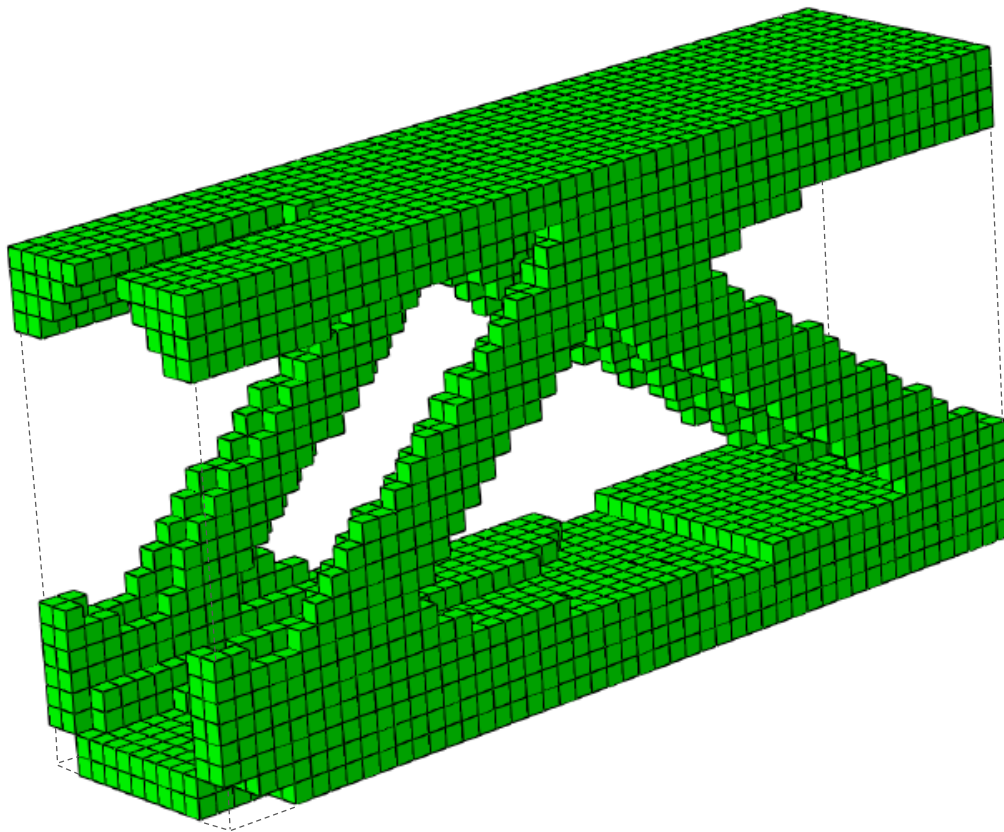*Figure 109: Top view (XY-plane).*

Figure 110: Perspective view.

D.2.5 OVERVIEW OF RESULTS

An overview of the results is presented below. In case of the dominant bending moment and shear force, the results are compared with reference models.

**Equally weighted bending moment and shear force**

The result can be considered as a combination between the results of the dominant moment and the dominant shear force; the recognizable patterns are still present, but less material is used for both patterns. The found result is a logic result as both the loads are equally weighted in the object function.
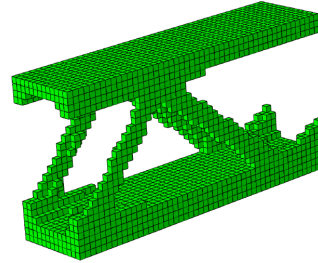
Dominant bending moment

The optimized result (left) with a dominant moment (load case 1) clearly corresponds to the reference model (right) with only a moment applied.
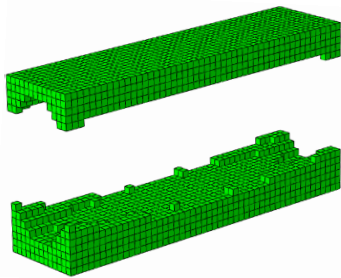
Result   *Reference model*

Dominant shear force

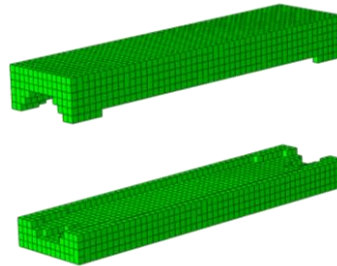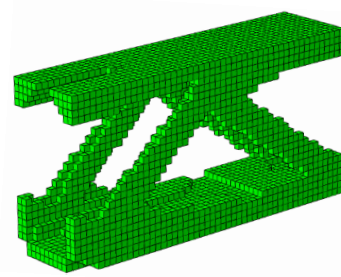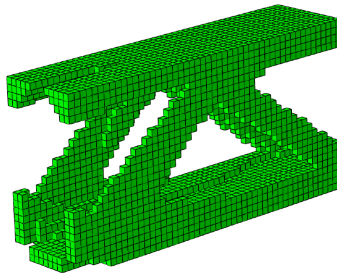Also, the optimized result (left) with a dominant shear (load case 2) force clearly corresponds to the reference model (right) with only a shear force applied.

Result   *Reference model*

D.3 FILTER RADIUS

Next to the option to apply multiple load cases, the filter radius is a setting which can be controlled by the engineer.

Stress values of elements influence the optimization process. To prevent the occurrence of slender (instable) structures due to unrealistic high stress levels from singularities in the mesh, a modified stress filter is used. The filter radius, measured from the centre of a mesh element (Figure 111), determines to which extent mesh elements take neighbouring elements into account. By increasing the filter radius, stress values will be smoothed and instable structures can be prevented by applying a proper filter radius [27].
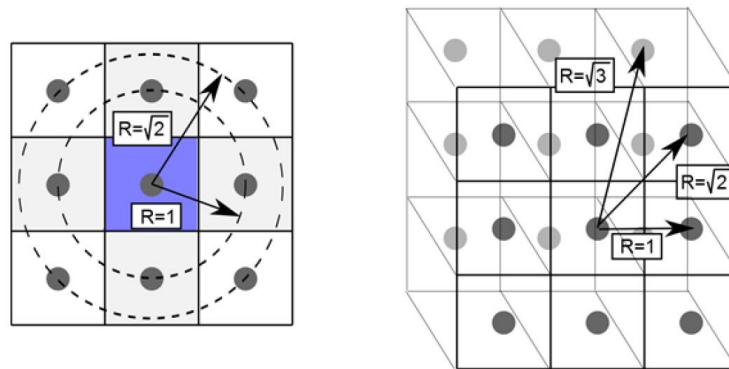

Figure 111: Filter radii (R) for 2D and 3D meshes [27].
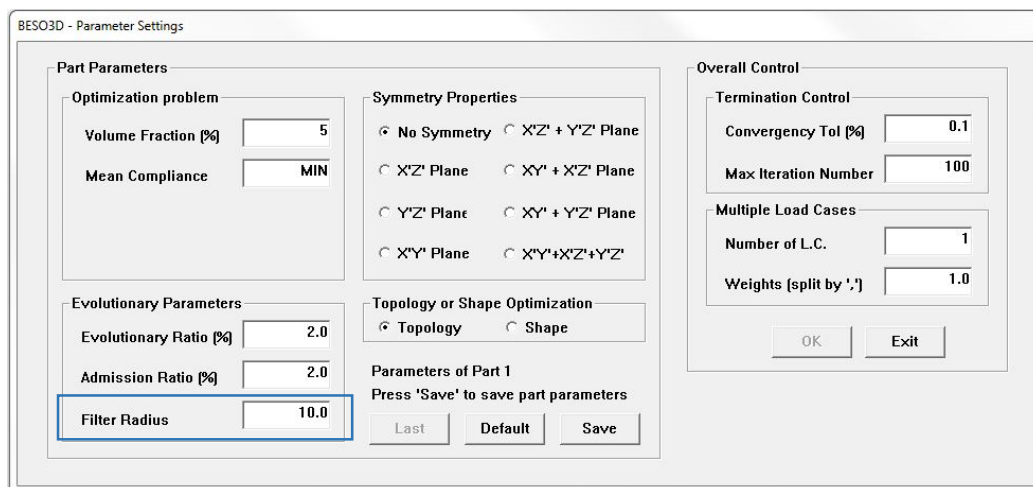
Figure 112: Filter radius input for BESO3D.

D.3.1 EXAMPLE

This example illustrates the effect of different filter radii on the optimization result.

Results are obtained by using BESO2D [28]. BESO2D is a simple brother of BESO3D and is able to solve 2D optimization problems. Similar to BESO3D, BESO2D minimises the mean compliance (maximises stiffness) by using a volume constraint.

The model as showed in Figure 113 has been used for tis example. The green part defines the optimization domain with a mesh width of 0,05.The domain is fixed at the left-hand side and a vertical force has been applied, located at the right-hand side. Optimization runs has been executed with four different filter radii: (i) 0,05; (ii) 0,15; (ii) 0,35; (iv) 0,55. The object constraint has been set to a volume fraction of 50%. An example of the input for filter radius 0,05 is depicted in Figure 114.

Figure 113: Optimization domain (mesh width 0,05) with predefined boundary conditions and vertical load.
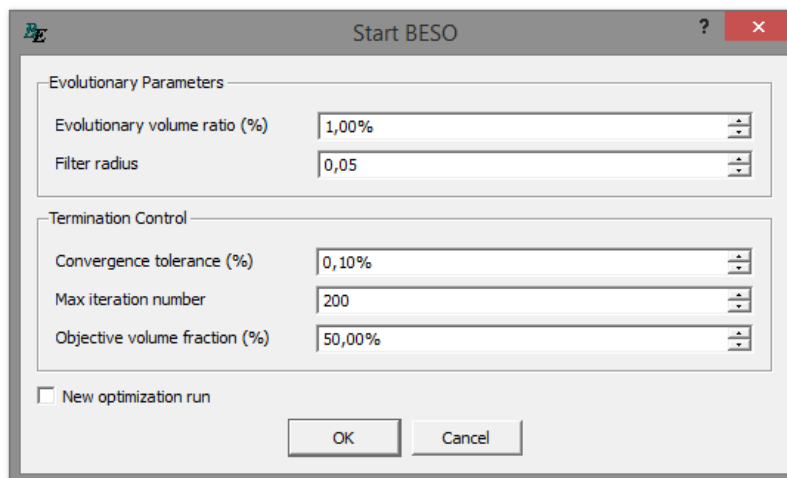
Figure 114: Example settings using filter radius of 0,05. The stiffness of the structure is maximised while the volume fraction is set to 50%.

D.3.2 OPTIMIZATION RESULTS
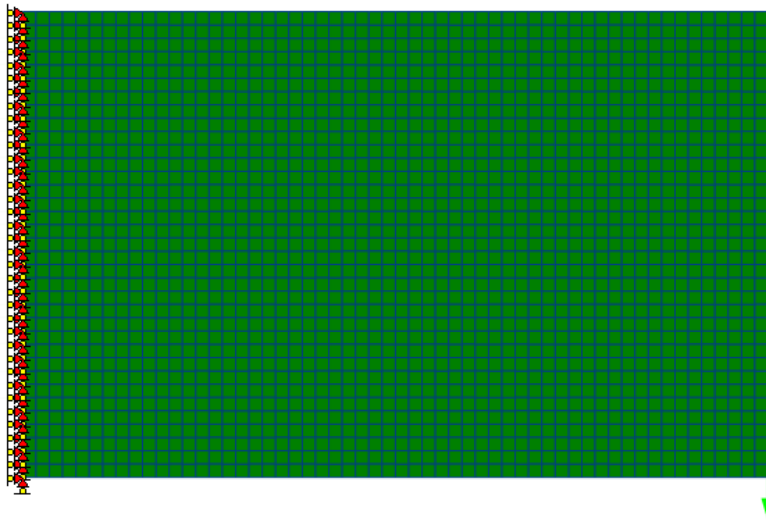
The results of the optimization runs are shown in Figure 115. The structure depicted at the left top contains very slender structures. These slender structures disappear by increasing the filter radius. The results prove that larger filter radii result in less slender structures.

Although undesired slender structures can be prevented, it is also important to note that applying larger filter radii result in less optimal structures. This is demonstrated by comparing the optimized mean compliance for the obtained structures by applying filter radii 0,05 and 0,55 (left top and right bottom in Figure 115 respectively). Figure 116 and Figure 117 show the optimized mean compliance for both optimization runs. The mean compliance with filter radius 0,05 is significantly lower to mean compliance when applying a filter radius of 0,55, i.e., a lower filter radius results in a stiffer structure compared to a higher filter radius.
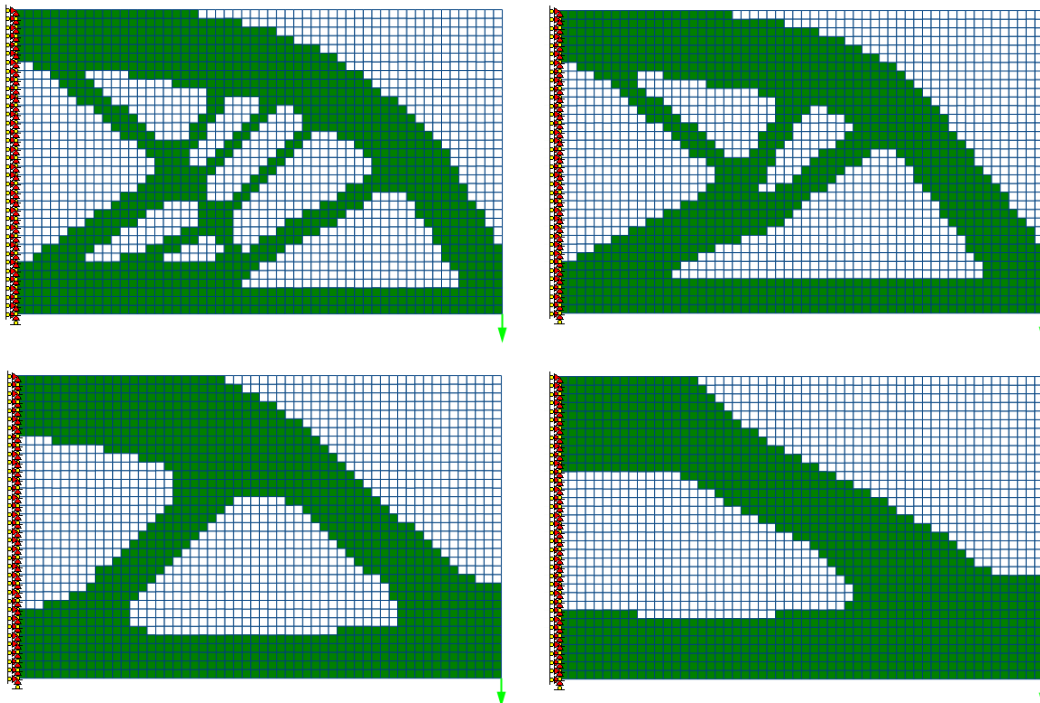
Figure 115: Top left: filter radius 0,05. Top right: filter radius 0,15. Bottom left: filter radius 0,35. Bottom right: filter radius 0,55.
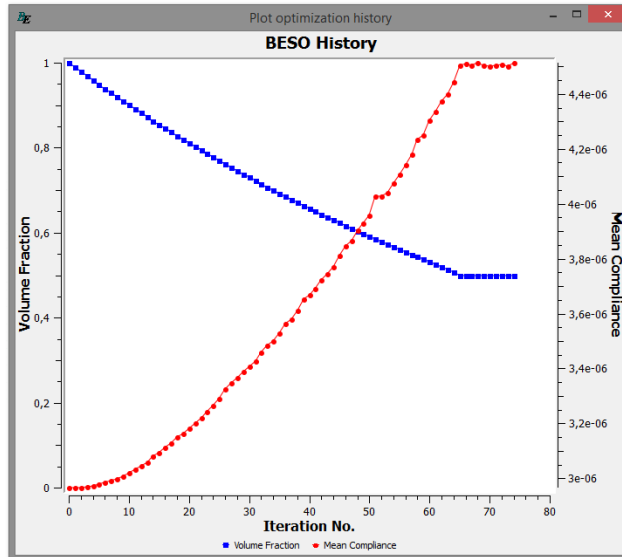
Figure 116: Optimized mean compliance for filter radius 0,05.
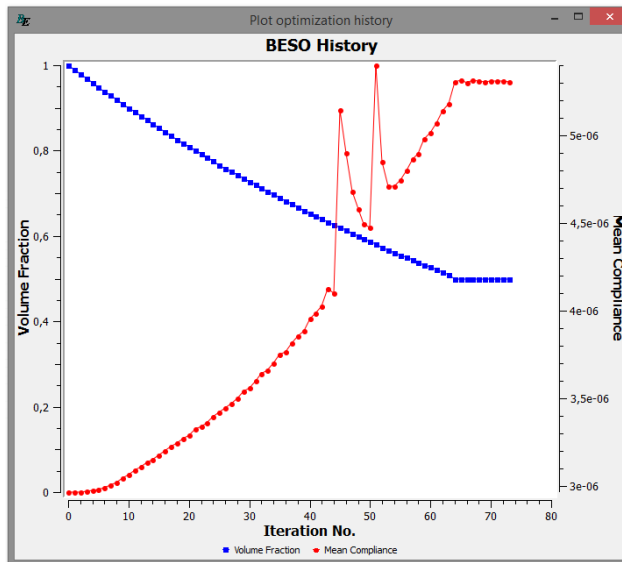
Figure 117: Optimized mean compliance for filter radius 0,55.

D.4 CONCLUSION

The results of the various optimization problems have provided more insight in the application of BESO3D.

The results obtained for the simple optimization problems correspond to the expectations and the results can be explained. Moreover, the results of the example with multiple load cases meet the pre-stated expectations. Also, it is demonstrated that the filter radius influences the results of optimizations. Undesired slender structures can be prevented by applying a proper filter radius. However, applying a large filter radius will result in not the most optimal structure. By using BESO3D for the optimization of structures, the engineer should decide which filter radius suits best for each problem.

It can be concluded that BESO3D acts as expected and can be applied in order to optimize complex problems, such as joints in gridshells.

E

DATA & CALCULATIONS

E.1   DATA OF THE BEAMS

Table 5, Table 6 and Table 7 present the data that have been used to classify the obtained topology optimization results in section 3.3.6.

Table 5: Member properties adjacent to joint 1.

#	l_0 [mm]	E [N/mm^2]	I [mm^4]	σ [N/mm^2]	$W_{p,l}$ [N/mm^3]	k_{beam} [Nmm/rad]	$M_{e,u}$ [Nmm]
1	2090	2,10E+05	3,68E+07	460	4,91E+05	3,70E+09	2,26E+08
2	2825	2,10E+05	1,83E+07	355	2,28E+05	1,36E+09	8,09E+07
3	1984	2,10E+05	3,68E+07	460	4,91E+05	3,89E+09	2,26E+08
4	2276	2,10E+05	3,68E+07	460	4,91E+05	3,39E+09	2,26E+08
5	2828	2,10E+05	3,68E+07	460	4,91E+05	2,73E+09	2,26E+08
6	1993	2,10E+05	1,83E+07	355	2,28E+05	1,93E+09	8,09E+07

Table 6: Member properties adjacent to joint 2.

#	l_0 [mm]	E [N/mm^2]	I [mm^4]	σ [N/mm^2]	$W_{p,l}$ [N/mm^3]	k_{beam} [Nmm/rad]	$M_{e,u}$ [Nmm]
1	2059	2,10E+05	2,27E+07	355	2,82E+05	2,32E+09	1,00E+08
2	3027	2,10E+05	2,27E+07	355	2,82E+05	1,57E+09	1,00E+08
3	2105	2,10E+05	2,27E+07	355	2,82E+05	2,26E+09	1,00E+08
4	2057	2,10E+05	1,51E+07	355	1,85E+05	1,54E+09	6,57E+07
5	3050	2,10E+05	1,51E+07	355	1,85E+05	1,04E+09	6,57E+07
6	2133	2,10E+05	2,27E+07	355	2,82E+05	2,23E+09	1,00E+08

Table 7: Member properties adjacent to joint 3.

#	l_0 [mm]	E [N/mm^2]	I [mm^4]	σ [N/mm^2]	$W_{p,l}$ [N/mm^3]	k_{beam} [Nmm/rad]	$M_{e,u}$ [Nmm]
1	2194	2,10E+05	1,50E+07	355	1,85E+05	1,43E+09	6,57E+07
2	3073	2,10E+05	1,50E+07	355	1,85E+05	1,02E+09	6,57E+07
3	2166	2,10E+05	1,50E+07	355	1,85E+05	1,45E+09	6,57E+07
4	2158	2,10E+05	1,50E+07	355	1,85E+05	1,45E+09	6,57E+07
5	3063	2,10E+05	1,50E+07	355	1,85E+05	1,02E+09	6,57E+07
6	2174	2,10E+05	1,50E+07	355	1,85E+05	1,44E+09	6,57E+07

E.2 EXAMPLE CALCULATION OF DETERMINATION COEFFICIENTS α & β

This example calculation for the stiffness and plastic moment capacity are based on the moment-rotation diagram for joint 1 in direction 1, see Figure 118. The data of the attaching beam, presented in Table 5, is used for this calculation.

Calculation determination coefficient α

For the stiffness k_1 of the joint in direction 1:

$$k_1 = \frac{M_1}{\theta_1} = \frac{202 \cdot 10^6}{0,005} = 4,04 \cdot 10^{10} \, Nmm \cdot rad^{-1}$$

Using the derived stiffness k_1 it yields:

$$\alpha_1 = \frac{k_1}{E_1 I_1 / L_{0,1}} = \frac{4,04 \cdot 10^{10}}{2,1 \cdot 10^5 \times 3,68 \cdot 10^7 / 2,09 \cdot 10^3} = 10,94$$

Calculation determination coefficient β

For the plastic moment capacity $M_{j,u,1+}$ in a positive direction of the joint in direction 1:

$$M_{j,u,1+} = 1,98 \cdot 10^2 \, kNm$$

Using the found the plastic moment capacity $M_{j,u,1+}$, it yields:

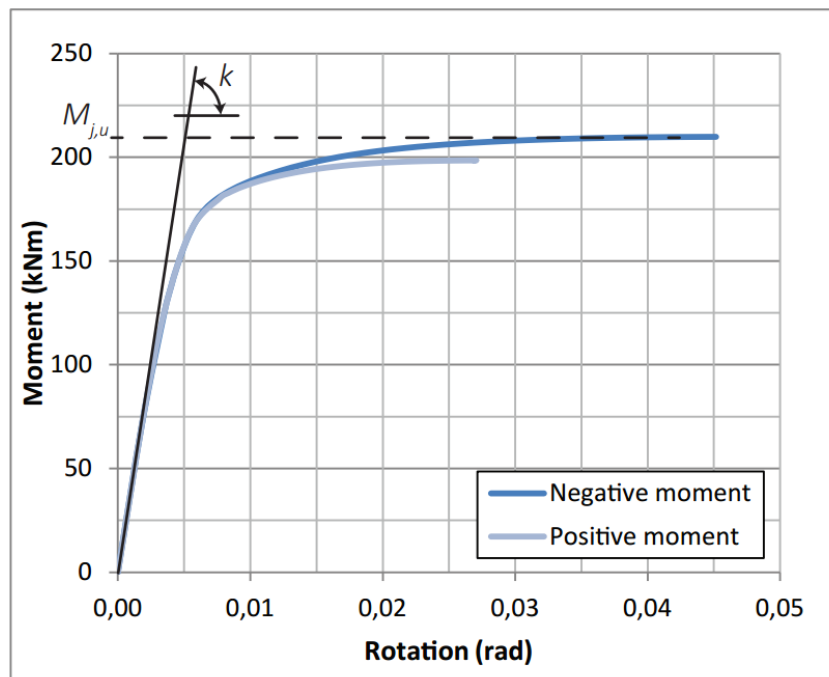$$\beta_1 = \frac{M_{j,u,1+}}{M_{e,u,1}} = \frac{1,98 \cdot 10^8}{2,26 \cdot 10^8} = 0,88$$

Figure 118: Moment-rotation diagram for joint 1 - direction 1.

E.3   CALCULATION OF PRETENSION FORCE

The pretension in the bolts prevent the plates to give way when loaded. By means of applying pretension the clamping force per bolt will equal $175\ kN$. A monolithic connection is obtained until the force tension force exceeds the clamping force. The calculation presented below is made to derive the clamping force. An example calculation has been used as reference [29]. Figure 119 gives some more information with respect to the calculation.

The stressed cross-section of the bolt:

$$A_t = \frac{\pi}{4} \cdot d_0^2 = \frac{\pi}{4} \cdot 21{,}185^2 = 352{,}49\ mm^2$$

The elastic limit of the material of the bolt:

$$R_{p0,2} = 1080\ MPa$$

When the bolt is pretensioned to 80% of the elastic limit of the material, the pretension stress becomes:

$$\sigma_t = \sigma_t' \cdot R_{p0,2} = 0{,}80 \cdot 1080 = 864\ MPa$$

The maximum pretension force in the bolt equals:

$$F_{0,2} = A_t \cdot \sigma_t' \cdot R_{p0,2} = 352{,}49 \cdot 0{,}80 \cdot 1080 = 380{,}69\ \text{kN}$$

The pretension force:

$$F_i = \sigma_t \cdot A_t = 864 \cdot 352{,}49 = 304{,}55\ kN$$

The change of force in the bolt P_b:

$$P_b = F_{0,2} - F_i = 380{,}69 - 304{,}55 = 76{,}14\ kN$$

The joint stiffness factor (the stiffness ratio of the bolt to the clamped parts) is:

$$C_m = 0{,}37$$
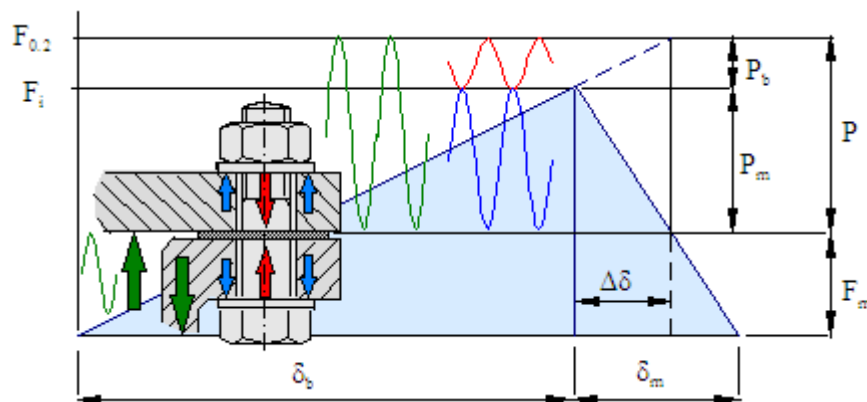
Figure 119: Notations used to calculate the pretension in the bolt [29].

The change of force on the clamped plates equals:

$$P_m = \frac{P_b \cdot (1 - C_m)}{C_m} = \frac{76{,}14 \cdot (1 - 0{,}37)}{0{,}37} = 129{,}64 \; kN$$

The clamping force on the clamped force yields:

$$F_m = F_i - P_m = 304{,}55 - 129{,}64 = 175{,}91 \; kN$$

The maximum force on the bolt after pretensioning is:

$$P = P_b + P_m = 76{,}14 + 129{,}64 = 205{,}78 \; kN$$

The stiffness ratio of the bolt to the clamped plates is derived by an online calculator [30]. The calculator makes use of the model as shown in Figure 120.

Figure 120: Model of the bolt clamping the plates [30].

E.4 CALCULATION OF REQUIRED TORQUE

In this calculation, the pretension force F_i, calculated in the previous paragraph, is used.

The required torque is the torque equalling the screw moment M_G and the moment M_{WD} occurring due to the friction between the nut and the thread:

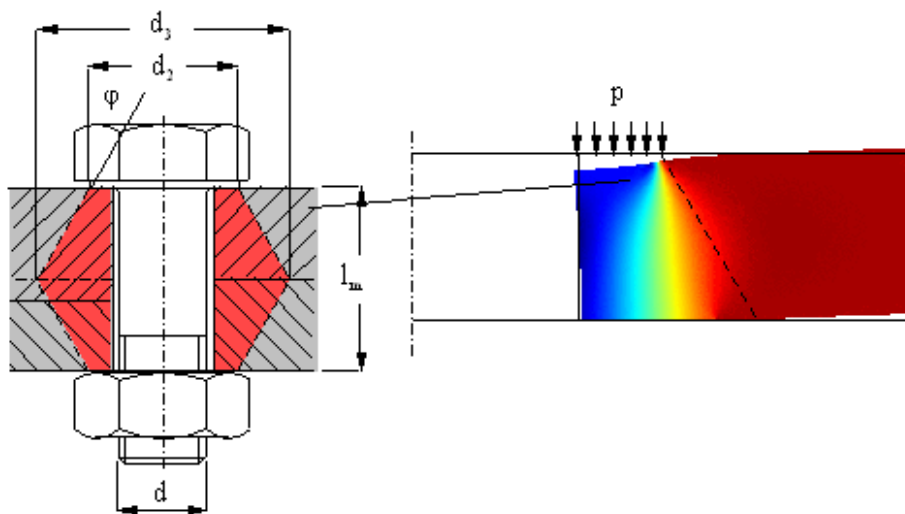$$M_A = M_G + M_{WD}$$

In order to calculate the torque in the thread, the pitch angle φ and the friction angle ρ' need to be determined (see Figure 121). With $P = 3\ mm$ the pitch of the bolts:

$$\varphi = \arctan\left(\frac{P}{\pi \cdot d_2}\right) = \arctan\left(\frac{3}{\pi \cdot 22{,}051}\right) = 0{,}0433\ rad = 2{,}48\ deg$$

With the steel to steel friction coefficient $\mu = 0{,}15$:

$$\rho' = \arctan\left(\frac{\mu}{\cos(\beta/2)}\right) = \arctan\left(\frac{0{,}15}{\cos(60/2)}\right) = 0{,}17\ rad = 9{,}83\ deg$$

For the moment M_G yields:

$$M_G = F_i \cdot \frac{d_2}{2} \cdot \tan(\varphi - \rho') = 304{,}55 \cdot \frac{22{,}051}{2} \cdot \tan(0{,}0433 - 0{,}17) = 546{,}77\ Nm$$

The moment due to friction of the nut to the thread:

$$M_{WD} = \mu_k \cdot F_i \cdot \frac{1{,}3d}{2} = 0{,}15 \cdot 304{,}55 \cdot \frac{1{,}3 \cdot 24}{2} = 712{,}7\ Nm$$

Finally, the required torque can now be derived by:

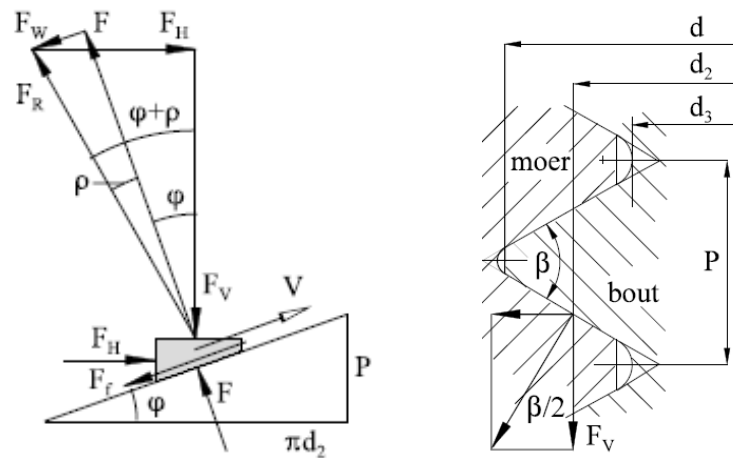$$M_A = M_{WD} + M_G = 712{,}7 + 732{,}5 = 1445{,}2\ Nm$$

Figure 121: Forces acting on the screw thread [29].

F

COST ITEMS

F.1 COST ITEMS

The cost items included in the cost comparison are specified in this section.

F.1.1 TRADITIONAL JOINT

Material

The joints are cut out of 20 cm thick forged steel plates. Most joints are made of steel S355, only some of S455. The average weight of the traditional joint is approximately $40\ kg$. The material costs of the thick steel plates are estimated to: $2\ €/kg$. Hence, the costs for the material:

Material $= 40 \cdot 2 = 80\ €$

Waste material

By cutting the star-formed joints out of steel plates, the waste generated will be around 200 % of the volume of the joint. Taking into account that selling the waste material would lead to a revenue of $0,3\ €/kg$, leads to the following costs:

Waste material $= 40 \cdot 2 \cdot (2 - 0,3) \approx 140\ €$

Fabrication

The fabrication of the joints took place by a special developed cutting machine. A welding robot was rebuilt to cut the steel plates. The cutting takes place either by laser of plasma. The estimated time to cut one joint is 15 minutes. The costs per hour for the machine including labour, energy and development of the machine is $400\ €/h$. Hence:

Cutting $= \frac{1}{4} \cdot 400 = 100\ €$

After fabrication, the joints need to be marked, removed from the remainder of the steel plate and brought to storage. This takes one man 10 minutes at a rate of $60\ €/h$:

Processing $= \frac{1}{6} \cdot 60 = 10\ €$

The total fabrication costs are:

Fabrication $= 100 + 10 = 110\ €$

Preparation beams

The beams need to be prepared to be installed in a ladder or to fill the gaps between the ladders on site. A CNC router was used to cut the beams into the exact geometry and shape at the tips

172

of the beams. Each beam end required 2 cuts. The time for placing the beam in the machine and to apply 4 cuts is estimated to 20 minutes. The costs for the CNC router including labour, energy and development of the machine is 150 €/ℎ. As each beam is attached to 2 joints, the costs for the preparation of the beams for 1 joint are:

$$\text{Cutting} = \frac{1}{3} \cdot 150 \cdot \frac{6}{2} = 150 \text{ €}$$

Next to cutting the correct geometry, the beams need to be provided with bevelled ends required for the weld process which takes 20 minutes. Again, each beam is connected to 2 joints, therefore:

$$\text{Weld preparation} = \frac{1}{3} \cdot 150 \cdot 3 = 150 \text{ €}$$

The total costs for the preparation for the beams are:

$$\textbf{Preparation beams} = 150 + 150 = 300 \text{ €}$$

Connection

The costs for the connection are built by the welding of the beams to the joints and the costs made to fit and install the beams at the site.

To attach 1 end of a beam to a joint, the length of the weld (2 welds at the top of 0,15 m, 2 at the bottom of 0,15 m and 2 sides of 0,2 m) is $4 \cdot 0,15 + 2 \cdot 0,2 = 1,0 \ m$. This implies that the total weld length per joint (6 beams) is 6,0 m (= 600 cm). The number of required weld beads depends on the wall thickness of the beams, therefore the following is assumed:

Table 8: Number of weld beads required per type RHS profile.

RHS profile	Number of weld beads
200x200x16,0	5
200x200x12,0	4
200x200x8,0	3
200x200x5,0	2

Most profiles consist of a wall thickness of 5,0 or 8,0 mm, therefore the average number of applied weld beads is set to 3. Because of welding on site, overhead welding and physical limitations made welding difficult, the time for welding is multiplied by a factor 2. With a weld speed of 10 cm/min, the time to weld one joint equals:

$$\text{Weld time} = \frac{600}{10} \cdot 3 \cdot 2 = 360 \ min = 6 \ h$$

Due to the difficulties with respect to the welding, classified welders were necessary at a cost of 80 €/ℎ for labour and equipment, the costs for welding are:

$$\text{Welding} = 6 \cdot 80 = 480 \text{ €}$$

At the site, the beams had to be hoisted into the exact place in order to apply tack welds before the welding process could start. In order to carry out this precision works, 4 man at a rate of 50 €/ℎ are required to install the beams. In 2 hours the 6 adjacent beams will be connected. Approximately 1500 of the 7123 members need to be hoisted in place, hence:

$$\text{Hoisting} = \frac{1500}{2300} \cdot 4 \cdot 2 \cdot 50 \approx 260 \text{ €}$$

The total costs for connecting the beams (fitting and welding) are summed to:

173

Connection $= 480 + 260 = 740 \, €$

Transport

Most transportation moves are similar for the traditional joint as well as the AM produced joint. Whereas in case of the traditional joint the weight was higher, an extra of 50 € is charged:

Transport $= 50 \, €$

Scaffolding

Scaffolding is required to prop the ladders and also to be able to install the beams between the ladders. The plan of the gridshell is approximately $10.000 \, m^2$. With an average height of $15 \, m$, the total amount of required scaffolding is $150.000 \, m^3$. The scaffolding will remain in place for 9 to 10 months for $2,5 \, €/m^3$, leading to the following costs for the scaffolding:

Scaffolding $= \frac{150000}{2300} \cdot 2,5 = 160 \, €$

Engineering/Inspection

The engineering for the joints is estimated to 50 € per joint. The inspection of the joint takes about 20 minutes per joint at a rate of $100 \, €/h$:

Engineering $= 50 + 0,33 \cdot 100 \approx 85 \, €$

F.1.2 AM PRODUCED JOINT TODAY

The costs for the optimized joint are based on data provided by EOS in Munich (Germany):

- Printing speed*: $2,2 \, mm/h$;
- Printing costs**: $80 \, €/h$.

*Printing speed on of the EOSINT M290 machine
**Including costs for post-processing

Material

The average weight of the traditional joint is approximately $12 \, kg$. The material costs of the powder of Stainless Steel GP1 are estimated to: $110 \, €/kg$. Hence, the costs for the material:

Material $= 12 \cdot 110 = 1320 \, €$

Waste material

Although the production by AM is associated with no waste material, support structure required during production can be considered as waste material. Assuming that 5 % extra material needs to be produced as support structure, the costs for the waste material are:

Waste material $= 0,05 \cdot 1320 \approx 70 \, €$

Fabrication

The total printing costs depend on the number of joints that fit in the building chamber. Because the printing process needs to be finished, the entire height of the building chamber of $400 \, mm$ needs to be filled with powder. As exemplified in Figure … (Appendix …) multiple joints or parts, with an average of 4 joints, will fit in the building chamber. The total printing costs equal:

Fabriation $= (\frac{400}{2,2} \cdot 80)/4 \approx 3640 \, €$

Note: the unused powder will be filtered and can be re-used.

Preparation beams

Contrary to the traditional situation, the beams can now be cut perpendicular to the axis of the beam and can therefore be cut by simple equipment, e.g. saw. Moreover, only one cut is required to cut the beams at the proper length. 6 beams can be handles and cut in $1\,h$. The costs for labour and equipment are $60\,€/h$. As each beam is connected to 2 joints, the costs for cutting are:

$$\text{Cutting} = 0,1 \cdot 60 \cdot 3 \approx 20\,€$$

The gusset plates to create the bolted connection are welded in the RHS members. The costs for a gusset plate is estimated to $5\,€$ and 12 are required per joint.

The length of the required (1 weld at the top or bottom of $0,1\,m$, 2 at the 4 sides of $0,05\,m$) is $1 \cdot 0,1 + 2 \cdot 0,05 = 0,2\,m$. With a weld speed of $10\,cm/min$ and with 12 required gusset plates (6 for each beam), the time to weld one joint equals:

$$\text{Weld time} = \frac{0,2 \cdot 12 \cdot 100}{10} \cdot 3 = 72\,min = 1,2\,h$$

Only 500 of the 2300 joints contain gusset plates. With the costs of $60\,€/h$ for labour and equipment, the costs for welding are:

$$\text{Welding + gusset plates} = \frac{500}{2300} \cdot (1,2 \cdot 60 + 12 \cdot 5) \approx 30\,€$$

The total costs for the preparation of the beams are:

$$\textbf{Preparation beams} = 20 + 30 = 50\,€$$

Connection

The ladders contain welded connections between the beams and the joints. To attach 1 end of a beam to a joint, the length of the weld (1 weld at the top of $0,1\,m$, 2 at the bottom of $0,1\,m$ and 4 sides of $0,05\,m$) is $2 \cdot 0,1 + 4 \cdot 0,05 = 0,4\,m$. This implies that the total weld length per joint (6 attaching beams) is $2,4\,m$ (= $240\,cm$). The number of required weld beads depends on the thickness of the weld, see Table 8. Similar to the traditional joint, the average number of weld beads of 3 is applied. With a weld speed of $10\,cm/min$, the time to weld one joint equals:

$$\text{Weld time} = \frac{240}{10} \cdot 3 = 72\,min = 1,2\,h$$

Note: with no difficulties of accessibility, no extra time is reserved as in case for the traditional joint.

With the costs of $60\,€/h$ for labour and equipment, the costs for welding are:

$$\text{Welding} = 1,2 \cdot 60 \approx 80\,€$$

At the site, bolts need to be prestressed with the required torque. As a considerable torque is required, this process will take up to 1,5 hour per joint. With the costs of $50\,€/h$ for labour and equipment, the costs for installation of the bolted connections per joint are:

$$\text{Bolts} = 1,5 \cdot 50 \approx 75\,€$$

At the site, the beams will be hoisted into place in order to be fixed by bolts that are pretensioned afterwards. In 1,5 hour 2 man will be able to install 6 beams to the joint. The costs

for labour and equipment are 50 €/ℎ. Approximately 1500 of the 7123 members need to be hoisted in place, hence::

$$\text{Hoisting} = \frac{1500}{2300} \cdot 2 \cdot 1{,}5 \cdot 50 \approx 100 \text{ €}$$

With the costs for the 1800 welded connections, 500 bolted connections and the hoisting, the total connection costs are summed:

$$\textbf{Connection} = \frac{1800}{2300} \cdot 80 + \frac{500}{2300} \cdot 75 + 100 \approx 180 \text{ €}$$

Scaffolding

Contrary to the required scaffolding of 9 to 10 months when the traditional joints are applied, the scaffolding is only needed for a period of 6 to 7 months. Therefore, assumed is that the costs for the scaffolding are reduced by approximately 20 %:

$$\textbf{Scaffolding } = 0{,}8 \cdot 160 \approx 130 \text{ €}$$

Engineering

The engineering is split in a part for the engineering for the joints and in a part of inspection for the applied welds. The engineering for the joints is estimated to 100 € per joint due to the long computational time of the topology optimization. The inspection of the joint takes about 5 minutes per joint and costs 100 €/ℎ:

$$\textbf{Engineering } = 100 + \frac{1}{12} \cdot 100 \approx 110 \text{ €}$$

F.1.3   AM PRODUCED JOINT 5 YEARS

The costs for the production of topology optimized joints by AM in 5 years are based on expected developments in the future with respect to AM techniques. The two most interesting developments will be the increase of printing speed, due to more powerful lasers and the application of multiple lasers in the same building chamber, and a larger building chamber. Therefore the following data is used for the calculations:

- Printing speed: $10 \ mm/h$;
- Printing costs*:   80 €/ℎ.
- Dimensions of building chamber: $500 x 500 x 500 \ mm$

*Including costs for material and post-processing

Material

Due to an increase in interest and demand, material costs will be reduced in the coming years. This interest can also come from firms in the building industry. Indications are Arup's research in additive manufacturing, but also Dutch companies are investing in research on AM, such as BAM and Heijmans.

Similar to the AM produced joint today, the average weight of the traditional joint is approximately $12 \ kg$. With future estimated costs of 20 €/kg

$$\textbf{Material} = 12 \cdot 20 = 240 \text{ €}$$

Waste material

5% extra material needs to be produced as support structure, the costs for the waste material are:

Waste material $= 0,05 \cdot 240 \approx 10$ €

Fabrication

The total printing costs again depend on the number of joints that fit in the building chamber. As the size of the building chamber is increased to $500x500x500$ *mm,* an average of 6 joints will fit in the building chamber. Using the higher printing speed, the total future printing costs can be calculated:

Fabrication $= (\frac{500}{10} \cdot 80)/6 \approx 670$ €

Preparation beams

The costs to prepare the beams correspond to the AM produced joint today:

Preparation beams $= 50$ €

Connection

The costs to prepare the beams correspond to the AM produced joint today:

Connection $= 180$ €

Scaffolding

The costs to prepare the beams correspond to the AM produced joint today:

Scaffolding $= 130$ €

Engineering

With increasing computational power the part for the engineering of the joints will be reduced to 50 € per joint. The inspection costs remain the same, hence:

Engineering $= 60$ €